Development of MALDI Mass Spectrometry Imaging Methods for Probing Spatial Lipid Biochemistry of Amyloid Plaques in Alzheimer's Disease

Ibrahim Kaya

Department of Psychiatry and Neurochemistry
Institute of Neuroscience and Physiology
Sahlgrenska Academy, University of Gothenburg

UNIVERSITY OF GOTHENBURG

Gothenburg 2020

Cover illustration: Ibrahim Kaya

Development of MALDI Mass Spectrometry Imaging Methods for Probing Spatial Lipid Biochemistry of Amyloid Plaques in Alzheimer's Disease

ibrahim.kaya@neuro.gu.se

ISBN 978-91-7833-918-1 (PRINT)
ISBN 978-91-7833-919-8 (PDF)

Printed in Borås, Sweden 2020
Printed by Stema Specialtryck AB

Sevgili Annem ve Ağabeyime

Development of MALDI Mass Spectrometry Imaging Methods for Probing Spatial Lipid Biochemistry of Amyloid Plaques in Alzheimer's Disease

Ibrahim Kaya

Department of Psychiatry and Neurochemistry, Institute of Neuroscience and Physiology

Sahlgrenska Academy, University of Gothenburg

ABSTRACT

Alzheimer's disease (AD) is the most prevalent cause of neurodegenerative dementia. Aggregation of amyloid β (Aβ) peptides into extracellular Aβ plaques is one of the major neuropathological features of AD. However, Aloysius Alzheimer reported remarkable lipid granule accumulations in multiple glial cell types and intense lipid granules in the plaque core in AD brain along with the proteopathic features of AD in his initial reports. While the role of lipids in AD has until recently not received as much attention, a body of molecular, immune, genetical, biochemical evidence closely links aberrant lipid metabolism to several stages of AD pathogenesis. Therefore, plaque-associated lipid molecular information in specific brain regions would be a strong asset to dissect spatial lipid biochemistry of amyloid plaques which would also provide a basis for further investigation of cell signaling and metabolic pathways that are disrupted in AD. This thesis represents the development of matrix-assisted laser desorption/ionization (MALDI) mass spectrometry imaging (MSI) methods for single-plaque resolution spatial lipidomics across the brain tissue sections of transgenic AD mouse models. The developed methods include "static" MALDI for high-spatial resolution (at 10 μm) lipid imaging using low-energy laser pulses which can be followed by immunofluorescence imaging of the same brain tissue section, dual polarity MALDI-MSI on the same pixel points for spatial correlation of lipid species ionized in both negative and positive polarities and "trimodal" MALDI-MSI which allows spatial correlation of lipid species in dual polarity with peptide/protein species within the same brain tissue sections at 10 μm spatial resolution. These MALDI-MSI methods in combination with immunohistochemistry revealed plaque-associated alterations of several phospholipids, lysophospholipids, and sphingolipids along with the Aβ peptide truncations and leveraged the understanding of molecular, structural and immune signatures of Aβ pathology. For instance, we observed amyloid

plaque-associated myelin lipid architecture loss, apolipoprotein E (APOE) mediated sulfatide depletion, region-specific and long chain base specific accumulations of monosialogangliosides, and accumulations of several lysophospholipids in amyloid plaques in transgenic AD mouse brain.

In summary, lipids are important components of amyloid plaques and above mentioned novel MALDI-MSI methods in combination with other modalities have great potential for probing spatial lipid molecular pathology of amyloid plaques which can provide novel insights into AD pathogenesis.

Keywords: Alzheimer's disease, amyloid plaques, lipids, MALDI, mass spectrometry imaging, static MALDI, dual polarity MALDI-MSI on the same pixel points, trimodal MALDI-MSI, APOE, immunohistochemistry, Aβ peptides, myelin, neurodegeneration, myelin lipids, sphingolipids, phospholipids, lysophospholipids, sulfatides, gangliosides

ISBN 978-91-7833-918-1 (PRINT)
ISBN 978-91-7833-919-8 (PDF)

SAMMANFATTNING PÅ SVENSKA

Alzheimers sjukdom (AD) är den vanligaste orsaken till neurodegenerativ demens. Det typiska neuropatologiska fyndet vid denna sjukdom är att peptider, kallade amyloid β /Aβ), klumpar ihop sig och bildar extracellulär plack. Emellertid rapporterade redan Aloysius Alzheimer 1907, i sin ursprungliga redogörelse för neuropatologin vid AD, att han hade funnit lipidkorn i flera gliacellstyper och även i centrum av placken. Betydelsen av lipider vid AD har tidigare inte uppmärksammats, men nu finns flera studier som talar för att störningar i lipidmetabolismen kan kopplas till sjukdomsutvecklingen vid AD. Det är därför av intresse att undersöka plack-associerade lipider i specifika delar av hjärnan. Denna information kan ge en grund för fortsatt kartläggning av vilka störningar i cellsignalering och metabola reaktioner som sker vid AD. I denna avhandling beskrivs utvecklandet av en metod för avbildande masspektrometri, ”matrix-assisted laser desorption/ionization (MALDI) mass spectrometry imaging (MSI)”, MALDI-MSI. Metoden, som tillåter visualisering av enstaka plack i ett vävnadssnitt, användes för att undersöka plack-associerade lipider i olika delar av hjärnan i en transgen musmodell för AD. Metoden gör att lipider kan visualiseras med en upplösning av 10 µm. Då laserstrålning med låg energi används bevaras vävnaden och samma vävnadssnittsnitt kan användas för både MALDI-MSI och immunhistokemiska färgningar för proteiner. Både positivt och negativt joniserade lipider kan visualiseras i samma punkt och denna analys kan i samma vävnadsnitt följas av analys av proteiner och peptider. Med MALDI-MSI-metoden i kombination med immunhistokemi påvisades plack-associerade förändringa av flera fosfoliper, lysofosfolipider och sphingolipider tillsammans med Aβ peptidfragmenten. Fynden kan bidra till förståelsen för de molekylära, strukturella och immunologiska kännetecknen för AD. Bland det som observerades var förlust av myelinets arkitektur, apolipoprotein E (APOE)-medierad sulfatidnedbrytning i amyloida plack samt regionspecifika och kedjespecifika anhopningar av monosialogangliosider och flera typer av lysofosfolipider i de amyloida placken.

Denna avhandling visar att lipider utgör en viktig del av de amyloida placken vid AD. De nya MALDI-MSI-metoderna i kombination med andra metoder kommer att bli användbara verktyg för att analysera lipiders molekylära patologi, vilket kan ge nya kunskaper om sjukdomsutvecklingen vid Alzheimers sjukdom.

LIST OF PAPERS

This thesis is based on the following studies, referred to in the text by their Roman numerals.

I. Kaya, I.; Michno, W.; Brinet, D.; Iacone, Y.; Zanni, G.; Blennow, K.; Zetterberg, H.; Hanrieder, J. Histology-Compatible MALDI Mass Spectrometry Based Imaging of Neuronal Lipids for Subsequent Immunofluorescent Staining. Analytical Chemistry 2017; 89: 4685-4694.

II. Kaya, I.; Brinet, D.; Michno, W.; Başkurt, M.; Zetterberg, H.; Blennow, K.; Hanrieder, J. Novel Trimodal MALDI Imaging Mass Spectrometry (IMS3) at 10 μm Reveals Spatial Lipid and Peptide Correlates Implicated in Aβ Plaque Pathology in Alzheimer's Disease. ACS Chemical Neuroscience 2017; 8: 2778-2790.

III. Kaya, I.; Zetterberg, H.; Blennow, K.; Hanrieder, J. Shedding Light on the Molecular Pathology of Amyloid Plaques in Transgenic Alzheimer's Disease Mice Using Multimodal MALDI Imaging Mass Spectrometry. ACS Chemical Neuroscience 2018; 9: 1802-1817.

IV. Kaya, I., Jennische, E., Dunevall, J., Lange, S., Ewing, A. G., Malmberg, P., Baykal, A. T., and Fletcher, J. S. Spatial Lipidomics Reveals Region and Long Chain Base Specific Accumulations of Monosialogangliosides in Amyloid Plaques in Familial Alzheimer's Disease Mice (5xFAD) Brain. ACS Chemical Neuroscience 2019; 11: 14-24.

V. Kaya, I., Jennische, E., Lange, S., Baykal, A. T., Malmberg, P., and Fletcher, J. S. Brain Region-Specific Amyloid Plaque-Associated Myelin Lipid Loss, APOE Deposition and Disruption of the Myelin Sheath in Familial Alzheimer's Disease Mice. Journal of Neurochemistry 2020.

Reprints were made with permissions from the publishers.

PAPERS NOT INCLUDED IN THE THESIS

Following studies are not included in the thesis, referred to in the text by their Roman numerals.

I. Carlred, L., Michno, W., Kaya, I., Sjövall, P., Syvänen, S., and Hanrieder, J. Probing Amyloid-β pathology in transgenic Alzheimer's disease (tgArcSwe) mice using MALDI imaging mass spectrometry, Journal of Neurochemistry 2016; 138: 469-478.

II. Kaya, I., Jennische, E., Lange, S., and Malmberg, P. Dual polarity MALDI imaging mass spectrometry on the same pixel points reveals spatial lipid localizations at high-spatial resolutions in rat small intestine, Analytical Methods 2018; 10: 2428-2435.

III. Kaya, I., Brülls, S. M., Dunevall, J., Jennische, E., Lange, S., Mårtensson, J., Ewing, A. G., Malmberg, P., and Fletcher, J. S. On-tissue chemical derivatization of catecholamines using 4-(N-Methyl) pyridinium boronic acid for ToF-SIMS and LDI-ToF mass spectrometry imaging, Analytical Chemistry 2018; 90: 13580-13590.

IV. Oomen, P. E., Aref, M. A., Kaya, I., Phan, N. T., and Ewing, A. G. Chemical analysis of single cells, Analytical Chemistry 2018; 91: 588-621.

V. Kaya, I., Brinet, D., Michno, W., Syvänen, S., Sehlin, D., Zetterberg, H., Blennow, K., and Hanrieder, J. r. Delineating Amyloid Plaque Associated Neuronal Sphingolipids in Transgenic Alzheimer's Disease Mice (tgArcSwe) Using MALDI Imaging Mass Spectrometry, ACS Chemical Neuroscience 2017; 8: 347-355.

VI. Michno, W., Kaya, I., Nyström, S., Guerard, L., Nilsson, K. P. R., Hammarström, P., Blennow, K., Zetterberg, H., and Hanrieder, J. r. Multimodal chemical imaging of amyloid plaque polymorphism reveals Aβ aggregation dependent anionic lipid accumulations and metabolism, Analytical Chemistry 2018; 90: 8130-8138.

VII. Kaya, I., Johansson, E., Lange, S., and Malmberg, P. Antisecretory Factor (AF) egg-yolk peptides reflects the intake of AF-activating feed in hens, Clinical Nutrition Experimental 2017; 12: 27-36.

VIII. Michno, W., Nyström, S., Wehrli, P., Lashley, T., Brinkmalm, G., Guerard, L., Syvänen, S., Sehlin, D., Kaya, I., and Brinet, D. Pyroglutamation of amyloid-βx-42 (Aβx-42) followed by Aβ1–40 deposition underlies plaque polymorphism in progressing Alzheimer's disease pathology, Journal of Biological Chemistry 2019; 294: 6719-6732.

TABLE OF CONTENTS

ABBREVIATIONS

AA	Arachidionic acid
ABC	ATP-binding cassette
ABCA7	ATP-binding cassette subfamily A member 7
ACH	Amyloid cascade hypothesis
AChE	Acetylcholinesterase
AD	Alzheimer's disease
AEC	3-amino-9-ethyl carbazole
AICD	APP intracellular domain
APOE	Apolipoprotein E
APOJ	Apolipoprotein J
APP	Amyloid precursor protein
ASA	5-aminosalicylic acid
ATT	6-aza-2-thiothymine
ATX	Autotaxin
Aβ	Amyloid β
BACE1	β-site APP cleaving enzyme 1
CA	Cornu ammonis
CAA	Cerebral amyloid angiopathy
Cer	Ceramide
CCS	Collision cross section
CD33	Sialic acid binding immunoglobulin-like lectin 3
CID	Collision induced dissociation
CI	Chemical ionization
Cl-CCA	4-chloro-α-cyanocinnamic acid
CLU	Clusterin
CNS	Central nervous system
$cPLA_2$	Cytosolic PLA_2
CSF	Cerebrospinal fluid
CTF	C-terminal fragment
CU-AP	Cognitively unaffected-amyloid positive
Da	Dalton
DAB	Diaminobenzidine
DAG	Diacylglycerol
DAN	Diaminonapthalene
DESI	Desorption electrospray ionization
DHA	Docosahexaenoic acid
DHB	Dihydroxybenzoic acid
DHAP	Dihydroxyacetophenone
DMCA	Dimethoxycinnamic acid

DPA	9,10-diphenylanthracene
DPH	1,6-diphenyl-1,3,5-hexatriene
DiFCCA	α-cyano-2,4-difluorocinnamic acid
EM	Electron microscopy
ENPP2	Ecto-nucleotide pyrophosphatase/phosphodiesterase-2 enzyme
EPHA1	Ephrin type-A receptor 1
ET	Electron transfer
EOAD	Early-onset Alzheimer's disease
EI	Electron impact
ESI	Electrospray ionization
FAB	Fast atom bombardment
FAD	Familial Alzheimer's disease
FDI	Field desorption ionization
FFPE	Formalin-fixed paraffin-embedded
FI	Field ionization
FTAA	Formyl thiophene acetic acid
FTICR	Fourier-transform ion cyclotron resonance
Gal-3	Galectin-3
GCIB	Gas cluster ion beam
GD1	Ceramide-N-tetrose-di-acetylneuraminic acid
GM1	Ceramide-N-tetrose-N-acetylneuraminic acid
GM2	Ceramide-triose-N-acetylneuraminic acid
GM3	Ceramide-lactose-N-acetylneuraminic acid
GT1	Ceramide-N-tetrose-tri-N-acetylneuraminic acid
GWAS	Genome-wide association studies
HCA	Hierarchical cluster analysis
HCCA	4-hydroxy -α-cyanocinnamic acid
HDL	High density lipoprotein
HPLC	High performance liquid chromatography
HRP	Horseradish peroxidase
Hz	Hertz
ICP	Inductively coupled plasma
InP_3	Inositol triphosphate
Ig	Immunoglobulin
IHC	Immunohistochemistry
IL-1β	Interleukin 1 beta
$iPLA_2$	Calcium independent PLA_2
IMS	Ion mobility separation
ISD	In source decay
ITAM	Immunoreceptor tyrosine-based activation motif
ITO	Indium tin oxide

LC	Liquid chromatography
LAESI	Laser ablation electrospray ionization
LDI	Laser desorption ionization
LESA	Liquid extraction surface analysis
LOAD	Late-onset Alzheimer's disease
LPA	Lysophosphatidic acid
LPAR	Lysophosphatidic acid receptor
LPC	Lysophosphatidylcholine
MAG	Monoacylglycerol
MALDI	Matrix-assisted laser desorption/ionization
MIBI	Multiplex ion beam imaging
MLR	Multiple linear regression
MS	Mass spectrometry
MSI	Mass spectrometry imaging
MW	Molecular weight
m/z	Mass-to-charge-ratio
NCX	Noncovalent complex
Nd:YAG	Neodymium-doped yttrium aluminum garnet
NEP	Neprilysin
NFT	Neurofibrillary tangle
NMDAR	N-methyl-D-aspartate receptor
NMR	Nuclear magnetic resonance
NRBF2	Nuclear receptor binding factor 2
NanoDESI	Nano desorption electrospray ionization
NanoSIMS	Nano secondary ion mass spectrometry
OCT	Optimal cutting temperature
OPLS	Orthogonal partial least squares
OPO	Optical parametric oscillators
PA	Phosphatidic acid
PC	Phosphatidylcholine
PCA	Principal component analysis
PCIS	Precursor ion selector
PDMS	Plasma desorption mass spectrometry
PE	Phosphatidylethanolamine
PentaFCCA	α-cyano-2,3,4,5,6-pentafluorocinnamic acid
PET	Positron emission tomography
PG	Phosphatidylglycerol
PI	Phosphatidylinositol
PIE	Pulsed ion extraction
PI3K	Phosphoinositide 3-kinase
PI3P	Phosphatidylinositol-3-phosphate
PKC	Protein kinase C

PLA_2	Phospholipase A_2
PLC	Phospholipase C
PLD	Phospholipase D
PLMS	Post LIFT metastable suppressor
PLS	Partial least squares
PNA	N-Phenyl-2-naphthylamine
ppm	Parts per million
PS	Phosphatidylserine
PSEN	Presenilin
QIT-MS	Quadrupole ion trap mass spectrometer
RF	Radiofrequency
SA	Sinapinic acid
SAD	Sporadic Alzheimer's disease
SHIP1	Phosphatidylinositol 3,4,5-trisphosphate 5-phosphatase 1
SIGLEC	Sialic acid-binding immunoglobulin-type lectin
SIMS	Secondary ion mass spectrometry
SPT	Serine-palmitoyl-CoA transferase
ST	Sulfatide
SYNJ1	Synaptojanin1
SYK	Spleen tyrosine kinase
S1P	Sphingosine-1-phosphate
TER	2,2':5',2''- terthiophene
TFA	Trifluoroacetic acid
tg	Transgenic
THAP	Trihydroxyacetophenone
TIMS	Trapped ion mobility spectrometry
TLC	Thin layer chromatography
TMB	Tetramethylbenzidine
TOF	Time of flight
TPPN	Bis(trispyrrolidinophosphazenyl) naphthalene
TREM2	Triggering receptor expressed on myeloid cells 2
TYROBP	Transmembrane immune signaling adaptor
UV	Ultraviolet
UVPD	Ultraviolet photo dissociation
Vps34	Class III phosphatidylinositol 3-kinase
9AA	9-aminoacridine
3-NBA	3-nitro benzyl alcohol
3-SBASE	3-sulfobenzoic acid
4-SPITC	4-sulphophenyl isothiocyanate
2,5-cDHA	(E)-4-(2,5-dihydroxyphenyl)but-3-en-2-one
3-HC	3-hydroxy coumarin
4-HNE	4-hydroxynonenal

1 INTRODUCTION

1.1 Alzheimer's Disease

Research into Alzheimer's disease (AD) has been traditionally focused on the central nervous system (CNS).[1] However, recent studies demonstrated significant link between AD and a number of peripheral and systemic anomalies including systemic immunity disorders,[2, 3] metabolic disorders,[4, 5] blood anomalies,[6, 7] cardiovascular diseases,[8, 9] hepatic and renal dysfunctions,[10, 11] respiratory and sleep disorders,[12-16] disturbed microbiota, gut-brain axis,[17, 18] infection[19] and systemic inflammation.[20, 21] These peripheral and systemic abnormalities along with the aging-related pathological states can be associated not only with the progression of the AD pathological features; amyloid and tau pathologies, neurodegeneration, and glial responses, degeneration of the glia and apoptosis but also with the possible initiative mechanisms of AD.[19, 22-24] While keeping an open mind for the fact that strong evidence suggests AD is not simply/only initiated and progressed by β amyloid peptide, a peptide fragment of an integral membrane protein named amyloid precursor protein (APP),[25] primary neuropathological criteria for the diagnosis of AD are widely accepted to be amyloid β plaques and tau neurofibrillary tangles which are currently detectable in vivo by PET imaging and/or fluid (blood and CSF) biological marker analysis without the need for the examination of the post-mortem brain at autopsy.[26-30] Although, amyloid based explanation is not a definitive explanation of the whole AD pathology, it acts as a framework which has galvanized AD research for the last three decades.[31] Either the pathological features of AD are a cause or a result/response of the AD pathogenesis. Therefore, understanding molecular, structural or immune aspects of amyloid plaques would be a strong asset to dissect the molecular and biochemical mechanisms leading to Alzheimer's disease state.

In this thesis, I will focus on the lesions in the AD brain parenchyma, with amyloid pathology in the spotlight, rather than a systemic approach or fluid biomarkers (blood and CSF) of AD pathogenesis. I will particularly focus on the lipid connection to amyloid pathology and neuroimmunopathology of AD. Then, I will shed light on the need for developing novel mass spectrometry imaging methods in combination with other modalities (e.g. immunohistochemistry) for probing spatial lipid biochemistry of amyloid plaques in AD and will discuss the results obtained from transgenic AD mouse models using the newly developed multimodal chemical imaging methods in this thesis.

1.1.1 Overview of Alzheimer's Disease

While not being synonymous with dementia, Alzheimer's disease (AD) is the most prevalent cause of neurodegenerative dementia which describes a progressive decline in memory and other cognitive domains differing intra-individually.[32, 33] The clinical symptoms of dementia associated with AD follows a progressive pattern with the onset of amnestic cases which are early impairment in episodic memory, followed by later disabilities in language, complex memory, executive function, praxis, gnosis and behavior throughout the disease course and which ends with severe dementia and inevitable death typically within the 5-12 years of symptom onset.[33, 34] The vast majority of the cases of AD are late-onset, which occurs after age 65, with no demonstrated evidence neither for a pattern of inheritance (even if familial clustering is common, linked to the *APOE* gene, see below) nor another known cause (sporadic Alzheimer's disease, SAD), while the cases below this age rarely occurs which constitutes less than 5% of all cases and termed early-onset AD (EOAD). Only about 1% of AD cases have been found to be inherited with autosomal dominant fashion, called familial AD (FAD) which can present early clinical onset and faster progression of disease depending on the mutation type and background family genetics [35, 36]

The clinical symptoms of Aloysius Alzheimer's aforetime (1901) patient, Mrs. Auguste Deter, were memory loss and severe behavioral changes including hallucinations, delusions and aggression, and these were in line with symptomatic dementia which was similar of that seen in some individuals of advanced years but such a case was not previously described in a young woman at the age of 51 and who was 56 years old when she died.[37, 38] Therefore, Aloysius Alzheimer examined the brain at autopsy, and in the cerebral cortex (interestingly, there is no report on the hippocampus and entorhinal cortex) found neuropathological features. He reported neuronal loss, and impervious bundled fibrillary tangles in the cells suggesting the "chemical changes''. He also saw the existence of senile plaques as "miliary foci'' and noted that it is the deposition of a "particular substance" in the cerebral cortex which can be observed without chemical staining. The neurofibrillary tangles and plaques were the prominent lesions in AD brain, the latter having been previously described by neuropathologists Gheorghe Marinescu and Paul Oscar Blocq in an elderly epileptic[39] and by Oskar Fischer in "miliary sclerosis". [40] Alzheimer also reported glial proliferation in his reports where he enunciated that glia develops numerous fibres and many glial cells include adipose inclusion, the intracellular lipid deposits in AD brain.[37, 38] Modern-day analysis of Mrs. Deter's brain revealed possible peculiar mutations of *PSEN1* gene which is involved in familial Alzheimer's

disease (FAD).[41, 42] DNA extracted from the century-old specimen showed that Deter had been homozygous for *APOE ε3*[43] giving a clue about this modern AD risk factor, the *APOE* gene which encodes an important lipoprotein for lipid metabolism that is implicated in AD pathogenesis in an isoform dependent manner[44] (please see later text for a detailed review on APOE protein and more about neuroimmunopathology of AD). Abundant β amyloid plaques and tau neurofibrillary tangles in the cerebral cortex of Auguste Deter's brain have been also confirmed with modern-day neuropathological analysis,[43, 45] and they have been prominent pathological hallmarks of AD pathogenesis and primary standards for diagnosis of AD.[46-48]

In light of the initial studies of Dr. Alzheimer[37] and other early neuropathological studies including Oscar Fischer's work on AD neuropathology,[49] there has been extensive research on molecular pathology, neuropathology, genetics, and neuroimmunopathology of AD along with the biomarker hunting in CSF and blood.[27, 50] While AD is thought to be a disorder of protein aggregation which postulates aggregation of β amyloid and tau proteins are the critical players of AD pathophysiology, there are several additional cellular pathways, processes, and molecules, some are independent of amyloid pathology,[51] have been recently found/postulated to be implicated in AD pathogenesis which turned AD into a heterogeneous disease with complex and enigmatic pathobiology.[1, 28 52]

Several promising treatment strategies have been reported for AD including the use of acetylcholinesterase (AChE) inhibitors which have been found to be viable targets for symptomatic improvement in AD,[53] because cholinergic deficit (dysfunctioning of acetylcholine containing neurons) is a consistent and early finding in AD.[54] N-methyl-D-aspartate (NMDA) antagonists (e.g. memantine)[55] have been used to treat the excessive NMDAR (glutamate receptor) activity in AD brains which causes excitotoxicity and promotes cell death.[56] Further, there have been successful immunotherapies applied such as aducanumab (a.k.a. BIIB037) which is a high-affinity, fully human IgG1 monoclonal antibody against a conformational epitope found on Aβ.[57] BIIB037 binds aggregated forms of Aβ, not Aβ monomer and preferentially binds parenchymal over vascular amyloid in the brains.[57] BAN2401, a humanized monoclonal antibody, highly selectively binds to Aβ oligomers/protofibrils in the AD brain and eliminates them.[58] β-, γ-secretase (secretases that act for amyloidogenic cleavage of APP, see below in detail) inhibitors have been used to limit the production of Aβ which, in turn, reduce the production of neurotoxic fibrils and plaques.[59, 60] However, most of the treatment strategies that target the prominent neuropathological features,

mainly the amyloid cascade hypothesis (see below). Due to the complexity of AD disease pathogenesis, there is no certain disease modifying treatment that proves benefits on the disease symptoms.[28, 61] Therefore, scrutinizing the molecular pathology of pathological features of AD could contribute to the understanding of the molecular pathways leading to AD pathogenesis and would help with the development of better treatment strategies.

1.1.2 Neuropathology

As mentioned above, the key neuropathological features of AD have been described by Aloysius Alzheimer and Oscar Fischer both in 1907.[37, 49] Today, the neuropathological hallmarks of AD include several lesions in the post-mortem AD brains including amyloid plaques, neurofibrillary tangles, cerebral amyloid angiopathy, neuronal and synaptic loss, white matter degeneration, demyelination, oligodendrocyte degeneration, granular lipid inclusions and glial responses (astrogliosis and microgliosis) as well as immune-related proteins including microglial cell surface receptors and lipoproteins from glial cells.[62-64] Degeneration of postmortem human AD brain can be explicitly observed at the macroscopic level as atrophy (volume loss) which involves shrinkage of cerebral cortex and hippocampus along with the enlargement of the ventricles (Figure 1A). Plaques, neurofibrillary tangles and neuronal loss can be clearly observed at the microscopic level in AD brain (please see Figure 1B, C, Figure1F-H for plaques and tangles in the AD brain). Immunohistochemical staining reveals extracellular depositions of amyloid plaques (consists of several truncations, 38- to 43 amino acid, of Aβ peptide) which can be in different morphologies (diffuse and dense-core) and positive or negative with Thioflavin S or Congo Red staining along with the intracellular depositions of hyperphosphoprylated tau tangles (Figure 1C). Cerebral amyloid angiopathy (CAA) is also evident in many cases in the AD brain which can be visualized either with Aβ immunohistochemistry or Thioflavin S staining (Figure 1D, E). An amyloid plaque consists of fibrillary amyloid in β-sheet conformation along with the non-fibrillary forms of it such as amyloid oligomers. The “neuritic” plaques involve degenerating neurites, dendrites and axons (Figure 1B, C). The non-fibrillary Aβ in “diffuse” plaques can only be visualized with immunohistochemical staining, while the fibrillary Aβ in compact “dense-core” plaques can also be observed with standard microscopy techniques using either chromogenic staining (e.g. Congo Red) or fluorescence staining (e.g. Thioflavin S) and imaged with light microscopy.

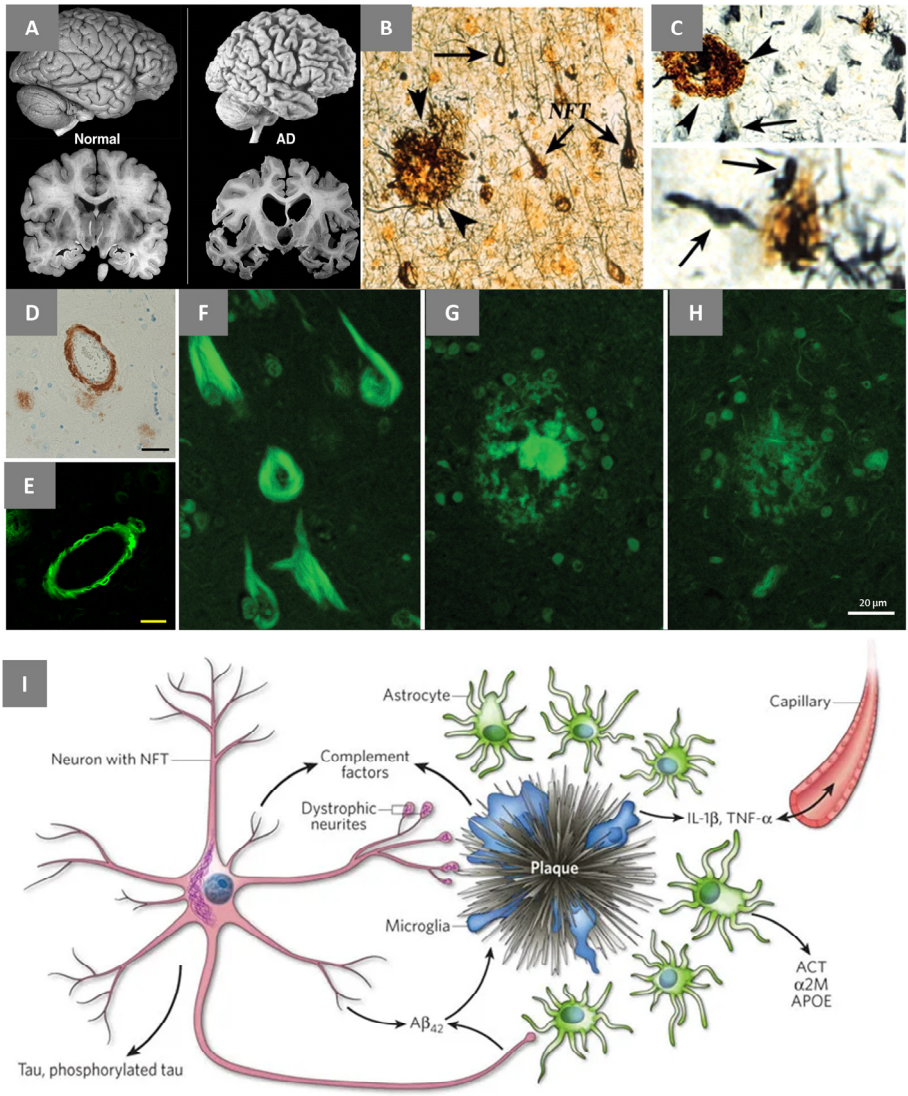

Figure 1. Neuropathology of Alzheimer's disease (AD). A) Postmortem brain tissue sections from AD diagnosed versus cognitively normal individuals reveal macroscopic atrophy in AD. Microscopic neuropathological features of AD brain include B) amyloid plaques (arrow heads) and neurofibrillary tangles (arrows) which are revealed by the Bielschowski silver stain. C) Immunostaining of paired-helical filament (PHF) tau (arrows) and β-amyloid (arrow heads) labels PHF-containing neurites associated with amyloid aggregates. Cerebral amyloid angiopathy (CAA) can be visualized e.g. in the frontal cortical sections in AD brain via D) Aβ immunohistochemistry or E) Thioflavin S staining.[65] Fluorescence micrographs of Thioflavin S stained F) neurofibrillary tangles, G) senile plaques with dense core, and H) senile plaques with neuritic elements.[66] I) A schematic illustration of AD neuropathology reveals extracellular accumulation of amyloid plaques in the brain. The plaques are

surrounded by immune cells; microglia and astrocytes which secrete several molecules including pro-inflammatory cytokines, complement components in the immune system, lipoproteins, apoptotic proteins and many more. Intracellular NFTs of tau can be observed in many neurons. AD related processes can be also regulated by the transport of the molecules through the blood vessels across the blood-brain barrier. Interleukin-1 (IL-1), tumor necrosis factor-α (TNFα), α-1 antichymotrypsin (ACT), α -2 macroglobulin (α2M), apolipoprotein E (apoE), and clusterin (a.k.a APOJ).[30] Scale bars are 40 μm in Panel D, E. Panel A, image credit: Bright Star Care. Panel B, C, adapted by permission[67] (Ref.67). Panel F-H, reprinted from The Lancet Neurology 10, Murray, M. E., Graff-Radford, N. R., Ross, O. A., Petersen, R. C., Duara, R., and Dickson, D. W. Neuropathologically defined subtypes of Alzheimer's disease with distinct clinical characteristics: a retrospective study, 785-796, Copyright (2011) with permission from Elsevier. Panel I, reprinted by permission from Springer Nature, Multimodal techniques for diagnosis and prognosis of Alzheimer's disease, Perrin, R. J., Fagan, A. M., and Holtzman, D. M. Copyright (2009).

Amyloid plaques are surrounded by proliferated active glial cells, microglia and astrocytes, with altered morphologies (Figure 1I). This underlies the implication of neuroinflammation in AD pathology. Neuroinflammation was presumed to be only a response to pathophysiological pathways in AD. Recently, the innate immune system related events have been demonstrated to be regulating and contributing to the disease pathogenesis[52, 68] while there is also evidence that neuroinflammation has protective roles in AD-associated neurodegeneration.[69, 70] Reactive astrogliosis and microgliosis are among the prominent pathological features of AD and whole-genome sequencing and genome-wide association studies (GWAS) analyses revealed that a number of immune-related, apoptotic and proinflammatory genes including *TREM2, CD33, SHIP1, APOE, IL-1β, ABCA7, EPHA1* are potential risk factors for AD.[71-74] AD research during the past three decades has particularly highlighted the importance of the innate immune-associated events that are primarily driven by the resident microglia in the CNS.[68, 75, 76] *TREM2, CD33* and *APOE* genes are differentially expressed in the AD disease models of Aβ deposition compared to tau pathology AD models and the corresponding encoded proteins APOE, CD33, and TREM2 are upregulated in amyloid plaques and its surrounding disease-associated glial cells.[77-81] Consequently, neuroimmunopathology becomes an updated/modern version of the classical neuropathology of AD and reshapes the pathogenesis of AD into a complex meshwork of genetics, innate immune system, cell signaling, and molecular pathology.

Although AD is traditionally a grey matter disease due to the prevalent neuronal pathological hallmarks, senile plaques and NFTs in the grey matter, a body of recent evidence revealed that white matter degeneration and demyelination can also be important pathological features of AD and they might be risk factors and/or can contribute to the disease progression.[63]

Myelin and the myelinating cells of CNS, oligodendrocytes, has been demonstrated to be degenerated through Aβ toxicity, tauopathy as well as other mechanisms such as ischemia and oxidative stress.[63] Clinically, myelin degeneration can contribute or cause the AD symptoms including cognitive decline.[82] Alterations of axonal conduction by demyelination or axonal damage could directly and/or indirectly affect cognition.[83] Notably, myelin degeneration might precede or can be independent of the formation of plaques and NFTs in the AD brain.[51, 84] This is significant considering the weak association of grey matter pathology with the clinical symptoms of AD.[85]

Aloysius Alzheimer reported the intracellular lipid deposits in multiple cell types in the AD brain in his original reports, but the research on lipids in AD has been passed over in silence for many years. Nevertheless, Alzheimer himself placed significant emphasis on these pathological features of AD brain.[86] Using erstwhile analytical staining methods (e.g. Mann staining, or Herxheimer reaction), he reported existence of colored lipid granules both at the core of plaques and in the surrounding fibrillary glial cells. However, the staining of lipids was not as stable as the staining of the proteopathic features of the AD brain. Lipid-associated neuropathological features have until recently not attracted enough attention compared to the protein aggregation based pathological features of AD, likely due to the limited analytical capability for lipid analysis during the initial AD research studies. However, current advanced lipidomics techniques reveal strong association of various lipid species with several stages of AD pathogenesis[87, 88] (see later discussion for a detailed review).

1.1.3 Neuroimmunopathology

It is known that FAD cases are derived from the mutations of genes regulating the production, structure or the ratio of Aβ truncations, (importantly, Aβ 1-42/Aβ 1-40), such as *APP*, *PSEN1*, *PSEN2* (see below). However, the majority of the AD cases are either SAD or show reasonable familial clustering. In addition to the aging-related pathological states, recent genome-wide association studies (GWAS) and whole genome candidate gene studies reveal significant portion of the gene variants implicated in the innate immune cell processes that are the prominent risk factors of late-onset AD.[89, 90] Therefore, innate immune-associated processes are non-negligible in AD pathogenesis. Activated glia is another pathological feature of AD along with the neurotoxic protein aggregation. Indeed, chronic neuroinflammation can cause neurodegeneration and neuronal death via certain pathways including toxic substances secreted from the activated glial cells such as reactive

oxygen species (ROS) and microglial phagocytosis and death of neurons due to the inflammatory stress.[91] In addition, neuroinflammation can induce neurodegeneration in an indirect way by affecting/contributing amyloid and tau pathologies.

Several prevalent AD risk gene variants, validated by functional genomics, such as *TREM2*, *APOE*, *CLU*, *INPP5D*, *ABCA7,* and *CD33* are associated with microglial and innate immune cell functions.[71, 92-94]Recently, *FAM222A* has been also suggested to be a putative brain atrophy susceptibility gene for AD, and the encoded protein by *FAM222A* has been found to be increased in the CNS and focally in amyloid plaques in the post-mortem human AD brain and transgenic AD mouse brains. The data has suggested that encoded protein by *FAM222A* has an affinity to physically bind to Aβ that facilitates its aggregation.[95] It has been also suggested that overexpression of encoded protein by *FAM222A* exacerbates neuroinflammation and cognitive decline[95]

APOE (which encodes apolipoprotein E (APOE)) is the prominent immune-related risk gene which has been discovered in 1993.[96] APOE protein has been implicated in AD pathogenesis with an isoform dependent manner.[97] In human, three abundant alleles of *APOE* present including; ε2, ε3, ε4 alleles and *APOE ε4* is the highest risk factor for AD,[98, 99] while *APOE ε2* is protective compared to *APOE ε3*.[1, 100] APOE protein is a major component of neuritic plaques[100-102] and has a strong affinity to Aβ.[96] APOE is expressed mostly in astrocytes (and with a less amount in microglia) in the CNS and it is a lipoprotein which is involved in the transport, delivery and regulation of lipids in the nervous system.[103-105] *CLU* (which encodes Clusterin a.k.a APOJ) is another prominent genetic risk factor of LOAD. Like APOE, its predecessor protein called clusterin (which is a multifunctional glycoprotein) is also associated with lipid transport and immune function in the AD brain and it is also secreted by astrocytes in the CNS.[106] Clusterin is involved in disease-associated pathways such as cell death and survival, oxidative stress, and proteotoxic stress in AD pathogenesis.[106-108] For instance, clusterin facilitates the clearance of late apoptotic cells via phagocytosis with a specific binding affinity which abrogates apoptotic cell-induced immune responses.[109] Further, clusterin accumulates in amyloid plaques and in fact promotes amyloid plaque formation[110] via sequestering oligomeric Aβ in the extracellular space as a chaperone.[111] Sedimentation of amyloid peptides by clusterin can promote oxidative stress in AD brain which can trigger neurotoxicity.[112] PDAPP, clusterin$^{-/-}$ mouse has revealed markedly less fibrillary Aβ (amyloid) deposits and plaque-associated neuritic dystrophy compared to PDAPP mouse with natural clusterin expression.[113]

TREM2 (which encodes triggering receptor expressed on myeloid cells 2 (TREM2)) is another risk variant of LOAD and R47H is the prominent *TREM2* variant which increases risk for AD significantly.[114-116] TREM2 is a cell surface receptor expressed by microglia in the CNS and it promotes microglial survival and modulates inflammatory signaling. TREM2 facilitates phagocytosis of amyloid β in soluble (oligomeric) and non-soluble forms which can alleviate amyloid-associated pathology of AD.[117-119] Transgene expressions of *TREM2* knockout (TREM2 KO) and *TREM2* R47H in mouse augment amyloid pathology and tau pathology in/around the neuritic plaques.[120, 121] Recently, it has been reported that *TREM2* deletion reduces Aβ plaque formation at late stages, but elevates Aβ1-42/Aβ1-40 ratio and enhances axonal dystrophy and dendritic spine loss.[122] TREM2 protein evidently plays key roles in microglial response to amyloid pathology and microglial viability in the CNS.[123, 124] The extracellular domain of TREM2 binds polyanionic ligands (e.g. lipopolysaccharides) and anionic and zwitterionic lipids (e.g. phospholipids, sulfatides).[125-127] Upon ligand binding, TREM2 transmits intracellular signals through association with an adaptor protein (DAP12, a.k.a TYROBP). DAP12's cytosolic tyrosine based activation motif (ITAM) activates spleen tyrosine kinase (SYK) upon its phosphorylation. Activation of SYK initiates several cellular signaling events e.g. protein tyrosine phosphorylation, phosphoinositide 3-kinase (PI3K) activation promoting proliferation, survival and phagocytosis that are important for the viability and immune function of TREM2.[124, 128-130] Recently, galectin-3 (gal3) protein has been demonstrated to be an endogenous TREM2 ligand which attenuates TREM2/DAP12 signaling mediated microglia-associated immune responses in AD.[131] Further, *LGALS3* gene, which encodes gal3 protein, has been suggested to be another genetic risk factor for AD.[131]

CD33 (which encodes a sialic acid binding immunoglobulin-like lectin 3 (CD33)) is another microglial risk factor for LOAD.[92, 132] CD33 is an abundant immunoglobulin-type lectin (SIGLEC) in the CNS microglia and its activity requires sialic acid.[133] CD33 inhibits microglial uptake of Aβ. Knocking out *CD33* in APP/PSEN AD mouse model has been demonstrated to attenuate amyloid oligomers and plaque burden in the brain parenchyma.[80] Another AD risk gene expressed in myeloid cells of the CNS is *SPI1* and it is also associated with phagocytosis. *SPI1* encodes PU.1 protein which is a transcription factor and critical for the development and function of myeloid cells. Lower expression of PU.1 protein has been found to delay the onset of AD via regulating myeloid gene expression and cell function.[134]

ABCA7 (which encodes ATP-binding cassette subfamily A member 7 (ABCA7)) is another highly predominant genetic AD risk factor. ABCA7 protein is expressed in microglia and myeloid cells and promotes phagocytosis of the apoptotic cells.[135] Further, deletion of *ABCA7* has been found to enhance and accelerate amyloid plaque pathology in the AD brain.[136, 137] *INPP5D* which encodes phosphatidylinositol 3,4,5-trisphosphate 5-phosphatase 1 (SHIP1) protein is also expressed in microglia. SHIP1 has been found to inhibit TREM2/DAP12 activation of PI3K signaling which suggests an association of SHIP1 with the disease-associated microglia in AD.[138]

Importantly, most of these genetic risk markers of AD and corresponding encoded immune proteins are directly or indirectly implicated in lipid metabolism and cellular signaling pathways in AD. They are strongly associated with the disease-associated amyloid pathology, neurodegeneration, and glial cell degeneration. This underlies the significance of lipids in AD pathogenesis and motivates for the need for lipidomics research in AD.

1.2 Amyloid Pathology in Alzheimer's Disease

Alzheimer's disease encompasses a complex pathogenesis but amyloid pathology has been widely accepted to be the prominent driving factor of the AD pathogenesis and a body of the research in AD has put amyloid in the center.[139] A few decades ago, the close link between FAD and mutations in the APP protein or the presenilins (PSEN1 or PSEN2- both APP proteases) along with the neuropathological and biochemical findings in the AD brains eventually led to the formulation of the amyloid cascade hypothesis (ACH). ACH postulates that Aβ peptide plays a central and causative part in AD and initiates its pathogenesis.[140] However, several clinical trials based on amyloid cascade hypothesis have failed. This suggests that amyloid plaques are important pathological features of the AD brain; however, the initiative and progressive events of the disease pathogenesis involve complex pathobiology and molecular mechanisms (as also mentioned above).[141, 142] Moreover, Aβ pathology without neuritic plaques or tangles, has been found in non-demented, cognitively unaffected-amyloid positive (CU-AP) subjects.[143] Nevertheless, amyloid plaques are a result of a complex meshwork of various genetic, biochemical, biophysical, cellular and immunological events in the AD brain. Therefore, dissecting the molecular composition of amyloid plaques would contribute to the understanding of amyloid-associated AD pathogenesis and would also provide a basis for further investigations of cell signaling and metabolic pathways that are impaired in AD.

In this section, I will start with a description of APP processing and amyloid cascade hypothesis, and introduce transgenic AD rodent models, particularly APP/PSEN mouse models used for probing Aβ deposition. Then, I will cover the role of lipids in AD pathogenesis with a strong emphasis on amyloid-associated aberrant lipid metabolism.

1.2.1 APP Processing and Amyloid Cascade Hypothesis

Amyloid cascade hypothesis (ACH) has been postulated as a result of combined interpretation of genetics, molecular biology and neuropathology of AD subjects.[140] The Aβ peptide was initially sequenced and identified in cerebral blood vessels[144] and then in the parenchyma of post-mortem human AD brains.[145] This has been followed by sequencing and identification of *APP* gene which encodes amyloid precursor protein (APP, a.k.a amyloid-β-A4 protein).[146-148] These findings initiated the formulation of ACH which postulates that amyloid peptides initiate and drive the rest of the disease pathogenesis including tau pathology, synaptic dysfunction and neuronal cell death (Figure 2).[31, 140] APP is a transmembrane protein with an amino terminus within the extracellular space and a carboxyl terminus within the cytosol.[147, 149] APP is proteolytically processed by α-, β-, γ-secretases each involved in specific cleavage steps.[150] Two principal processing pathways of APP can be described: one leads to Aβ generation (the amyloidogenic pathway) and the other doesn't generate pathologically relevant Aβ (the non-amyloidogenic pathway).[151] Amyloidogenic cleavage of APP protein is facilitated by β-site APP-cleaving enzyme 1 (BACE1)[152] which liberates the soluble ectodomain of APP (sAPPβ). Then, the resulting carboxy-terminal fragment (CTF), with 99 or 89 amino acid length (which are termed C99 or C89), are cleaved by γ-secretase proteolysis within the single hydrophobic transmembrane domain which generates several C-terminally truncated Aβ peptide species of varying lengths [151, 153] along with the transcriptionally active APP intracellular domain (AICD).[154] Further, presenilin 1 and 2 (*PSEN1*; *PSEN2*) have been reported to be novel genes for early-onset FAD (EOFAD)[155-157] and they have been identified as the catalytical domains of the protease activity of γ-secretase.[158, 159] Missense mutations of *PSEN1*, *PSEN2* and *APP* genes can increase Aβ production and enhance propensity of Aβ for aggregation which leads to a fully penetrant disease state.[160-162] The non-amyloidogenic pathway involves the cleavage of APP by α-secretase which produces C-terminal fragment, C83, followed by γ-secretase cleavage generating P3 peptide (which apparently is pathologically irrelevant) along with the secreted ectodomain (sAPPα) and AICD.[151, 153, 163]

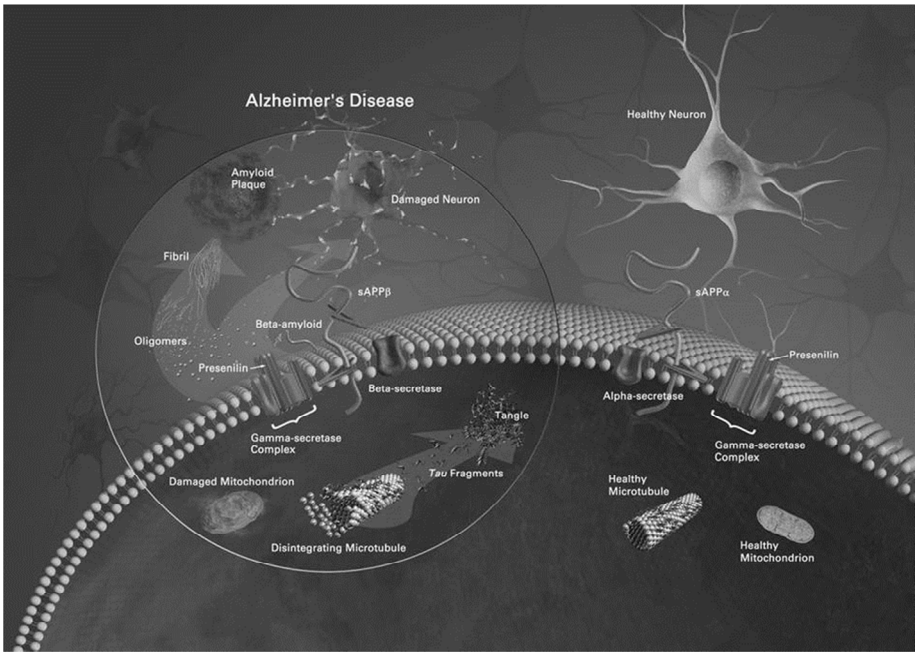

Figure 2. A schematic illustration of the amyloidogenic (on the left) and non-amyloidogenic (on the right) pathways of amyloid precursor protein (APP) processing and the amyloid cascade hypothesis (ACH). Amyloidogenic cleavage of APP protein is facilitated by β-site APP-cleaving enzyme 1 (BACE1) which liberates the soluble ectodomain of APP (sAPPβ). Then, the resulting carboxy-terminal fragments are cleaved by γ-secretase complex proteolysis within the single hydrophobic transmembrane domain which generates several C-terminally truncated Aβ peptide species of varying lengths. The non-amyloidogenic pathway involves the cleavage of APP by α-secretase which produces C-terminal fragment, C83, followed by γ-secretase cleavage generating P3 peptide (which apparently is pathologically irrelevant) along with the secreted ectodomain (sAPPα). According to the ACH (see the left side of the image), Aβ aggregates into oligomers, protofibrils, and fibrils, eventually leading to the formation of extracellular diffuse and neuritic plaques which have been suggested to cause dysfunction and loss of synapses and neurons, hyperphosphorylation of tau, formation of neurofibrillary tau tangles and disintegration of microtubules along with the mitochondrial damage. Adapted image courtesy of the National Institute on Aging/National Institute of Health (NIH).

Due to the combined activity of several enzymes during APP processing, Aβ peptides at various lengths are produced including C-terminally and N-terminally truncated species along with the post-translational modification product species of Aβ peptides including oxidation, glycosylation, phosphorylation and isomerization.[164-168] Depending on the site of γ-secretase cleavage, several C-terminally truncated Aβ peptides, varying in length (Aβx-37 to Aβx-43), are generated and are liberated into extracellular fluids such as cerebrospinal fluid (CSF), plasma or interstitial fluid.[164] N-

terminally truncated Aβ peptides (such as Aβ1-x, Aβ3-x, Aβ4-x, Aβ5-x, and Aβ11-x as common species) are produced independent of the α-secretase or β-secretase activities and they are possibly produced by the activity of Aβ degrading secretory proteases such as insulin degrading enzyme and neprilysin (NEP).[164, 169] N-terminally truncated Aβ peptides are abundant in human AD subjects but they exist with a lesser degree in the brains of transgenic AD mouse models.[170-173]

Modern ACH suggests differential role of amyloid peptides in different stages of aggregation including insoluble aggregates of Aβ such as fibrils along with the soluble oligomeric Aβ assemblies including dimers, trimers and higher order oligomers such as dodecamers.[174, 175] Aβ aggregates into oligomers and forms diffuse and neuritic plaques in the brain parenchyma which have been suggested to cause dysfunction and loss of synapses and neurons. [174, 176 139, 177] While the disease mechanism is relatively clear in FAD in the frame of ACH, which is a result of missense mutations of APP and PSENs and increased Aβ peptides (particularly $A\beta_{1-42}$),[162] amyloid based explanation of the disease initiation and progression in sporadic AD is more complex. It is known that concentration of Aβ is increased gradually in an age-dependent manner.[178, 179] Aβ peptides are regulated by proteolytic degradation and clearance in normal conditions.[180] Therefore, it has been hypothesized that SAD involves an imbalanced rates of production and clearance of Aβ levels without a certain cause yet.[181, 182]

Modern ACH in its current form postulates that the intracellular and extracellular accumulation and oligomerization of amyloid peptides are the initiative factors of the disease which results in a cascade of events leading to the disease state.[139, 183-185] According to ACH, Aβ oligomers firstly cause subtle effects on synaptic function and later gradually deposit and form diffuse plaques.[186-188] Various assembly stages of Aβ peptides initiate the innate inflammatory responses, mainly with microglial and astrocytic activation, along with the accompanying immune responses.[189-192] Further, Aβ oligomers can misbalance the neuronal ionic homeostasis and cause oxidative stress.[193] In addition, genes that promote β-amyloidogenesis in AD (*APP, PSEN1/2*, and *APOE4*) have primary role on the abnormalities in endolysosomal network which implicates this crucial cytopathology in AD.[67, 194] Amyloid oligomers can also alter the activities of phosphatases and kinases and this can cause imbalances of certain signaling pathways and lead to the phosphorylation and aggregation of tau protein forming intracellular neurofibrillary tangles.[195-199] Eventually, these processes lead to synaptic dysfunction, neuronal loss together with the attendant neurotransmitter deficits.[200, 201] Recent findings also demonstrate the toxicity of amyloid

peptides, particularly oligomeric amyloid assemblies, to oligodendrocytes (the myelinating cells of the CNS) which suggest a connection between amyloid pathology and the white matter degeneration in the AD brain.[63] Axonal damage during the myelin degeneration can clinically contribute or cause the AD symptoms including cognitive decline.[82] Therefore, rather than a sole neuronal focus, it is important to consider the role of amyloid in the AD brain within the scope of interrelated dysfunctioning of neurons and glial cells including astrocytes, microglia, and oligodendrocytes along with the cerebral vascular cells.[202]

1.2.2 Genetics and Transgenic AD Mouse Models

Amyloid cascade hypothesis promoted the generation of transgenic AD mouse/rat models mainly through the overexpression of APP and PSEN mutations, harboring one or multiple mutations, along with the mutations in tau. [203-206] Genes encoding APP protein are located on the chromosome 21 and genes encoding two γ-secretase component proteins (PSEN1/2); *PSEN1* and *PSEN2* are located on chromosomes 14 and 1, respectively.[153] Iowa (D694N),[207] Dutch (E693Q),[208] London (V717I),[209] Indiana (V717F),[210] Swedish (K670N/ M671L),[211] Florida (I716V),[212] and Arctic (E693G)[213] are the prominent mutations of *APP* which are linked to FAD (Figure3). A number of mutations in *PSEN1* and *PSEN2* linked to FAD have also been reported.[214, 215] The majority of the FAD mutations cause aberrant APP processing which results in the generation of more amyloidogenic Aβ peptide species, notably $A\beta_{1\text{-}42,}$ or results in increased $A\beta_{1\text{-}42}/A\beta_{1\text{-}40}$ ratio.[203] There are also AD mouse models designed for the investigation of the pathological role of N-terminally truncated Aβ peptide species which are prevalent in the senile plaques (e.g. $A\beta_{3\text{-}42}$) in human AD brains.[172, 216]

The first transgenic AD model was PDAPP mouse which overexpresses human *APP* transgene (containing Indiana mutation).[217] The Indiana mutation (V717F), located in the transmembrane domain of APP, generates senile plaques (primarily composed of $A\beta_{1\text{-}42}$)[218] in the mouse brain.[218] PDAPP displays age-related deposition of amyloid in the cortex and hippocampus along with the amyloid-associated neuroinflammation (reactive astrocytes and activated microglia), however, no overt neuronal loss.[219] One of the most widely used transgenic AD mouse model is Tg2576 (APPSwe) and it overexpresses human *APP* transgene containing the Swedish mutation (K670N/M671L) which is located outside the N-terminus of the Aβ domain (Figure 3) of APP (and favors β-secretase cleavage in *vitro*).[220] Tg2576 is associated with age-dependent increase of $A\beta_{1\text{-}40}$ and predominantly $A\beta_{1\text{-}42}$ levels leading amyloid plaque formation.[221]

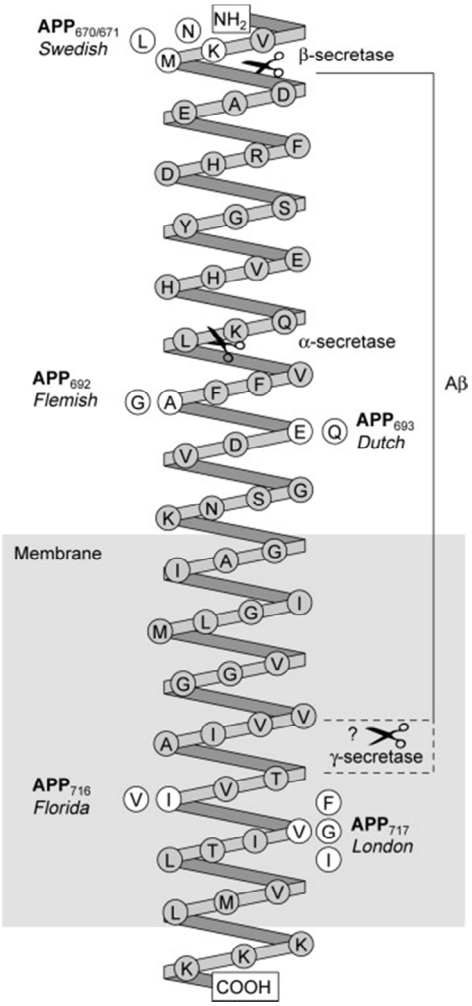

Figure 3. A schematic of some of the well-known APP mutations showing the relationship between the sites of the mutations and the sites of cleavage of APP around the Aβ part of the molecule.[161]*Reprinted from Hardy, J. Amyloid, the presenilins and Alzheimer's disease, Trends in neurosciences 20, 154-159., Copyright (1997), with permission from Elsevier.*

Tg2576 displays amyloid plaque-associated gliosis and dystrophic neurites without overt neuronal loss in CA1.[222] Further, Tg2576 exhibits deficits in synaptic plasticity and decreased dendritic spines in the hippocampus, and impaired spatial memory prior to severe Aβ deposition which is apparent at the age of 18 months.[223]

Many other transgenic AD mouse models have been developed by driving the overexpression of *APP* transgenes containing not only single but also

multiple FAD mutations such as TgCRND8 mouse (expressing Swedish and Indiana mutations)[224] and tgArcSwe (Swedish and Arctic mutations) mouse.[225, 226] TgCRND8 displays an aggressive neuropathology including early Aβ deposition (rich in $A\beta_{1-42}$), starting at the age of 3 months in the brain parenchyma, and cognitive decline while the neurodegeneration was absent.[224] TgArcSwe mouse exhibits intraneuronal immunoreactivity of Aβ and particularly N-terminus of Aβ. Further, compared to tgAPPSwe mice, the amyloid plaque deposition is markedly accelerated in tgArcSwe mouse brain parenchyma.[225] Mouse models expressing multiple APP and PS1 mutations exhibit early neuropathology in the brain parenchyma including intraneuronal Aβ accumulation and Aβ plaque deposition, and notably marked neuronal loss.[227-229] 5xFAD mouse overexpresses human APP with Florida, Swedish and London mutations along with the PS1 (M146L/L286V) mutations. 5xFAD is a widely used transgenic AD mouse model and it exhibits rapid neuropathology of FAD including intraneuronal Aβ accumulation, neuronal loss, neuroinflammation, synaptic loss and $A\beta_{1-42}$-rich amyloid plaques in the brain parenchyma.[229]

Mouse models have also been developed in order to study the pathological role of the toxic Aβ oligomers. For instance, tgAPP(OSK) which overexpresses APP with Osaka mutation (E693Δ) has been developed.[230] TgAPP(OSK) mouse displays age-dependent accumulation of intraneuronal Aβ oligomers and impaired hippocampal synaptic plasticity and memory loss starting from 8 months, however, there were no detected extracellular amyloid plaques in aged brains.[230]

Transgenic AD mouse exhibiting both amyloid plaques and NFT-like lesions in the brain have also been produced using combined FAD mutations and mutations of tau.[231] For instance, 3xTg-AD mouse has been developed which expresses human APP Swedish (K670N/M671L) and FTD-17 Tau (P301L) mutations (from exogenous transgenes combined with an endogenous PS1 mutation (M146V).[231] This triple-transgenic AD mouse model exhibits age-dependent intraneuronal Aβ accumulation which precedes clear extracellular Aβ deposits, with particularly prominent effect of $A\beta_{1-42}$. Tau pathology in 3xTg-AD mouse brain is only evident on the later stages of the disease pathology (in 1 year-old mouse brain) while Aβ plaques are readily apparent at earlier stages.[231, 232]

N-terminally truncated Aβ peptides are abundant in human AD subjects. In order to investigate pathological role of individual N-terminally truncated Aβ peptides, mouse models including TBA2[233] and tg4-42[172] have also been developed. TBA expresses only N-terminal $A\beta_{3-42}$ peptide in neurons which

exhibits neurotoxicity in *vivo* and neurological deficits including loss of motor functions.[233] Transgenic mouse expressing $A\beta_{4\text{-}42}$ (Tg4-42) exhibits a massive CA1 pyramidal neuron loss in the hippocampus which is in line with the age-dependent spatial reference memory deficits observed using the Morris water maze test.[172]

Along with the mutations in APP and PSENs for enhancing the accumulation of amyloid in the brain, mouse species lacking APP secretases including PSENs,[234, 235] BACE1[236] and lacking Aβ-degrading enzymes such as neprilysin[237, 238] have also been developed. Importantly, mouse lacking the major Aβ-degrading enzyme neprilysin and the ATP-binding cassette (ABC) transporter ABC1, a major contributor to amyloid-β clearance, exhibits pathological (e.g. astrogliosis and loss of synapses) and clinical (e.g. memory loss and anxiety) impairment which mimic sporadic AD.[237]

Nevertheless, new AD mouse models termed $APP^{NL\text{-}F}$ and $APP^{NL\text{-}G\text{-}F}$ harboring Swedish and Beyreuther/Iberian mutations with and without the Arctic mutation in the *APP* gene have been developed. These AD mouse models have endogenous APP levels and thus they develop robust Aβ amyloidosis.[239] This is important due to the fact that overexpression of APP used in several mouse models may cause Aβ-independent artifacts through the high levels of APP and its proteolytic fragments. $APP^{NL\text{-}F}$ and $APP^{NL\text{-}G\text{-}F}$ AD mouse models induce synaptic degeneration and memory impairment and they are more-reliable models to examine Aβ-associated pathology in AD.[240]

Recent findings about the role of innate immune system in AD as a result of GWAS and whole genome candidate gene studies have stimulated the development of mouse models for probing the immunopathological role of the proteins encoded by the AD risk genes notably *APOE*,[241, 242] *TREM2*,[120, 243] *CD33*,[80, 244] *ABCA1*.[245, 246] These transgenic mouse models have great potential to dissect the immune-associated lipid metabolism in AD pathogenesis.

Although none of the mouse/rat models fully recapitulate the AD pathogenesis (particularly the pathogenesis of SAD) they have been utilized to gain valuable molecular, biochemical, immune, structural insights into the neuropathological features of AD including amyloid β and tau pathologies, and importantly amyloid β oligomers.[203, 230, 247, 248]

1.2.3 The Lipid Connection to Amyloid Pathology

The first lipid connection to AD was originally reported by Aloysius Alzheimer in his initial reports in which he devoted significant space to remarkable lipid granule accumulations in multiple glial cell types and intense lipid granules in the plaque core within the post-mortem AD brain.[249] However, the research into the role of lipids in AD pathogenesis was widely ignored in the ensuing years, likely due to the better suitability of the aforetime analytical and biochemical techniques for probing the prominent proteopathic AD pathological features, senile plaques and NFTs.[249] Today, several molecular, immune, genetical, biochemical evidences closely link aberrant lipid metabolism to AD.[87, 88, 100, 250] While aberrant lipid metabolism and lipid biochemistry can also be associated with amyloid-independent AD pathogenesis such as the phosphorylation of tau (p-tau),[24, 251] here I will review the role of lipids in association with APP processing and amyloid pathology.

The lipid connection to amyloid pathology can be categorized into several mechanistic subtitles including: 1) The interactions of amyloid (Aβ) peptides and/or Aβ oligomers with the cellular membranes defect/alter the membrane lipid homeostasis, the organization and physicochemical properties of the membrane bilayer which can potentially alter APP processing and/or lipid metabolism.[252, 253] 2) On the other hand, Aβ, Aβ oligomers and AICD play functional roles in the regulation of lipid metabolism pathways either directly (e.g. via altering the activities of the phospholipases) or by transcriptional pathways, affecting the gene expressions encoding for APP, β-secretase, β-site APP cleavage enzyme (BACE1) or the Aβ-degrading protease neprilysin (NEP).[254-257] 3) Changes in lipid metabolism can directly modulate the functions of target proteins in APP processing such as APP and APP-cleaving secretases.[258-261] 4) Lipids, such as ceramide-N-tetrose-N-acetylneuraminic acid (GM1) play seeding and/or catalyzer roles in amyloid aggregation stages.[262, 263] 5) Lipids such as cholesterol and sphingolipids can also revert inert Aβ amyloid fibrils to soluble neurotoxic protofibrils which importantly suggest that insoluble Aβ aggregates can be activated by exposure to lipids.[264] 6) The interaction of cell membranes with a variety of assembly stages of Aβ peptides, particularly amyloid oligomers at various sizes, can dysregulate the signaling pathways within the neurons and surrounding glial cells either directly or via altering the activities of phosphatases, kinases and lipases or via resulting lipid-metabolite signaling molecules.[265, 266] 7) The functional groups of the lipids in the cell membrane (e.g. sialic acid, anionic head groups) can regulate the activity of the cell surface receptors in the surrounding glial cells in AD, prominently the cell

surface receptors in the microglial cells.[125, 133] 8) Autophagic-lysosomal dysfunction can defect lysosomal turnover of the lipids as well as proteins and this can result in the accumulation of lipids in autophagic vacuoles and lysosomes which can lead to a cascade of dysregulated lipid-protein interactions and impaired autophagic flux.[267, 268] 9) Oxidative stress and mitochondrial dysfunction in AD can impair lipid metabolism via reactive oxygen species (ROS)-induced lipid peroxidation[269, 270] which is evidenced by the increased amount of lipid-peroxidation end products; malondialdehyde (MDA) and 4-hydroxynonenal (4-HNE) in AD brains.[271] Importantly, 10) whole-genome sequencing and GWAS analyses revealed a number of immune-related, apoptotic and proinflammatory genes as a risk factor for AD including *TREM2, CD33, SHIP1, APOE, cPLA$_2$, IL-1β, PLD3* and these are directly or indirectly implicated in lipid metabolism or cellular membrane dynamics.[71-73, 272] Therefore, alterations and/or functions of several lipid and lipid-derived molecules including sphingolipids,[273] glycosphingolipids,[274] cardiolipins,[275] glycerophospholipids,[276] glycerolipids,[88, 277] plasmalogens,[278] fatty acids,[279] sterols (cholesterol, bile acids, cholesterol ester),[280-282] lysophospholipids,[283] phosphoinositides,[284] eicosanoids[276, 285] and endocannabinoids[286] have been implicated in AD pathogenesis.

Sphingolipids (SLs) are a class of lipids containing a backbone of sphingoid bases and a set of organic aliphatic amino alcohol sphingosines. SLs are essential constituents of eukaryotic cells. SLs and cholesterol abundantly present in lipid rafts which are subdomains of the plasma membrane and SLs are implicated in various cell signaling pathways.[287-289] Along with being structural components of the cellular membranes, many sphingolipids, such as ceramide, ceramide-1-phosphate, sphingosine, sphingosine-1-phosphate (S1P), and lyso-sphingomyelin act as bioactive signaling molecules involved in the regulation of cell growth, differentiation, senescence, and apoptosis.[287, 289] BACE1, γ-secretase and APP C-terminal fragments are localized in sphingolipid and cholesterol rich lipid rafts which suggest that amyloidogenic processing of APP occurs in lipid rafts and this strongly links sphingolipid metabolism to amyloid pathology in AD.[290] Further, the APP intracellular domain (AICD) has been found to decrease the expression of the catalytic subunit (SPTLC2) of the serine-palmitoyl-CoA transferase (SPT), the enzyme initiates the sphingolipid biosynthesis, which decreases the SPT activity and downregulates sphingolipid synthesis.[255] In addition, a body of evidence implicates several sphingolipids in subcellular transport, proteolytic processing and degradation/clearance of APP and APP processing enzymes along with the aggregation of Aβ peptides.[273] Cell studies indicated that inhibition of glycosphingolipid synthesis by inhibiting glycosyl ceramide synthase, which catalyzes the first step in glycosphingolipid biosynthesis,

reduces the secretion of APP and Aβ peptides, whereas addition of gangliosides stabilizes APP and increased the amount of secreted APP and of Aβ.[291, 292] Further, using a cell-permeable analog of ceramide, C6-ceramide, and several biochemical inhibitors of the sphingomyelin/glycosphingolipid biosynthetic pathway, it has been found that ceramide stabilizes BACE1 and promotes Aβ biogenesis.[293] It has also been demonstrated that S1P specifically binds to full-length BACE1 and increases its proteolytic activity in mouse neurons, suggesting that cellular S1P directly modulates BACE1 activity.[294] GM1 has been found to bind the N-terminus of APP specifically and induce a conformational change which decreases secreted APP and thus involves GM1 in APP proteolysis in AD.[295, 296] Further, accumulation of sphingolipids can impair the autophagic clearance of AD-associated proteins and can promote Aβ accumulation and aggregation.[268, 297] Indeed, it has been reported that cell surface GM1 binds to Aβ which alters its conformation from random coil to more structured β sheets, and therefore acts as a seed for amyloid aggregation in neurons.[262, 274] Importantly, the act of GM1 as a seed increases by age and it is facilitated by cholesterol-rich environments, suggesting that this process might be facilitated in lipid rafts.[274, 298]

Lipidomics studies using cells and brain tissues revealed alterations of several sphingolipids including ceramides, sphingosine-1-phosphate (S1P), sphingomyelins and glycosphingolipids (including gangliosides and sulfatides).[88, 267, 299] Depletion of sulfatides and elevations of long-chain ceramides from AD brain tissue extracts have been consistently reported.[299, 300] Depletion of sulfatides has been demonstrated to be mediated by an APOE-mediated pathway where APOE released from astrocytes removes sulfatides from cells with a hypothesized "kiss and run mechanism" (see below).[301, 302] Elevation of ceramides are potential degradation products of sulfatides, but other explanations for their elevations in AD brains include Aβ induced membrane oxidative stress, Aβ-mediated activation of sphingomyelinases (SMases) catalyzing the breakdown of SM to ceramide.[303-305] While an overall reduction of total ganglioside content of AD brain tissue extracts has been reported, there is a general elevation of simple gangliosides (e.g., GM2, GM3) and depletion of major, complex gangliosides (e.g., GM1, GD1a, GD1b, GT1b) in the AD brains.[273] Nevertheless, localized examinations of cells and histopathological regions reveal more specific focal alterations of ganglioside species in the AD brains.[306, 307] Importantly, GM1 and GM2 levels have been found to be elevated in lipid raft fractions derived from the cortical region of AD patients.[307] Several ganglioside species including GM1, GM2, GM3, GD3, and GD1a have been found to be accumulated in autophagic vacuoles and lysosomes in the tgCRND8 AD mouse brain, implicating defective turnover of lipids in

macroautophagy.[267] Further, increased expressions of cholinergic neuron-specific GMs in AD brain such as GT1aα may reflect altered cholinergic neurogenesis in AD brains.[308]

Another major lipid component of lipid rafts, cholesterol, has also been implicated in AD pathogenesis. [280] Astrocytes are a major site of cholesterol synthesis in the CNS and cholesterol is secreted by astrocytes in the form of apolipoprotein E-containing HDL-like particles. Cholesterol produced in astrocytes is also essential for myelination of oligodendrocytes in the CNS.[309, 310] Importantly, neurons are thought to reduce their cholesterol synthesis after birth and their cholesterol uptake relies predominantly on astrocytes.[311] Thus, the implication of apolipoprotein E (*APOE*) gene, which encodes APOE protein (particularly associated with cholesterol transport) closely associates cholesterol with the pathogenesis of AD.[280] Cell studies have revealed that cholesterol modulates α-secretase cleavage of APP which suggests that the alteration of cholesterol could contribute to the disease progression.[312] Cholesterol esters, the storage products of excess cholesterol, have been found to be accumulating in AD brains[88] and they can facilitate amyloidogenic processing of APP which, in turn, result in excessive Aβ production.[313] Importantly, cholesterol and cholesterol esters have also been found to be accumulating in autophagic vacuole fractions and lysosomes isolated from TgCRND8 mouse brain implicating impeded turnover of sterol metabolism in the cells due to the autophagic-lysosomal dysfunction associated with amyloid pathology in AD.[267]

Phospholipids are composed of a glycerol molecule substituted by one or two fatty acids and one additional polar group including phosphocholine, ethanolamine, serine or inositol.[314] A number of reports from cells studies, brain tissues from transgenic AD mouse models and patients with AD have indicated significant alterations of the composition and metabolism of several phospholipids including phosphoinositides (phosphorylated derivatives of phosphatidylinositols), plasmalogens and lysophospholipids[276, 278, 283, 284, 315] as well as changes in the levels and activity of phospholipases including phospholipase A_2 (PLA_2),[316, 317] phospholipase D (PLD),[318-320] phospholipase C (PLC),[321, 322] and phosphoinositide kinases and phosphatases.[323-325]

PLA_2 represents a group of enzymes which are characterized by their specific ability to hydrolyze phospholipids generating arachidonic acid implicated in inflammatory responses and lysophospholipids involved in cell membrane remodeling and regulation of membrane fluidity.[326] Aβ oligomers induce MAPK-mediated phosphorylation/activation of cytosolic PLA_2 ($cPLA_2$) and calcium-independent PLA_2 ($iPLA_2$) in a brain region-specific manner in

tgAPP(OSK) mice (which specifically expresses Aβ oligomers).[256] Lipidomics analysis revealed accumulations of *sn-2* lysophosphatidylcholine (LPC) and 4-hydroxynonenal indicating cleavage of phospholipids via oxidative stress and lipid peroxidation, respectively. Complementary immunofluorescence staining and spatial lipidomics revealed that activity of $cPLA_2$ is implicated with arachidonic acid (AA) accumulation in the myelin-rich white matter areas whereas the activity of $iPLA_2$ is implicated with docosahexaenoic acid (DHA) accumulation in pyramidal-neuron rich regions in the gray matter.[256] The activation of $cPLA_2$ by oligomeric Aβ, which can mediate/permit the migration of Ca ions into the cytosol, can stimulate AA mediated inflammatory signaling pathways along with the mitochondrial dysfunction and cell death.[327]

Plasmalogens are a subclass of phospholipids mainly found in the cell membranes and they are characterized by having an ether bond in position sn-1 to an alkenyl group. Overt depletion of plasmalogens has been consistently reported in the brains of patients with AD and transgenic AD mouse models.[278, 328, 329] Oxidative stress[329] and inflammation[330] are the prominent mechanisms for the depletion of plasmalogens in AD brain. Indeed, plasmalogens are particularly susceptible to oxidative stress due to a vinyl-ether group in their molecular structure.[278] Amyloid plaques and NFTs are focal, discrete structures in AD brains which can stimulate inflammation and activate PLA_2 enzymes which can hydrolyze the plasmalogens.[331] Another lipid species susceptible to oxidative stress is cardiolipins which are essential components of mitochondrial membrane. Indeed, oxidative stress in AD brains can cause mitochondrial damage and along with the plasmalogens, cardiolipins have also been found to be significantly depleted in AD brains which can be implicated in mitochondrial dysfunction via a damage in the inner membrane of the mitochondria.[275, 332]

Phosphoinositides represent seven species of reversibly phosphorylated derivatives of phosphatidylinositols. They play fundamental roles in controlling membrane-cytosol interfaces through interactions mediated by their head groups.[324] Phosphoinositides have functions in the regulation of membrane traffic, the cytoskeleton, the permeability and transport functions of membranes, synaptic vesicle recycling along with the signal transduction at the cell surface.[324, 333] Immunostaining experiments reveals an abnormal accumulation of a PLC isozyme (PLCδ) in NFTs, the neurites surrounding plaque cores along with the neuropil threads in AD brains.[321] PLC is a phosphoinositide-specific phospholipase (hydrolyzes phosphatidylinositol bisphosphate) which is important in signal transduction and it is implicated in the regulation of the secretion of APP in AD. This is facilitated by the

activity of the PLC-activity resulting secondary messengers; diacylglycerol (DAG) via activating protein kinase C (PKC) and inositol triphosphate (InP_3) via releasing Ca ions from intracellular stores.[334] In line with this, Berman et al. demonstrated that incubation of primary cortical neurons with oligomeric Aβ decreases phosphatidylinositol-4,5-bisphosphate (PtdIns(4,5)P2) levels.[253]

Deficiency of PIP species and PI kinases in the brains of patients with AD and transgenic AD mouse models has been previously reported.[284, 325, 335] Furthermore, phosphatidylinositol-3-phosphate (PI3P) species have been found to regulate sorting, and processing of APP through the endosomal system. PI3P is primarily synthesized by a PI3P kinase termed Vps34 whose disruption impairs autophagy, lysosomal degradation as well as lipid metabolism and promotes secretion of exosomes enriched in APP C-terminal fragments (APP-CTFs) and specific sphingolipids.[336] It is evidenced that PI3P levels are deficient in post-mortem human AD and transgenic AD mouse (with APP and PSEN mutations) brain tissues.[325] In addition, the NRBF2 (nuclear receptor binding factor 2), a key component and regulator of the PIK3C3/Vps34 containing PtdIns3K complex, has been found to be involved in APP-CTFs homeostasis in AD cell models. NRBF2 overexpression has been found to promote degradation of APP-CTFs and reduce $A\beta_{1–40}$ and $A\beta_{1-42}$ levels in human mutant APP-overexpressing cells. Interestingly, NRBF2 expression levels are reduced in the hippocampus of 5xFAD mouse brain.[337]

The phosphoinositide phosphatase, synaptojanin 1 (SYNJ1), is the main phosphoinositol (4,5)-bisphosphate phosphatase which is a key regulator of synaptic function. SYNJ1 has been implicated in both FAD and SAD where excess SYNJ1 has been found to contribute to cell dysfunction and memory impairment in the aging hippocampus[338] whereas the reduction of SYNJ1 has been found to accelerate Aβ clearance and ameliorate cognitive decline in APP/PSEN1 AD mouse model.[339]

PLD hydrolyzes the phosphodiester bond of the glycerophospholipid, phosphatidylcholine (PC), generating phosphatidic acid (PA) and free choline. PAs are bioactive molecules which can modify both the physical and signaling properties of lipid bilayers.[340] Similar to phosphoinositides, PAs are also involved in the regulation of the membrane-cytosol interface through a direct interaction with effector proteins, such as PIP kinases and SNARE proteins.[341] Nevertheless, PAs can also be converted to other bioactive signaling molecules such as diacylglycerol (DAG) and lysophosphatidic acid (LPA).[340] Elevated PLD1 has been found in the brains of patients with AD and transgenic AD mouse models.[319] Further, cell studies

reveals that Aβ peptides (particularly oligomeric $A\beta_{42}$) stimulate the activity of PLD not only in neurons but also in astrocytes and microglial cells.[318] It has been demonstrated that aberrant PLD activity contributes to the synaptic dysfunction and underlying memory deficits driven by amyloidogenic proteins in AD.[319] In line with this, ablation of PLD isoforms ameliorated Aβ pathology-associated synaptic dysfunction and cognitive deficits in transgenic AD mouse models expressing APP and APP/tau mutations.[319, 320] Another possible/suggested role of PLD activity in association with AD is ATX-LPA signaling.[342] Autotaxin (ATX, ENPP2) is an ecto-nucleotide pyrophosphatase/phosphodiesterase-2 enzyme (ENPP2) with lysophospholipase D activity that hydrolyzes lysophospholipids (particularly LPCs) into the lipid mediator LPA.[343] Therefore, apart from the phospholipase (PLD and/or PLA_2) activities, ATX enzyme activity might be another pathway for the aberrant production of LPAs in the AD brains. Indeed, increased autotaxin expression has been reported in the frontal cortex of Alzheimer-type dementia patients.[344, 345] LPA signaling through lysophosphatidic acid receptors (LPARs) is an important growth factor in the CNS.[346] LPA signaling increases the number of differentiating oligodendrocytes (but not the mature ones) and enhances membrane sheath formation in myelinating oligodendrocytes.[347] Shi et al. has reported that LPA increases the production of Aβ by upregulating the expression of β-secretase (BACE1) without altering the expression of APP or γ-secretase complex proteins as evidenced in vitro using mouse neuroblastoma N2a cell line stably expressing wild-type presenilin 1 and Swedish mutant APP.[348] Therefore, upregulated LPA levels in AD brains might be a result of feed forward cycle between LPA and Aβ production in which Aβ stimulates the activity of phospholipases and ATX resulting in LPA accumulation. Eventually, the aberrant LPA signaling can result in dysregulated LPA signaling in surrounding glial cells and neurons through LPARs which can have impairment in the AD brains, notably myelinopathy.

Recent findings reveal strong-association of immune-associated AD risk genes specifically with Aβ pathology including *APOE*, *TREM2*, *CD33* and *INPP5D*. The encoded proteins by these genes, notably APOE, TREM2 and CD33 have been implicated in microglial response and/or aberrant lipid metabolism in AD pathogenesis.[349] The content of sulfatides in the CNS is modulated by APOE protein in an isoform-dependent manner through APOE-containing CNS lipoproteins.[105] APOE, the lipid transport protein expressed mainly by astrocytes[103] and by microglia with a lesser amount[350] and it is implicated in the disruption of sphingolipid and sterol metabolism in AD,[351] notably sulfatide depletion in the brains of patients with AD and transgenic AD mouse models.[301] Han et al.[352] proposed a working mechanism

which suggests APOE-associated lipoprotein particles released from astrocytes can acquire sulfatides from myelin sheath through a ‘’kiss-and-run’’ mechanism which can be followed by metabolism and degradation of the resulting sulfatide-containing APOE-associated lipoprotein particles through endocytic pathways associated with the low density lipoprotein (LDL) receptor family in neuronal cells. This hypothesis has been reinforced using brain tissue extracts of transgenic AD mouse models where APOE-mediated depletion of sulfatides in AD brain has been found to be associated with amyloid pathology in APP transgenic AD mouse models.[301]

CD33, which is expressed on microglia in the CNS, inhibits microglial uptake of Aβ and its activity requires sialic acid recognition.[80, 133] Therefore, the sialic acid residues in the structure of gangliosides and sialylated glycoproteins (e.g. APOE and APOJ) masking the Aβ aggregates are possible activating agents for CD33 which can defect amyloid cleansing in the AD brains. This implicates gangliosides, the complex glycosphingolipids, in AD neuroimmunopathology.[353] TREM2 is a cell surface receptor expressed by microglia in the CNS and it promotes microglial survival and modulates inflammatory signaling. TREM2 lipid sensing has been evidenced to sustain microglial response and metabolic fitness around the amyloid plaques and limit the diffusion and toxicity of amyloid plaques[354] in the brain of Aβ-deposition AD mouse models. Further, human TREM2 reporter cells are stimulated with various phospholipids and non-phosphate anionic and zwitterionic lipids including sulfatides.[126, 128]

The lipids are closely associated not only with APP processing and Aβ pathology but also with the innate-immune system in AD and thus, investigation of the plaque-associated lipid biochemistry would leverage the understanding of the molecular mechanisms leading to the complex amyloid-associated disease progression and this would provide insights into the disease pathogenesis.

2 AIMS

2.1 General Aim

Lipids are abundant structural components of the brain and lipid-mediating signaling regulates various processes of brain function. They have been increasingly implicated in neurodegenerative disorders including AD. From lipid granular inclusions in multiple cell types and the core of the extracellular plaques reported in Dr. Alzheimer's original reports today's genetic, immune, biochemical and molecular research, there is a body of evidence linking lipids to several stages of AD pathogenesis including APP processing and amyloid-associated pathology. Therefore, there is an apparent need for developing novel chemical imaging methods in order to dissect the role of lipid biochemistry in amyloid pathology in AD which shall provide a framework for approaching the research into the disease pathogenesis from lipid-centered perspective and adding another important piece into the complex molecular puzzle of amyloid plaques.

The overall aim of the work in this thesis was to develop novel chemical imaging methods based on MALDI mass spectrometry imaging and implicate them for probing spatial molecular pathology of amyloid plaques in transgenic AD mouse brains in order to leverage the understanding of amyloid-associated lipid biochemistry across the brain regions and provide a basis for further investigation of cell signaling and metabolic pathways that are disrupted in AD.

2.2 Specific Aims

The specific aims and motivations are explained for each communication, referred to in the text by their Roman numerals.

Paper I: Development of "gentle" (or "static") MALDI mass spectrometry imaging and implications for probing amyloid-plaque pathology

The majority of the commercial MALDI-MSI instruments employ nanosecond pulse duration lasers. Along with the mechanical damage, nanosecond lasers can induce thermal damage on the tissue surfaces imaged with MALDI which can induce damage in the tissue structure and epitopes and this can impair the correlation of the MSI data with the following immunofluorescence imaging of the same tissue section. Therefore, the

purpose of this study was to investigate a "gentle" MALDI-MSI approach for lipid imaging to minimize/diminish the laser-induced damage on the tissue surfaces for enabling a successful subsequent immunofluorescence imaging while preserving the spectral and MS imaging quality. Further, the final aim was utilizing the newly-developed MALDI-MSI method for correlating plaque-associated lipid alterations with fluorescence amyloid plaque imaging in transgenic AD mouse brain.

Paper II: Development of dual polarity MALDI-MSI on the same pixel points and "trimodal" MALDI mass spectrometry imaging (IMS3) and implications for probing amyloid plaque pathology

Despite the high abundance of lipids and the efficient ionization behavior of a number of them during MALDI process, the structural diversity of lipids and the complexity of the laser desorption/ionization process limit comprehensive lipid profiling within a single IMS analysis. The first aim of this study was to develop a dual polarity MALDI-MSI method to detect/image lipids ionized in both negative and positive polarities from the same raster spots/pixel points which should provide a "static" MALDI-MSI approach and enhance the lipid molecular information correlated with the very same histo/pathological features over the brain tissue sections.

Secondly, the level of laser powers used for lipid MALDI-MSI is significantly lower than the level used for peptide/protein MALDI-MSI analysis. After performing dual polarity MALDI-MSI on a brain tissue section, there still shouldn't be significant mechanical or thermal damage of the tissue surface which could prevent/impair a subsequent peptide/protein MALDI-IMS analysis of the same imaging region. Therefore, the final purpose of this study was to develop a "trimodal" MALDI-MSI (IMS3) method which involves dual polarity MALDI-MS lipid imaging on the same pixel points (using the principles of "static" MALDI) followed by peptide/protein MALDI-MS imaging of the same imaging area over brain tissue surfaces.

Finally, the ultimate aim of this communication was to utilize this novel trimodal MALDI-MSI method for probing amyloid plaque-associated lipids and peptides to gain enhanced molecular information from a single amyloid plaque in a specific brain region over the brain tissue sections of transgenic AD mouse models.

Paper III: An extensive implication of "trimodal" MALDI mass spectrometry imaging for probing molecular pathology of amyloid plaques

An amyloid plaque consists of a plethora of cellular, molecular, structural and immune components which reflects final scenery of the complex APP and amyloid-associated pathology in APP transgenic AD mouse brain. The purpose of this communication was to utilize IMS3 for probing molecular pathology of individual amyloid plaques to gain deeper understanding of both plaque-associated pathological events and molecular mechanisms involved in amyloid pathology leading to amyloid plaque formation.

Paper IV: Investigation of the brain region-specific (2 and 3D) alterations of lipid composition in amyloid plaques in 5xFAD mouse brain

5xFAD is one of the most widely used transgenic AD mouse models. 5xFAD expresses human APP and PSEN1 transgenes with a total of five AD-linked mutations. While several histopathological and/or molecular investigations have been performed on 5xFAD mouse brain, including studies of plaque pathology in conjunction with lipid metabolism-related immune proteins, the lipid molecular information in amyloid plaques still remain largely unknown. Therefore, the aims of this communication were both to investigate brain region-specific alterations of lipid composition in amyloid plaques and to correlate the lipid molecular information obtained using MALDI-IMS with the wealth of other published molecular, structural and immunopathological findings associated with amyloid plaques in 5xFAD mouse brain.

Paper V: Investigation of the molecular, immune and structural signatures of focal amyloid plaque-associated myelin lipid architecture loss in a spatial region-specific manner in 5xFAD mouse brain

There is emerging evidence that Aβ aggregation and plaque formation can lead to impairment of the lipid-rich myelin sheath and glial cells called oligodendrocytes. In this communication, the aim was to shed light on the brain region-specific lipid molecular, structural and APOE-associated aspects of plaque-associated myelin degeneration in 5xFAD mouse brain using a combination of MALDI-MSI and fluorescence/immunofluorescence staining.

3 METHODS

3.1 Overview of Mass Spectrometry

The fundamental experiments of mass spectrometry were originally designed for measuring elemental masses and isotope abundances which was initiated by Joseph John (J.J.) Thomson's experiment in which he calculated the charge-to-mass ratio of positive rays along an axis *x* deflected by parallel electric and magnetic field on axis *y* which makes them strike on a photographic plate on a specific parabolic arc, so one could capture m/z information.[355] This was followed by a design of a mass spectrograph by Francis Aston which could focus the rays as line forms hitting the plate at a specific point on a focal plane which increased the intensity, accuracy and resolution and allowed determination of the existence of ^{20}Ne and ^{22}Ne proving for the first time that stable elements can be isotopic.[356] Important efforts were later made by Francis Aston and Arthur Dempster on the determination of the isotopic abundance and mass of the elements including uranium whose splitting released a large amount of energy which was shown by others. In the ensuing years, Alfred Nier, many call him the "father of modern mass spectrometry" isolated ^{235}U and ^{238}U and this led the discovery of ^{235}U which is responsible for slow neutron fission. The "Manhattan Project" during World War II was started in order to isolate ^{235}U for the production of nuclear weapons. In part stimulated during the Manhattan Project, the development of several ionization techniques and instrumentation galvanized the use of mass spectrometry which has become an indispensable technology not only for chemical research but also for various fields of biomolecular and elemental research including proteomics, metabolomics, lipidomics, metallomics and it is an important tool for systems biology, cellular biology, immunopathology and structural biology.

The earliest ionization technique was 'electron impact' (EI) which was initially described by Walker Bleakney; he focused the electrons generated from a tungsten filament into a narrow beam for positive ray analysis.[357] The EI technique has been used to determine ionization energies of several elements such as mercury and it has been utilized to generate highly ionized species via electron ionization, such as Cs^{7+}. EI mass spectrometer, later described by Alfred Nier, has been used for the measurement of relative isotopic abundances of many elements such as carbon, nitrogen and oxygen.[358]

Nevertheless, the EI technique, while it became a widely-used technique for many years, was not gentle enough for the analysis of intact organic molecules due to the fragmentation of the molecular ion and this stimulated the developments of 'softer' ionization techniques. In the mid-1950s, ionization of intact organic molecules (e.g. acetone) was reported from the tungsten tip of a field emission microscope via high electrical field which is termed field ionization (FI).[359] The use of multiple dense arrays of needle-like tips on a tungsten wire increased the sensitivity of the FI method, called field desorption (FD), which allowed ionization of thermally labile organic molecules including monosaccharides, glycosides, nucleotides and small peptides.[360] Another attempt towards soft ionization was chemical ionization (CI) which involves mixing of analyte molecules and methane gas that is subjected to collide with the electrons and the resulting methane ions (exclusively ionized) mediates the ionization of the analyte molecules.[361]

Introduction of an ion source producing a beam of positive ions by Richard Herzog and Franz Viehböck was another milestone for MS; the beam of positive ions can be used to bombard the surface of a solid which facilitates ionization and ejection of atoms as 'secondary ions'.[362] In the ensuing years, this ionization technique, also named 'sputtering' was used for secondary ion mass spectrometry (SIMS) analysis of neutrals and charged species in dual polarity from metal surfaces e.g. silver.

While development of ionization techniques from EI to FI, FDI, and CI allowed detection of small organic molecules, the diversity and wide mass range of biomolecules inspired development of a number of new ionization techniques for sensitive ionization of labile, nonvolatile large molecules, notably large proteins. In the 1970s, the high-energy particles from radioactive ^{252}Cf nuclear decay were used to bombard surfaces for plasma desorption mass spectrometry (PDMS) by Ronald Macfarlane and David Torgerson. This allowed detection of large organic molecules including tetrodetoxin (a neurotoxin), oligonucleotides and small proteins.[363] In the same context, Alfred Benninghoven introduced low primary ion dose density (static) SIMS for the sensitive detection and identification of nonvolatile thermally unstable molecules.[364, 365] This was taken a step further by Michael Barber in 1981 with the introduction of a new ionization technique similar to SIMS, termed fast atom bombardment (FAB), which involved the use of a beam of high-energy argon atoms focused onto the surface of the sample which was embedded in electrically insulating low-volatility matrix molecule such as glycerol or 3-nitro benzyl alcohol (3-NBA). FAB mass spectrometry provided high-quality spectra of small proteins and oligosaccharides.[366, 367]

Another source for the ionization of organic compounds and elements, which was concurrently developing with FAB, SIMS and PD after 1960s, was laser irradiation. The use of lasers for generating ions started soon after the invention of the first lasers and was utilized for MS analysis in the ensuing years.[368-371] However, the sensitivity of laser-based MS instruments as well as FAB and PD instruments was still low for high-throughput biological applications, while FABMS and PDMS were capable of detecting high-mass proteins up to ~20 kDa.[372] Therefore, several attempts were concurrently made to enhance the sensitivity of laser desorption/ionization including the use of organic and inorganic matrices to assist the laser desorption/ionization of large non-volatile, labile molecules.[373] The introduction of a chemical matrix for laser desorption/ionization by Franz Hillenkamp and Michael Karas led the discovery of a new ionization technique which is termed matrix-assisted laser desorption/ionization (MALDI) and it significantly enhanced the sensitivity of the MS detection of large, nonvolatile and labile biomolecules.[374] Further, Koichi Tanaka used a similar approach; he prepared the sample mixed with cobalt nanoparticles in glycerol (similar to FABMS preparation) which facilitated laser/desorption ionization MS analysis of large molecules up to m/z 100 000[375] (Please see later chapter on MALDI mass spectrometry for a detailed review). In addition to this, electrospray ionization (ESI) introduced by John Bennett Fenn,[376] another sensitive soft-ionization technique for large, labile molecules, was concurrently developed with MALDI. The discovery of ESI for large molecules was based on Lord Rayleigh's fundamental work on the equilibrium of liquid conducting masses charged with electricity in 1882 which reported that evaporating solvent gradually increases the charge density on the surface of a "charged liquid droplet" until the columbic repulsive forces overcome surface tension, causing the droplet to dissociate and leave a stream of ions.[377] One crucial part of Fenn's analysis on large molecules was the observation of multiply charged ions along with the singly charged ions of the analytes with intensities depending on the composition and concentration of the solutions. This increased the mass range of the mass analyzers by a factor equal to the number of charges on a multiply charged analyte ion which stimulated the use of ESI for MS analysis of macromolecules (notably large proteins).[378] Therefore, ESI and MALDI (together with other laser desorption/ionization techniques) have become the two most-widely used ionization techniques for the molecular analysis due to their soft ionization and versatility.

While initial experiments of MS development were based on elemental and isotopic analysis, the low sensitivity of early ionization techniques hindered both molecular analysis and sensitive and high-throughput elemental analysis. The inductively coupled plasma (ICP), invented by Thomas Reed in

1961,[379] is an ionization technique which facilitates highly-sensitive (down to part-per-trillion (ppt) range depending on the species) MS detection of all metals and even some metalloids and non-metals.[380] ICP mass spectrometry employs an inductively coupled argon plasma torch which atomizes and ionizes a sample, which is usually introduced as an aerosol or via laser ablation. The generated singly charged ions in ICP are then transferred to a mass spectrometer through an orifice and analyzed. Modern ICP-MS systems allow rapid, simultaneous screening of multiple elements at trace levels in variety of samples. ICP-MS can be used to simultaneously measure multiple antigens on single cells and tissue sections using attached lanthanide tags to antibodies against cell-surface antigens which significantly impacts the research in cellular biology and immunopathology.[381]

Along with the development of several ionization techniques, concurrent instrumental developments such as mass analyzers, mass filters along with the development of tandem mass spectrometry and separation techniques coupled to MS have significantly impacted on the development of chemical and biological mass spectrometry.

During the fundamental mass spectrometry discoveries, the sector mass spectrometers using static electric or magnetic sector (or a combination of the two) had low range of mass-to-charge ratio (m/z) that could be analyzed at any given time. This hindered the analysis of short-lived and/or unstable analytes. To circumvent these limitations, a new design of mass spectrometer was introduced by W.E. Stephens in 1946 which uses microsecond pulses of ions accelerated by an electrical field so that ions with different m/z reach the detector at different times allowing their 'time of flight' (TOF) separation and detection and give a spectrum that can be acquired in just hundreds of microseconds. However, in the early experiments, the result of initial energy and spatial distributions resulted in poor mass resolution due to the dispersions in the measured times of the ions at the same m/z. Therefore, to compensate for the initial ion spatial and energy distributions for improved mass resolution, an ion source with two accelerating regions (for pulsed (delayed) ion extraction) was developed by W.C. Wiley and I.H. McLaren in 1955[382] and electrostatic reflector by B.A. Mamyrin in 1973.[383] TOF, pulsed ion extraction and reflector will be revisited in the context of the UltrafleXtreme MALDI-TOF/TOF MS instrument in a later chapter.

Another dimension of the development of mass spectrometry instrumentation is trapping mass analyzers which utilize a combination of electric or magnetic fields to capture or “trap” ions and currently they provide the highest accuracy and resolution in MS analysis. In the 1940s, John Hipple combined

magnetic sector mass spectrometers with the principles of the cyclotron[384] which is a particle accelerator invented by Ernest Lawrence in 1932; an ion cyclotron uses a constant magnetic field in which charged particles follow an outward spiral, accelerated by a rapidly varying radiofrequency (RF) field. Hipple utilized this ion cyclotron resonance (ICR) mass spectrometer for trapping and detecting hydrogen ions where RF field frequency was tuned to resonance with the cyclotron frequency ensuring target ions at charge-to-mass ratio would be accelerated and pushed along the exact spiral trajectory to hit the detector.[385] In 1974, Melvin Comisarow and Alan Marshall utilized the principle that ions in a magnetic field rotate around that field at their cyclotron frequency. Instead of detecting the charged particles directly (turning off the RF), the resulting image current generated by the charges as they pass close to the detector plates can be recorded and converted to mass spectrum using Fourier transform which forms the basis of FT-ICR mass spectrometry.[386] Mass accuracy and resolution of FT-ICR mass spectrometry improved with the use of superconducting magnets, generating magnetic field up to 21 Tesla, which makes ICR-based MS the highest-performance mass spectrometers significantly impacting biological research such as spatial neurolipidomics[387] and proteomics.[388]

Another approach to trap charged particles is the electrostatic field trap, without a need for magnetic fields, which was introduced by Kenneth Kingdon in 1923. A "Kingdon trap" consists of a cylinder with a central wire along the *x* axis with end cap electrodes on both ends where a static voltage can be applied resulting in a radial logarithmic potential in which the charged particles can be trapped and orbit until they loses their transverse velocity and hits the wire.[389] In 2000, Alexander Makarov designed a new ion trap mass analyzer called the Orbitrap, based on the concept of the Kingdon trap. The Orbitrap replaces the wire and cylinder in Kingdon trap with a spindle-shaped electrode and barrel-like electrode, respectively which traps ions in an orbital (spiral trajectory) motion around the spindle, trapping them in an electrostatic harmonic potential where the resulting harmonic oscillations can be used to identify the charge-to-mass ratio of the ions.[390]

Another ion trap mass analyzer is the quadrupole ion trap developed by Wolfgang Paul.[391, 392] The quadrupole consists of four parallel metal rods that have both direct-current and oscillating RF voltages applied in a constant ratio between the opposing pairs in which the trajectories of the ions depends on their mass-to-charge ratios which would determine the transmission of the ions through the quadrupole and reach to a detector. One major advancement of the quadrupole ion trap introduced by Jim Morrison was the use of triple-stage quadrupole mass spectrometer to isolate a specific ion in the first filter,

which can be fragmented using light in the second and detected in the third which was an innovative approach for the structural determination of a specific ion. This approach was later significantly improved and used widely in the analysis of complex molecules and proteins with the introduction of collision-induced dissociation (CID) into the first and second quadrupole of the triple-stage quadrupole mass spectrometer by Richard Yost et al. in which the collisions of the analyte molecules with the neutral gas molecules (e.g. argon) at high pressures in electrical field generate fragmentation of the ions.[393]

Nevertheless, the initial findings on MS/MS and CID date back to 1960s. T.W. Shannon and Fred McLafferty demonstrated that the 'metastable ion' can decompose between the source and the detector and can give specific fragments of the parent ion.[394] However, the decomposition of a parent ion to give metastable ions is dependent on its internal energy and often gives metastable fragment ions of labile groups and thus this is generally not enough to obtain the complete structural information of the parent ion. Later, Keith Jennings introduced neutral gas into the mass spectrometer which collides with the stable molecular ions and provides specific fragment ions of the parent ion.[395] These developments initiated tandem mass spectrometry and later followed with several sensitive fragmentation techniques such as electron capture dissociation (ECD) developed by Roman Zubarev and Neil Kelleher which involves the direct introduction of low-energy electrons to trapped gas-phase ions for structural elucidation of peptides and proteins in tandem mass spectrometry.[396]

While mass spectrometry rapidly developed, the deconvolution of spectra comprising multiple analytes as well as distinct physicochemical properties of analyte molecules was hindering high-throughput simultaneous molecular MS analysis. Therefore, various separation methods were coupled to MS instruments. A very early example of this is coupling of gas chromatograph to a TOF mass analyzer by Roland Gohlke and Fred McLafferty in 1955 which provided separation and fast MS analysis of a mixture of organic species.[397] However, GC separation was not suitable for non-volatile and thermally unstable molecules. Therefore, the introduction of direct liquid injection and charged droplet evaporation techniques in late 1960s and 1970s[398-400] significantly stimulated the developments of the liquid chromatography (LC) MS (particularly with the successful trials with ESI) which has been an indispensable tool for the MS detection and identification of trace analytes in various samples considering the flexibility, sensitivity along with the speed and precision of modern LC-MS instruments .[401] Charge droplet evaporation involves forcing liquid through a heated capillary in

which the analytes chemically ionized through at high pressures which provides a nebulization producing gas-phase ions.[399]

Ion-mobility separation (IMS) is another gas phase separation technique similar to GC which involves separation of ionized molecules in the gas phase based on their mobility in a carrier buffer gas. Initially, IMS was utilized to monitor gas-phase reactions but a real landmark was the development of an IMS-based mass spectrometer by David Clemmer and colleagues in 1998. They demonstrated that IMS could separate different conformations of intact proteins that have identical m/z values and this approach since then has become an indispensable tool for structural biology of large proteins.[402]

3.2 Emerging Lipidomics in Neuroscience

Lipids play crucial roles in the physiology of cells, organs and organisms evidenced by a number of genetic, immune, molecular studies as well as studies implicating aberrant lipid metabolism in the pathogenesis of many diseases including cancer,[403] diabetes,[404] infectious diseases[405] and neurodegenerative diseases.[406] The burst in functional analysis in genes has stimulated the analysis of molecules directly related to genes including DNA, RNA and proteins. However, genomics, transcriptomics and proteomics do not investigate the entire metabolism and one should consider all the molecules affecting not only metabolism but also signaling and gene regulation including lipids which are not genetically encoded but are generated and metabolized by enzymatic activities that are regulated peculiar to the given biological system and its influencing environment.[407, 408]

From a neuroscience point of view, myelin is abundant in the human brain accounting for ~ 30% of its dry weight and myelin is enriched in lipids which accounts for 70%–85% of its dry weight.[409, 410] Further, advances in the fields of cell biology, synaptic physiology and receptor pharmacology have demonstrated that lipids contribute to the structure and dynamics of biological membranes, convey messages in all cellular levels (including the nucleus), contribute to energy homeostasis and play crucial roles in various regulatory and signaling events including gene regulation. This gives rise to the interest in the field of neurolipidomics; an emerging field of systems-level analysis of lipids and non-lipid mediators (e.g. lipoproteins) which interact within the metabolome as well as physicochemical studies on lipid function such as lipid-protein interactions in the lipid rafts in cell membranes.[411]

The relatively small size and large chemical diversity of the lipid molecules along with the dynamic nature of their structure in the cell hinders the analysis of many of them with the well-established techniques such as optical microcopy in combination with specific antibodies and/or fluorescent tags. Further, NMR spectroscopy,[412] native mass spectrometry[413] and/or ion mobility mass spectrometry[414] have been successfully used for the study of lipid-protein interactions. Here I will focus on the high-throughput analysis of the complex lipid mixtures with a spotlight on mass spectrometry-based developments for neurolipidomics.

The nervous system comprises the largest diversity of lipid classes and lipid molecular species with a broad mass range in comparison to other organs and/or systems in mammals and it contains a large portion of complex sphingolipids, particularly glycosphingolipids, and many of them are specific to the nervous system.[411] Nevertheless, according to collaborative project entitled "lipid metabolites and pathways strategy" (LIPID MAPS, http://www.lipidmaps.org/) led by Edward Dennis and colleagues,[415] lipids are classified as small amphipathic molecules containing both hydrophobic and hydrophilic groups, derived from carbanion-based condensations of alpha-ketoacyl subunits and/or carbocation-based condensations of isoprene subunits and are subtitled as fatty acyls, glycerolipids, glycerophospholipids, saccharolipids, sphingolipids polyketides, sterol lipids, and prenol lipids and they comprise staggering structural diversity. Mass spectrometry has been the optimal tool of choice for the analysis of lipids, particularly in the nervous system, due to its capability of simultaneous detection of many lipids by their m/z with high sensitivity and resolution which can sort out the complexity of lipid structures and allow their comprehensive interrogation.[416-418]

In the early research on the MS analysis of lipids, fragmentation of lipid molecules during ionization via fast-atom-bombardment and chemical ionization was a drawback for the assignment of labile groups in the lipid molecular structure including head groups, fatty acids and backbones, particularly when analyzing complex lipid mixtures. MS analysis of lipids was further limited due to the requirement of thermal stability and volatility in gas-phase measurements and many lipids that occur in nature are nonvolatile. Therefore, "softer" ionization techniques including ESI,[416] MALDI,[419] and cluster ion beam SIMS[420, 421] (notably via gas cluster ion beam (GCIB) sputtering, see below)[422] as well as tandem mass spectrometry (notably since the development of CID) have been used for the MS analysis of complex lipid mixtures which circumvents these limitations. However, ESI has been, by far, the most widely-used ionization technique for the lipidomic analysis of crude extracts from cells and tissues owing to its

extraordinary sensitivity for lipid molecules (comprising a variety of structural diversity) and with minimal in-source fragmentation. Thus ESI has become a workhorse for systems biology for the comprehensive interrogation of lipid metabolism of a given organelle, cell type, organ and biological system. Further, ESI is efficiently coupled with LC, microfluidic techniques, and patch clamp systems for sensitive and quantitative lipidomics analysis. Notably, LC separation overcomes ion suppression effects due to the matrix effects and competitive ionization of the analyte species observed when direct analysis of complex lipid mixtures is performed with either of these ionization techniques.[423, 424] Coupling ESI with patch clamp, microfluidic techniques and other cell-content removal and extraction techniques facilitate sensitive and high-throughput lipidomics analysis of single cells and even subcellular compartments.[425, 426] Nevertheless, cluster ion beam SIMS and MALDI are better suited for mass spectrometry imaging of lipids over cell and tissue surfaces due to the easy focusing of the ion and laser beam (see below in the next chapter).

The initial MS analysis of complex lipid mixtures using soft ionization techniques e.g. ESI were reported in the 1990s and since then it has been rapidly developing.[427, 428] Large structural diversity of lipids in cells and tissue hinders their comprehensive MS analysis in a single experiment although significant improvements have been reported, notably using multidimensional mass spectrometry-based shotgun lipidomics.[429] ESI analysis of lipids can be performed via three different approaches including multi-dimensional MS-based shotgun lipidomics after intrasource separation, the HPLC coupled ESI/MS method, and the tandem mass spectrometry-based shotgun lipidomics.[430] The "shotgun lipidomics" approaches can be used via direct infusion of the lipid extract from a biological sample which can provide global analyses of the individual lipid molecular species without pre-chromatographic separation, whereas HPLC-ESI-MS approach can provide high-sensitivity detection and quantitation for even least abundant lipid molecular species.[430] Multidimensional mass spectrometry-based shotgun lipidomics utilizes multiplexed extractions (e.g. under acidic, basic, and/or neutral conditions) for a good recovery of most of the lipid classes followed by intrasource separation and selective ionization to resolve and ionize lipid classes in crude lipid extract based on their intrinsic electrical properties depending on the nature of the polar head groups and this provide a comprehensive lipidomics analysis of a given biological sample.[429] These shotgun lipidomics approaches have proven to be immensely valuable for the investigation of lipid alterations of neurodegenerative diseases, notably Alzheimer's disease, using the extracts from brain tissue and cells [88, 281, 299, 336] However, these approaches, unless specific extraction of a subcellular feature

or micro-dissection of localized features on tissues are performed, lack the spatial information of a lipid within heterogeneous environment of tissue or cell and this can convolute significant but highly-localized lipid alterations within the bulk analysis of cells and tissues. Fluorescent protein-tagged specific probes (e.g. for phosphoinositides), fluorescent-tagging of lipids (e.g. via rhodamine labels) are used to study trafficking and partitioning into specialized subcellular compartments and membrane in living cells.[407, 431] However, these techniques are not applicable for many lipid species, very few lipid antibodies exist with questionable specificity and the fluorescent-tagging might interfere with in-vivo function whereas the capability of imaging lipids in living cells is a clear advantage of these techniques.

Mass spectrometry imaging (MSI) has emerged as a powerful analytical method for spatial lipidomics in neuroscience, owing to its ability for high-throughput, simultaneous and semi-quantitative spatial analysis of many ionized lipid species (a spatial shotgun lipidomics) within their native environment from tissue sections[432] to the subcellular level.[433]

3.3 Mass Spectrometry Imaging

The first use of mass spectrometry for imaging (mass spectrometry imaging; MSI) was first introduced by Raymond Castaing and Georges Slodzian in 1962, using the principles of SIMS. They utilized high energy 'primary ions' such as Cs^+, Ar^+, Ga^+ and In^+ to bombard the surface of a metal-alloy to eject 'secondary ions' of elements and isotopes from defined points which allows generation of the ion images of those elements and isotopes present at a particular position on the sample surface.[434] This was followed by Pierre Galle's experiments on biological applications of SIMS imaging in 1970; he investigated spatial distributions of sodium and potassium on renal tissue sections and red blood cells.[435] These applications demonstrated the power of MSI, which combines chemical information content of MS detection with chemical imaging technology, and today MSI has become a rapidly developing analytical method concurrently with the development of ionization techniques, instrumental developments and advances in methodologies in the MS field.[436-445]

From the MSI perspective, there is a minute quantity of various analytes with distinct ionization characters in a pixel point across the surface of the analyte. This has led the complementary use of several desorption/ionization methods for high-throughput and/or selective mass spectrometry imaging of analytes; elements, small molecules to large proteins at high-spatial resolutions to

understand the functioning/dysfunctioning of subcellular compartments, cells, histological and histopathological features, organs and organisms.

MALDI and ESI are more recognized with their capability of detecting large molecules. However, these two soft ionization techniques are versatile and they have been utilized for the MS analysis of a variety of molecules including small metabolites, lipids, peptides, nucleotides, saccharides, proteins and many more in a wide spectral mass range. The use of MALDI for mass spectrometry imaging was introduced by Bernhard Spengler and Richard Caprioli in the 1990s while the first uses of LDI-MS detection of salts and elements with focused laser beam from the surfaces date back to early 1960s[369, 371] (Please see a detailed review of LDI, MALDI and imaging mass spectrometry in the next chapter). Nevertheless, the search for application of ESI for the detection of molecules from the surfaces led to development of a new method, an ambient ionization technique, called desorption electrospray ionization (DESI) by Zoltan Takáts and colleagues which is performed by directing electrosprayed charged droplets and ions of solvent onto the analytes surface (conductive or insulator) whose impact produces gaseous ions of the molecules present on the surface.[446] One of the advantage of using DESI is that the spraying solution can be changed to selectively ionize particular compounds with distinct ionization characters without the chemical labeling or prior chemical treatment of the surface.[446] This allows detection and imaging of a variety of molecules including small metabolites, drugs, lipids, peptides and proteins in a large mass range from the biological tissue sections.[447-449] However, to extend the mass range of DESI for large molecules such as proteins (>45 kDa), liquid sample DESI was introduced which involved DESI analysis of protein samples from liquid surfaces and increases mass range of protein detection up to 150 kDa and allows detection of large protein complexes (>45 kDa), preserving the weak non-covalent interactions likely due to the protective hydrate shell in the liquid phase extraction/ionization.[450] Another novel surface profiling technique, which is similar to liquid-DESI, is liquid extraction surface analysis (LESA) which is carried out by micro-liquid extraction from a solid surface followed by MS analysis.[451] This technique has been utilized for the detection of large (~800 kDa) non-covalent protein complexes[452] and demonstrated for the spatial detection of non-covalent hemoglobin complex directly from thin tissue sections of mouse liver and this is significant because it suggests a pathway for native mass spectrometry imaging.[453] Recently, a novel workflow; microLESA was introduced which combines non-destructive autofluorescence microcopy to spatially recognize micro-scale (~110 μm diameter) histopathological features and spatially targeted

liquid droplet micro-digestion for in-situ digestion followed by LESA-MS spatial proteomics analysis.[454]

The lower spatial resolutions achieved with DESI, liquid-DESI or LESA mass spectrometry imaging experiments compared to imaging with MALDI and SIMS is a drawback. This due to the challenge of reducing the sampling area in accordance with the optimization of experimental parameters in DESI, liquid DESI and LESA experiments.[455] Another derivative of the DESI method is nano-DESI which is carried out by desorption of the solvent from the sample surface into a solvent bridge formed between two capillaries followed by high-resolution MS analysis which improves the sensitivity and signal stability.[456] Improved stepping size between line scans (≤ 10μm) has been achieved for nanoDESI mass spectrometry imaging using a combination of shear force microscopy with nanoDESI to precisely control the distance between the sample and nanoDESI probe which provides better focusing at shorter stepping sizes.[457]

Another ambient ionization technique called laser ablation electrospray ionization (LAESI) was introduced by Peter Nemes and Akos Vertes in 2007. LAESI combines infrared laser ablation producing a plume intercepted with electrospray at right angle and provides postionization in the atmospheric pressure.[458] LAESI facilitates ionization and MS detection and/or imaging of samples from small metabolites, lipids[459] to large proteins (up to 66 kDa) from diverse surfaces (e.g. biological fluids, tissue sections with water content).[458]

Although SIMS was one of the first ionization techniques for the MS detection of intact organic compounds that were not amenable to electron impact ionization, the first SIMS instruments were operated in the "dynamic" mode with high primary ion currents causing huge surface damage on the sample surface. While "static" SIMS, using low primary ion doses, provides efficient ionization of the molecules from the top surface of the analytes, the bombardment process with high ion doses (> ~1% of the number of surface molecules, the so called static limit) causes damage to the surface resulting a carbon residue accumulation from molecular fragmentation of the surface which suppresses the ionization.[364] However, SIMS was still an attractive ionization technique for surface analysis and mass spectrometry imaging due to its surface sensitivity and sub-micrometer imaging capability (with easy focusing of ion beams in the vacuum) with limited sample preparation.

The use of cluster ion beams (e.g. SF_6) composed of molecular clusters rather than single atomic particles was introduced in late 1980s[460, 461] and has

become another landmark (after static SIMS) for TOF-SIMS analysis. Cluster ion beam sources decrease the accumulated damage over the surfaces via distribution of overall kinetic energy in between the components of the clusters leading to deposition of the energy closer to the surface and providing better desorption/ionization with less depth of damage, and exhibiting a simpler MS spectra and extended mass range.[420, 461] Au_3^+, Bi_3^+ and C_{60}^+ ion beams have been widely used for cluster ion beam SIMS imaging of tissue sections to single cells due to their convenient use, easy focusing and relatively high lifespan. These ion beams provided enhancement in the ion signals and detection/imaging of high-mass ion yields (for small molecules) with less fragmentation compared to single atomic ion beam such as Ga^+,[462-466] but C_{60}^+ exhibits less subsurface damage accumulation on the analyte compared to Au_3^+, likely due to the lower kinetic energy of carbon atom than gold atom and, hence, this renders C_{60}^+ a useful tool for not only for 2D molecular imaging but also for nanoscale 3D molecular depth profiling and 3D imaging of even single cells.[467-469]

Another landmark for SIMS imaging analysis was the introduction of gas cluster ion beams (GCIBs, e.g. Ar_{4000}^+ or $(CO_2)_{6000}^+$)[470-473] which are generated by supersonic expansion and consist of thousands of atoms or molecules and they are accelerated to >10 keV to provide focusing and sufficient kinetic energy for molecular desorption/ionization. The key aspect of GCIBs is that the kinetic energy is divided in between the components of the GCIB which reduces the energy of each particle to a level which is comparable to chemical bond strengths and thus molecular fragmentation and subsurface damage is reduced. This increases the signal intensity and enhances the mass range in SIMS analysis. GCIB-TOF-SIMS, particularly with cluster beam incorporating CO_2 due to the enhanced beam cohesion and hence focusability, has been applied for molecular imaging. These include imaging of small metabolites and high-molecular weight species such as cardiolipins from tissue sections to single cells at high-spatial resolutions but are limited, so far, to around 1-3 μm.[474-476] In between the attempts for increased ion yields and minimized molecular fragmentation, the introduction of the water cluster ion source producing water cluster ion beams is notable as it increases the SIMS ion yields compared to argon cluster ion beams.[477] Recently, high-energy water cluster ion beams (water cluster beams with cluster beams composed of pure argon, argon and 10% CO_2, and pure CO_2) have been demonstrated to increase the GCIB-TOF-SIMS molecular ion yields in dual polarity and enhanced focusability, which allowed imaging of high-molecular-weight lipid molecules from rat brain tissue sections and single HeLa cells at 1 μm spatial resolution.[478]

While a majority of SIMS instruments employ TOF analyzers due to the need for high-speed data collection for high-spatial resolution imaging experiments, there have been attempts to couple SIMS with high-mass resolving analyzers.[479] A combination of C_{60} primary ion source with FTICR mass spectrometer providing a mass resolving power in excess of 100 000 ($m/\Delta m_{50\%}$) has been demonstrated and used to image cholesterol in rat brain tissue section at 40 μm pixel size.[480] However, in these experiments, the signal-to-noise ratio was low for even the abundant cholesterol molecule and the imaging was slow as FTICR was used and only 15s/pixel was achieved for even large pixel sizes. This is a drawback for 2D and 3D SIMS imaging analysis at high-spatial resolutions. Therefore, this led a landmark development in SIMS instrumentation, which is called 3D OrbiSIMS.[481] 3D OrbiSIMS uses a hybrid mass analyzer design to combine the strengths of high-speed TOF imaging with the high mass-resolving power, high mass accuracy and MS/MS capability of the Q Exactive HF Orbitrap (Thermo Fisher Scientific, Germany).[482] 3D OrbiSIMS utilizes polyatomic and gas cluster ion beams and provides high spatial resolution SIMS imaging (~200 nm for inorganic species and ~2 μm for biomolecules) with the high mass-resolving power of an Orbitrap (>240,000 at m/z 200). It has been utilized to image neurotransmitters from mouse hippocampus and 3D imaging and single-cell metabolic profiling of rat alveolar cells incubated with amiodarone drug.[481]

Another remarkable instrumental development was the introduction of J105-3D Imaging TOF-SIMS instrument to circumvent the drawback that long pulses required for high-spatial spatial resolution SIMS imaging results in poor mass resolution.[483] J105 utilizes a continuous primary ion beam combined with a bunched secondary ion stream which allows the generation of high-spatial resolution ion images, independent of sample height, with consistent mass accuracy (1-5 ppm) and mass resolution ($m/\Delta m$ ~10 000). Briefly, the continuous stream of primary ions produces a continuous stream of secondary ions, which are extracted into a RF-only quadrupole filled with inert gas (e.g. N_2) for collisional cooling of the ions and focusing them. This is followed by energy filtering of the ions by an electrostatic analyzer providing secondary ions with a 1 eV energy spread for injection into a linear buncher. The buncher provides a time focus at the entrance of the TOF analyzer by suddenly applying an accelerating field that varies from 7 kV at the entrance of the buncher to 1 kV at the exit and this makes the mass resolution dependent on the quality of this focus and independent of the sputtering process and sample surface topography. The large, 6 keV energy spread between the ions, and thus such that the path of the ions are analyzed using a harmonic field TOF reflectron which is filled with reflectron plates

and doesn't have field free region providing separation of the secondary ions depending on their mass and charge, not the energy. [483]

Static SIMS has been widely used for molecular SIMS and imaging starting in late 1990s. However, concurrent with the developments in static SIMS, Georges Slodzian and coworkers introduced a new ion beam configuration which is described with a highly focused primary ion beam with minimal distances to the sample surface, and orthogonally impacts it and acts coaxially with the secondary ion beam extraction (but it requires opposite polarity for primary and secondary ions). This is particularly useful for high-lateral resolution "dynamic" SIMS measurements in which relatively large amounts of material are removed, as primary ion doses exceed the so called "static limit", and so do not capture molecular information (which is limited) but sensitive and accurate elemental information.[484, 485] This orthogonal primary ion beam configuration has been coupled to a magnetic sector mass spectrometer for SIMS analysis and commercialized by CAMECA as the NanoSIMS. The NanoSIMS typically employs reactive primary ion beams, where Cs^+ is used for negative ion analysis and O^- (or rarely O_2^-) for positive secondary ion analysis and the secondary ion collection and detection via a double-focusing design, incorporating both an electrostatic sector and a magnetic sector which provides both high transmission and high mass resolution conditions. Therefore, along with the extensive use of NanoSIMS imaging in geological sciences, there are several studies for the elucidation of spatial metal accumulation in biological samples or to visualize stable isotope incorporation, indicative of metabolic uptake into organisms and tissues, at the subcellular level at spatial resolutions down to few tens of nanometer.[485-489] Recently, NanoSIMS has been demonstrated for subcellular MSI and absolute quantitative analysis across organelles and this allows subcellular quantification of drugs and metabolites in single cells and suggests a significant potential for pharmaceutical development.[490]

Most MSI methods, unless a specific enhancement and/or labeling strategies are applied (e.g. chemical derivatization, isotopic labeling), are non-targeted and label-free, allowing mainly the detection of abundant compounds if they are ionized efficiently depending on the applied ionization technique and methodology. However, a biological sample, either a tissue section or even single cell or organelle, is composed of a myriad of biochemical compounds with enigmatic regional roles, but due to low-abundance and/or poor ionization behavior of most of them such as certain immune proteins (e.g. microglial cell surface receptors) are not detected/imaged with MSI. Therefore, targeted MSI methods such as imaging mass cytometry and multiplex ion beam imaging have been developed for simultaneous and

selective imaging of low-abundance species (notably proteins). Imaging mass cytometry involves tissue sections and cells immobilized on slides are stained/labeled with antibodies or other probes carrying a high mass tag (commonly rare earth elements) which is scanned with a pulsed laser ablation and transferred by a stream of inert gas into ICP ion source. The ions from each measured spot are then detected by TOF mass spectrometry.[491, 492] Imaging mass cytometry has been widely used for the interrogation of spatial immunopathological investigations such as human breast cancer samples to investigate tumor heterogeneity via simultaneous detection of >30 proteins at subcellular resolution.[493] Multiplex ion beam imaging (MIBI) is another technique which combines the sensitive selectivity of antibodies (with similar preparation to imaging mass cytometry) with mass spectrometry imaging using the principles of dynamic SIMS. Here, the sample surface is sputtered with a primary ion beam continuously that, in turn, produces a continuous stream of secondary ions which are then separated by a magnetic sector, where each mass of interest is projected onto a separate ion detector.[494] However, the use of a magnetic sector in parallel to the number of ion detectors limits the number of masses that can be detected using dynamic SIMS. To circumvent this, MIBI-TOF instrument has been recently introduced. The MIBI-TOF is an orthogonal time-of-flight mass spectrometer that uses the principles of static SIMS to image, so far, up 36 metal-tagged antibodies at subcellular resolution (<300 nm) in clinical tissue sections.[495] Recently, TOF-SIMS based multiplex ion beam imaging of proteins within the tissue sections has also been demonstrated using metal oxide nanoparticle (MONP)-conjugated antibodies with <300 nm spatial resolution.[496]

In summary, MSI is an emerging powerful analytical methodology for spatial interrogation of elements and biomolecules from tissue sections to subcellular level using complementary use of several ionization techniques in combination with other modalities and smart method developments. MSI allows detection of analytes in 2D and 3D within single cells and tissue sections and even develops towards to imaging of molecules with their tertiary (e.g. using ion mobility and/or specific chemical derivatization) and quaternary (e.g. noncovalent complexes) molecular structural information.

3.4 MALDI Mass Spectrometry Imaging

MALDI mass spectrometry imaging is a rapidly developing "molecular histology" technique and recently it has been also developing for single cell MSI analysis. In this section, I will focus on the desorption/ionization process in MALDI and introduce the development of MALDI mass spectrometry and imaging of tissues and cells. Further, I will particularly review MALDI mass spectrometry imaging of lipids in detail. Finally, I will introduce the UltrafleXtreme MALDI-TOF/TOF instrument used for the MS and MSI experiments in this thesis.

3.4.1 The Desorption/Ionization Process in MALDI

Matrix-assisted laser desorption/ionization (MALDI) has become one of the most widely used and rapidly-growing, indispensable analytical ionization technique in mass spectrometric analysis of a variety of synthetic and natural organic molecules.[373] Indeed, MALDI has been developed in a highly empirical manner and fundamental mechanisms of MALDI ionization still remain incomplete; [373, 497, 498] thus, a better understanding of the ionization mechanisms would be beneficial for the development and design of efficient MALDI-MS and MALDI-MSI methods and shall enhance interpretation of resulting mass spectrometric data.

The desorption/ionization from laser-absorbing surfaces e.g. porous silicon,[499] nanowires[500] or ultrafine metal powders (such as cobalt nanoparticles)[375] are primarily dependent on the physical properties of the substrates which mainly comprise thermal mechanisms at high temperatures reached upon short-pulse laser irradiation of the surface with poor thermal conductivity. However, MALDI achieved using UV-absorbing organic matrix molecules[374] encompasses more complex ionization mechanisms of matrix and analyte molecules which comprise a widely-agreed two-step mechanism including the primary ionization mechanisms, which are often matrix-derived species, mainly explained with cluster ionization and the photoexcitation/pooling during and shortly after the laser pulse interaction with the matrix-coated sample surface (or matrix/analyte incorporated crystal) and secondary reactions (particularly involves analyte ionization) in the expanding laser desorption/ablation plume which involves complex charge generation and electron and charge transfer processes.[497]

A simplified schematic of MALDI process and ion generation is depicted in Figure 4. Here, I will describe the MALDI process in a detailed look. The primary ionization mechanisms require dense concentrated energy and

therefore occur upon the interaction of the laser pulse and shortly after it which enables generation of processes for the creation of separated ion pairs. The cluster model refers to various sizes of clusters which carry analyte ions, separated in sample preparation solution and retained in the solid matrix, which can undergo neutralization in the desorption plume by electrons or matrix anions in the case of positive analyte ions but this is an incomplete stochastic process which generates detectable ions, the "lucky survivors".[501] One reason for the stochastic nature of this process is the possibility of the internal migration of the charge via proton, cation or electron transfer like secondary ionization mechanisms within the clusters.[502] Further, the photoexcitation/pooling model involves combined excitation energy in the matrix followed by concentration of this energy in "pooling" which refers to the redistribution of the electronic excitation energies of two nearby molecules.

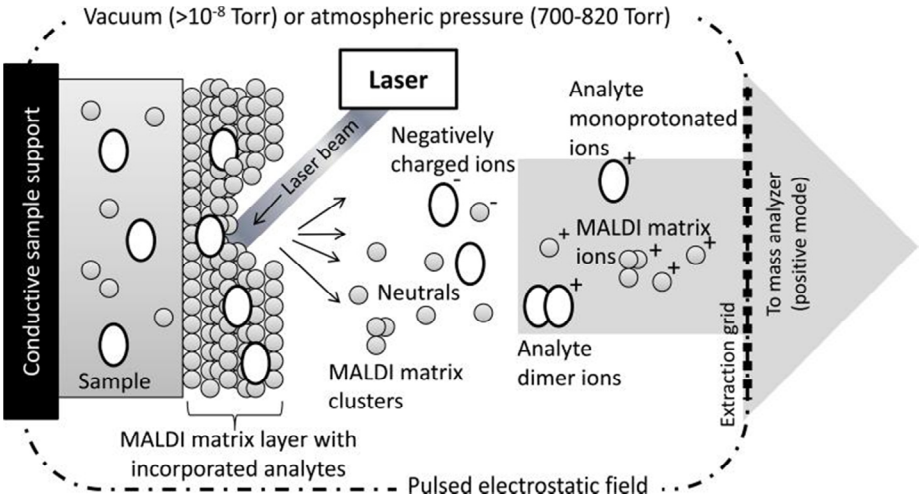

Figure 4. Schematic of laser desorption/ionization process and ion generation (in positive ion mode) in MALDI. Reprinted by permission from Springer, mass spectrometry imaging, a mass spectrometry primer for mass spectrometry imaging, Rubakhin, S. S., and Sweedler, J. V., pp 21-49, (2010). [503]

Direct ionization of several free-state matrix molecules (e.g. 2,5-DHB) and matrix-analyte complexes are not generally favored with two- or multi-photons from commonly used N_2 and Nd:YAG lasers[504] which supports the onset of pooling events during MALDI for the ionization of the matrix[505] together with the finding that fluorescence quenching occurs at laser fluences around the desorption threshold.[506] It is important to note that, the photoexcitation/pooling model involves excitation and ionization mediated

by pooling events that are second order and depend on the local temperatures and pressures in the expanding "molecular beam" plume which are determined by the rate of energy conversion from the excited electronic states of the species (including ions) to heat and the resulting pressure gradient.

Secondary mechanisms are favored during the reduced density of energy in the MALDI plume which occurs when the energy is converted to heat and the plume is physically expanded to relax the physical and chemical processes. A typical MALDI plume contains excess amount of neutral matrix molecules and therefore the ion and neutral matrix biomolecular collisions are likely to occur often. In the expanding plume several cascades of secondary reactions occur including electron transfer, proton transfer (via de/protonation) and cation transfer. Charge transfer reactions in the laser-desorption plume involve extensive matrix-analyte and analyte-analyte reactions and understanding the dynamics of these reactions would help to interpret the MS spectrum. Depending on the physicochemical properties of the matrix molecule including ionization potential, electron and proton affinities, and the acidity of the matrix and matrix ions, various type of matrix ions can be observed in the MS spectrum (particularly when analyte concentration is low) such as $m^{\cdot+}$, $m^{\cdot-}$, mH^+, mNa^+, mH^- along with the non-thermal decay products; m-H_2O and m-CO_2 and rarely but possible $(m\text{-}nH)^+$ and $(m+2H)^+$ species. The concentration ratios of matrix and analyte ions have significant effect on the plume reactions which is reflected in the MS spectra as e.g. matrix suppression[507] and analyte suppression.[508] As it is implied in the term, all the matrix ion species in the spectrum can be completely suppressed when the physicochemical properties of the matrix and analyte molecules are matched such as the suppression of the protonated primary ions of a matrix by a strongly basic analyte which suggests strong evidence of the onset of the secondary reactions in the plume. In this case, neutral matrix molecule-mediated interconversion of matrix-derived ions such as $m^{\cdot+}$, mH^+, mNa^+ is possible and this was demonstrated before.[508] Analyte suppression implies more complicated secondary reactions which can significantly affect the relative intensities of multiple analytes detected in MS spectra. Analyte suppression involves varying sensitivity factors of the multiple analytes which can undergo reactions with the matrix ions and with each other and it is possible to observe suppressed ionization of one type of analyte by the others and this phenomenon depends on several parameters including exothermic nature of the expanding plume reactions, the kinetics of various charge transfer reactions along with the relative abundance of the analytes with each other and the matrix.[508]

Matrix-analyte secondary reactions can explain the ionization of several analytes. Proton transfer can partially explain the protonation of peptides/proteins which are one of the most important analytes in MALDI analysis. One common observation (while not the only factor) is that basic residues such as arginine (with high gas-phase proton affinity) in the protein structure can favor its protonation whereas less basic residues such glycine (with low gas-phase proton affinity) in the structure of protein might not favor its protonation.[509, 510] In line with this, oligonucleotides, which generally have weak basicity, are mainly measured as deprotonated ions.[511]

Some molecules with low proton affinities or acidities which may have no polar groups in their structure might be better desorbed/ionized with cationization. This includes the detection of these molecules, notably certain polymers or sterols, as alkali (e.g. Na^+, K^+) adducts or as transition metal (e.g. Cu^+, Ag^+) complexes such as via d-π complexation with their aromatic side chains.[512, 513]

Along with the cationized and de/protonated ion species, radical cations and anions are also observed in MALDI via electron transfer. Matrix radical anion and cation species are commonly observed while analyte radical ions observed from the low polarity molecules. Radical cations of analytes have been observed with a secondary reaction involving electron transfer from neutral analytes to molecular radical matrix cations.[514]

A brief introduction into the ionization mechanisms in MALDI was given above. A number of experimental parameters interrelated with each other for the MALDI process can be taken into account to interpret the observed MALDI mass spectrum including; the choice of the matrix which is dependent on its physicochemical properties, the chemical and physical properties of the analyte molecule, matrix/analyte ratio and their concentrations and sample preparation method, the characteristics of the lasers such as wavelength, pulse duration, geometry (axial, orthogonal, transmission), beam profile (temporal pulse shape), the desorption environment such as ambient pressure, substrate temperature and ion extraction method (e.g. delay extraction).[497, 515] Therefore, a body of research has been carried out for the optimum ionization, detection and identification of several synthetic and organic molecules with MALDI-MS considering the ionization mechanisms and instrumental parameters along with the dedicated instrumental (e.g. detectors, mass analyzers) and/or methodological (e.g. laser post ionization) developments.

3.4.2 MALDI Mass Spectrometry and Imaging

Since it was introduced in the 1990s as a new molecular ion imaging tool,[516, 517] MALDI has been rapidly developing as a versatile ionization technique for the MS detection and imaging of a variety of biomolecules including metabolites,[518, 519] lipids,[443, 520] peptides[521-523] and proteins[439, 524] within the tissue sections and single cells with potentially subcellular resolution.[425, 436, 438] Given the empirical nature and complexity of the MALDI process, a body of research has been performed to improve the detection limit, sensitivity, selectivity, and spectral range of biomolecules for high-spatial resolution MALDI-MSI using new matrix molecules with compatible sample preparation strategies along with the instrumental and methodological developments.

Matching of the laser-wavelength with the optical absorption and physicochemical properties of the matrix molecules are important parameters for an efficient MALDI-MS analysis of nonvolatile compounds.[525] In this regard, design and synthesis of new matrix molecules and/or studies on the wavelength dependence of UV-MALDI-MS analysis have been performed.[526-529] Results indicate that design of the new matrix molecules with low proton affinity value potentially provide better ionization of peptides via proton transfer when the excitation wavelength is matched with the absorption maxima (particularly at the red side) of the new matrix molecule.[526] For instance, 4-chloro-α-cyanocinnamic acid (Cl-CCA), a derivative of commonly used commercial 4-hydroxy-α-cyanocinnamic acid (HCCA) matrix molecule, has been successfully designed and synthesized to enhance the MALDI-MS detection limit and spectral coverage of peptides.[529] However, unpredictable physicochemical features of new matrices can also have effects on the efficiency of MALDI-MS analysis. Along with its low proton affinity compared to the proton affinity of its commercial derivate HCCA matrix, Cl-CCA matrix provided more compact matrix crystals which suggest better incorporation with the peptide molecules and this can contribute to the MALDI efficiency.[529] Further, α-cyano-2,4-difluorocinnamic acid (DiFCCA), another matrix molecule with low proton affinity, has been designed and synthesized to improve the detection limit of peptides. DiFCCA has been utilized to improve detection limit of several peptides, when the laser wavelength was matched with the red side of its absorption maxima. However, addition of more fluorine in the benzene ring structure of HCCA matrix, such as the synthesis and use of α-cyano-2,3,4,5,6-pentafluorocinnamic acid (PentaFCCA) did not improve the MALDI-MS detection limit of the same peptides in spite of its lower proton affinity than HCCA's and DiFCCA's. This was due to the increased

hydrophobicity of the multiply fluorinated matrix molecule which hinders matrix-analyte incorporation. Further, increased fragmentation of matrix and analyte molecules has been observed due to the drastic shift in the absorption maxima of PentaFCCA to the blue side of the UV spectrum.[526]

New matrix molecules have also been developed considering the physicochemical properties of peptide molecules. 2-Hydroxy-5-octyloxybenzoic acid (o-alkylated DHB) is a hydrophobic, alkylated-derivative of commonly used commercial 2,5-dihydroxybenzoic acid (2,5-DHB) matrix molecule and it was synthesized as a matrix additive to increase the incorporation of the hydrophobic peptides with matrix crystals which improves the MALDI-MS sensitivity of several hydrophobic peptides.[530] In line with this, 1-(2,4,6-Trihydroxyphenyl)octan-1-one (ATHAP) molecule has been synthesized which is a hydrophobic, alkylated-derivative of the commonly used commercial 2,4,6-trihydroxyacetophenone (THAP) matrix molecule. ATHAP worked as a selective matrix molecule for sensitive detection of hydrophobic peptides in MALDI-MS analysis.[531]

For the MALDI-MS detection of large proteins, 2,5-dimethoxy-4-hydroxycinnamic acid (sinapinic acid) (and some other cinnamic acid derivatives; ferulic and caffeic acids) and 2,5-dihydroxyacetophenone (2,5-DHAP) are the prevalent matrix molecules. This is because of their high optical absorptivity at the commonly used UV wavelengths (e.g. 355 nm and 335 nm) along with their salt tolerance and low photochemically-generated matrix adduct peaks of the proteins quasimolecular ion signals in MALDI-MS analysis.[532, 533] Sinapinic acid and 2,5-DHAP have also been utilized for high-spatial resolution (at 5-10 μm using commercial instruments) MALDI-MSI of proteins on tissue sections.[388, 534] 2,5-DHAP has been particularly found to be sensitive for protein MALDI-MSI analysis and provided MALDI-MSI of proteins at cellular and subcellular scales[535, 536] but the vacuum stability of this molecule is not enough for long-acquisition times for high-spatial resolution analysis of large imaging areas with vacuum-based MALDI instruments. To tackle this, a vacuum stable derivative of 2,5-DHAP which is a ketone-based matrix named (E)-4-(2,5-dihydroxyphenyl)but-3-en-2-one (2,5-cDHA) has been designed and synthesized. 2,5cDHA provides small matrix crystal size (1-2μm) and this allows high spatial-resolution MALDI MS imaging of proteins in large areas in cerebellum region of mouse brain tissue sections.[537]

Other strategies including chemical derivatization have been applied for the N-terminal derivatization of peptides/proteins followed by MALDI-MS/MSI analysis to increase /enhance either the detection limit and/or their de novo

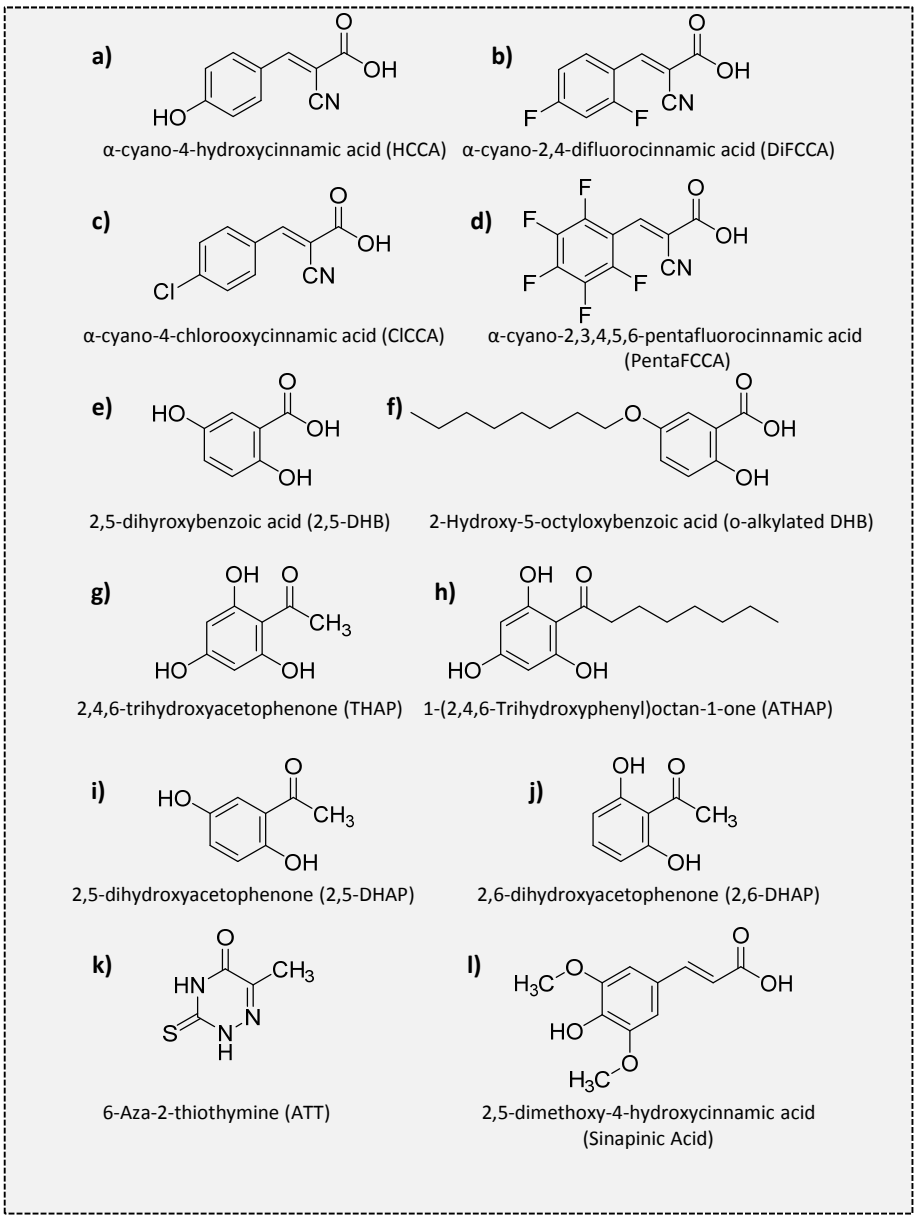

Figure 5. Molecular structures of the commonly used MALDI matrix molecules and some of their halogen- substituted or alkylated derivatives as new generation matrix molecules.

sequencing and fragmentation/identification. Coumarin based tags have been utilized to increase the peptide MALDI-MS sensitivity and this was dependent on the incorporation of the commercial matrix molecule (e.g. 2,5-

DHB and 2,5-DHAP) and the derivatized structure of the peptides.[538] Further, the coumarin tag, Alexa Fluor 350 that contains an anionic sulfo group has been found to increase LC-MALDI-TOF/TOF-MS peptide/protein detection and identification via inducing specific fragmentation which yields high-intensity signals of those fragments in MALDI process.[539] In addition, sulfonation agents, such as 4-sulphophenyl isothiocyanate (4-SPITC) and 3-sulfobenzoic acid (3-SBASE) have been used to N-terminally derivatize tryptic peptides directly on tissue sections which adds a negative charge at the N-terminus of a tryptic digest peptide and this generates a complete y fragment series of peptides/proteins directly from the tissue sections which allows MALDI-MSI with enhanced identification of peptides and proteins on their spatial locations over the brain tissue sections.[540] Notably, certain matrix molecules such as 1,5-diaminonapthalene (1,5-DAN) and 5-aminosalicylic acid (5-ASA) perform as reductive matrices for MALDI in source decay (ISD) fragmentation of peptide/protein molecules which provides specific fragmentation ions for molecular identification.[541, 542] As reductive matrices, these molecules have high hydrogen donating (the hydrogen radical transfer from matrix to analyte) ability which can reduce the S-S bonds in the peptide and protein molecules and facilitate specific de novo sequencing of molecules.[542] MALDI ISD using 1,5-DAN has been applied for direct de novo sequencing and imaging of protein fragments on the tissue sections.[543] This methodology has been successfully demonstrated with a selective approach, using MALDI-FT-ICR-MSI, where protein standards were spotted next to the tissue sections and the radically induced ISD fragments via 1,5-DAN were compared with the ISD fragments obtained from tissue sections which provided high-confidence identification and imaging of proteins.[544] Therefore, along with the ionization of intact peptide/protein molecules mainly via proton transfer from the matrix-derived ions, ISD fragmentation is also possible depending on the radical hydrogen donating ability of the matrix molecules.

Along with the development of matrix molecules, instrumental developments have also impacted on MALDI-MS/MSI of proteins such as use of active pixel detector for MALDI-MS detection of high-mass proteins up 400 kDa[545] and use of high-mass resolving mass analyzers coupled to MALDI such as FT-ICR.[388, 546] MALDI-TOF MS provides high-sensitivity, but it lacks the resolving power and mass accuracy for protein imaging with high confidence which is particularly skewed for tissue imaging due to the ion suppression effects and possible surface charging of the insulating tissue matrix. Modern instrumentation with improved ion optics and availability of higher magnetic fields improved the sensitivity of FT-ICR instruments at higher mass ranges. A 15T Bruker MALDI FT-ICR mass spectrometer has been utilized to image

large proteins (at m/z 12 kDa) from tissue sections with high mass resolving power (~75,000 at m/z 5000) and mass accuracy (<5ppm) using 2,5-DHA matrix molecule with high-acid containing washing protocol and matrix solution.[388, 547]

The exact nature of the "soft" ionization feature of MALDI is not well understood in all its aspects, notably for the detection of noncovalent complexes (NCXs) and no really coherent understanding has been settled so far. An isomer of 2,5-DHAP, 2,6-dihydroxyacetophenone (2,6-DHAP), and 6-Aza-2-thiothymine (ATT) are among the matrix molecules which have been reported to be useful for the detection of NCXs such as the non-covalent molecular aggregates of streptavidin protein.[548] Analysis of NCXs required optimal sample preparation conditions such as high-pH buffer solvents and this has been found to secure the quaternary structures of non-covalent peptide/protein complexes in the MALDI plume.[549, 550] Along with the matrix selection and solvent preparation conditions (notably the pH of the solvent), laser pulse energy has also been found to be important for MALDI-MS detection of NCXs. A hot MALDI plume induced by high-energy laser pulses can denature the quaternary structure of the NCXs and result in increased monomer and gas cluster ion signals in MALDI-MS analysis.[551] In line with this, a more recent study has revealed that protein-peptide NCXs are detected more efficiently at a wavelength matching with low optical absorptivity of the ATT matrix molecule and this suggests that a cooler MALDI plume is more efficient to detect the NCXs.[527]

One of the disadvantages of conventional low-proton-affinity acidic matrices such as 2,5- DHB, sinapinic acid, and HCCA is that they are typically unsuitable for MALDI-MSI analysis of relatively low-molecular-weight (LMW) analytes such as lipids, drugs and metabolites due to many matrix-related interfering peaks in the low m/z range (<800 m/z) and their relatively low performance in negative ion mode and their unsuitability for neutral analytes.

MALDI has some specific advantages compared to other soft ionization techniques such as its high tolerance to salts, buffers and contaminants, uncomplicated spectra with almost exclusive generation of singly charged ions, high sensitivity, and high throughput analysis which has stimulated the reassessment of the role of MALDI-MS for the analysis of LMW and neutral compounds. Thus, in order to overcome the problem of matrix interference, several attempts and developments have been reported such as derivatization of the analytes or matrix, addition of dopants, enhanced matrix deposition techniques, matrix-analyte incorporation techniques, use of rationally

designed organic matrices, ionic liquids, inorganic matrices, and nanostructured surfaces as well as instrumental developments of MALDI-MS/MSI instruments.

9-Aminoacridine (9AA) (Figure 6a) has been introduced as an efficient matrix molecule for negative ion mode due to the gas phase basicity of this matrix producing deprotonated analyte molecules needed for MALDI-MS.[552] A number of LMW compounds including phenols, carboxylic acids, sulfonates, and alcohols along with oligosaccharides, phospholipids and sphingolipids have been sensitively detected using 9AA as the MALDI matrix.[553, 554] Further, norharmane (9H-β-carboline) which contains strongly basic nitrogen in a heterocycle in its molecular structure, similar to 9AA, has also been found to be an efficient matrix for lipids and oligosaccharides.[555, 556] Several other organic matrices have been described for the detection and imaging of LMW compounds including N-(1-naphthyl) ethylenediamine dihydrochloride,[557] 1,6-diphenyl-1,3,5-hexatriene (DPH)[558], 1,5-diaminonapthalene (1,5-DAN),[559, 560] N-phenyl-2-naphthylamine (PNA),[561]3,4-Dimethoxycinnamic acid (DMCA)[562] along with the binary, hybrid (organic-inorganic), and nanomaterial-based matrices such as hexagonal boron nitride nanosheets,[563] graphene,[564] TiO_2 nanoparticles,[565] and a binary matrix of 3-hydroxycoumarin (3-HC) and 6-aza-2-thiothymine (ATT)[566] to name but a few.

Matrix deposition strategies for enhancing the analyte matrix incorporation have been developed such as electrowetting-assisted drying of matrix/analyte solutions which leads to substantially smaller and more homogeneous sample spots on special electrowetting-functionalized e-MALDI target plates.[567] This significantly increases the ion yields of LMW pharmaceutical molecules. The heterogeneity of the drying spots, which is accelerated by Marangoni flows as a result of changing substrate temperatures to create temperature gradients across droplets, can be circumvented by drying droplets on a 5 °C substrate while keeping the surroundings at ambient conditions. This typically reduces the spot heterogeneity and allows better quantification in MALDI-MS analysis.[568] Further, superhydrophobic surfaces[569] and binary matrix mixture with hygroscopic glycerol[570] have also been used to confine the dried droplets and increase the sensitivity and reproducibility of MALDI-MS analysis of a variety of analytes.

DPH (Figure 6b), a commonly used fluorescence probe for studying cell membrane-lipids due to its affinity toward the acyl chains in the phospholipid bilayers, has been utilized to detect and image LMW fatty acids in brain tissue sections with minimal matrix interference in the MALDI-MS spectra.

DPH has also low volatility in the vacuum which makes it suitable for high-spatial resolution MALDI-MSI [558] Further, along with the reductive properties of 1,5-DAN (also mentioned above), it has more recently been demonstrated that 1,5-DAN can work as an electron transfer (ET) matrix molecule. Thus, it has been utilized for the sensitive detection of chlorophylls where ET deposits a limited energy excess responsible for the virtually fragmentation free detection of the odd molecular ion.[571]

Another approach for the detection of LMW compounds as well as neutral molecules was the discovery of the use of very strong bases ("proton sponges") as MALDI matrices such as 1,8-bis(dimethylamino)naphthalene (DMAN),[572] 1,8-di(piperidinyl)naphthalene (DPN),[573] 3-(4,5-bis(dimethylamino)napthalen-1-yl)furan-2,5-dione (4-maleicanhydridoproton sponge ("MAPS"),[574] and bis(trispyrrolidinophosphazenyl) naphthalene (TPPN).[575] The discovery of proton sponges was initiated with general framework of a rational protocol for matrix selection based on Brønsted-Lowry acid-base theory where the proton sponge matrix is supposed to be capable of deprotonating an acidic analyte in the liquid-phase in the matrix solution and in the gas phase after laser irradiation.[576] In this regard, DMAN (Figure 6c) was particularly capable deprotonating and facilitating the detection of a number of LMW acidic metabolites (e.g., carboxylic acids, fatty acids, amino acids, vitamins) as well as lipid species, but its low vacuum stability was not suitable for MSI experiments.[577, 578] Further, rationally-designed stronger base proton sponge matrix molecules including DPN, MAPS and TPPN have been synthesized. Notably, vacuum stabilities of these new matrices were higher than DMAN's. Thus, MAPS has been utilized to detect and image metabolites of a human diffuse glioma tissue section.[574] Further, TPPN (Figure 6d) has been found to be efficient to deprotonate and facilitate the detection of neutral saccharides and sterols (e.g. cholesterol, with a detection limit of 3 pmol/spot) with MALDI-MS.[575, 576]

Recently, IR 780 (Figure 6f) has been introduced as a novel MALDI matrix which has a larger collision cross sections (CCS) (along with the above mentioned suitable optical properties and salt tolerance) facilitating the carriage of relatively high-molecular-weight analytes such as large lipid molecules including gangliosides, cardiolipins and phosphoinositides into the gas phase. IR 780 increases the chance of collisions between this larger size matrix and the analytes in the MALDI plume, which eventually improves the ionization efficiency of the high-molecular-weight analytes.[579]

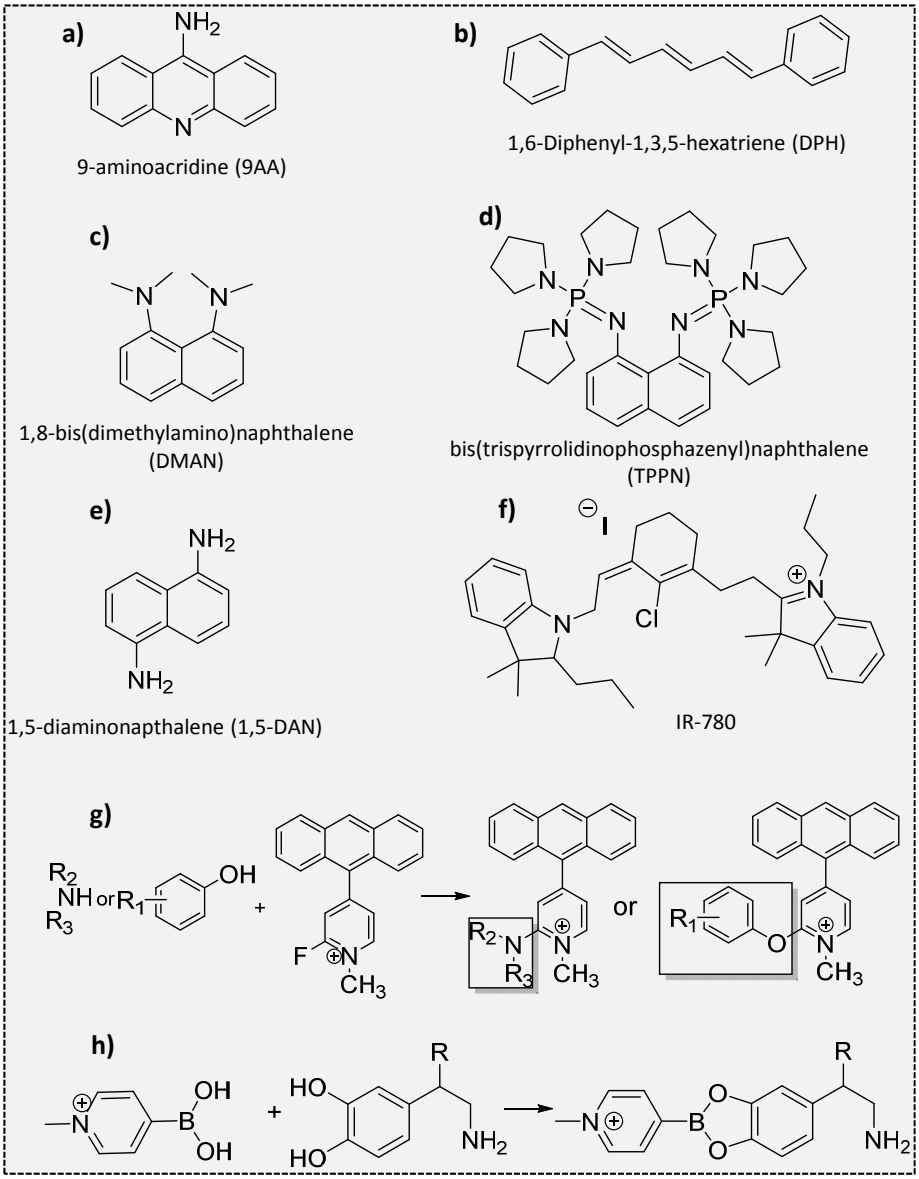

Figure 6. Molecular structures of several matrix molecules with different physicochemical properties used in the detection of low-molecular-weight compounds and/or various lipid species along with some neutral compounds. Reaction schemes of the reactive matrices were provided for g) 4-(anthracen-9-yl)-2-fluoro-1-alkylpyridin-1-ium (FMP-10) with phenolic hydroxyl and primary and secondary amines groups in the structures of neurotransmitters and their metabolites and for h) 4-(N-Methyl)pyridinium boronic acid with catechol (1,2-benzene diol) in the structures of catecholamines.

Another approach for the detection of LMW and neutral compounds is using "reactive matrices" for selective derivatization of the target molecules to increase their ionization yield with permanent charges and/or to change their structure for better ionization/detection in MALDI-MS analysis.

Carboxymethyl) trimethylammonium chloride hydrazide (a.k.a. Girard's reagent T), 2,4-dinitrophenylhydrazine (DNPH), DMNTH (4-dimethylamino-6-(4-methoxy-1-naphthyl)-1,3,5-triazine-2-hydrazine) have been used to selectively derivatize and detect/image carbonyl containing compounds such as corticosteroids.[580-582] Further, the aromatic compounds, 2,4-dihydroxybenzaldehyde and 2,5-dihydroxyacetophenone have been utilized as reactive matrices for the sensitive detection of polyamines.[583] A screen of pyrylium salts revealed that the 2,4-diphenyl-pyranylium ion efficiently derivatizes primary amines and it can be used as a reactive matrix for the detection and imaging of biogenic amines and amino acid chemical messengers in rodent brain tissue sections.[584, 585] Catecholamine neurotransmitters can also be detected and imaged with boronic acid compounds via boronic acid-diol reactions due to the high-association constant of the resulting boronate esters from boronic acid-catechol (1,2-benzene diol) reactions.[586, 587] For instance, 4-(N-Methyl)pyridinium boronic acid worked as a reactive matrix for the detection and imaging of catecholamines (Figure 6h) with LDI and SIMS ionization techniques on porcine adrenal gland tissue sections. Here, the boron atom reflects a unique isotopic pattern (^{10}B and ^{11}B natural abundances of 19.9 and 80.1%, respectively) for derivatized catecholamines in the MS analysis.[587] Several reactive matrices have been developed to target a specific group of neurotransmitter molecule, but these derivatization strategies only target specific molecules and thus a comprehensive mapping of neurotransmitters and their metabolites are hindered. For this reason, methylated 4-(anthracen-9-yl)-2-fluoro-1-alkylpyridin-1-ium (FMP-10) cation has been recently developed as a novel reactive matrix. FMP10 selectively targets phenolic and primary amine groups simultaneously and reacts with them via a nucleophilic aromatic substitution reaction of the phenolic hydroxyl and primary and secondary amine groups (Figure 6g) which facilitates the MALDI MS imaging of the catecholaminergic and serotonergic signaling systems including precursors and metabolites in brain tissue sections.[588]

Along with the rational approaches considering the physicochemical properties of the matrices and targeted analytes and chemical derivatization, instrumental, technical and methodological developments have been also introduced for the enhanced detection of LMW and neutral compounds. High-performance instruments with advanced mass analyzer such as Fourier

transform ion cyclotron resonance (FTICR) and Orbitrap are capable of distinguishing target small metabolite compounds of interest with high mass accuracy from the large chemical background in the low-m/z region of a MALDI spectrum (typically less than m/z 1000) which contains a large population of ions from endogenous tissue compounds as well as matrix-related adduct clusters and fragments.[387, 518, 589, 590] Further, a wavelength-tunable postionization laser-based ionization strategy (MALDI-2) has been introduced to initiate secondary MALDI-like ionization processes in the gas phase likely involving the ionization of the molecules via resonant two-photon ionization-derived matrix (m) ions; $m^{+\bullet}$ ions and free e^- by laser post ionization along with the proton transfer to or from neutral analyte molecules in subsequent collisions. This new ionization strategy has been demonstrated to increase the ion yields for numerous lipid classes and liposoluble vitamins, and saccharides. Importantly, MALDI-2 allows MALDI MS imaging of neutral molecules in the gas phase such as cholesterol and vitamins in mouse cerebellum.[591] MALDI-2 has been shown to be useful in pharmaceutical research for the detection and imaging of LMW drugs[592] and it has also significantly impacted on spatial lipidomics research in cells and tissues when it is combined with advanced mass analyzers and ion extraction geometries.[433, 536, 593]

3.4.3 MALDI Mass Spectrometry Imaging of Lipids

Owing to its versatile capability to mediate desorption/ionization of several important lipid classes, MALDI is one of the most prevalent ionization techniques used for lipid MSI of biological tissue sections and it has been rapidly developing for single cell MSI. Various lipids are highly abundant in biological tissues and single cells because they constitute the external and internal defining membranes of each cell. Many lipids such as phospholipids, anionic/cationic glycosphingolipids (e.g. sulfatides and sphingomyelin) are already ionized as they have either phosphate-sulfate anions or nitrogen-centered cations in their molecular structure and this generates abundant positive or negative ions during the MALDI process. Further, the general mass range of various lipids including a number of fatty acids, phospholipids, sphingolipids, sterols and glycerolipids is below 1000 Da which is optimal for the most sensitive operation of modern mass spectrometers with high mass-resolving analyzers, advanced ion extraction strategies, MS/MS structural identification capabilities which can be coupled to MALDI process.

Nevertheless, biological lipids comprise various groups of naturally occurring molecules which includes fatty acids, waxes, eicosanoids, glycerolipids, glycerophospholipids, lysolipids, sphingolipids, sterols, fat-

soluble vitamins (such as vitamins A, D, E and K) and others which have a diversity of molecular structures in a wide molecular mass range. In addition, the concentration and composition of lipid molecules in each biological tissue type and individual cells vary significantly.[407] Therefore, sensitive, selective and high-throughput MALDI-MSI analysis of lipids require a careful design of experiments with consideration of a complex meshwork between ambient/substrate conditions, instrumental features and parameters along with the physicochemical properties of matrix and targeted analyte molecules which dictate a unique desorption/ionization dynamics for each individual laser-shot MALDI process. Therefore, lipid molecular imaging with MALDI-MSI has been rapidly developing in parallel not only with the development of advanced mass spectrometers ("technology") but also with the methodological developments ("chemistry").

Glycerophospholipids (GPs), also referred to as phospholipids (an imprecise term as other lipids can have phosphate in their structure), are a major class of lipids present in all cells and they are quite ubiquitous in living organisms. The molecular structure of glycerophospholipids has three parts: a three-carbon backbone of glycerol, two long-chain fatty acids esterified to hydroxyl groups on two carbons of the glycerol, phosphoric acid esterified to the central carbon hydroxyl group of glycerol and polar head groups; mainly ethanolamine, choline, serine, or inositol (Figure 7a). Plasmalogens are GPs which have an ether bond in position sn-1 to an alkenyl group in their molecular structure (Figure 7b). Glycerolysophospholipids are GPs which have only a single fatty acid moiety (usually in the sn-1 position) in their structures (Figure7c). Further, molecular structure of diphosphatidylglycerol (also known as "cardiolipins") consists of two phosphatidic acid moieties connected with a glycerol backbone in the center to form a dimeric structure (Figure 7d).

GPs are key components of the lipid bilayers of cells and they are primary components of cellular membranes; they can act as binding sites for intra- and extracellular proteins and as an anchor for the membrane proteins. They are involved in the metabolism and signaling in eukaryotic cells. GPs such as phosphatidic acid or membrane-derived second messengers (e.g. diacylglycerol (DAG) and inositol triphosphate) are important signaling molecules.[594] Owing to their high abundance and polar head groups, several phospholipids including phosphatidylcholines (PCs), phosphatidic acids (PAs), phosphatidylethanolamines (PEs), phosphatidylinositols (PIs) and phosphatidylglycerols (PGs), lysophospholipids, and plasmalogens have been spatially mapped over the tissue sections and single cells using MALDI-MSI.[432, 433, 520, 595]

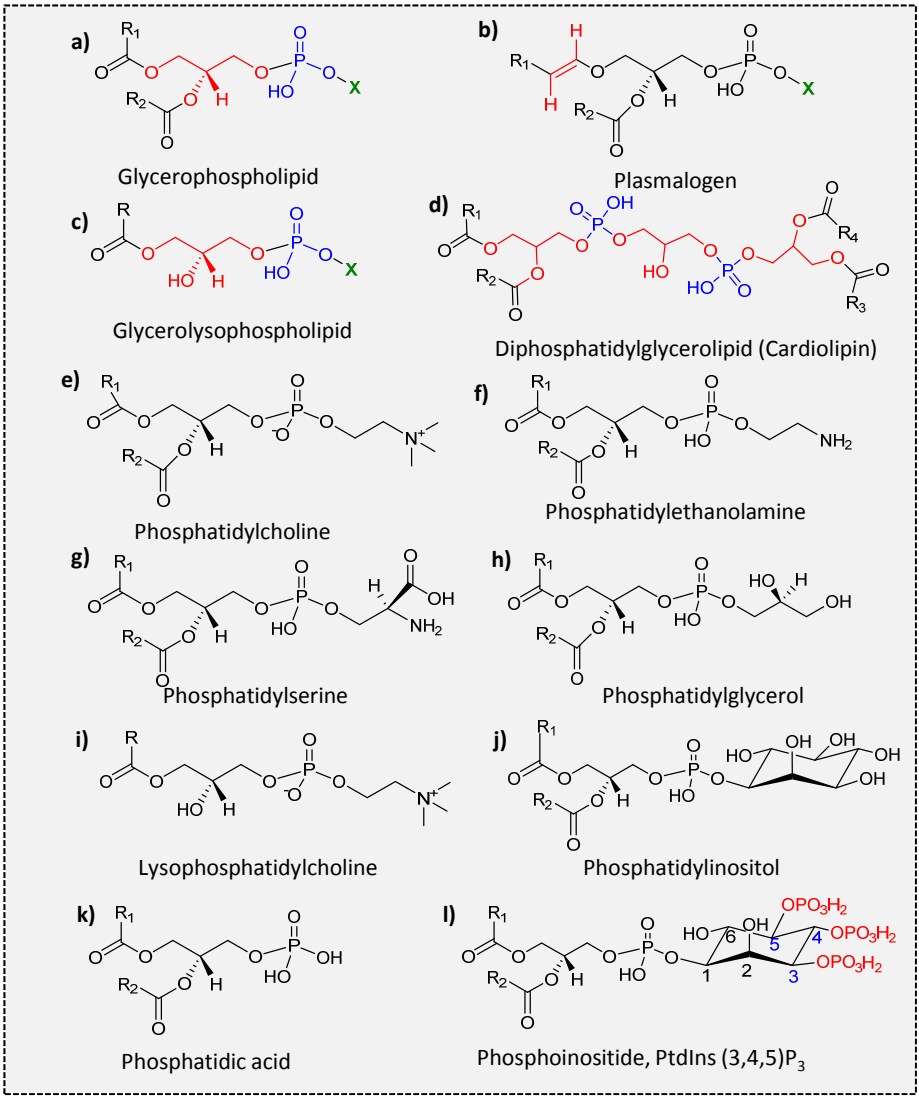

Figure 7. Molecular structures of glycerophospholipids including a) glycerophospholipid (GP) whose molecular structure has three parts: a three-carbon backbone of glycerol (in red), two long-chain fatty acids esterified to hydroxyl groups on two carbons of the glycerol (in black), phosphoric acid esterified to the central carbon hydroxyl group of glycerol (in blue) and polar head groups (X, in green). b) Plasmalogens are GPs which have an ether bond in position sn-1 to an alkenyl group in their molecular structure. The alkenyl group in its molecular structure is indicated in red, c) glycerolysophospholipids are GPs which have only a single fatty acid moiety (usually in the sn-1 position) in their molecular structure. The molecular structure of d) diphosphatidylglycerolipid (a.k.a. cardiolipin) consists of two phosphatidic acid moieties connected with a glycerol backbone in the center to form a dimeric structure, e)

phosphatidylcholine, f) phosphatidylethanolamine, g) phosphatidylserine, h) phosphatidylglycerol, i) lysophosphatidylcholine, j) phosphatidylinositol, k) phosphatidic acid, l) phosphoinositides are the phosphorylated derivatizes of phosphatidylinositols which can be reversibly phosphorylated (in red) at the 3rd, 4th, 5th (in blue) carbon positions to generate seven different species of phosphoinositides and this has been exemplified with the common PtdIns (3,4,5)P_3 species in panel l.

Several matrix molecules have been utilized for lipid MALDI-MSI analysis. However, due to the presence of acidic, basic and zwitterionic head groups of many phospholipids, matrix molecules functioning in dual polarity have been widely used for lipid MALDI-MSI including the prevalently used matrices; norharmane (9H-β-carboline),[596] 2,5-DHB,[597] 1,5-DAN.[598] LMW of lipids and their high-concentrations in tissues facilitate their efficient diffusion into a matrix molecule, but sublimation-based matrix-coating has been found to provide cleaner matrix crystals compared to the wet matrix application methods (e.g. robotic spraying of matrix solution). Sublimation also provides smaller crystal size and thus facilitates both better sensitivity and high-spatial resolution imaging of several lipid species with MALDI-MSI.[598, 599]

Nevertheless, certain matrix molecules such as dithranol and 2,6-DHAP rapidly evaporate in the low pressure which hinders their use for long MSI experiments for high-spatial resolution and/or high-mass resolution. To overcome this, a high-speed MALDI-TOF-MSI instrument (Bruker rapifleX MALDI Tissuetyper™ TOF instrument) has been developed to provide acquisition rates up to 50 pixels/s which was made possible by the use of a 10 kHz laser and two rotating mirrors that allow the laser beam to be moved over and synchronized with the rapidly moving sample. Hence, this allowed the use of dithranol and 2,6-DHAP matrices, applied via sublimation, for MALDI-MSI imaging of large areas of rodent sagittal brain tissue sections without losing any signal intensities of phospholipids within the analysis time.[600]

Cardiolipins are important and abundant components of the inner mitochondrial membrane. They have been detected and/or imaged with MALDI-MSI (using organic matrix molecules or silver nanoparticles) in tissue sections from the organs where they are abundant such as heart.[601, 602] However, standard protocols were unsuccessful to detect/image cardiolipins, particularly the diverse species of these mitochondria-unique lipids, which are essential for cellular and mitochondrial physiology of the brain. Therefore, in order to detect/image cardiolipins in rodent brain tissue sections, ion suppressive effects of highly-abundant amino- and choline-

containing lipid species can be eliminated using cross-linking of carboxyl/amino containing molecules on tissue using 1-ethyl-3-[3-(dimethylamino)propyl]-carbodiimide-hydrochloride and this can be followed by phospholipase C treatment to remove phosphatidylcholine head groups. Then, 2,5-DHB matrix application can be applied for MALDI-MSI of several cardiolipins in the coronal rodent brain tissue sections.[603] This methodology has been utilized to spatially map the cardiolipins in the brains of traumatic brain injured-rats which revealed loss of polyunsaturated cardiolipins in the cortical contusion, hippocampus, and thalamus.[604] Recently, IR-780 matrix has been introduced (Figure 6f). IR780 has a larger collision cross section (CCS) compared to commercial matrices and this makes it efficient for the MALDI of high molecular weight lipids. Thus, IR780 has been found to be efficiently facilitating the detection and imaging of high-molecular-weight cardiolipins in brain tissue sections using MALDI-MSI without the need of tissue treatment prior to matrix deposition.[579]

Phosphoinositides are a family of minority acidic phospholipids which are the phosphorylated derivatives of phosphatidylinositols which can be reversibly phosphorylated at the 3rd, 4th, 5th carbon positions to generate seven species of phosphoinositides including PtdIns $(3,4,5)P_3$ (Figure 7l). They are critically important for numerous cellular signaling pathways such as membrane trafficking, cytoskeleton rearrangement, and ion channel regulation, transporter function and signal transduction in eukaryotic organisms.[324] While certain species of phosphoinositides have been detected and imaged with MALDI-MSI using tissue washes (volatile buffer wash) followed by matrix application or high CC-value IR780 matrix in negative ion mode,[579, 605] their low abundance and high polarity hinder their comprehensive MALDI-MSI analysis in tissue sections.

Sphingolipids represent one of the major classes of lipids in eukaryotes and they contain a backbone of sphingoid bases including sphingosine, dehydrophytosphingosine, dihydrosphingosine and phytosphingosine which are the characteristic building block of sphingolipids. Sphingosine (Figure 8a) is the most abundant sphingoid base in animals, which can be formed from palmitoyl-CoA and serine, catalyzed by the enzyme named serine palmitoyl transferase and used by cells to form ceramides. Ceramides are incorporated into various complex sphingolipids, and they are formed through the union of long-chain fatty acids with sphingosine (Figure 8b). Sphingomyelins usually consists of phosphocholine and ceramide, or a phosphoethanolamine head group and they do not contain a glycerol

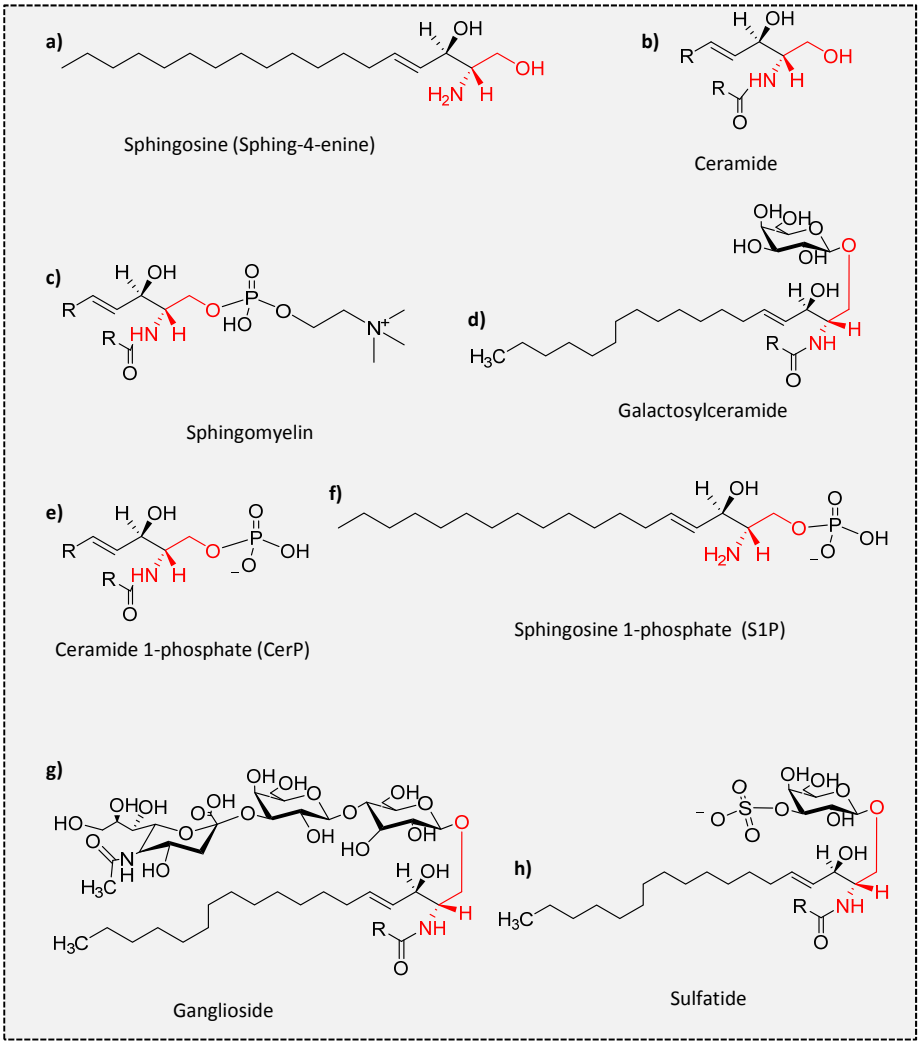

Figure 8. Molecular structures of several sphingolipids. a) Sphingosine (sphing4-enine) was chosen as the characteristic building block for d) galactosylceramide, f) sphingosine-1-phosphate (S1P), g) ganglioside, and h) sulfatide.

backbone (Figure 8c). Cerebrosides such as galactosylceramides (Figure 8d) are glycosphingolipids which are formed through linkage of either glucose or galactose to a ceramide. Gangliosides are glysocsphingolipids composed of a glycosphingolipid (ceramide and oligosaccharide) with one or multiple sialic acids (e.g. the prevalent N-acetylneuraminic acid) which makes them anionic at the physiological pH (Figure 8g). Sulfatides are anionic glycosphingolipids and they are the sulfated forms of galactocerebrosides (Figure 8h).

Sphingolipids are major constituents of the plasma membrane, where they are enriched in lipid micro domains together with cholesterol. Bioactive sphingolipids including sphingosine (Figure 8a), ceramide (Figure 8b), ceramide-1-phosphate (Figure 8e) and sphingosine-1-phosphate (S1P) (Figure 8f) exert distinct functions by acting on specific protein targets, including kinases, phosphatases, lipases and other enzymes and membrane receptors. Further, bioactive sphingolipids play critical roles in the modulation of a plethora of cell biological processes including growth regulation, cell migration, adhesion, apoptosis, senescence and inflammatory responses.[606]

The sphingolipidome is highly complex with distinct molecular species, and therefore comprehensive MALDI-MSI analysis of sphingolipids within a single experiment is challenging. Several acidic sphingolipids contain an ionized charged group such as sulfate, phosphate or sialic acid. Among them are sulfatides, ceramide phosphates, and gangliosides have been imaged with MALDI-MSI at high-spatial resolutions using acidic or basic matrix molecules including 2,5-DHB,[607] 1,5-DAN,[598] 9AA.[554] However, MALDI-MSI of neutral cerebrosides with no ionized charged group in their molecular structures is challenging due to their low-ionization efficiency and suppressed ionization in the MALDI plume. Therefore, similar for the MALDI-MS detection of cardiolipins, on-tissue phospholipase C digestion has been applied to degrade abundant PC species on the tissue sections prior to 2,5-DHB matrix application which increased the alkali adduct ion signal intensities of mono-, di-, and oligohexosylceramides by up to 10-fold.[608] Another strategy to increase the ion yields for imaging of cerebrosides was to increase the cationization via sodium doping of the tissue sections prior to 2,5-DHB matrix sublimation which significantly enhanced MALDI-MSI of neutral cerebrosides.[609]

MALDI-MSI of abundant gangliosides e.g. certain mono- di- tri-sialogangliosides is feasible with standard sublimation or spray-coating matrix application of several matrices such as 1, 5-DAN.[610, 611] However, due to the low abundance and/or high polarity of certain ganglioside species, the signal intensities of many other gangliosides are low for MALDI-MSI analysis. 2,6-DHAP is an efficient MALDI matrix not only for labile proteins but also for lipid species, particularly for gangliosides. However, the rapid sublimation time of 2,6-DHAP under vacuum (low pressure) at the extended time necessary to complete both high spatial and mass resolution is a drawback for MSI. Therefore, 2,6-DHAP has been utilized for atmospheric

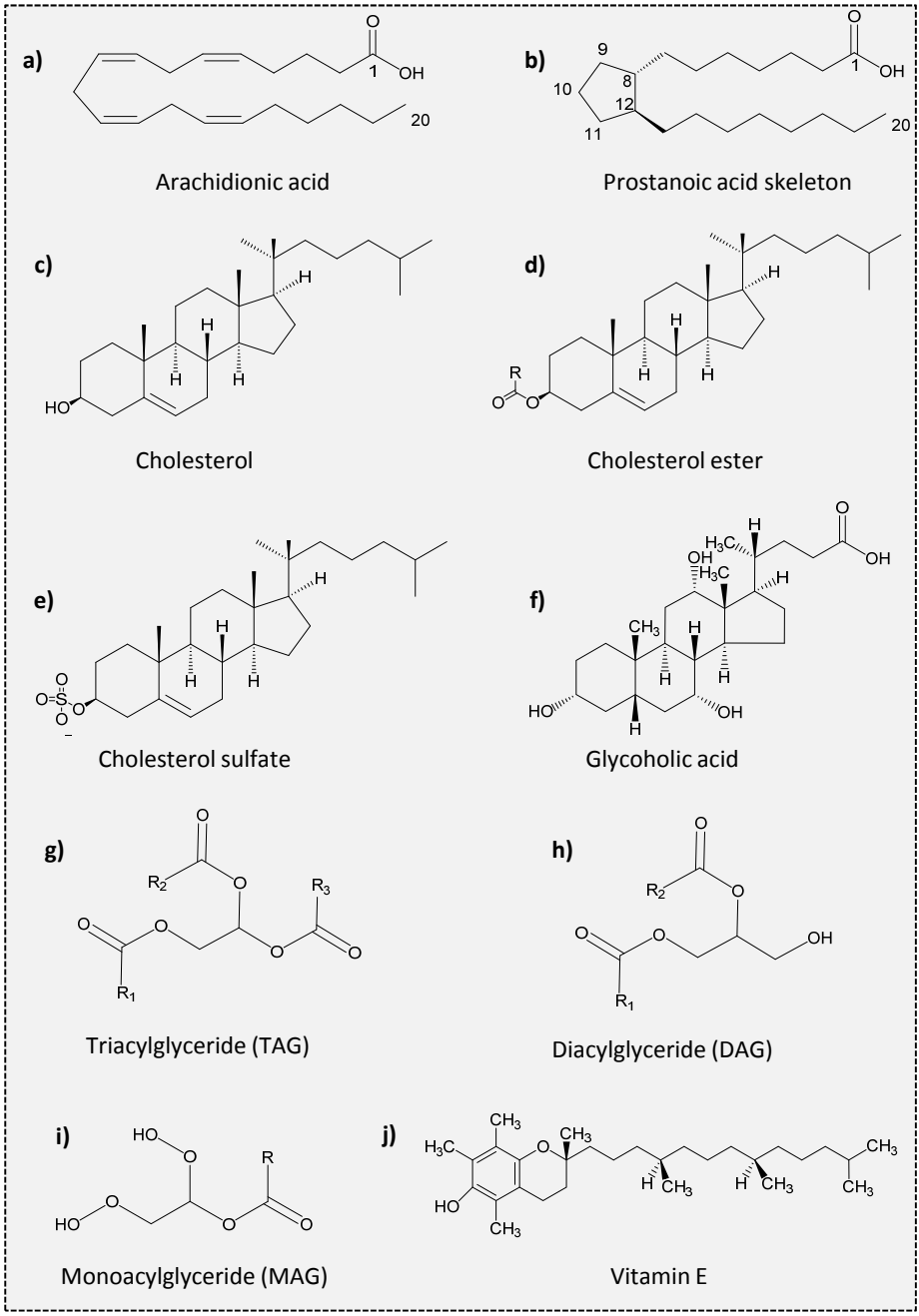

Figure 9. Molecular structures of a) arachidionic acid as an example of fatty acids, b) prostanoicacid skeleton, the building block of prostaglandins which is a subclass of eicosanoid signaling molecules derived from arachidionic acid, c) cholesterol, d) cholesterol esters, e)

cholesterol sulfate, f) glycoholic acid as an example of bile acids, g) triacylglyceride (TAG), h) diacylglyceride (DAG), i) monoacylglyceride (MAG), and j) vitamin E.

pressure (AP) MALDI-MSI in order to obtain high-spatial resolution ganglioside imaging in the brain using a high-mass-resolution mass spectrometer which yielded good-quality MALDI MS imaging of low-abundant GD_1 ganglioside species in the rodent brain tissue sections along with the abundant gangliosides including GM1, GM2 and GM3 species.[612] Another approach to circumvent high-volatility of 2,6-DHAP in low pressure and to utilize it for MALDI-MSI was chemical treatment of the matrix molecule. This has been achieved by adding heptafluorobutyric acid (HFBA) into the matrix solution, which increases its stability in the vacuum and thus allowing its use for tissue imaging. This approach has facilitated the detection and imaging of rare ganglioside species such as tetrasialoganglioside (GQ) and the O-acetylated forms of GD1, GT1, and GQ1 in rat coronal brain tissue sections.[613]

Signal intensities of ceramides are generally low during MALDI-MSI analysis. However, several studies have reported sensitive detection of elevated ceramide species, particularly long-chain ceramides, in tissue sections from disease models including kidney tissue from Farber disease mouse model,[614] brain tissue from traumatic brain injury rodent models[615, 616] and transgenic Alzheimer's mouse models.[617] Another signaling sphingolipid, S1P, which is low-abundant in rodent brain tissue sections has been also imaged with high-mass-resolution MALDI-MSI in brain tissue sections from traumatic brain injury rat model.[618]

The fatty acyls (FA) represent a diverse group of molecules synthesized by chain elongation of an acetyl-CoA primer with malonyl-CoA (a.k.a. methylmalonyl-CoA) groups that may contain a cyclic functionality and/or are substituted with heteroatoms. As the main structural building blocks of the many complex lipids, FAs represent one of the most fundamental categories of biological lipids. Eicosanoids are the derived group of signaling molecules from arachidonic acid (Figure 9a) which includes prostaglandins (Figure 9b), leukotrienes, and other structural derivatives. Disease associated oxidative stress or various other pathological events such as inflammation can mediate the oxidation of polyunsaturated FA groups to many different species of varying complexity from simple addition of an oxygen atom to form a conjugated diene hydroperoxide to very complex esterified isoprostanes.[619, 620] MALDI-MSI analyses of free FAs have been performed on tissue sections using organic matrices such as 1,5-DAN[560] or inorganic matrices such as silver nanoparticles.[621] Nevertheless, DPH, a commonly

used fluorescence probe, has been introduced to be a specific matrix for MALDI-MSI of various fatty acids in rodent brain tissue sections. This is feasible due to the high affinity of DPH for the acyl chains in the phospholipid bilayers.[558] However, the detection and MALDI-MSI imaging of several eicasonoids species within the tissue sections and single cells still remain as a challenge in the field.

Neutral lipid species including glycerolipids such as triacylglyceride (TAG) (Figure 9g), diacylglyceride (DAG) (Figure 9h) and monoacylglyceride (MAG) (Figure 9i), cholesterol (Figure 9c), cholesterol esters (Figure 9d) and various fat soluble vitamin species including vitamin E (Figure 9j) mainly require chemical treatment of tissue sections prior to matrix deposition (e.g. sodium doping),[609, 622] use of nanoparticles as the desorption/ionization substrate,[602] nanophotonic surfaces (e.g. silicon nanopost arrays)[623, 624] or signal enhancement techniques (e.g. laser post ionization)[591] for MALDI-MSI unless their abundance is elevated within the analytes (tissue sections, single cells) due to their disease-associated alterations. For instance, MALDI-MS detection/imaging of cholesterol within the tissue sections is not feasible using classical organic MALDI matrices unless a highly-basic proton sponge molecule, e.g. TPPN, is used as the matrix to deprotonate weakly-acidic cholesterol molecule.[575] Silver-assisted desorption/ionization can be used to detect cholesterol and other olefinic compounds including free fatty acids and TAGs using d-π complexation of silver metal and double bonds.[625] Nevertheless, nanophotonic ionization on silicon nanopost arrays can be used for selective ionization of neutral lipids such as TAG, cholesterol and hexylceramide species which facilitates their LDI MS imaging in brain[626] and skin tissue sections[627] along with their spatial subcellular detection.[626] Further, laser post ionization, a technique stimulates the ionization of the matrix molecules and analytes in the laser-induced desorption plume, facilitates the imaging of neutral liposoluble vitamins including vitamin E within the cerebellum of mouse brain tissue sections.[628] However, the charged derivatives of neutral lipids such as anionic bile acids (e.g. glycoholic acid), and cholesterol sulfate are readily ionized in MALDI using classical matrices such as 1,5-DAN and 9AA and imaged with MALDI-MSI within the tissue sections from e.g. rat small intestine and/or mouse liver.[560, 629]

As mentioned above, due to both high abundance and ionization efficiency of many lipid species in MALDI process and implications of lipids in critical biological processes, the progress in spatial lipidomics is strongly correlated with the rapid ongoing improvements in mass spectrometry technology and MSI methodology. MS analyzers with high mass resolving powers such

FTICR and Orbitrap are capable of distinguishing several species of lipids in different lipid classes with high mass accuracy and this facilitates the visualization of lipid molecules in complex tissue surfaces using MALDI-MSI.[556, 595, 630, 631] However, low-abundance and/or low ion yields of certain lipids species and analyte ion suppression effects or low ionization efficiency of certain lipids (e.g. neutral lipids) in MALDI plume require methodological advancements to enhance the spatial chemical coverage obtained from analyte surfaces at high-spatial resolutions. Note that, this is highly dependent on the properties of matrix molecules, its application and the molecular composition of the analytes. In order to increase sensitivity, while providing a high mass-resolving power, a novel interface has been designed combining MALDI at elevated pressure and electrospray ionization with Orbitrap mass spectrometer which facilitates low-abundance and low MALDI-ionization efficient molecules (e.g. cholesterol) within transversal rat brain tissue sections at high-spatial resolutions (15-30μm).[590] Another approach was combining the MALDI-2 ionization strategy with Orbitrap mass spectrometry which facilitates both enhanced ionization of abundant lipid species and ionization of neutral lipid species (e.g. GalCers, and cholesterol) while increasing chemical coverage with high mass resolving power.[589]

One important objective of MSI is to map molecular distributions of a wide range of biomolecules within their native environment at high-spatial resolutions. Further, one of the challenges in MALDI-MSI is spatial mapping of molecules at subcellular levels due to the minute small quantity of analytes in cells, along with the variety of cellular constituents with distinct ionization characters.[425] Commercial MALDI-MSI instruments provide spatial resolutions down to 5-10 μm[632, 633] at high data acquisition speeds (about up to 50 pixel/second)[600] while experimental instruments can provide down to ~1 μm.[433, 536, 595] With the performance of the commercial MALDI-MSI instruments, tissue imaging from whole body to cellular levels, including the cellular-layer levels such as Purkinje cell layer in the cerebellum of mouse brain or goblet cells in rat small intestine are possible.[560, 634, 635]

Transmission geometry principle has introduced as an efficient approach to focus the laser beam to low-micron levels which facilitated protein MALDI mass spectrometry imaging directly correlated to individual Purkinje cells within the cerebellum of rodent brain tissue.[536] However, decreased laser spot sizes are often associated with decreased analyte ion signal intensity, and thus, in order to circumvent this, the transmission geometry has been combined with the MALDI-2 ionization strategy which increases the analyte ion yields without sacrificing spatial resolution.[593] Further, combination of

this strategy with high mass-resolving Orbitrap mass spectrometer has been utilized for high-throughput lipid molecular information with high mass accuracy at subcellular levels (at 1μm spatial resolution).[433]

Another important objective of MALDI-MSI is three-dimensional (3D) molecular imaging of tissue sections. Due to the low-surface sensitivity and heterogeneous laser ablation process, layer by layer 3D MALDI-MSI of the tissue surfaces or MALDI-MSI on 3D surfaces with heterogeneous topography is challenging. Therefore, 3D MALDI-MSI experiments are often achieved by 2D imaging of strict consecutive tissue sections collected at an equal distance. The resulting data are processed with dedicated software to construct 3D ion images of individual analyte signals, thus enabling the use of virtual z-stacks and 3D volume renderings to investigate differential localization patterns of a variety of molecules including lipids and peptide/proteins.[636, 637] In order to image lipids on irregular 3D surfaces of (e.g. plants, parasites), an autofocusing MALDI-MSI strategy has also been developed which uses long-distance laser triangulation on a micrometer scale to simultaneously obtain topographic and molecular information.[638]

A rapidly developing perspective of MALDI-MSI is four-dimensional (4D) imaging which is an important objective and potentially provides a biophysical aspect via providing structural information of the analytes imaged with MALDI-MSI. Combination of ion mobility with MALDI can distinguish isobaric lipid, peptide, and oligonucleotide molecular ions which are pre-separated in the mobility cell before MS analysis.[639, 640] Notably, the potential of MALDI-ion mobility-MS analysis indicated a clear shift within the comparison of the structural isomers of GD1a standard with a GD1b, to higher drift times for GD1a.[641] Recently, a new instrument design, which combines ion-trap and ion mobility, trapped ion-mobility spectrometry (TIMS), has been introduced, providing TIMS-based imaging of analytes. This initial TIMS-based imaging strategy has facilitated the separation in the gas phase and MALDI imaging MS of closely isobaric $[PC(32:0) + Na]^+$ and $[PC(34:3) + H]^+$ (3 mDa mass difference) from whole-body mouse pup tissue.[642] TIMS can also resolve matrix peaks from metabolite signals and separate both isobaric and isomeric metabolites with different localizations within the kidney tissue sections and thus allows 4D spatial metabolomics using MALDI-MSI.[643]

Other approaches for 4D lipidomic to detect/image structurally defined lipid species include fragmentation using ultraviolet photo dissociation (UVPD, e.g. using 193 nm photons) by enabling fragmentation following electronic excitation which facilitates fragmentation pathways not accessible with low

energy CID (vibrational excitation). UVPD can cleave C=C bonds and facilitate identification of C=C isomers of both phospholipids and sphingolipids.[644, 645] Further, various on-tissue chemical derivatization strategies including Paternò–Büchi,[646, 647] ozone-induced dissociation,[648] meta-chloroperoxybenzoic acid (m-CPBA) epoxidation reaction[649] followed by tandem MS analysis have been introduced to identify and/or image the position of the double bonds in the molecular structures of unsaturated lipids using MALDI-MSI.[650] Importantly, benzophenone (BPh) has been introduced as a novel reactive matrix for MALDI which facilitates desorption/ionization providing functionalization of unsaturated PLs during the MALDI process via a laser-light driven Paternò Büchi reaction. Thus, this has been utilized to image C=C isomers of PC species via tandem mass spectrometry imaging in mouse cerebellum at high-spatial resolutions.[647]

3.4.4 MALDI MSI with UltrafleXtreme MALDI-TOF/TOF

The basic principle of a mass spectrometer involves generation of multiple ions from the analytes under investigation which is followed by their separation according to their specific mass-to-charge ratio (m/z), and then recording the relative abundance of each ion type. Therefore, a typical mass spectrometer consists of three main components; an ion source, a mass analyzer, and a detector. Here I will describe the important features of the UltrafleXtreme MALDI-TOF/TOF mass spectrometer including the unique modified 'smart beam' (termed by Bruker) laser profile which refers to structured focus profiles of frequency-tripled Nd:YAG laser (at 355 nm)[651] and the novel 'LIFT' technique (MALDI LIFT-TOF/TOF MS).[652] Then, I will introduce the suitability of this instrument for high-throughput MALDI-MSI analysis. In a detailed brief, the LIFT-TOF/TOF mass spectrometer consists of a gridless MALDI ion source pulsed ion extraction (PIE, a.k.a. delay extraction) electronics, a high-resolution timed ion selector which is also called pre cursor ion selector (PCIS) based on Bradbury-Nielsen principle, a "LIFT" device for raising the potential energy of the ions, a further velocity focusing stage with subsequent post-acceleration (source 2), a post lift metastable suppressor (PLMS), a gridless space-angle and energy focusing reflector, and fast multiple-dynode ETP electron multiplier ion detectors for the linear and reflector modes.

Several solid-state, dye and gas lasers have been utilized for MALDI-MS. Due to the need for rapid energy transfer to the analyte surface which should be shorter than the thermal diffusion time, only pulsed lasers are useful for MALDI. Further, the most common type of mass analyzer used for MALDI

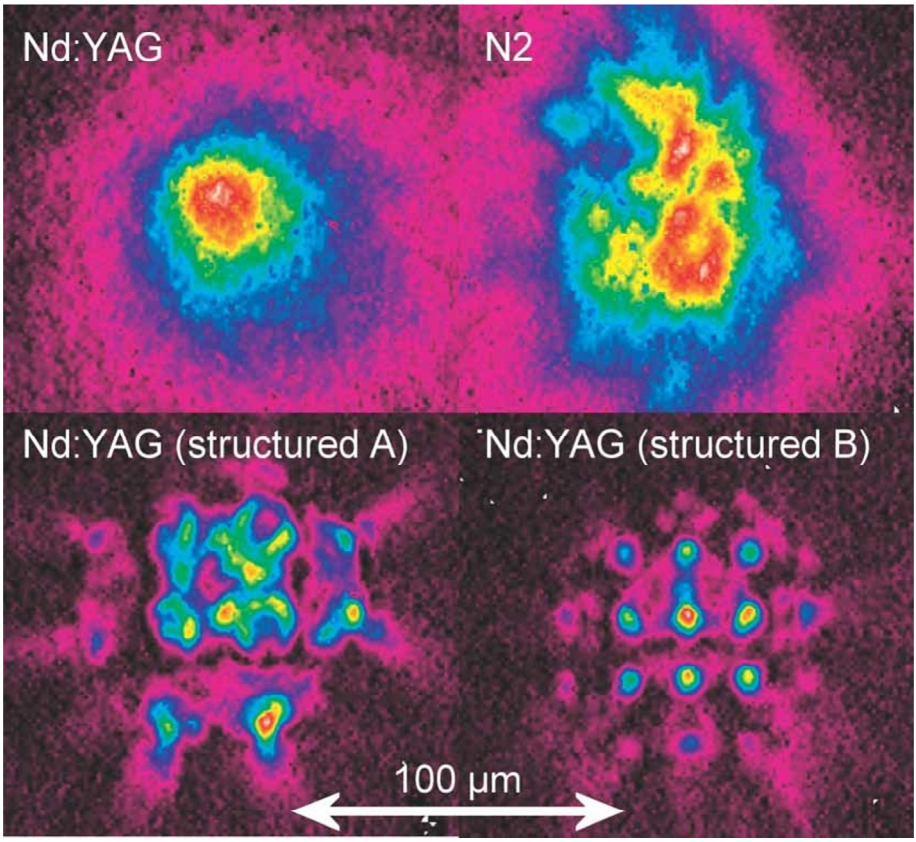

Figure 10. Comprarison of the beam profiles with high-resolution CCD images of the frequency-tripled Nd:YAG laser at 355 nm with a Gaussian beam profile, nitrogen (N_2) laser at 337 nm, and structured frequency-tripled Nd:YAG laser profiles; Nd:YAG (structured A), Nd:YAG (structured B).[651] *Reprinted by permission from Wiley, optimizing UV laser focus profiles for improved MALDI performance, Holle, Armin; Haase, Andreas; Kayser, Markus; Hoehndorf, Journal of Mass Spectrometry 2006, 41, 705-716.*

applications, axial time-of-flight (TOF) analyzers, also require a short laser pulses for a good time and mass resolution.[373, 515]

The lasers are characterized by their emission features including wavelength, pulse width, and pulse energy along with the beam features such as beam diameter, divergence and beam shapes. Nitrogen (N_2) gas lasers are commonly used for ultraviolet-MALDI (UV-MALDI) due to their simplicity, small size, and relatively low cost. Emission wavelength of N_2 lasers which is 337 nm is close to the absorption maxima of many commonly-used matrices including 2,5-DHB and HCCA. However, N_2 lasers have limited pulse repetition frequency (typically <100Hz) and limited laser life time which

hinder their use in high-throughput analysis, notably for MSI. Therefore, for MALDI-MSI analysis, diode-pumped Nd:YAG solid state laser with a wavelength of 355 nm and pulse repetition rates up to 1 kHz or more with relatively higher life span have been increasingly used in MALDI ion sources. For less commonly used infrared MALDI (IR-MALDI), lasers emitting in the OH- or NH stretch vibration range near 3 μm are usually employed such as Er:YAG lasers with a wavelength of 2.94 μm and optical parametric oscillators (OPO) which are tunable typically from about 1.7 to 2.5 μm or less common CO_2 lasers with a wavelength around 10 μm., The emission pulse width (or pulse duration) for UV lasers ranges from ~0.5 ns and 25 ns (with 3–10 ns most frequently used) and 5–100 ns in the IR lasers. Picosecond and femtosecond laser pulse durations have been also studied for MALDI analysis which can dictate distinct desorption/ionization dynamics including distinct ionization, fragmentation of the analyte and matrix molecules along with the different laser ablation profiles.[515, 653]

Beam shape characteristics of the lasers are also important for MALDI. The important laser beam parameters which determine the optimal coupling of the laser beam into the mass spectrometer includes the laser near-field beam diameter, the divergence of the beam, and the energy distribution across the beam in the near field and the far field, the region far from the focus and measured in the focal plane of a lens focusing the beam. The optimal MALDI performance in MALDI is achieved using laser spots with a smooth fluences or irradiance distribution without any "hot spots". Thus, it is crucial to place the target precisely in the focal plane of the lens to localize the far field of the laser beam on the target for the best MALDI performance.

The UltrafleXtreme utilizes special irradiation geometry of frequency-tripled Nd:YAG laser (at 355 nm) called "smart beam" which is a modified structured beam profile of Gaussian beam shape (Figure 10). The fast pulse repetition rates and high life span render Nd:YAG solid state lasers optimal for MALDI-MSI experiments; however, the Gaussian beam shape diode-pumped Nd:YAG solid state laser with a wavelength of 355 nm (Figure 10) offers worse MALDI ionization efficiency of peptides from HCCA thin-layer sample preparation compared to N_2 lasers which operate at 337 nm (Figure 10). This is likely due to the heterogeneous (with significant shot to shot variation), structured beam profile of the N_2 lasers which involves needle-type local maxima in the beam profile and thus provides hot beam spots for MALDI. Therefore, in order to mimic the N_2 laser, the Gaussian beam profile of diode-pumped Nd:YAG solid state laser has been modified which yielded

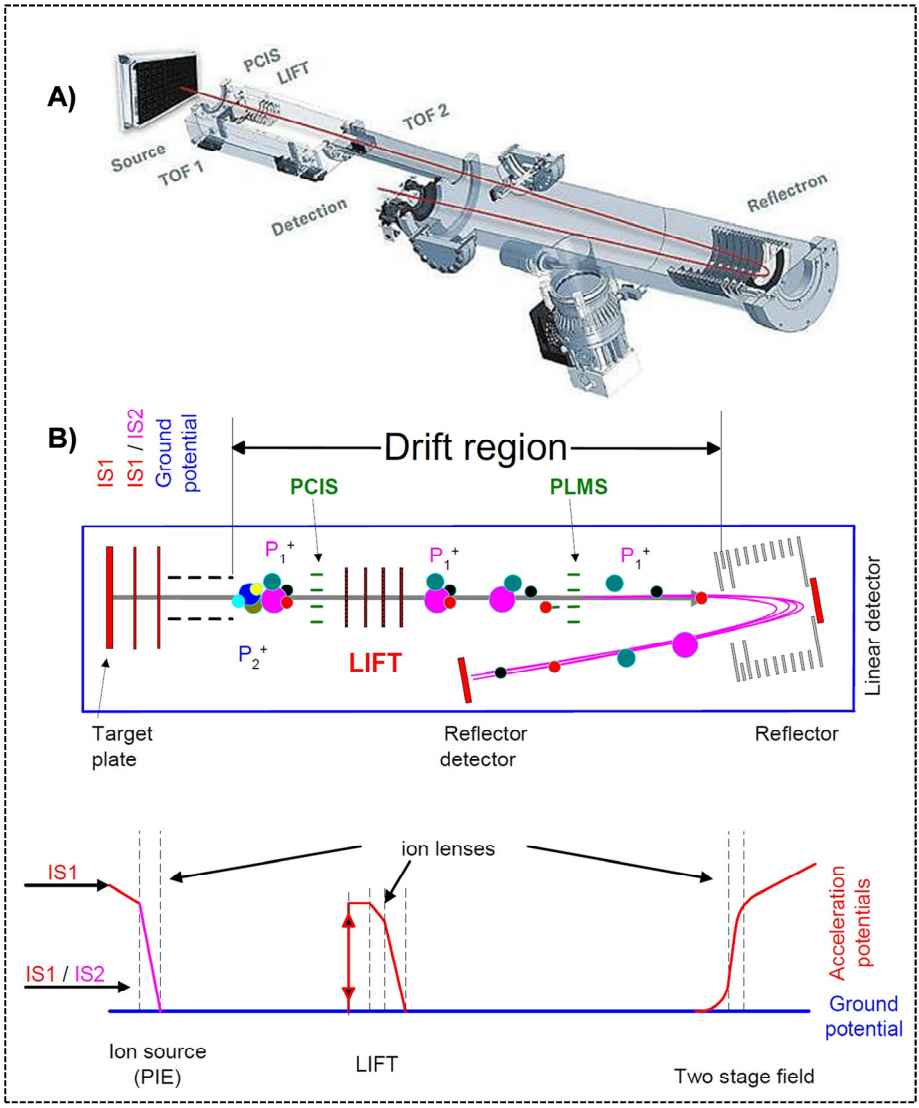

Figure 11. The schematic of UltrafleXtreme MALDI-TOF/TOF mass spectrometer A) in 3D which employs "smart beam" laser beam profile of frequency-tripled Nd:YAG laser. In a detailed brief, B) the LIFT-TOF/TOF mass spectrometer consists of a gridless MALDI ion source with pulse ion extraction (PIE) electronics, a high-resolution timed ion selector which is also called precursor ion selector (PCIS), a "LIFT" device for raising the potential energy of the ions, a further velocity focusing stage with subsequent post-acceleration (source 2), a post lift metastable suppressor (PLMS), a gridless space-angle and energy focusing reflector, and fast multiple-dynode ETP electron multiplier ion detectors for the linear and reflector modes. Panel A, image credit: Bruker Daltonics. Panel B, adapted from Ultraflex III user manual (Bruker Daltonics).

structured beam profiles such as Nd:YAG (structured A) and Nd:YAG (structured B) (Figure 10). These 'smart beam' profiles enhanced the MALDI-MS ion yields obtained from several analyte molecules (e.g. peptides) compared to Nd:YAG (Gaussian) and N_2 lasers.[651] This suggests the beam shape is an additional and important parameter in MALDI process and should be considered for further studies including MALDI-MSI.

MS analysis of ions produced from MALDI plume can be performed using a variety of mass analyzers including quadrupole ion trap mass spectrometers (QIT-MS), FT-ICR, Orbitrap, ion mobility, trapped ion mobility spectrometer (TIMS) and time of flight (TOF).[503] The use of these mass analyzers often involves a tradeoff between the cost, speed, dynamic range and throughput. The advantages of using each mass analyzer for biological mass spectrometry including spatial lipidomics have been mentioned in the previous chapters for the MALDI-MS and MALDI-MSI analysis above. Nevertheless, MALDI usually generates a pulse of ions several nanoseconds wide which makes it particularly suited for TOF analyzers and therefore TOF is the dominant mass analyzer for MALDI-MS instruments. MALDI can generate ions of very large masses (e.g. large proteins at hundreds of kDa) with dominant singly charged ions and this also makes TOF analyzer suited for MALDI due to its, in principle, unlimited mass range, while the high initial axial velocity of MALDI ions and their broad kinetic energy distribution can limit the mass resolution in TOF instruments.

The most common type of mass analyzer for MALDI applications is the axial TOF spectrometer while orthogonal and transmission geometry instruments have been also used. In axial TOF instruments, all ions of charge q are first accelerated by a potential difference U, between the sample support and a nearby grid or open electrode, to a kinetic energy E_k before they travel down a field (and force) free path of typically about 1 m length to the detector.

Thus,

$E_k = zeU$

where z is the charge state and e the elementary charge. Potential differences, U, of 20 kV are typically used in modern TOF instruments. Ions with the same kinetic energy, E_k, will have different velocities, v, based on their mass, m, following the equation

$$E_k = \frac{1}{2}mv^2 \text{ or } v = \sqrt{\frac{2E_k}{m}} = \sqrt{\frac{2zeU}{m}}$$

Thus, the arrival time will be:

$t = L\sqrt{\frac{m}{2E_k}} = \sqrt{\frac{m}{2zeU}}$ where L is the flight tube length.

This can be inverted to: $\frac{m}{z} = 2eU\left(\frac{t}{L}\right)^2$

In TOF mass spectrometers, the initial velocity distribution of the ions extracted from the MALDI plume can cause at heterogeneous arrival times for the ions of a particular mass to the detector. This broadens the peaks and degrades mass resolution. In addition, an irregular analyte surface will cause diverse initial positions of the ions in the potential gradient and this affects their final velocity distribution. Repulsive electrical forces within the MALDI plume can also contribute to the initial energy distribution of the ions of a particular mass. Thus, the pulsed-ion extraction (a.k.a. delay extraction) mode of operation[382, 654] is employed to compensate the initial velocity distributions of the ions of a particular mass in which the electric field between the sample surface and the first electrode is initially kept at zero or very low (here the fast ions will move farther towards to electrode) and switched on after a delay time which is typically tens of nanoseconds.

In the UltrafleXtreme, the pulse ion extraction mode of operation involves the target plate (P1) where the analyte is dropped on, the second voltage plate (P2) which is an electrode mounted some mm apart opposite to the sample position, and the following grounded acceleration electrode where the delay extraction is performed between the P1 and P2 (Figure 11b) and the ions are accelerated by the delayed applied electrical field and focused by a lens system before they leave the source.

Ion reflectors invented by Mamyrin et al.,[383] which are designed to re-focus the ion packets onto the detector, are another alternative to contribute to the compensation of the initial velocity/energy distribution of MALDI ions. The reflector increases the travel time of the ions in TOF with the same mass but higher velocities where high-velocity ions penetrate the electric field to a greater depth, thus equalizing the arrival time of the ions with the same m/z to the detector which compensates their initial energy dispersion. Modern commercial TOF mass spectrometers including the UltrafleXtreme have both reflectrons and delayed ion extraction mode of operation. A reflectron (ion mirror) refers to a series of ring electrodes which ideally create a constant electric field near their center through a linear voltage gradient that slows

down the ions and reflects them around and send to a second detector with the aid of larger potential of the last electrode than the acceleration potential of the ions. The UltrafleXtreme uses a gridless reflector with ion lenses, with a double stage design where the first stage's field is stronger, in order to minimize residence times of ions inside the reflector which removes fragment ions arise inside the reflector and decrease chemical background and creates a space focusing effect for better sensitivity. Thus, in the UltrafleXtreme instrument, the delay extraction and the reflectron can compensate for the flight time dispersion due to the initial velocity distribution and energy dispersion (e.g. as a result of irregular sample surface), respectively which renders mass resolving power up to 40,000 and 1 ppm mass accuracy for the highest confidence. Note that, for MALDI-MSI experiments, the values of mass resolving power and mass accuracy will be lower due to the sample surface heterogeneity and complex molecular composition of the sample surfaces such as the surfaces of the tissue sections.

Tandem mass spectrometry is a highly informative methodology used for the structural analysis of various types of molecules (including lipids, peptides, and proteins). Tandem mass spectrometry involves selection of a precursor ion, fragmenting it, and generation of a mass spectrum of the fragment ions of the precursor ion. In the MALDI plume, ions mainly emerge as a result of the following processes; ions are excited via absorption of some of the laser pulse energy directly and/or they become 'hot' by collisions with the excited matrix molecules which also absorbed laser light. The collisional activation of the ions dragged in the matrix plume occurs via the applied electric field in the source. Chemical reaction-induced fragmentations such as hydrogen and proton transfer occur inside the plume and have certain exothermicities associated with them. These internal energetic processes can cause fragmentation of the analyte molecules, particularly labile molecules such as phospholipids with labile head groups (e.g. choline), phospho- or sulfo-peptides and sialylated/sulfated glycolipids. They dissociate before (or during) the detection depending on the relative stability of the cleavage of the bond via unimolecular decay of the precursor ions which is activated by vibrational energy transferred in the dense MALDI plume.

In axial TOF analyzers, the structural information of the target analyte molecules can be obtained using either metastable decay (in which ion selection is avoided such as in-source decay fragmentation) or externally induced fragmentation such as collision induced dissociation (CID) of the selected precursor ion or increased laser-induced unimolecular decay of metastable molecules which is called "LID". Metastable ion fragmentation often produces fragment ions of labile groups in the molecular structure of

the analyte molecules which is not enough to obtain all the structural information of interest. Metastable decay fragments can be generated in source on a time scale that is short compared to the delay time of the ion extraction and these ions are called "in-source decay ions" which are often the result of chemical reactions of hydrogen radicals.[655, 656] Precursor ions, decaying in the field-free region of the flight tube are called "post source decay" (PSD) fragment ions which are generally reduced by delayed extraction due to the loss of the high pressure of the MALDI plume via adiabatic expansion before the application of the ion extraction potential reducing collisional activation of the ions with the dense neutrals.[657] Therefore, to increase the internal vibrational energy of the metastable ions and thus to enhance their fragmentation, one option is to induce collisions with neutral gas molecules in a specially designed collision cell. In this mode, an ion gate in front of the collision cell is operated with an optimum delay time to pass the precursor ions of interest into the collision cell which is then acts as the fragment ion source for the second high-resolution reflectron TOF mass spectrometer in TOF/TOF instruments where the fragment ions are accelerated to a high velocity once again and then allowed to time separate.

In my research, I utilized increased metastable unimolecular decay of lipid and peptide molecules using LID-LIFT-TOF/TOF MS/MS mode of operation in the UltrafleXtreme instrument. Parent ions and PSD fragment ions formed in the drift region will have the same velocity as the PSD precursor ion and travel side by side in the TOF and thus goes undetectable in linear TOF. The total kinetic energy of the precursor ion will be split between the fragments in the ratio of their masses and the fragment ions will be dispersed and poorly focused onto the second detector which generates unresolved peaks around the baseline noise level of the instrument or they will not be detected at all in the reflectron. These PSD ions can be refocused onto the detector by reducing the reflectron voltage.[657, 658]

In the UltrafleXtreme, the gridless reflector can be used to focus some of the fragment ions with less energy than the precursor ion in time and space but the ions that have even less energy do not hit the detector. The initial accelerating voltage for fragments and corresponding precursor ion is 8 kV which is low and provides a long flight time of about 10–20 μs during which fragments arise (via unimolecular decay). These fragments and the precursor ion will reach the timed pre cursor ion selector (PCIS) at the same time which is also the case for the other fragments and their corresponding precursor ions. Thus, here PCIS offers the capability of selecting the ions under investigation with very short selection times and thus improves the resolving power. PCIS consists of deflector plates arranged in vertical layers below

each other. Consecutive electrodes are coupled to a high voltage supply with alternating polarity, according to the Bradbury-Nielsen shutter principle (an electronic ion gate for ion selection).[659] An electrostatic field perpendicular to the ion flight direction is generated due to the potential difference between the plates and this electrostatic field deflects all the ions entering this electrode. PCIS operates as follows; when the selected ions enter the deflection field, the deflection is switched off just in the same moment and the potential between the plates is kept to zero until the ions leave the deflector. In this moment the deflection is switched on again with the reverse polarity to compensate the partial deflection, which occurs in the stray areas at both front ends of the electrodes.

The basic idea of LIFT is to raise the kinetic energies of parent and fragment ions to a level that the energy difference between parent and smallest fragments is suitable (not too high) for the reflectrons focusing capability. Thus, in this case, all the fragments can be simultaneously detected with the parent ion. LIFT is a chamber in the drift region which consists of three stages between four grids (Figure 11B): the first stage is the LIFT chamber with a potential of the electrode 1 and 2 raised from ground to 19 kV when the ions entered in and where the ions continue moving as before; however on this increased electrical potential of 19 kV. Then, the ions move from the first stage to the second stage at this increased potential. While the precursor and fragment ions are still inside the second stage, they are accelerated towards to third stage by reduced 2-3 kV potential on the third grid (in the third stage the electrode 4 is ground). Thus, the second stage acts as a pulsed (delayed) acceleration stage and thus when entering the third stage, a further acceleration of the particles takes place according to the remaining voltage difference and full speed and time-focused onto the reflector detector. The UltrafleXtreme employs a second deflection unit called PLMS (post lift metastable suppressor) (Figure 11B) located between LIFT and the reflector which removes daughter ions (if switched on) that are formed after the LIFT procedure by deflecting the parent ion and prevents undesired fragment ion formation after post-acceleration.

The UltraleXtreme employs ETP electron multiplier ion detectors with multiple discrete-dynodes which displays amplification at each successive dynode and this can facilitate cascading process results in gains up to 10^8 being achieved with ~21 dynodes. ETP electron multiplier detectors can provide better sensitivity for high masses up to 10^6 Da with low saturation in linear mode compared to multichannel plate detectors. Their life time is reasonable and it can be efficient for a long time with a careful operation

while their gain will fall very gradually over time by aging and voltage requirement will periodically increase.

In conclusion, the UltraleXtreme MALDI-TOF/TOF is a well-designed modern MS instrument which is in line with the versatility of the MALDI-MSI research and empirical nature of desorption/ionization process in MALDI.

3.5 Sample Preparation for MALDI-MS/MSI

Successful MALDI-MS or MALDI-MSI analyses depend very largely upon good sample preparation due to the empirical nature of desorption/ionization process in MALDI. A number of factors, which can interrelatedly effect the final sample form and so the desorption/ionization process, should be considered for a successful MALDI analysis including the physiochemical properties of the analyte compound such as its solubility in organic solvents, charge state of the analyte in the matrix solution along with the purity and concentration of the analyte, the choice of the matrix molecule, and the mass range of the MS analysis.

A typical MALDI-MS experiment involves resuspension of the analyte (either in solution or lyophilized) in an aqueous matrix solution of 50% (v/v) acetonitrile, 0.1% (v/v) trifluoroacetic acid (TFA) using ultra high purity water and the resulting solution is spotted on MALDI target plates such as MTP ground steel or AnchorChip. The majority of the matrix compounds are acids (e.g. commonly used HCCA, 2,5-DHB) and in acidic matrix solution, most proteins and peptides (especially tryptic peptides) are basic and thus they are mostly positively charged and detected in positive ion mode. Acidic compounds such as phosphopeptides and oligonucleotides are best observed in negative ion mode but it is less sensitive and this requires alternative sample preparation and suitable matrix choice. For example, use of ATT matrix co-crystalized with the analyte (at pH~7 to avoid DNA depurination) in volatile ammonium salts (e.g. ammonium citrate) increases the detection of oligonucleotides and suppresses the peak broadening caused by the multiple alkali adducts.[660] A number of matrices have been empirically determined for each compound class and particular mass ranges. While MALDI-MS is more tolerant to salts and detergents compared to several other MS methods, the contamination can still interfere with the matrix/analyte crystallization and/or desorption/ionization. Therefore, sample purification can be applied for improved MALDI-MS such as reversed phase separation or sample washing using a volatile buffer such as ammonium acetate.

A number of sample preparation strategies have been developed empirically for improved MALDI-MS analysis of peptides and proteins considering the importance of matrix selection, matrix and analyte concentration, pH adjustment, crystallization conditions and the use of matrix additives.[661] For example, a widely-used two-layer sample preparation for efficient analysis of complex mixtures involves a first layer of densely packed matrix microcrystals on the MALDI spot which is done by fast solvent evaporation of a matrix solution and this is followed by addition of matrix/analyte

solution to the first layer which provides uniform well-incorporated matrix/analyte molecules in microcrystals for better desorption/ionization.[662]

For MALDI-MSI, even subtle differences in sample integrity or molecular density can have profound effects on the signal intensity, types of molecules being ionized, molecular identity of analyte compounds as well as their native spatial distribution.[438, 663] The initial crucial step of sample preparation is the dissection or collection of organ or tissue biopsies which requires a step to halt enzyme activity to reduce degradation and delocalization (e.g., diffusion across the tissue) of the molecules which is generally performed by directly freezing the tissue sample in liquid nitrogen or isopentane after dissection, cooling on dry ice and storing at −80°C until use. Thus, it is of greatest importance to perform the removal and freezing of the tissue from death as fast as possible because major degradation of peptides/proteins can occur in brain tissue within the first minutes after death.[664] Paraformaldehyde (PFA) fixation is a common immunohistochemical method to block postmortem degradation of proteins and peptides within the tissue sections. However, due to the cross-linking of proteins via methylene bridges, direct MALDI-MSI analysis is not straightforward while several methodologies have been developed including deparaffinization followed by 9AA matrix application for the analysis of metabolites,[665] and peptides and protein MALDI-MSI of formalin-fixed paraffin-embedded (FFPE) tissue sections via chemical derivatization or tissue digestion followed by matrix application.[666, 667]

The frozen tissue samples are inserted into a sample stage (−15 to −25°C) in a cryostat using an embedding material and sectioned with a stainless steel microtome blade at 10–20 μm thick at −20°C, which is optimal for ensuring that enough analyte molecules are available for extraction while keeping the optimal insulating properties of the tissue. This is followed by mounting the tissue sections onto MALDI plates such indium tin oxide (ITO) conductive glass slides. ‘Optimal cutting temperature’ compound (OCT) is a commonly used embedding material for sectioning although its inattentive use can result in suppression effects during MALDI process. Therefore, for more delicate experiments, alternative options are available such as carboxymethyl cellulose (CMC)[668] and gelatin[669] which are more compatible with mass spectrometry imaging.

Brain tissue is one of the most widely examined tissue type with MALDI-MSI analysis owing to its molecular complexity and spatial heterogeneity of

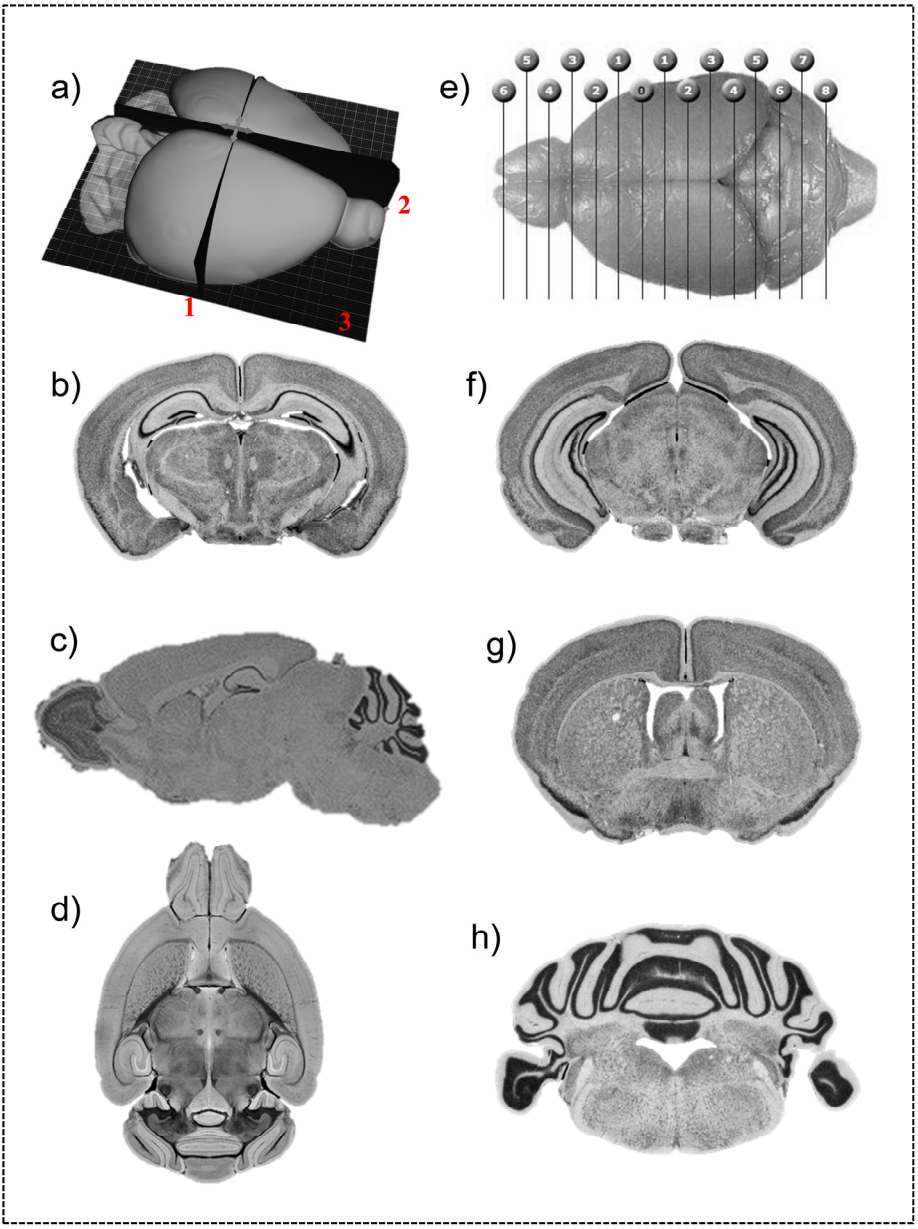

Figure 12. Dissection of mouse brain and resulting histology. a) 3D view of mouse brain sketched in 3D viewer of Allen brain atlas. 1, 2, 3 numbers in red represent dissection of the mouse brain from three different planes which provides b) coronal, c) sagittal and d) transversal views of the brain, respectively. e) The histological views of the coronal mouse brain sections obtained from mouse brain atlas: DBA/2J Coronal at different bregma points

including f) at the level 3 on the right side of the bregma point (zero point), g) at the bregma point which is the zero point, and h) at level 6 on the right side of the bregma point.

the brain tissue structure in 2D and 3D. Mouse and rat brains are usually used for the MALDI-MSI experiments. The mouse brains are usually dissected in three different planes depicted in Figure 12a which provide coronal (Figure12b), sagittal (Figure 12c) and transversal (Figure 12d) views. Coronal and sagittal brain tissue sections have been widely used in many experiments including the experiments in this thesis. I mainly used coronal mouse brain tissue sections from several levels according to bregma points in mouse brain atlas: C57BL/6J coronal (Figure 12e). The markers C57BL/6J coronal mouse brain atlas is spaced 1 mm apart and corresponds to levels of the atlas. The zero coordinate is the bregma point, a landmark visible on the skull. Distinct brain regions can be observed from different levels of coronal mouse brain tissue sections such as level 2 in Figure 12b (right side of the bregma point), level 3 in Figure 12 f (right side of the bregma point), level 0 in Figure 12 g (the bregma point) and level 6 in Figure 12h (right side of bregma point). These sections reveal several histological regions including hippocampus, cerebellum, cortex, corpus callosum, subventrical zone, thalamus and many more specific regions in both 2D and 3D in mouse brain.

Another crucial step in sample preparation of MALDI-MSI is the application of the matrix onto the tissue sections which should be optimal for the sensitive desorption/ionization of analyte molecules from small raster spots while ensuring minimal damage on the spatial integrity of the sample and minimal analyte migration. Several matrix deposition strategies have been reported such as thin-layer chromatography (TLC) sprayer[670] which provides effective analyte incorporation, but can also lead to substantial spatial spreading of the analyte molecules. ImagePrep (Bruker Daltonics, Bremen, Germany)[671] which utilizes 'vibrational vaporization' to generate a spray of matrix droplets and the SunCollect sprayer (SunChrom, Friedrichsdorf, Germany) which utilizes pneumatic sprayer[672] are commercial instruments and they can both provide crystal sizes below 50 μm in diameter which is not optimal for high-spatial resolution MALDI mass spectrometry imaging. CHIP-1000 (Shimadzu Corp., Kyoto, Japan) which is based on piezoelectric technology, and the spotter from Labcyte (Sunnyvale, CA, USA) which is based on acoustic droplet deposition are spotting devices both provide good desorption/ionization but the spot sizes which is ~200 μm are not optimal for high-spatial resolution.[673] HTX TM-Sprayer (HTX Technologies, Carrboro, NC, USA) (Figure 13a) allows users to adjust both gas flow rate and nozzle

velocity to control drying time which has a heated nozzle making a narrow aerosol of matrix droplets and this prevents analyte delocalization while providing well matrix/analyte incorporation and small crystal sizes for high-spatial resolution MALDI-MSI.[554] This sprayer has been utilized for high-spatial resolution imaging of several analytes within the tissue sections including lipids, metabolites, peptides and proteins.[388, 554, 588, 632]

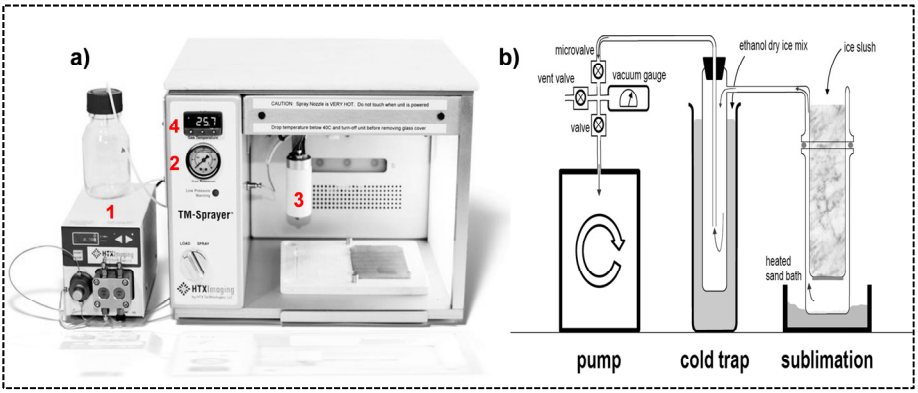

Figure 13. Matrix-coating strategies for high-spatial resolution MALDI-MSI. a) The schematic of HTX TM-Sprayer combined with an a1) isocratic pump. HTX TM-Sprayer allows users to adjust both a2) gas flow rate and a3) nozzle velocity to control drying time which has a a4) heated a3) nozzle making a narrow aerosol of matrix droplets and this prevents analyte delocalization while providing well matrix/analyte incorporation and small crystal sizes for high-spatial resolution MALDI-MSI. b) The schematic of sublimation-based matrix coating experiment. The sublimation apparatus is connected to a primary vacuum pump via a connection valve. To capture sublimated matrix particles, a cold trap is inserted between the sublimation system and the vacuum pump. For the sublimation, the matrix is homogenously dispersed in the bottom of the sublimation chamber and the system is closed and after stabilization of vacuum was assured, sublimation is initiated by placing the bottom of the sublimation apparatus in a sand bath which is pre-heated. Panel a, image credit: HTX Technologies. Panel b, reprinted by permission from ASMB, From whole-body sections down to cellular level, multiscale imaging of phospholipids by MALDI mass spectrometry, Chaurand, P., Cornett, D. S., Angel, P. M., and Caprioli, R. M. Molecular & Cellular Proteomics 2011, 10, O110. 004259.

Another matrix application strategy for high-spatial resolution MALDI-MSI is sublimation-based matrix coating.[599] Figure 13b depicts a sublimation apparatus which is connected to a primary vacuum pump via a connection valve. To capture sublimated matrix particles, a cold trap is inserted between the sublimation system and the vacuum pump. For the sublimation, the matrix is homogenously dispersed in the bottom of the sublimation chamber

and the system is closed and after stabilization of vacuum was assured, sublimation is initiated by placing the bottom of the sublimation apparatus in a sand bath which is pre-heated.[674] Matrix-sublimation provides small crystal sizes (depending on the matrix molecule) and purified matrix coating over the tissue sections which is optimal for high-spatial resolution imaging analysis.[598, 599] However, a molecule should be easily sublimated without the need for high-temperatures and the molecular integrity should be protected at the sublimation temperatures. To increase the incorporation of the analyte/matrix molecules, sublimation can be followed by recrystallization which provides better sensitivity while preserving the spatial resolution.[675] Matrix sublimation/recrystallization is particularly efficient for high-spatial resolution peptide/protein MALDI-MSI due to the need for matrix/analyte incorporation and thus their efficient desorption/ionization.[534]

While lipid MALDI imaging MS analysis can be often performed without a tissue treatment prior to matrix deposition. Peptide and protein MALDI imaging MS require a washing step to remove the lipids and salts from the tissue surface which decreases ion suppression effects, increases the incorporation of peptide/protein molecules within the matrix crystals and thus provides better desorption/ionization. However, washing process can potentially increase molecular diffusions by removal of the lipid compartmental substructure and might impair the tissue integrity. A combination of several organic solvents including acetonitrile, ethanol, methanol, propanol, acetone along with the solutions of trifluoroacetic acid, acetic acid and more aggressive chemical reactive solvents like dichloromethane, chloroform and hexane is used for tissue washing prior to matrix deposition for protein MALDI-MSI.[534, 676, 677] On the other hand, tissue treatment with buffer solutions have also been applied prior to matrix deposition (either via spraying or sublimation) for some lipid MALDI-MSI analysis to decrease the salt adducts and/or increase the signal intensity of lipids in MALDI-MSI analysis.[605, 678]

3.6 Immunohistochemistry and Microscopy

The term Antikörper (the German word for antibody) was first introduced by Paul Ehrlich in the conclusion of his article "Experimental Studies on Immunity," published in October 1891. Paul Ehrlich described his theory of antibody in 1897 proposing that the receptors on the cell surface could specifically bind to toxins and stimulate the production of antibodies.[679] The concept of attaching a fluorescent dye to an antibody to localize its respective antigen in a tissue section was introduced by Albert H. Coons[680] and together with later developments this has become a milestone for many fields of biomedical research to detect and localize individual or multiple antigens in situ.

An antibody, also known as an immunoglobulin (Ig), is a large Y-shaped glycoprotein, used by the immune system to neutralize pathogens such as bacteria and viruses and other infectious agents. There are five classes of antibodies: IgG, IgA, IgM, IgE and IgD in mammals, and IgG which is one of the most abundant proteins in serum, provides the majority of antibody-based immunity. This binds the antigen and recruits other cells against the antigens of invading pathogens and which are generated during the secondary immune response and produced by B lymphocytes. IgM, which is another important antibody, eliminates pathogens in the early stages of B cell mediated immunity before there is sufficient IgG.

The "Y" shaped IgG molecule consists of four polypeptide chains including two identical light and two identical heavy chains which are connected by disulfide bonds. The forked portions of the "Y" on the antibody are called Fab (Fragment, antigen binding) which is the responsible region for antigen binding. Further, being the most abundant immunoglobulin in the serum, IgG is often used in the production of antibodies for immunoassays.

Polyclonal antibodies are produced by immunization of suitable animals, usually mammals, and are derived from different types of immune cells. IgG specific for the antigens injected into the animal are produced by B lymphocytes as immune response which is followed by the purification of these immunoglobulins from the animal's serum. In contrast, monoclonal antibodies are identical because they are derived from a single immune cell line which is a clone of single parent cells. Monoclonal antibody production uses a fusion method called "hybridoma" which involves the fusion of cancer cells and mammalian cells that produces an antibody in immunized animal and this fusion replicates the cells endlessly and stimulates the production of the antibody. Goats, horses, guinea pigs, hamsters, mice, rats, sheep and

chickens are mostly used for the production of polyclonal antibodies whereas rabbit and mice (more often) are also used for monoclonal antibody production.

Antigen-antibody immunoreaction can be observed in the microscope via labeling of the antibody with enzyme, fluorophore, colloidal gold or biotin. While enzyme labels such as commonly used horseradish peroxidase (HRP) and calf intestinal alkaline phosphatase (AP) are usually coupled to secondary antibodies or to avidin, they can be visualized in the light microscope via enzyme-histochemical chromogenic reactions. For example, histochemical detection of peroxidase is based on the conversion of aromatic phenols or amines, such as widely-used enzyme substrate diaminobenzidine (DAB), into water-insoluble brown pigments in the presence of hydrogen peroxide (H_2O_2). Several other enzyme substrates are available such as 3-amino-9-ethyl carbazole (AEC, red) and tetramethylbenzidine (TMB, blue) producing distinct colored pigments and this can be used for multicolor immunostaining of the antigens within the tissue sections. However, large deposits of chromogen molecules prevent a second antigen staining in the same cellular compartments such as nucleus, membranes or cytosol and thus prevent their simultaneous visualization. Nevertheless, multicolor fluorescence immunostaining can allow simultaneous immune visualization of multiple antigens down to subcellular levels using fluorescent antibodies. Primary antibodies can be labeled with fluorescent dye before their use for the antigen binding or primary antibodies and can be applied without labeling which is followed by their visualization with secondary antibodies that are labeled with fluorescent dyes. While primary antibodies that are produced in different species can be labeled and used for the visualization of multiple tissue/cell antigens, the appropriate combination of primary antibodies from different host species is often not available. This is because, primary antibodies produced in the same host species (e.g. rat or mouse) and the secondary species-specific antibodies can cross-react with each of the primary antibodies.[681] However, if primary antibodies of the same species belong to different IgG isotypes, they can be selectively detected with secondary antibodies directed against the corresponding isotype.

The use of directly labeled antibodies is advantageous in many aspects including elimination of secondary reagents, lower backgrounds, faster analysis and lower perturbation of the tissue/cell due to less washing and chemical treatment. Advanced spectroscopic techniques such as Fourier-transform spectroscopy-based hyperspectral imaging can be used to simultaneously image multiple antigens via covalently labeled primary antibodies.[682] Further, as also explained in detail above in the MSI section,

imaging mass cytometry[492] and multiplex ion beam imaging[495] are emerging methods for the visualization of multiple antigens using primary antibodies.

Although it is not usually practiced, gold-labeled antibodies are also used in general histochemical analysis due to the high electron density of the gold particles which makes them visible in the electron microscope without further treatment. For electron microscopical immunolabeling, gold particles are available with sizes from 6 to 25 nm. Gold nanoparticles can be enlarged with subsequent use of silver enhancement technique which involves the reduction reaction of silver causing its build up preferentially on the surface of the gold particles and resulting their intense brown/black staining conjugated to proteins A and G or to antibodies on the analyte specimen. Therefore, gold particles can be visualized at much lower magnifications; even in the light microscope which provides a greater overall sensitivity and far greater resolution than other immunocytochemical method and can be counterstained with other staining techniques.

Bacterial proteins; protein A and protein G can bind to Fc“tail” (Fragment, crystallizable) region of an antibody composed of two heavy chains on the C-terminal side. Protein A and protein G can be used in immunohistochemistry using secondary anti-IgG antibodies to make an antigen–IgG complex which is then visualized by incubation with labeled protein A or protein G. Molecular weights of protein A and protein G (MW~40 kD) which is far smaller than IgG (MW ~150 kD), and therefore they can be exploited in electron-microscopy immunohistochemistry via colloidal gold tagging (protein A, G-gold) complexation which is followed by monoclonal and/or polyclonal primary antibody reaction for the detection/visualization of several antigens directly under the electron microscope.[683, 684]

3.7 Multivariate Analysis

MSI data are usually analyzed with direct spatial visualization of single ion images, each of which is assigned to a color code. However, the combination of spatial and mass resolution in MALDI-MSI results in large and complex data sets in which single ion images do not identify the spatially localized correlations between analytes that are latent in the data. Therefore, a set of multivariate analysis techniques are used for the analysis of data sets that contain more than one variable which are especially valuable when working with correlated variables.

Principal component analysis (PCA) is the most widely used unsupervised multivariate method that transforms a number of (possibly) correlated variables into a number of uncorrelated variables called principal components (PC). PCA was invented as an analogue of the principle axis theorem in mechanics by in Karl Pearson in 1901.[685] Several MS spectrum in large MSI data becomes like a collection of points in multidimensional space. The first PC is the "best fitting" line which minimizes the average squared distance from a point to the line which is then followed by the next best-fitting lines which are orthogonal to one another and this means that different individual dimensions of the data are uncorrelated. Thus PCA reduces the dimensionality of the data with these vectors (PCs) to a 2D or 3D coordinate system which makes it possible that those spectra with similar variation characteristics can be clustered together and the differences between sample groups can be readily visualized in the system.[686] The initial PCs (one or two) often cover the majority of variance between the samples, which turns original multidimensional data matrix in a 2D plot such as PC2 vs PC1. The PCA score plot indicates the similarities and differences between the ion patterns of the mass spectra obtained from the samples. The loading plots reveal the information about the contribution of each ion signal to the variance covered by each respective principle component.

Another approach for multivariate analysis is partial least square (PLS) regression analysis which is a supervised multivariate approach that addresses the multicollinearity problem by computing latent vectors which explains both the independent and the dependent variables.[687, 688] PLS regression analysis combines PCA and multiple linear regression (MLR). MLR relies purely on factors extracted from predictive (X) and observed variables (Y). However, PLS also performs regression modelling of covariance in these predictive and observed variables (X/Y) and projects these into a new space. For PLS regression, the score of the units as well as the loadings of the variables can be plotted as in PCA, and the

dependent variables can be estimated as in MLR. Orthogonal partial least squares (OPLS)[689] is a common variant of PLS which aims to relate a set of predictor variables (X) to one or more responses (Y) and uses orthogonal signal correction to maximize the explained covariance between X and Y on the first latent variable (LV), while the remaining LVs capture variance in the predictors which is orthogonal, i.e. statistically uncorrelated to the response variables which filters out the structured noise in the data and reduces the model's complexity by lowering the number of LVs, and thus allows the analysis and investigation of the main source of orthogonal variation.

Cluster analysis is another unsupervised multivariate approach along with the PCA. Cluster analysis aims for the detection of natural partitioning of the objects by grouping observations that are similar into homogeneous subsets which may reveal patterns related to the phenomenon under study. Most common clustering analysis techniques used in MALDI-MSI data analysis are hierarchical cluster analysis (HCA) and K-means clustering.[690] HCA finds relatively homogeneous clusters of cases based on dissimilarities or distances between objects. It starts with each case as a separate cluster, and then combines the clusters sequentially, reducing the number of clusters at each step until only one cluster is left. A resulting hierarchical tree diagram (dendrogram) indicates the linkage points: the clusters are linked at increasing levels of dissimilarity.[691] Kmeans uses an iterative algorithm which partitions the dataset into Kpre-defined distinct non-overlapping subgroups (clusters) where each data point belongs to only one group and it iterates the similarity of the inter-cluster points whereas keeping the clusters as different as possible.

A number of multivariate image analysis methods have been used to interrogate MALDI-MSI data from tissues and single cells such as spatial segmentation of histological and/or histopathological features within the tissues[692, 693] along with the studies of metabolic heterogeneity of cells.[694]

4 RESULTS AND DISCUSSION

In this chapter, I will discuss the results of each paper included in this thesis focusing on the major findings with an updated look.

4.1 Paper I

Development of "Static" MALDI for Subsequent Fluorescence and Immunofluorescence Analysis of the Same Tissue Section: Implications for Probing Spatial Amyloid Plaque-Associated Lipid Biochemistry

MALDI-MSI of lipids and a subsequent immuno/fluorescence staining of the same tissue section can be a strong asset to correlate spatial lipidomics MSI data with the optical microscopy imaging and this can be useful to dissect the region-specific lipid biochemistry in association with the histological and/or histopathological features. While MALDI is an efficient ionization technique for variety of lipids as explained in detail before, the laser desorption process can induce mechanical and chemical damage of the tissue surface particularly when nanosecond lasers used which can induce thermal effects and which are employed by majority of the commercial MALDI instruments. However, the laser ablation process during MALDI is dependent on the matrix (along with the instrumental parameters) which can determine dynamics of the laser desorption/ionization such as the thermal diffusion over the matrix-coated analyte surface (e.g. a tissue section). Hence, the physicochemical nature of a matrix molecule might be used to circumvent undesired laser ablation effects.

Proton affinity and ionization energy of a matrix molecule affect energy transfer involved in proton and electron transfer. As mentioned before, several matrix (m) ions are observed in MALDI MS spectrum such as $m^{\cdot+}$, $m^{\cdot-}$, $(m+H)^+$, mNa^+, $(m-H)^-$ and it has also been reported that rare species such as H atoms also exists in the MALDI plume which can make the existence of radicals like $(m-H)^{\cdot}$ likely.[695] Several common matrices are able to form radical ions; however, their electron transfer ability is not efficient, being the competing proton transfer much more favored in the MALDI plume. 1,5-DAN matrix is an interestingly effective matrix for many purposes including the reductive properties for peptide/protein in-source decay fragmentation,[542] and it is an efficient electron transfer matrix.[571] 1,5-DAN leads to formation of odd electron molecular ions $M^{+\cdot}$ with remarkably high yield which is contrary to what is usually observed for many common MALDI matrices, whereby the formation of protonated adducts $[M + H]^+$ is prevailing.[696]

This can be explained with the low-ionization energy of 1,5-DAN which is i.e., 6.74±0.2 eV[697] and this can allow the formation of radical matrix ions of 1,5-DAN through two photon ionization mechanisms. Hence, this can also favor the electron transfer reactions for the ionization of analyte molecules yielding analyte radical ions and neutral matrix molecules in the MALDI plume.[514]

While there are other electron transfer matrices such as 2,2':5',2''-terthiophene (TER),[698] trans-2-[3-(4-t-butyl-phenyl)-2-methyl-2-propenylidene] malononitrile (DCTB),[699] and 9,10-diphenylanthracene (DPA),[700] these molecules are non-polar and they are mainly used for MALDI-MS analysis of electroconjugated polymers and/or coordination compounds. Therefore, 1,5-DAN is more favorable for lipid MALDI-MSI analysis, in part, for the following reasons. Firstly, 1,5-DAN is a polar basic molecule and can provide electron transfer ionization of analytes along with the charge transfer reactions in MALDI plume which can provide ionization of a wide-range of molecules with different ionization behaviors and secondly, the physicochemical properties of 1,5-DAN molecule is optimal for the efficient matrix application strategies, notably, the sublimation approach for high-spatial resolution MALDI-MSI of lipids on tissue sections.

I used sublimation-based matrix coating because it provides small crystal size with uniform morphologies favoring higher effective temperature via hindered heat dissipation during laser irradiation of the surface which can increase the analyte ion signals at high-spatial resolutions. Considering the features of "smart beam" (above mentioned in detail) which is a modified structured beam profile containing needle-like local maxima and the ionization features of 1,5-DAN matrix molecule, MALDI ionization of several lipid molecules at low laser fluences should be possible. Thus, 1,5-DAN, via sublimation approach, outperforms several common MALDI matrices for MALDI-MSI of lipids of tissue sections in both negative and positive polarities.[598, 635]

I firstly optimized the matrix thickness and homogeneity of the matrix distribution over the brain tissue sections. I concluded that a thin-layer of matrix is highly efficient for lipid ionization at low laser fluences when the laser pulse energies and number of laser shots are carefully optimized.[635] I investigated the efficiency of 1,5-DAN matrix for MALDI-MSI of lipids on mouse brain tissue sections at different number of laser pulses and laser pulse energies. I observed that using high laser pulse energies (e.g. either with 5 or 50 laser shots) during MALDI-MSI of lipids in negative polarity can induce mechanical damage on tissue surface which is visible with fluorescence

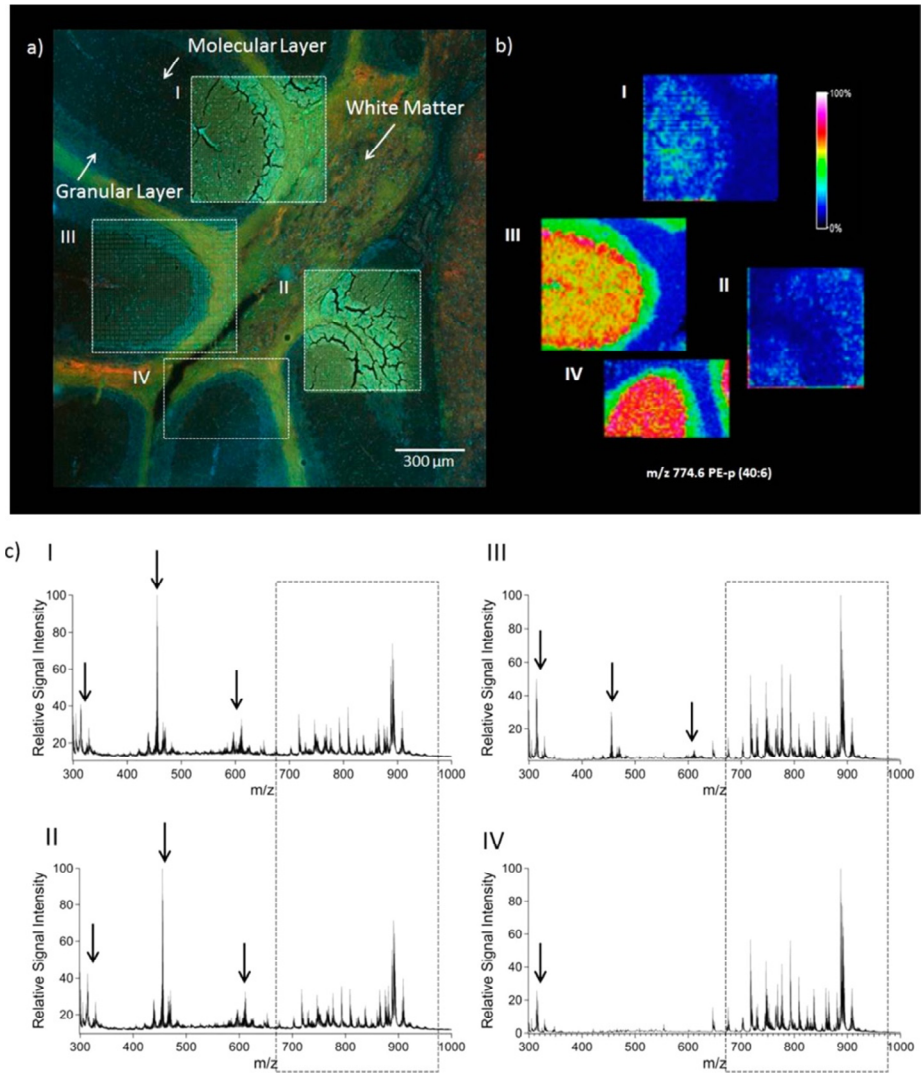

Figure 14. Four different sections on mice cerebellum region analyzed with different parameters of MALDI imaging mass spectrometry: (aI) 100 of 50% energy laser shots, (aII) 5 of 50% energy laser shots, (aIII) 100 of threshold-energy laser shots, and (aIV) 5 of threshold-energy laser shots in reflective negative ion mode followed by immunohistochemistry and fluorescent staining. Corresponding single-ion images of PE-p (40:6, m/z 774.6) and full-range MS spectra of the same sections are shown in panels bI−IV and cI−IV, respectively. Highlighted regions in the spectra (650−950 Da) show relative signal intensity of lipids. Arrows in between 300 and 650 Da mass range indicate 1,5-DAN matrix cluster ions. Percent energy stands for density wheel setting. Imaging data were acquired with a spatial resolution of 10 µm. Antiglial fibrillary acidic protein (GFAP, green), anti-βIII-tubulin (red), and

fluorescent stain 4,6-diamidino-2-phenylindole (DAPI, blue) were used to visualize radial glial cells, cytoskeleton, and cell nuclei, respectively, allowing us to highlight the molecular layer, the granular layer, and the white matter. Reprinted with permission from Kaya, I., Michno, W., Brinet, D., Iacone, Y., Zanni, G., Blennow, K., Zetterberg, H., and Hanrieder, J. r. Histology-Compatible MALDI Mass Spectrometry Based Imaging of Neuronal Lipids for Subsequent Immunofluorescent Staining, Analytical Chemistry 89, 4685-4694, copyright (2017), American Chemical Society.

microscopy imaging of the cerebellum region in the same brain tissue section which was immuno-stained (Figure 14a I, II). The mechanical damage observed with fluorescence microscopy was prevalent in the grey matter compared to the white matter which indicates tissue-type specific laser ablation dynamics (Figure 14a I, II). Further, high laser pulse energies also resulted in extensive matrix oligomer formation and lower lipid signal intensity as observed in the MS spectrum (Figure 14 c I, II). Some of the possible molecular structures of dimeric, trimeric and tetrameric oligomers of 1,5-DAN were shown in Figure 15. I observed signals of these oligomers along with the signals of 1,5-DAN monomers in the MS spectra obtained with both polarities[635] and some of these oligomeric structures have been previously observed and proposed within LDI-MS spectrum of 1,5-DAN using high-mass resolution mass spectrometer.[696]

Low-energy laser pulses (only 5-10) provide better ionization of lipids when using only few number laser shots (Figure 14 cIV) and there was no laser ablation effects observed with fluorescence microscopy imaging of the following immunofluorescence staining (Figure 14 aIV). I observed diminished trimeric and tetrameric matrix oligomers and increased lipid signal intensities when low-energy five laser shots were used for MALDI-MSI of lipids in negative polarity (Figure 14 cIV). Increased number of laser pulses (such as 100 laser shots), even at low-energies, still induced laser ablation signatures which were observed in the microscopy images of the subsequent immunofluorescence staining of the same cerebellum regions (Figure 14 aIII). Please read the original paper for the details of laser ablation effects on the tissue surfaces. Further, increasing the number of laser shots didn't increase lipid signal intensities and resulted in extensive matrix oligomer signals as observed in the MS spectrum (Figure 14 cIII). The effects of laser pulse energy and/or number of laser shots on the quality of PE-p (40:6, m/z 774.6) ion images are visualized in Figure 14b.

Consequently, the results suggest that when the matrix thickness is optimized carefully, 1,5-DAN mediates ionization of lipids with low-energy few number of laser pulses and the quality of the lipid MS spectra decreases with

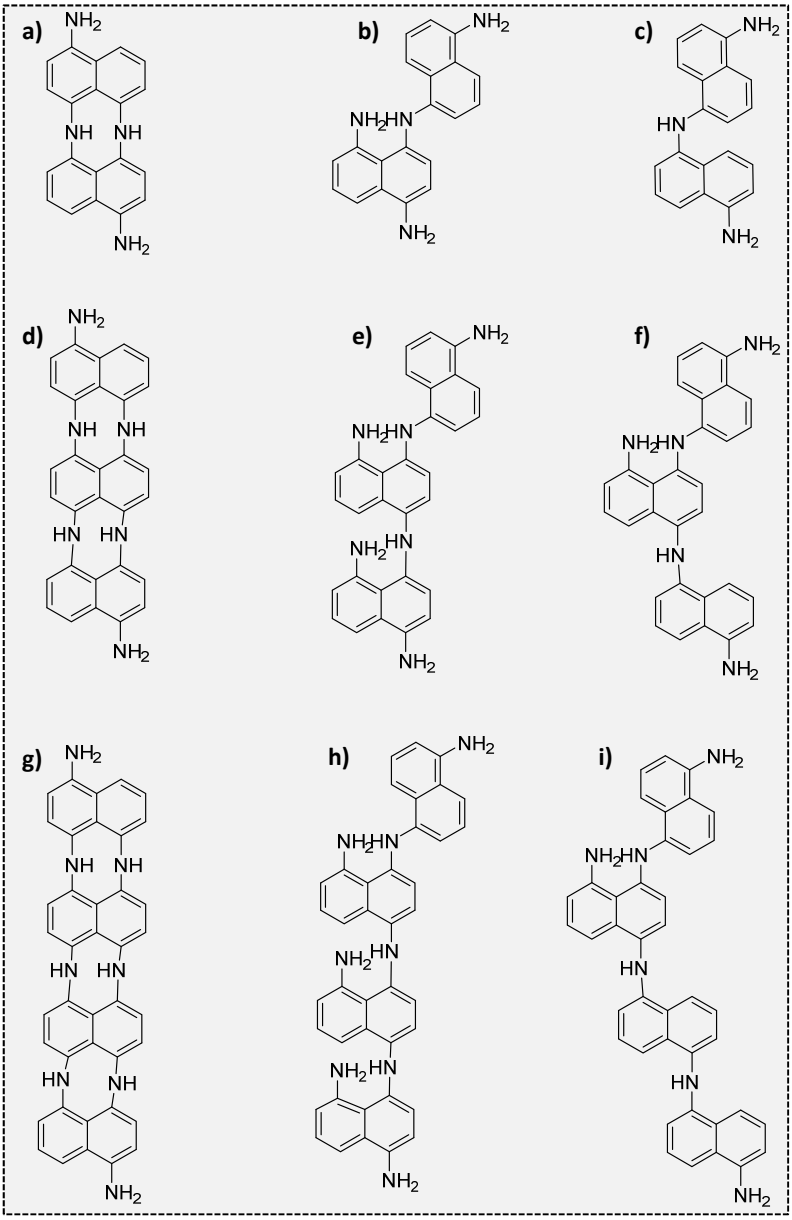

Figure 15. Possible molecular structures of several laser-irradiation induced oligomeric; a, b, c) dimeric, d, e, f) trimeric and g, h, i) tetrameric matrix clusters of 1,5-diaminonapthelene (1,5-DAN) observed in both MALDI-MSI of the tissue sections and LDI-MSI analysis of the matrix molecule alone when high laser pulse energies and/or high-number of laser shots are used. These oligomeric 1,5-DAN matrix clusters are observed in both negative and positive polarities in MALDI-MSI and LDI-MS analysis.

the increasing laser pulse energies and number of laser shots. This can be explained as follows; 1,5-DAN ionizes with low-energy and produces radical $m^{\bullet+}$, m^{-} matrix ions (along with the other matrix ions) which can mediate efficient ionization of brain lipids in both polarities. The initial few number of laser pulses at low pulse energies provides optimum ionization of lipids via electron transfer together with the other mechanisms including charge transfer as the matrix/analyte ratio is optimal. Note that, electron transfer reactions will result in neutralized radical matrix ions. Lipid molecules which have intrinsic charge on their molecular structures will be also readily desorbed into the gas phase and detected with MS using only low-energy few numbers of laser shots and thus this will minimize the undesired gas-phase reactions leading matrix cluster formation and lipid fragmentation. However, increased laser energies and number of laser shots seemed to increase the matrix oligomer formation and lower lipid signals which suggest a competition between matrix oligomer formation and ionization of lipids via radical matrix ions. This suggests a kind of threshold for the optimum ionization of the lipids within the first few efficient laser pulses. Hence, this shall remind MSI scientists the low primary ion dose density ("static") SIMS developed by Alfred Benninghoven.[364] Static SIMS proposes and demonstrates that the initial low primary ion doses provides efficient ionization of the molecules from the top surface of the analytes, while the bombardment process with high ion doses causes damage on the surface resulting a carbon residue accumulation from molecular fragmentation of the surface which suppresses the ionization. Therefore, I can name this approach "static" MALDI-MSI of lipids which is possible when 1,5-DAN is used as the matrix via sublimation approach as explained in this paper and thesis.

Static MALDI does not only provide enhanced lipid MS spectrum at high-spatial resolutions but also makes it possible to perform subsequent immunofluorescence or fluorescence staining of the same tissue section analyzed with high-spatial resolution MALDI-MSI. Therefore, as a proof of concept, I utilized "static" MALDI-IMS for lipids in negative polarity (at 10 µm spatial resolution) for probing amyloid plaque-associated lipid biochemistry within a cortical region of a sagittal brain tissue section of an Aβ-deposition Alzheimer's mouse model (tgSwe). Then, this is followed by a subsequent staining of amyloid with a fluorescent amyloid probe called heptameric formylthiophene acetic acid (hFTAA) (Figure 16). Static MALDI has a great potential for correlative spatial lipidomics and fluorescent staining of the same tissue sections for dissecting region-specific lipid biochemistry.

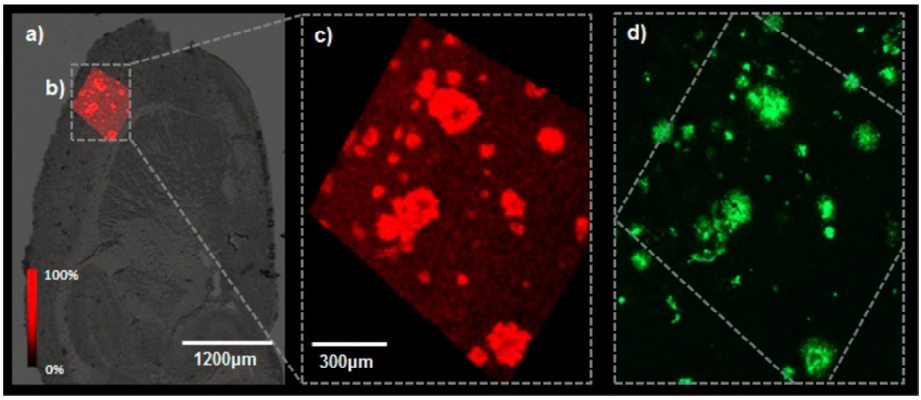

Figure 16. "Static" MALDI-IMS of lipids in negative polarity (at 10 µm spatial resolution) for probing amyloid plaque-associated lipid biochemistry within a cortical region of a sagittal brain tissue section of an Aβ-deposition Alzheimer's mouse model (tgSwe) which is followed by subsequent staining of amyloid of the same tissue section with a fluorescent amyloid probe called heptameric formylthiophene acetic acid (hFTAA). (a) Bright-field image of sagittal tgSwe mouse brain tissue section. (b) High-resolution (10 µm) MALDI-IMS-analyzed cortical region using static MALDI-MSI. (c) Ion image of ceramide [Cer (d18:1/18:0), m/z 564.6] species which is correlated with (d) high-resolution fluorescence microscopy image of amyloid aggregates. Reprinted with permission from Kaya, I., Michno, W., Brinet, D., Iacone, Y., Zanni, G., Blennow, K., Zetterberg, H., and Hanrieder, J. r. Histology-Compatible MALDI Mass Spectrometry Based Imaging of Neuronal Lipids for Subsequent Immunofluorescent Staining, Analytical Chemistry 89, 4685-4694, copyright (2017), American Chemical Society.

For example, in a follow-up study, we used static MALDI followed by fluorescent staining of amyloid aggregates for probing alterations of lipids in amyloid plaques with a structural specific manner (e.g. plaques which are cored/compact and diffuse).[701]

4.2 Paper II

Development of Dual Polarity MALDI-MSI on the Same Pixel Points and "Trimodal" MALDI Mass Spectrometry Imaging (IMS3): Implications for Probing Molecular Pathology of Amyloid Plaques

A tissue section is composed of a myriad of biomolecules such as lipids, metabolites, peptides, proteins and many more. While MALDI is a versatile ionization technique, majority of the MALDI-MSI experiments target a specific group of molecules such as lipids, proteins or metabolites due to the suitability of the matrix molecules for different range of molecules, different sample preparation requirements for many biomolecules and the need for optimal instrumental settings for targeted compounds. Therefore, correlation of different groups of molecules is usually hindered. Multimodal MALDI-MSI methods for probing different groups of molecules within the same tissue sections would enhance the molecular information obtained from the very same histological and histopathological features which would increase the understanding of molecular interrogation in functioning or dysfunctioning organs.

In this communication, I developed a three-step multimodal MALDI-MSI method for imaging of lipids in dual polarity and peptide/proteins within the same region in the mouse brain tissue sections. For this purpose, I used two matrix molecules; 1.5-DAN and 2,5-DHA for lipid and protein imaging, respectively. The success of this trimodal MALDI-MSI method lies behind the synergy of using these two matrix molecules with their distinct but complementary desorption/ionization mechanisms upon laser irradiation.

As mentioned above, static MALDI using 1,5-DAN matrix via sublimation-based matrix coating approach assists ionization of lipid species with low-energy few laser pulses, particularly in negative polarity. Therefore, it yields a good-quality lipid MS spectrum while inducing minimal perturbation (and limited matrix loss) on the laser irradiated pixel spot. Thus, a subsequent analysis of lipids in positive polarity should be possible on the very same pixel points. I tested this hypothesis and discovered that 1,5-DAN allows dual polarity MALDI-MSI of lipids on the mouse brain tissue sections at 10 µm spatial resolution (Figure 17a,b). The quality of the MS spectrum obtained with the subsequent positive polarity MALDI-MSI imaging on the analyzed pixel points was comparable with the one obtained from a non-irradiated pixel point.[632] Dual polarity MALDI-MSI on the same pixel points allows correlation of the ion images of various lipids obtained in negative and

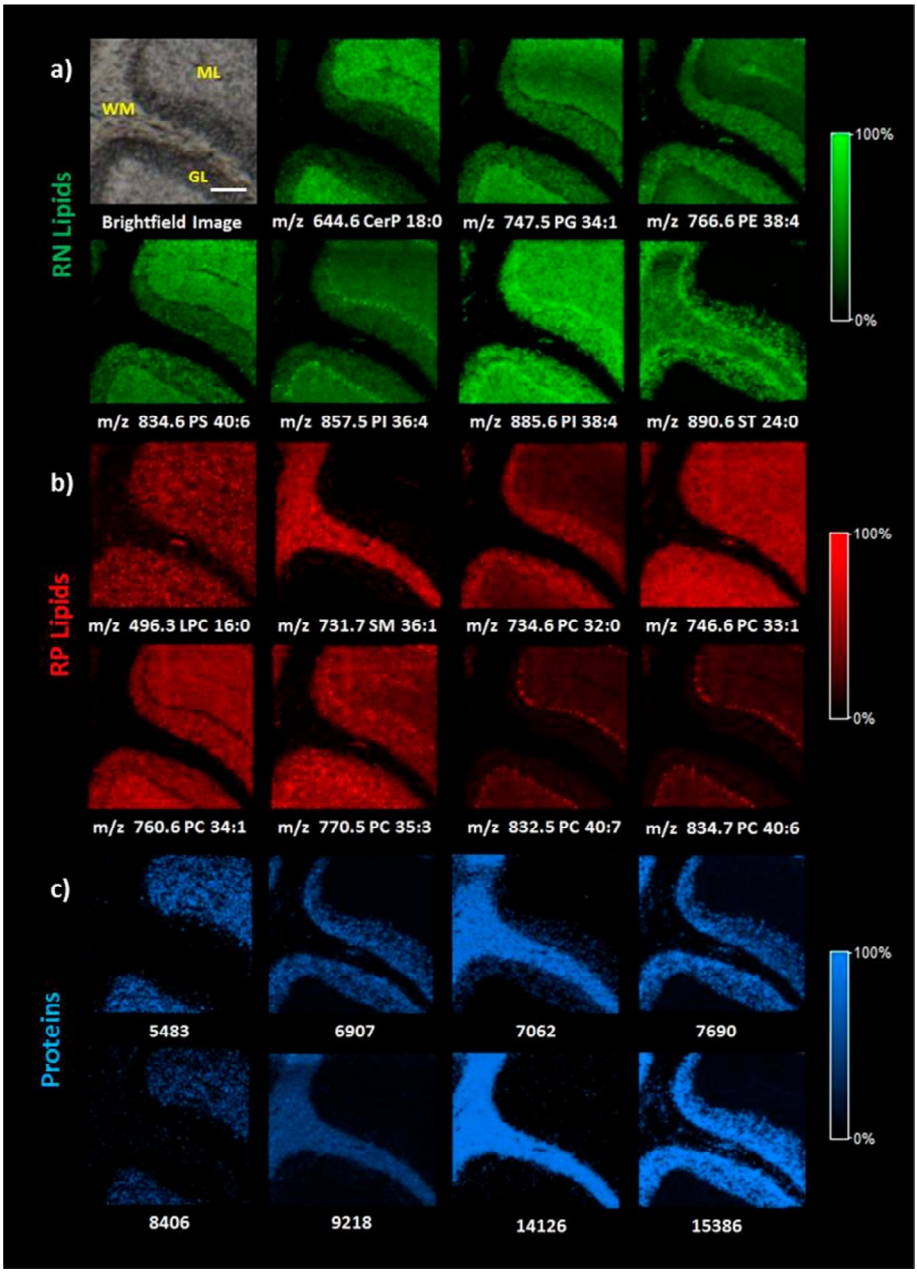

Figure 17. High-spatial resolution (10 µm) trimodal MALDI imaging MS data acquired on the same IMS region in mouse cerebellum. (a, b) Dual polarity MALDI-IMS of lipids in a) negative and b) positive ion modes was followed by c) high-spatial resolution (10 µm) protein imaging on the same IMS region. c) Protein signals were assigned based on the accurate mass

and literature values including: m/z 5483 cytochrome c oxidase 7c (Cox7c); m/z 6907 histone H2B $[M+2H]^{2+}$; m/z 7062 myelin basic protein (MBP) 14 kDa $[M+2H]^{2+}$; m/z 7690 histone H3 $[M+2H]^{2+}$; m/z 9218 MBP 18 kDa $[M+2H]^{2+}$; m/z 14 126 MBP 14 kDa; m/z 15 386 histone H3. m/z 8406 could not be assigned. WM, ML, and GL represent white matter, molecular and granular layers, respectively. Scales bar in panel a, 200 μm. Reprinted (adapted) with permission from Kaya, I., Brinet, D., Michno, W., Başkurt, M., Zetterberg, H., Blennow, K., and Hanrieder, J. r. Novel Trimodal MALDI Imaging Mass Spectrometry (IMS3) at 10 μm Reveals Spatial Lipid and Peptide Correlates Implicated in Aβ Plaque Pathology in Alzheimer's Disease, ACS chemical neuroscience 8, 2778-2790. Copyright (2018), American Chemical Society.

positive polarities from the same regions in the mouse cerebellum (Figure 17a,b). This methodology has been utilized to image various lipids in dual polarity within subtle histological regions on the tissue sections of rat small intestine in a parallel study.[560]

Nevertheless, even after applying dual polarity MALDI-MSI of lipids on the same pixel points, there is still shouldn't be a significant perturbation on the tissue surface. Thus, one could envision that dual polarity MALDI-MSI can be followed by a subsequent immunohistochemical staining or a subsequent protein MALDI-MSI analysis on the same region of the same tissue section. I hypothesized that subsequent MALDI-MSI analysis of peptides/proteins after dual polarity MALDI-MSI (using 1,5-DAN) should be feasible. However, 1,5-DAN cannot be used for desorption/ionization of proteins and peptides; it rather assists their in-source decay fragmentation as explained before.[702]

2,5-DHA is a highly sensitive MALDI matrix molecule for MS detection and MSI of proteins within the tissue sections.[388, 533, 536, 703, 704] While it absorbs UV light at 355 nm efficiently, experimental results of multiphoton dissociation and ionization indicate that the photoionization occurs in the gas phase after 2,5-DHA vaporizes from the solid phase and may not play an important role in the MALDI process.[705] This can explain the requirement of relatively high amount of acid content (≥2% TFA) in the matrix solutions of 2,5-DHA in the previous reports compared to other common matrixes.[388, 632]

It is likely that pre-protonated protein molecules can be easily desorbed using 2,5-DHA as the MALDI matrix. Therefore, after applying dual polarity MALDI-MSI of lipids in dual polarity on mouse cerebellum region, I washed away the remaining matrix molecules, lipids and salts with six-step washing protocol; 70% EtOH (30 s), 100% EtOH (30 s), Carnoy's fluid (6:3:1 EtOH/chloroform:acetic acid) (2 min), 100% EtOH (30 s), H_2O with 0.2% TFA (30 s), and 100% EtOH (30 s)[534] and applied 2,5-DHA matrix using

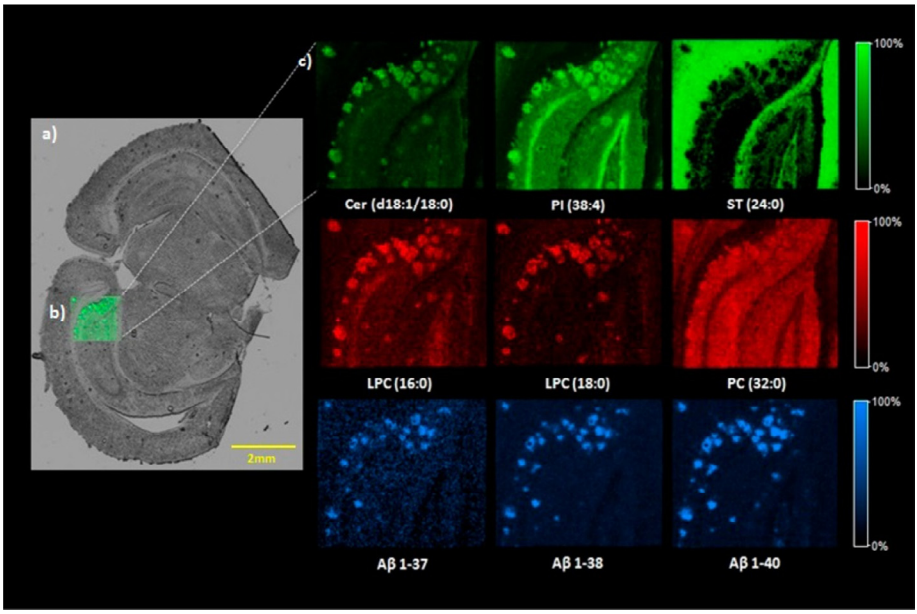

Figure 18. Hippocampal amyloid plaque-associated lipids in dual polarity (on the same points) and peptides (a) on a coronal mouse brain tissue section of transgenic AD mouse (tgArcSwe) were revealed by trimodal MALDI-IMS. (b) Hippocampal region analyzed with 10 µm spatial resolution. (c) Ion images of lipids: ceramides (Cer d18:1/18:0, m/z 564.6), phosphatidylinositols (PI 38:4, m/z 885.6), sulfatides (ST 24:0, m/z 890.6) acquired in negative ion mode (green) and ion images of lysophosphatidylcholines (LPC 16:0, m/z 496.3, (LPC 18:0, m/z 524.3) along with the posphatidylcholines (PC 32:0, m/z 734.6) acquired in positive ion mode (red). Subsequently, amyloid-β (Aβ 1–37, m/z 4002.7, Aβ 1–38, m/z 4060.3, Aβ 1–40, m/z 4257.6) peptide (blue) ion images within the same imaging region were acquired. Reprinted (adapted) with permission from Kaya, I., Brinet, D., Michno, W., Başkurt, M., Zetterberg, H., Blennow, K., and Hanrieder, J. r. Novel Trimodal MALDI Imaging Mass Spectrometry (IMS3) at 10 µm Reveals Spatial Lipid and Peptide Correlates Implicated in Aβ Plaque Pathology in Alzheimer's Disease, ACS chemical neuroscience 8, 2778-2790. Copyright (2018), American Chemical Society.

HTX TM sprayer which allowed sensitive protein MALDI-MSI at 10 µm spatial resolution.[632] Trimodal MALDI-MSI allows correlation of lipid ion images in dual polarity and protein ion images to the very same histological regions within the mouse cerebellum (Figure 17). Note that, protein MALDI-MSI in trimodal MALDI-MSI method is not on the same pixel points with the lipid imaging but only on the same histological regions due to the tissue metamorphosis during the washing protocol and wet matrix application of 2,5-DHA. Trimodal MALDI-MSI suggests a great potential for

simultaneous imaging of lipids and proteins within the same histological or histopathological features.

In order to reveal the potential of this methodology, I utilized trimodal MALDI-MSI (at 10 μm spatial resolution) for probing amyloid plaque-associated lipid (in dual polarity) and peptide alterations in the brain tissue sections of Aβ-deposition transgenic Alzheimer's mouse model (tgArcSwe). Trimodal MALDI-MSI ion images obtained from the hippocampal regions of coronal brain tissue sections revealed plaque-associated lipids in dual polarity which is correlated to the accumulations of multiple Aβ peptide species within the same amyloid plaque in a specific brain region (Figure 18).

4.3 Paper III

Shedding Light on the Molecular Pathology (Lipids in the Spotlight) of Amyloid Plaques in Transgenic Alzheimer's Disease Mouse Brain Using Multimodal MALDI Imaging Mass Spectrometry

With a sketchy description, amyloid plaques consist of accumulated amyloid-β peptides together with glial and neuritic debris. However, plaques contain a variety of other molecules with significant roles in AD pathology. While the symptoms of AD reflect a loss of neural circuit integrity in the brain, a body of evidence from molecular, immune, cellular and neuropathological studies reveals that AD is associated with the misbalance of the intricate interactions between neurons, astrocytes, microglia, oligodendrocytes and vascular cells. This makes the molecules involved in metabolism significantly important. Indeed, it might be described that the alterations of lipids in association with amyloid plaques are the mirrors of the metabolic dysfunction of the complex disease pathogenesis.

Lipidomics analyses of the brain tissue or cell extracts have been performed to interrogate the role of lipids in AD pathogenesis.[281, 299] However, these studies lack the spatial information of the individual lipid species. While one can perform lipidomics analysis of the single cells, a neuron or a glial cell does not work in isolation and an amyloid plaque is the final picture of the disease pathogenesis which reflects the interrelated pathology of the neurons and surrounding microenvironment including glial cells and extracellular matrix in situ. Therefore, single plaque-resolution lipidomics is a strong asset to interrogate lipid biochemistry of amyloid plaques. MSI makes it possible to perform region-specific single plaque-resolution lipidomics analysis and peptidomics/proteomics analysis within the post-mortem brain tissue sections of human AD patients and transgenic AD mouse models.[617, 706-712] However, all of these experiments target either lipids or peptides/proteins hindering the correlation of peptides/proteins and lipids in dual polarity to a single plaque aggregate. Hence, an extensive implication of trimodal MALDI-MSI for probing molecular pathology of amyloid plaques within brain tissue sections of transgenic AD mouse models (e.g. tgArcSwe) would be a strong asset to leverage the understanding of plaque-associated AD pathogenesis (Figure 19).

I applied trimodal MALDI-MSI on hippocampal regions in the brain tissue sections of 18-month-old tgArcSwe mouse brain at 30 µm and 10 µm spatial resolutions (Figure 19). While 30-µm imaging allows imaging of wider brain

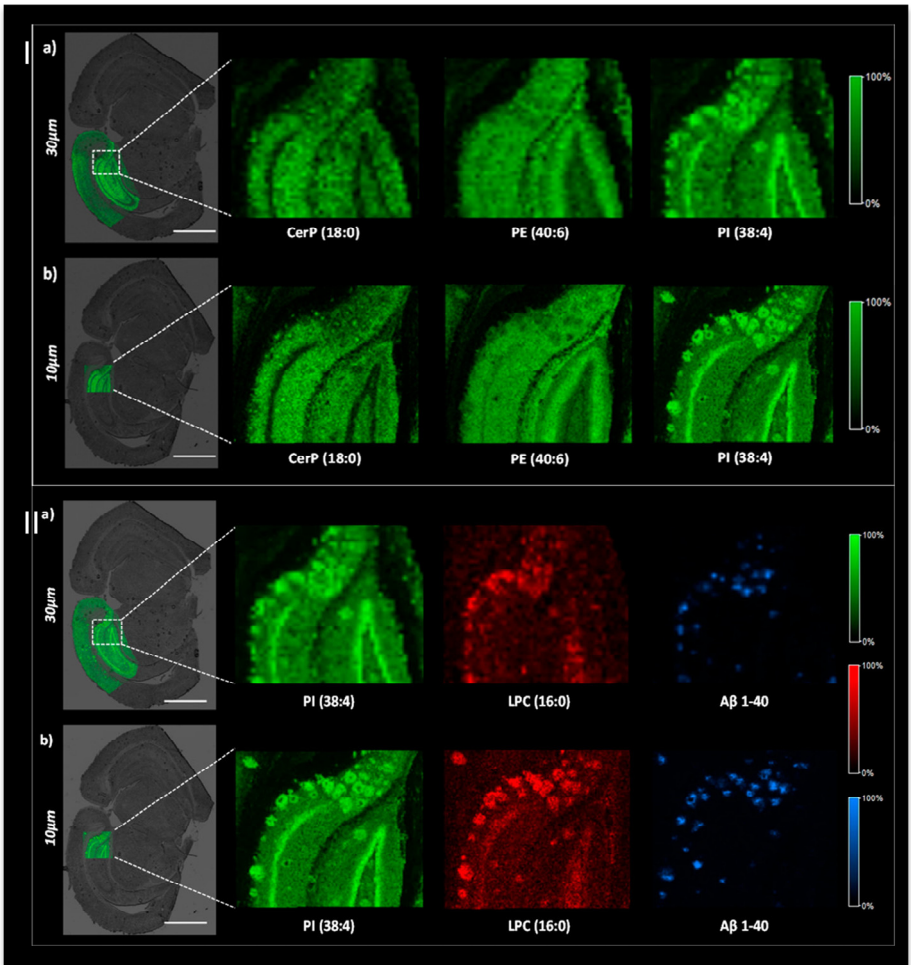

Figure 19. The power high-spatial resolution MALDI-MSI and trimodal MALDI-MSI for probing molecular pathology of amyloid plaques in tgArcSwe transgenic AD mouse model. MALDI-MSI of lipids in negative ion mode Ia) at 30 µm vs Ib) at 10 µm spatial resolutions reveal plaque-associated lipid species clearly resolved at 10 µm spatial resolution in tgArcSwe AD mouse brain.. Trimodal MALDI-MSI of lipids and peptides IIa) at 30 µm vs IIb) at 10 µm spatial resolutions reveal plaque-associated lipid species and Aβ peptides clearly resolved at 10 µm spatial resolution in tgArcSwe AD mouse brain. Reprinted (adapted) with permission from Kaya, I., Zetterberg, H., Blennow, K., and Hanrieder, J. r. Shedding light on the molecular pathology of amyloid plaques in transgenic Alzheimer's Disease mice using multimodal MALDI imaging mass spectrometry, ACS chemical neuroscience 9, 1802-1817. . Copyright (2018), American Chemical Society.

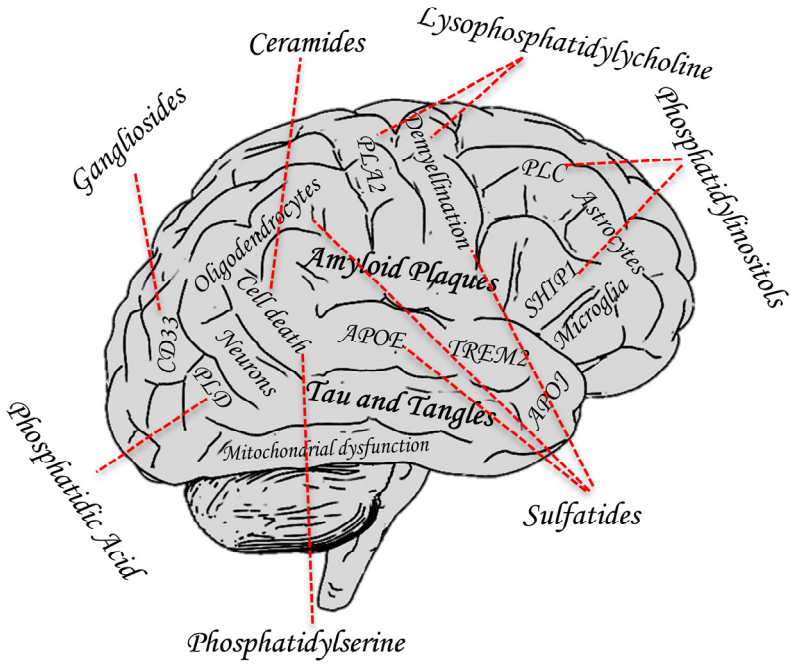

Figure 20. Alzheimer's disease (AD) is often characterized with extracellular amyloid plaques and intraneuronal hyperphosphorylated fibrillary tau tangles which are the prominent neuropathological features of AD. However, in a wider perspective, AD is associated with the misbalance of the intricate interactions between neurons, astrocytes, microglia, and oligodendrocytes. Indeed, a body of evidence links AD to innate immune system. TREM2, CD33, APOE are the prominent immune-related proteins associated with AD pathogenesis whose significance is also demonstrated by whole-genome sequencing and GWAS studies and they are directly associated with the aberrant lipid metabolism in AD. Further, phospholipases PLA_2, PLC, PLD are also associated with AD pathogenesis and lipid metabolism. Along with the plaques and tangles, demyelination and mitochondrial dysfunction are also the neuropathological features of AD which can link it to aberrant lipid metabolism. Therefore, single-plaque resolution lipidomics would help to interpret the role of lipids in amyloid plaques. Above I sketched an illustrative schematic to indicate the relevance of certain lipid species to amyloid-associated pathological features of the AD pathogenesis, immune proteins and disease-associated glial cells based on the data in the literature.

areas, 10-µm imaging reveals clearly-resolved lipid ion images in dual polarity and amyloid peptide ion images in amyloid plaques correlated to each other within hippocampal brain regions. Dual polarity MALDI-MSI analysis of lipids on the same pixel points revealed high-throughput lipid molecular information including glycerophospholipids, lysophospholipids and sphingolipids including glycosphingolipids (e.g. sulfatides, gangliosides)

which can be correlated to the ion images of individual amyloid β peptide isoforms at high spatial resolutions (10 μm). This high-throughput molecular information (particularly lipids) obtained from a single amyloid plaques in specific brain regions allowed us to interpret possible roles of lipids in association with amyloid pathology in AD. For instance, dual polarity MALDI-MSI on the same pixel points reveals accumulations of LPC species and depletion of sulfatide species within amyloid plaques which are both associated with focal amyloid plaque-associated myelin and myelin lipid degeneration. Several pathological features of AD including demyelination, mitochondrial dysfunction, glial responses (e.g. inflammation) and more specifically immune-related proteins such as TREM2, APOE, CD33 along with the phospholipases; PLA_2, PLC, PLD are associated with both amyloid pathology and amyloid-associated aberrant lipid metabolism (Figure 20). Thus, this underlies the significance of high-throughput spatial lipidomics of amyloid plaques. The roles of several lipid species in amyloid plaques were discussed in detail in this communication.[703]

Trimodal MALDI-MSI has a great potential for probing molecular pathology in diseases which are associated with simultaneous peptide/protein and lipid accumulations/alterations such as myocardial infarction, cancer, traumatic brain injury, Alzheimer's disease, Parkinson's disease to name but a few.

4.4 Paper IV

Spatial Lipidomics Reveals Region and Long Chain Base Specific Accumulations of Monosialogangliosides in Amyloid Plaques in Familial Alzheimer's Disease Mice (5xFAD) Brain

One would envision one of the biggest advantages of MALDI mass spectrometry imaging as its capability to visualize region-specific alterations of several biomolecules in histological and histopathological features in a single experiment. I have demonstrated the power of MALDI-MSI for probing single-plaque resolution molecular pathology in transgenic AD mouse models in previous publications; however, I haven't focused on the plaque to plaque differences in molecular pathology depending on the brain region.

One of the drawbacks of using vacuum MALDI-MSI is the limited area that can be imaged at high-spatial resolutions due to the rapid sublimation of many useful matrices including 2,5-DHA and 1,5-DAN in low-pressure sources. Therefore, performing trimodal MALDI-MSI in large brain regions would be unfeasible due to both rapid matrix sublimation and longer imaging times. However, 1,5-DAN can be used more than 10 hours (according to my experience) for MALDI-MSI in negative or positive ion mode without losing any signal intensity. Therefore, 1,5-DAN can also be utilized to image lipid molecules in large brain regions at high-spatial resolutions in single polarity.

It has been widely suggested that long chain (sphingosine) base (LCBs), C18:1-LCB and C20:1-LCB, containing gangliosides might play different roles in neuronal function in vivo.[713] I performed high-spatial resolution (10 μm per pixel) MALDI-MSI of lipids in negative polarity in the hippocampal and adjacent cortical regions of 12-month-old 5xFAD mouse coronal brain tissue sections from obtained from two different stereotaxic coordinates (bregma points, −2.2 and −2.7 mm) which elucidated region-specific aspects plaque-associated C18:1-LCB and C20:1-LCB monosialoganglioside (GM) accumulations in 2D and 3D (Figure 21).

The results reveal that GMs are important components of amyloid plaques and the accumulation of monosialogangliosides is region and LCB specific in 12-month-old 5xFAD mouse brain. I have discussed these observations in relation to amyloid-associated AD pathogenesis such as lipid-related immune changes in amyloid plaques, AD specific ganglioside metabolism, and, notably, AD-associated impaired neurogenesis in the subgranular zone.[610]

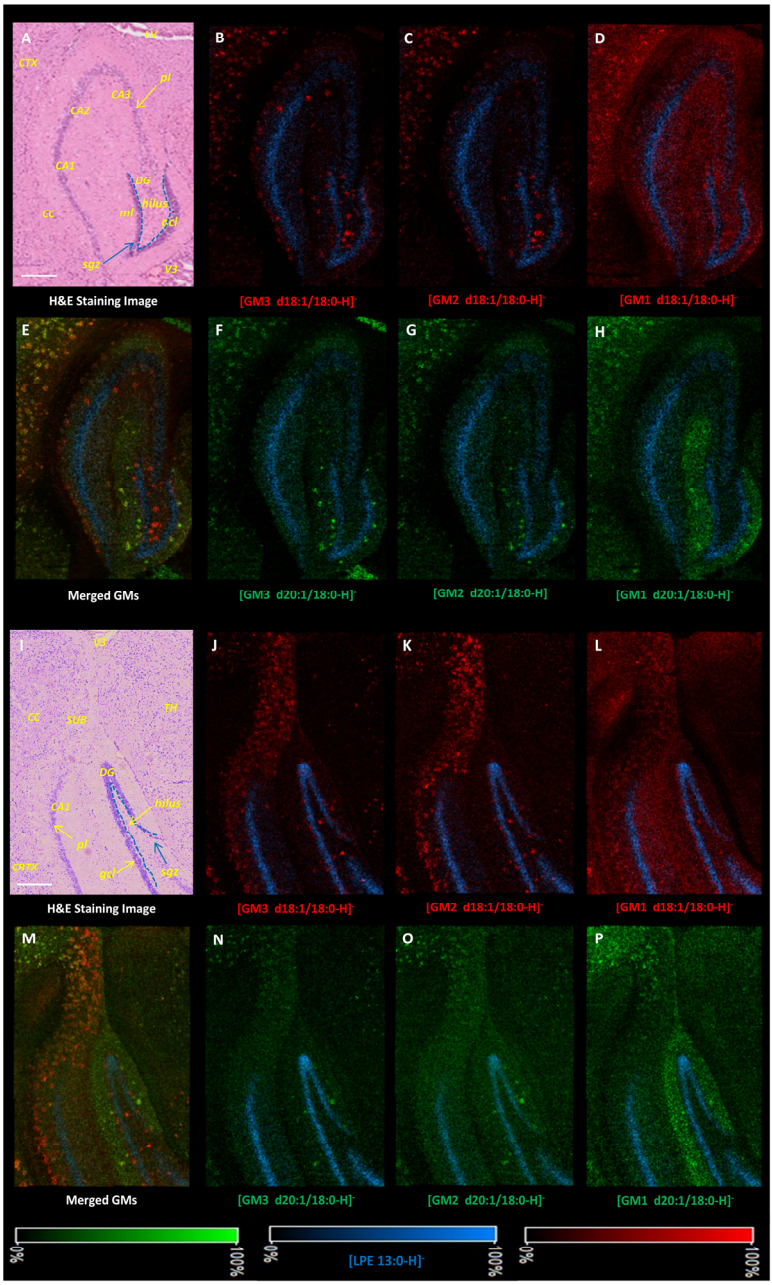

Figure 21. Regional and long-chain-base specific accumulations of monosialogangliosides (GMs) in amyloid plaques in hippocampal subfields and cortex in 12 month old 5xFAD mouse brain. High-spatial resolution (10 µm per pixel) MALDI-MSI of lipids in negative polarity in hippocampal and adjacent cortical regions of 12-month-old 5xFAD mouse coronal brain

tissue sections. Reprinted with permission from Kaya, I., Jennische, E., Dunevall, J., Lange, S., Ewing, A. G., Malmberg, P., Baykal, A. T., and Fletcher, J. S. Spatial Lipidomics Reveals Region and Long Chain Base Specific Accumulations of Monosialogangliosides in Amyloid Plaques in Familial Alzheimer's Disease Mice (5xFAD) Brain, ACS chemical neuroscience 11, 14-24. Copyright (2019), American Chemical Society.

For instance, CD33, a sialic acid binding immunoglobulin-like lectin, inhibits microglial uptake of Aβ[80] and its activity requires sialic acid binding.[133] Therefore, it could be hypothesized that accumulation of sialic acid-rich GMs in amyloid plagues of 5xFAD may contribute to the activation of siglec-3 (CD33) receptors which can mask Aβ plaques and suppress the function of microglia for cleansing of amyloid aggregates. Specific accumulations of C18:1-LCB containing GMs (which are associated with cell differentiation) in the polymorph layer of the DG (Figure 21B-D, and J−L), wherein neurogenesis occurs in the subgranular zone, might be associated with increased neurogenesis and cell differentiation during Aβ-associated impairment of neurogenesis in the DG of 5xFAD mouse brain.

Consequently, MALDI-MSI of lipids in large brain regions can reveal not only plaque-associated lipid alterations but also their region-specific aspect and it can be a great tool for probing brain-region specific molecular plaque pathology in 2D and 3D.

4.5 Paper V

Brain Region-Specific Amyloid Plaque-Associated Myelin Lipid Loss, APOE Deposition and Disruption of the Myelin Sheath in Familial Alzheimer's Disease Mice

Alzheimer's disease is traditionally characterized by its pathological features in the grey matter including extracellular amyloid plaques and intraneuronal neurofibrillary tangles. However, there is emerging evidence suggesting that Aβ pathology leads to impairment of the white matter and glia and causes demyelination in the AD brain.[63, 714]

The myelin sheath is a lipid rich, multilamellar extension of the plasma membrane of oligodendrocytes which contains remarkably high lipid levels accounting for 70%–85% of its dry weight.[410] Here, I investigated brain-region aspect of molecular, structural and immune signatures of amyloid plaque-associated demyelination in 5xFAD transgenic AD mouse brains.[715] MALDI-MSI analysis of coronal brain tissue sections revealed accentuated depletion of myelin-associated lipid species including sulfatides, galactosyl-ceramides, and specific plasmalogen phosphatidylethanolamines in amyloid plaques in the hippocampus, cortex, and on the edges of corpus callosum in the white matter.

Lysophospholipids including lysophosphatidylethanolamine (LPE) and lysophosphatidylcholine (LPC), implicated in neuroinflammation, were found to accumulated in amyloid plaques in 5xFAD mouse brain. Disruption of the lipid-rich myelin sheath was observed only clearly on the edges of corpus callosum which is specifically correlated with plaque-associated myelin lipid loss in this region (Figure 21A-C). Apolipoprotein E (APOE), which is implicated in the depletion of sulfatides in AD brains,[301] was deposited in all the Aβ plaques (Figure 21J-O) which suggest that APOE mediated depletion of sulfatides (Figure 21E-I) is an amyloid plaque-associated phenomenon and it suggest immune-associated disruption of myelin structure via APOE-mediated aberrant lipid metabolism. The data reveal amyloid plaque-associated disruption of lipid molecular architecture, particularly in the corpus callosum in the white matter, suggesting that amyloid pathology leads to myelin degeneration, in part, through the loss of myelin lipids (notably sulfatides and plasmalogens), and this can be partially explained by APOE-mediated sulfatide (abundant lipids in myelinating oligodendrocytes) depletion in amyloid plaques.

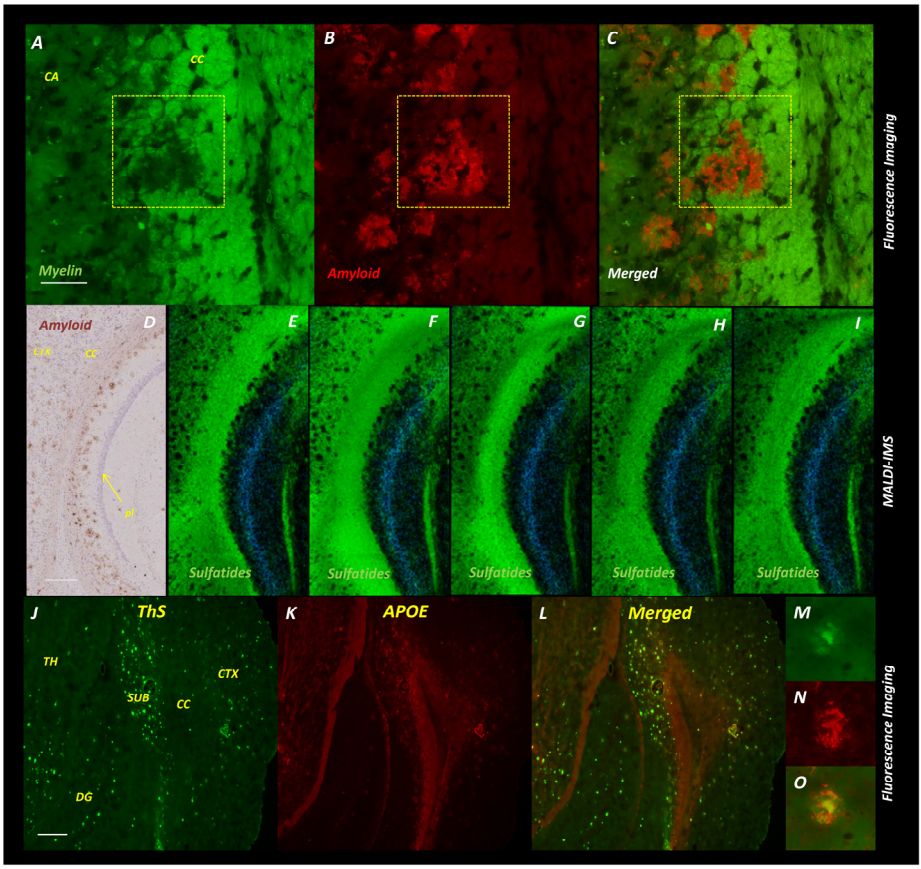

Figure 22. Amyloid plaque-associated myelin sheath disruption, myelin lipid loss and APOE accumulation in 12-month-old 5xFAD transgenic AD mouse brain. A-C) Double staining of coronal brain tissue sections with FluoroMyelin (in green), and anti-amyloid beta (Aβ) antibody (in red) reveals focal amyloid plaque-associated disruption of myelin on the edges of corpus callosum in the white matter. D) The spatial distributions of amyloid aggregates (brown aggregates) in the hippocampus and adjacent cortical regions were visualized with anti-beta amyloid antibody and counter staining with hematoxylin. E) MALDI-MSI analysis at 10 µm spatial resolution reveals depletion of E-I) several sulfatide species in amyloid plaques. J-O) Double staining of coronal brain tissue sections with thioflavin S and anti-apolipoprotein E (APOE) antibody reveals accumulation of APOE in fibrillary amyloid plaques in several brain regions. CC, corpus callosum; CTX, cortex; TH, thalamus; CA, Cornu Ammonis; SUB, subiculum; pl, pyramidal layer; gcl, granular cell layer. Scale bars, panels (A, D, J), 200 µm. Reprinted (adapted) with permission from Kaya, I., Jennische, E., Lange, S., Baykal, A. T., Malmberg, P., and Fletcher, J. S. Brain Region Specific Amyloid Plaque Associated Myelin Lipid Loss, APOE Deposition and Disruption of the Myelin Sheath in Familial Alzheimer's Disease Mice, Journal of Neurochemistry. Copyright (2020), Wiley.

5 CONCLUDING REMARKS

Although the role of lipids in AD has until recently not received as much attention, a body of molecular, immune, genetical and biochemical evidence closely links aberrant lipid metabolism to several stages of AD pathogenesis. Aggregation of Aβ peptides into extracellular Aβ plaques is one of the major neuropathological features of AD. Nevertheless, apart from Aβ peptides, an amyloid plaque consists of a plethora of constituents including lipids which are the "messengers" of amyloid-associated cell signaling, metabolic pathways, and innate immune responses that are disrupted in AD pathogenesis. Therefore, single plaque-resolution spatial lipidomics would be a strong asset to leverage the understanding of molecular pathology of amyloid plaques. This thesis involves both development of novel MALDI mass spectrometry imaging methods in combination with fluorescence and immunofluorescence staining and their implications for probing spatial amyloid plaque-associated lipid biochemistry in transgenic AD mouse brains.

This thesis contributes with the following knowledge to the field of MALDI mass spectrometry imaging and spatial lipidomics in AD:

i) 1,5-DAN matrix allows "static" MALDI-MSI of lipids in brain tissue sections at high-spatial resolution (10 μm) owing to its low-ionization energy and peculiar MALDI ionization mechanisms. Further, "static" MALDI can be followed by fluorescence and immunofluorescence staining of the same tissue section and this has been utilized to image amyloid plaque-associated lipids in the brain tissue sections of tgSwe AD mouse.
ii) 1,5-DAN allows dual polarity MALDI-MSI on the same pixel points at 10 μm spatial resolution and this enhances spatial lipid molecular information at the histological and histopathological features in brain tissue sections.
iii) Dual polarity MALDI-MSI (using 1,5-DAN matrix) on the same pixel points can be followed by peptide/protein MALDI-MSI (using 2,5-DHA matrix) of the same imaging areas in the same brain tissue section at 10 μm spatial resolution and this facilitates a novel "trimodal" MALDI-MSI approach. This has been utilized to image lipids in dual polarity (lipids ionized both in negative and positive polarities) and Aβ peptides from single amyloid plaques in the brain tissues of tgArcSwe AD mouse.

iv) Trimodal MALDI-MSI reveals amyloid plaque-associated alterations of several phospholipids, lysophospholipids and sphingolipids. This gives novel insights into biochemical, structural and immune signatures of amyloid plaque pathology. For instance, plaque-associated myelin lipid architecture loss, plaque-associated accumulations of lysophospholipids which are implicated in focal inflammation.
v) Spatial lipidomics using "static" MALDI in negative polarity revealed region and long chain base specific accumulations of monosialogangliosides in amyloid plaques in familial Alzheimer's disease mouse (5xFAD) brain. This demonstrates that MALDI-MSI facilitates lipid molecular imaging to dissect region-specific molecular amyloid plaque pathology.
vi) MALDI-MSI and fluorescence/immunofluorescence staining revealed brain region-specific amyloid plaque-associated myelin lipid loss, APOE deposition and disruption of the myelin sheath in familial Alzheimer's disease mouse (5xFAD). This demonstrates a strong complementarity of mass spectrometry imaging and immunohistochemistry and fluorescence staining for dissecting the role of lipids in structural, immune and molecular mechanisms of AD pathogenesis.

AD is the most common form of neurodegenerative dementia. However, a neuron doesn't work in isolation. While the symptoms of AD reflect a loss of neural circuit integrity in the brain, a body of evidence from molecular, immune, cellular and neuropathological studies reveals that AD is associated with the misbalance of the intricate interactions between neurons, astrocytes, microglia, oligodendrocytes and vascular cells. This makes the molecules involved in this complex metabolism including lipids significantly important and plaque-associated spatial lipidomics is a strong asset for dissecting the role of lipids in association with proteopathic features of AD pathogenesis.

ACKNOWLEDGEMENTS

I have spent significant amount of time during the last four years working on the development and applications of MALDI and SIMS mass spectrometry imaging methods. Apart from the "cool science" that we discovered, my journey as a “freelance” PhD student has taught me a lot about vigilance, patience and sacrifice while facing the struggles that being independent had to offer. However, before and during my PhD studies I was privileged to work with great people who contributed to achieving results in this doctoral thesis. I have learned something from each and every one whom I have met along the way. I hope I can fully express my gratitude with these following lines.

I would like to thank **Andrew G. Ewing** for accepting me in his amazing laboratory with unlimited resources and supervising my projects since my master studies while giving me independence to pursue my curiosity. Thank you for your encouragement, support, thoughtfulness and generous help with my studies.

My sincere gratitude to **Jörg Hanrieder** for providing a dynamic, collaborative and enthusiastic research environment in the beginning of my PhD studies and giving me independence for pursuing my challenging ideas.

I would like to thank **Kaj Blennow** and **Henrik Zetterberg** for accepting me in this challenging and exciting Alzheimer’s disease research at the Sahlgrenska Academy and providing endless information and valuable suggestions for my future career.

Per Malmberg, thanks for always being available, helpful, supportive and kind. Many of the achievements during my PhD studies wouldn’t be possible without your generous help and collaborative research network.

Eva Jennische, I was very lucky to work with you in your fantastic “little” laboratory. I am grateful for all the teaching, advice and great work we have been doing together. Thanks for all the didactic discussions and teaching me histology and immunohistochemistry.

John S. Fletcher, thanks for all the teaching about SIMS and J105 instrument and useful comments and discussions for my projects.

Stefan Lange, thanks for the teaching, kindness, support and the great and didactic discussions. I am grateful for the fantastic samples that you provided for my projects and a big thank you for teaching me neuroanatomy.

My sincere gratitude to my study director **Mia Ericson** for guidance and her patience with me throughout the years.

Dimitri Brinet, thank you for the kindness, support and the great scientific discussions and great work we did together. Thanks for providing a sane, friendly atmosphere during those hard times…

Johan Dunevall, thanks for the great scientific discussions and great work we did together. It was a pleasure to work with you.

Yasmine Iacone, thanks for being a friendly colleague and providing a sane atmosphere over those few months.

My thanks and appreciation to my coauthors **Mehmet Başkurt** and **Wojciech Michno** for their contributions.

Many thanks to **Stina Syvänen** and **Dag Sehlin** for the great collaboration and precious samples that they provided throughout the years.

My gratitude to **Lena von Sydow** for helping with my experiments at Astra Zeneca.

I would like to thank **Michael E. Kurczy** and **Aurélien Thomen** for the interesting and didactic seminars/meetings and scientific discussions.

Ahmet Tarık Baykal, thanks for the great collaboration and all the fantastic samples that you provided throughout the years.

My gratitude to **Steffen M. Brülls** and **Jerker Mårtensson** for the great collaboration and all the didactic discussions about chemical derivatization and organic chemistry.

I would like to thank the great scientists I have met in Mölndal **Johan Gobom**, **Erik Portelius**, **Ann Brinkmalm**, **Gunnar Brinkmalm**, and **Bruno Becker** for the wonderful group meetings and all the discussions and learnings about mass spectrometry and Alzheimer's disease research.

My thanks and appreciation to **Søren Andersen**, **Patrik Ek** and **German Cuellar** for the professional help with the instrumentation, software and all those didactic discussions.

I would like to thank my past and present office mates **Tina B. Angerer, Marwa Munem**, **Kim Long Le Vo**, **Keke Hu**, **Jun Wang**, **Xianchan Li**, and **Edward Zoet** for all the nice chats, scientific discussions, and afterwork beers and shared delicious stuff throughout the years.

Many thanks to **Jennifer Andersson** and **Maria Pavlovska** for patiently helping with the administration and ordering stuff throughout the years.

Many thanks to my colleagues **Alex S. Lima**, **Pieter E. Oomen**, **Alicia A. Lork**, **Mai Hoang Philipsen**, **Xinwei Zhang**, **Chaoyi Gu**, **Nguyen Duc Khanh Tho**, **Elias Ranjbari**, **Kelly D. Nilsson**, **Anthi Karagianni** and **Mohaddeseh A. Aref** for afterwork beers, movie nights, and great company for lunch breaks and all those fun conversations.

I would like to thank **everyone** I have met along the way in the laboratories in Mölndal, Sahlgrenska, Medicinareberget, Astra Zeneca and Chalmers for creating a stimulating research environment in the city of Gothenburg.

I would like to express my gratitude to my former supervisors; **Şerife H. Yalçın** for teaching me all about lasers and spectroscopy and, **Jaroslav Kvíčala** and **Melih Kuş** for teaching me experimental and theoretical organic chemistry. Many achievements in this doctoral thesis wouldn't be possible without the knowledge I acquired from you.

Annecim, senin bana olan katkılarını ve karşılıksız sevgini birkaç satırla açıklayamam. Ama yüz kere dünyaya gelsem, yine de senin oğlun olmak isterdim. İyiki varsın, herşey için çok teşekkür ederim.

Ağabeyim, bana sorgulamayı, şüphe duymayı ve araştırmayı daha çocukken öğrettiğin için teşekkür ederim. İyiki varsın.

REFERENCES

[1] Holtzman, D. M., Morris, J. C., and Goate, A. M. (2011) Alzheimer's disease: the challenge of the second century, *Science translational medicine 3*, 77sr71-77sr71.

[2] Zenaro, E., Pietronigro, E., Della Bianca, V., Piacentino, G., Marongiu, L., Budui, S., Turano, E., Rossi, B., Angiari, S., and Dusi, S. (2015) Neutrophils promote Alzheimer's disease–like pathology and cognitive decline via LFA-1 integrin, *Nature medicine 21*, 880.

[3] Zaghi, J., Goldenson, B., Inayathullah, M., Lossinsky, A. S., Masoumi, A., Avagyan, H., Mahanian, M., Bernas, M., Weinand, M., and Rosenthal, M. J. (2009) Alzheimer disease macrophages shuttle amyloid-beta from neurons to vessels, contributing to amyloid angiopathy, *Acta neuropathologica 117*, 111-124.

[4] Gasparini, L., Gouras, G. K., Wang, R., Gross, R. S., Beal, M. F., Greengard, P., and Xu, H. (2001) Stimulation of β-amyloid precursor protein trafficking by insulin reduces intraneuronal β-amyloid and requires mitogen-activated protein kinase signaling, *Journal of Neuroscience 21*, 2561-2570.

[5] Moreno-Gonzalez, I., Edwards III, G., Salvadores, N., Shahnawaz, M., Diaz-Espinoza, R., and Soto, C. (2017) Molecular interaction between type 2 diabetes and Alzheimer's disease through cross-seeding of protein misfolding, *Molecular psychiatry 22*, 1327-1334.

[6] Rosenberg, R. N., Baskin, F., Fosmire, J. A., Risser, R., Adams, P., Svetlik, D., Honig, L. S., Cullum, C. M., and Weiner, M. F. (1997) Altered amyloid protein processing in platelets of patients with Alzheimer disease, *Archives of neurology 54*, 139-144.

[7] Rogers, J., Li, R., Mastroeni, D., Grover, A., Leonard, B., Ahern, G., Cao, P., Kolody, H., Vedders, L., and Kolb, W. P. (2006) Peripheral clearance of amyloid β peptide by complement C3-dependent adherence to erythrocytes, *Neurobiology of aging 27*, 1733-1739.

[8] Luchsinger, J., Reitz, C., Honig, L. S., Tang, M.-X., Shea, S., and Mayeux, R. (2005) Aggregation of vascular risk factors and risk of incident Alzheimer disease, *Neurology 65*, 545-551.

[9] Zetterberg, H., Mörtberg, E., Song, L., Chang, L., Provuncher, G. K., Patel, P. P., Ferrell, E., Fournier, D. R., Kan, C. W., and Campbell, T. G. (2011) Hypoxia due to cardiac arrest induces a time-dependent increase in serum amyloid β levels in humans, *PloS one 6*.

[10] Wang, Y.-R., Wang, Q.-H., Zhang, T., Liu, Y.-H., Yao, X.-Q., Zeng, F., Li, J., Zhou, F.-Y., Wang, L., and Yan, J.-C. (2017) Associations between hepatic functions and plasma amyloid-beta levels—implications for the capacity of liver in peripheral amyloid-beta clearance, *Molecular neurobiology 54*, 2338-2344.

[11] Liu, Y.-H., Xiang, Y., Wang, Y.-R., Jiao, S.-S., Wang, Q.-H., Bu, X.-L., Zhu, C., Yao, X.-Q., Giunta, B., and Tan, J. (2015) Association between serum amyloid-beta and renal functions: implications for roles of kidney in amyloid-beta clearance, *Molecular neurobiology 52*, 115-119.

[12] Osorio, R. S., Ayappa, I., Mantua, J., Gumb, T., Varga, A., Mooney, A. M., Burschtin, O. E., Taxin, Z., During, E., and Spector, N. (2014) The interaction between sleep-disordered breathing and apolipoprotein E genotype on cerebrospinal fluid biomarkers for Alzheimer's disease in cognitively normal elderly individuals, *Neurobiology of aging 35*, 1318-1324.

[13] Sun, X., He, G., Qing, H., Zhou, W., Dobie, F., Cai, F., Staufenbiel, M., Huang, L. E., and Song, W. (2006) Hypoxia facilitates Alzheimer's disease pathogenesis by up-regulating BACE1 gene expression, *Proceedings of the National Academy of Sciences 103*, 18727-18732.

[14] Benedict, C., Blennow, K., Zetterberg, H., and Cedernaes, J. (2020) Effects of acute sleep loss on diurnal plasma dynamics of CNS health biomarkers in young men, *Neurology*.

[15] Musiek, E. S., Bhimasani, M., Zangrilli, M. A., Morris, J. C., Holtzman, D. M., and Ju, Y.-E. S. (2018) Circadian rest-activity pattern changes in aging and preclinical Alzheimer disease, *JAMA neurology 75*, 582-590.

[16] Ju, Y.-E. S., Ooms, S. J., Sutphen, C., Macauley, S. L., Zangrilli, M. A., Jerome, G., Fagan, A. M., Mignot, E., Zempel, J. M., and Claassen, J. A. (2017) Slow wave sleep disruption increases cerebrospinal fluid amyloid-β levels, *Brain 140*, 2104-2111.

[17] Zhan, X., Stamova, B., Jin, L.-W., DeCarli, C., Phinney, B., and Sharp, F. R. (2016) Gram-negative bacterial molecules associate with Alzheimer disease pathology, *Neurology 87*, 2324-2332.

[18] Seo, D.-o., Boros, B. D., and Holtzman, D. M. (2019) The microbiome: A target for Alzheimer disease?, *Cell research 29*, 779-780.

[19] Harris, S. A., and Harris, E. A. (2015) Herpes simplex virus type 1 and other pathogens are key causative factors in sporadic Alzheimer's disease, *Journal of Alzheimer's Disease 48*, 319-353.

[20] Bu, X. L., Yao, X. Q., Jiao, S. S., Zeng, F., Liu, Y. H., Xiang, Y., Liang, C. R., Wang, Q. H., Wang, X., and Cao, H. Y. (2015) A study on the association between infectious burden and A lzheimer's disease, *European journal of neurology 22*, 1519-1525.

[21] Gao, H.-M., and Hong, J.-S. (2008) Why neurodegenerative diseases are progressive: uncontrolled inflammation drives disease progression, *Trends in immunology 29*, 357-365.

[22] Herrup, K. (2010) Reimagining Alzheimer's disease—an age-based hypothesis, *Journal of Neuroscience 30*, 16755-16762.

[23] Wang, J., Gu, B. J., Masters, C. L., and Wang, Y.-J. (2017) A systemic view of Alzheimer disease—insights from amyloid-β metabolism beyond the brain, *Nature reviews neurology 13*, 612.
[24] van der Kant, R., Goldstein, L. S., and Ossenkoppele, R. (2019) Amyloid-β-independent regulators of tau pathology in Alzheimer disease, *Nature Reviews Neuroscience*, 1-15.
[25] Herrup, K. (2015) The case for rejecting the amyloid cascade hypothesis, *Nature neuroscience 18*, 794.
[26] Jack Jr, C. R., Bennett, D. A., Blennow, K., Carrillo, M. C., Dunn, B., Haeberlein, S. B., Holtzman, D. M., Jagust, W., Jessen, F., and Karlawish, J. (2018) NIA-AA research framework: toward a biological definition of Alzheimer's disease, *Alzheimer's & Dementia 14*, 535-562.
[27] Blennow, K., Hampel, H., Weiner, M., and Zetterberg, H. (2010) Cerebrospinal fluid and plasma biomarkers in Alzheimer disease, *Nature Reviews Neurology 6*, 131.
[28] Long, J. M., and Holtzman, D. M. (2019) Alzheimer disease: an update on pathobiology and treatment strategies, *Cell*.
[29] Zetterberg, B. K. d. L. M. (2006) H: Alzheimer's disease, *Lancet 368*, 387.
[30] Perrin, R. J., Fagan, A. M., and Holtzman, D. M. (2009) Multimodal techniques for diagnosis and prognosis of Alzheimer's disease, *Nature 461*, 916-922.
[31] Hardy, J. (2006) Alzheimer's disease: the amyloid cascade hypothesis: an update and reappraisal, *Journal of Alzheimer's disease 9*, 151-153.
[32] Jack, C. R., Holtzman, D. M., and Sperling, R. (2019) Dementia is not synonymous with Alzheimer's disease, American Association for the Advancement of Science.
[33] McKhann, G. M., Knopman, D. S., Chertkow, H., Hyman, B. T., Jack Jr, C. R., Kawas, C. H., Klunk, W. E., Koroshetz, W. J., Manly, J. J., and Mayeux, R. (2011) The diagnosis of dementia due to Alzheimer's disease: recommendations from the National Institute on Aging-Alzheimer's Association workgroups on diagnostic guidelines for Alzheimer's disease, *Alzheimer's & dementia 7*, 263-269.
[34] Vermunt, L., Sikkes, S. A., Van Den Hout, A., Handels, R., Bos, I., Van Der Flier, W. M., Kern, S., Ousset, P. J., Maruff, P., and Skoog, I. (2019) Duration of preclinical, prodromal, and dementia stages of Alzheimer's disease in relation to age, sex, and APOE genotype, *Alzheimer's & Dementia 15*, 888-898.
[35] Bateman, R. J., Xiong, C., Benzinger, T. L., Fagan, A. M., Goate, A., Fox, N. C., Marcus, D. S., Cairns, N. J., Xie, X., and Blazey, T. M. (2012) Clinical and biomarker changes in dominantly inherited Alzheimer's disease, *N Engl J Med 367*, 795-804.
[36] Wijsman, E. M., Daw, E. W., Yu, X., Steinbart, E. J., Nochlin, D., Bird, T. D., and Schellenberg, G. D. (2005) APOE and other loci affect

age-at-onset in Alzheimer's disease families with PS2 mutation, *American Journal of Medical Genetics Part B: Neuropsychiatric Genetics 132*, 14-20.
[37] Alzheimer, A. (1907) Uber eine eigenartige Erkrankung der Hirnrinde, *Allgemeine Zeitschrife Psychiatrie 64*, 146-148.
[38] Möller, H.-J., and Graeber, M. (1998) The case described by Alois Alzheimer in 1911, *European archives of psychiatry and clinical neuroscience 248*, 111-122.
[39] Blocq, P., and Marinescu, G. (1892) *Sur les lésions et la pathogénie de l'épilepsie dite essentielle*.
[40] Fischer, O. (1907) Miliare Nekrosen mit drusigen Wucherungen der Neurofibrillen, eine regelmässige Veränderung der Hirnrinde bei seniler Demenz, *Monatsschr Psychiatr Neurol 22*, 361-372.
[41] Müller, U., Winter, P., and Graeber, M. B. (2013) A presenilin 1 mutation in the first case of Alzheimer's disease, *The Lancet Neurology 12*, 129-130.
[42] Rupp, C., Beyreuther, K., Maurer, K., and Kins, S. (2014) A presenilin 1 mutation in the first case of Alzheimer's disease: Revisited, *Alzheimer's & Dementia 10*, 869-872.
[43] Graeber, M., Kösel, S., Grasbon-Frodl, E., Möller, H., and Mehraein, P. (1998) Histopathology and APOE genotype of the first Alzheimer disease patient, Auguste D, *Neurogenetics 1*, 223-228.
[44] Poirier, J., Bertrand, P., Kogan, S., Gauthier, S., Davignon, J., and Bouthillier, D. (1993) Apolipoprotein E polymorphism and Alzheimer's disease, *The Lancet 342*, 697-699.
[45] Enserink, M. (1998) First Alzheimer's diagnosis confirmed, American Association for the Advancement of Science.
[46] Beach, T. G., Monsell, S. E., Phillips, L. E., and Kukull, W. (2012) Accuracy of the clinical diagnosis of Alzheimer disease at National Institute on Aging Alzheimer Disease Centers, 2005–2010, *Journal of neuropathology and experimental neurology 71*, 266-273.
[47] Tanzi, R. E. (2013) A brief history of Alzheimer's disease gene discovery, *Journal of Alzheimer's disease 33*, S5-S13.
[48] Huang, Y., and Mucke, L. (2012) Alzheimer mechanisms and therapeutic strategies, *Cell 148*, 1204-1222.
[49] Goedert, M. (2009) Oskar Fischer and the study of dementia, *Brain 132*, 1102-1111.
[50] Olsson, B., Lautner, R., Andreasson, U., Öhrfelt, A., Portelius, E., Bjerke, M., Hölttä, M., Rosén, C., Olsson, C., and Strobel, G. (2016) CSF and blood biomarkers for the diagnosis of Alzheimer's disease: a systematic review and meta-analysis, *The Lancet Neurology 15*, 673-684.
[51] Tse, K. H., and Herrup, K. (2017) Re-imagining Alzheimer's disease–the diminishing importance of amyloid and a glimpse of what lies ahead, *Journal of neurochemistry 143*, 432-444.

[52] Heppner, F. L., Ransohoff, R. M., and Becher, B. (2015) Immune attack: the role of inflammation in Alzheimer disease, *Nature Reviews Neuroscience 16*, 358.
[53] Terry, A. V., and Buccafusco, J. J. (2003) The cholinergic hypothesis of age and Alzheimer's disease-related cognitive deficits: recent challenges and their implications for novel drug development, *Journal of Pharmacology and Experimental Therapeutics 306*, 821-827.
[54] Bierer, L. M., Haroutunian, V., Gabriel, S., Knott, P. J., Carlin, L. S., Purohit, D. P., Perl, D. P., Schmeidler, J., Kanof, P., and Davis, K. L. (1995) Neurochemical correlates of dementia severity in Alzheimer's disease: relative importance of the cholinergic deficits, *Journal of neurochemistry 64*, 749-760.
[55] Reisberg, B., Doody, R., Stöffler, A., Schmitt, F., Ferris, S., and Möbius, H. J. (2003) Memantine in moderate-to-severe Alzheimer's disease, *New England Journal of Medicine 348*, 1333-1341.
[56] Rogawski, M. A., and Wenk, G. L. (2003) The neuropharmacological basis for the use of memantine in the treatment of Alzheimer's disease, *CNS drug reviews 9*, 275-308.
[57] Sevigny, J., Chiao, P., Bussière, T., Weinreb, P. H., Williams, L., Maier, M., Dunstan, R., Salloway, S., Chen, T., and Ling, Y. (2016) The antibody aducanumab reduces Aβ plaques in Alzheimer's disease, *Nature 537*, 50-56.
[58] Lannfelt, L., Möller, C., Basun, H., Osswald, G., Sehlin, D., Satlin, A., Logovinsky, V., and Gellerfors, P. (2014) Perspectives on future Alzheimer therapies: amyloid-β protofibrils-a new target for immunotherapy with BAN2401 in Alzheimer's disease, *Alzheimer's research & therapy 6*, 16.
[59] Dovey, H., John, V., Anderson, J., Chen, L., de Saint Andrieu, P., Fang, L., Freedman, S., Folmer, B., Goldbach, E., and Holsztynska, E. (2001) Functional gamma-secretase inhibitors reduce beta-amyloid peptide levels in brain, *Journal of neurochemistry 76*, 173-181.
[60] Ghosh, A. K., Brindisi, M., and Tang, J. (2012) Developing β-secretase inhibitors for treatment of Alzheimer's disease, *Journal of neurochemistry 120*, 71-83.
[61] Hardy, J., and Selkoe, D. J. (2002) The amyloid hypothesis of Alzheimer's disease: progress and problems on the road to therapeutics, *science 297*, 353-356.
[62] Serrano-Pozo, A., Frosch, M. P., Masliah, E., and Hyman, B. T. (2011) Neuropathological alterations in Alzheimer disease, *Cold Spring Harbor perspectives in medicine 1*, a006189.
[63] Nasrabady, S. E., Rizvi, B., Goldman, J. E., and Brickman, A. M. (2018) White matter changes in Alzheimer's disease: a focus on myelin and oligodendrocytes, *Acta neuropathologica communications 6*, 22.

[64] Perl, D. P. (2010) Neuropathology of Alzheimer's disease, *Mount Sinai Journal of Medicine: A Journal of Translational and Personalized Medicine: A Journal of Translational and Personalized Medicine 77*, 32-42.

[65] DeTure, M. A., and Dickson, D. W. (2019) The neuropathological diagnosis of Alzheimer's disease, *Molecular neurodegeneration 14*, 1-18.

[66] Murray, M. E., Graff-Radford, N. R., Ross, O. A., Petersen, R. C., Duara, R., and Dickson, D. W. (2011) Neuropathologically defined subtypes of Alzheimer's disease with distinct clinical characteristics: a retrospective study, *The Lancet Neurology 10*, 785-796.

[67] Nixon, R. A. (2007) Autophagy, amyloidogenesis and Alzheimer disease, *Journal of cell science 120*, 4081-4091.

[68] Shi, Y., and Holtzman, D. M. (2018) Interplay between innate immunity and Alzheimer disease: APOE and TREM2 in the spotlight, *Nature Reviews Immunology 18*, 759-772.

[69] Lucin, K. M., and Wyss-Coray, T. (2009) Immune activation in brain aging and neurodegeneration: too much or too little?, *Neuron 64*, 110-122.

[70] McGeer, P. L., and McGeer, E. G. (1995) The inflammatory response system of brain: implications for therapy of Alzheimer and other neurodegenerative diseases, *Brain Research Reviews 21*, 195-218.

[71] Hollingworth, P., Harold, D., Sims, R., Gerrish, A., Lambert, J.-C., Carrasquillo, M. M., Abraham, R., Hamshere, M. L., Pahwa, J. S., and Moskvina, V. (2011) Common variants at ABCA7, MS4A6A/MS4A4E, EPHA1, CD33 and CD2AP are associated with Alzheimer's disease, *Nature genetics 43*, 429.

[72] Colangelo, V., Schurr, J., Ball, M. J., Pelaez, R. P., Bazan, N. G., and Lukiw, W. J. (2002) Gene expression profiling of 12633 genes in Alzheimer hippocampal CA1: transcription and neurotrophic factor down-regulation and up-regulation of apoptotic and pro-inflammatory signaling, *Journal of neuroscience research 70*, 462-473.

[73] Efthymiou, A. G., and Goate, A. M. (2017) Late onset Alzheimer's disease genetics implicates microglial pathways in disease risk, *Molecular neurodegeneration 12*, 43.

[74] Lambert, J.-C., Ibrahim-Verbaas, C. A., Harold, D., Naj, A. C., Sims, R., Bellenguez, C., Jun, G., DeStefano, A. L., Bis, J. C., and Beecham, G. W. (2013) Meta-analysis of 74,046 individuals identifies 11 new susceptibility loci for Alzheimer's disease, *Nature genetics 45*, 1452.

[75] Kiialainen, A., Hovanes, K., Paloneva, J., Kopra, O., and Peltonen, L. (2005) Dap12 and Trem2, molecules involved in innate immunity and neurodegeneration, are co-expressed in the CNS, *Neurobiology of disease 18*, 314-322.

[76] Griciuc, A., Patel, S., Federico, A. N., Choi, S. H., Innes, B. J., Oram, M. K., Cereghetti, G., McGinty, D., Anselmo, A., and Sadreyev, R. I. (2019) TREM2 Acts Downstream of CD33 in Modulating Microglial Pathology in Alzheimer's Disease, *Neuron*.

[77] Matarin, M., Salih, D. A., Yasvoina, M., Cummings, D. M., Guelfi, S., Liu, W., Solim, M. A. N., Moens, T. G., Paublete, R. M., and Ali, S. S. (2015) A genome-wide gene-expression analysis and database in transgenic mice during development of amyloid or tau pathology, *Cell reports 10*, 633-644.

[78] Namba, Y., Tsuchiya, H., and Ikeda, K. (1992) Apolipoprotein B immunoreactivity in senile plaque and vascular amyloids and neurofibrillary tangles in the brains of patients with Alzheimer's disease, *Neuroscience letters 134*, 264-266.

[79] Frank, S., Burbach, G. J., Bonin, M., Walter, M., Streit, W., Bechmann, I., and Deller, T. (2008) TREM2 is upregulated in amyloid plaque-associated microglia in aged APP23 transgenic mice, *Glia 56*, 1438-1447.

[80] Griciuc, A., Serrano-Pozo, A., Parrado, A. R., Lesinski, A. N., Asselin, C. N., Mullin, K., Hooli, B., Choi, S. H., Hyman, B. T., and Tanzi, R. E. (2013) Alzheimer's disease risk gene CD33 inhibits microglial uptake of amyloid beta, *Neuron 78*, 631-643.

[81] Rangaraju, S., Dammer, E. B., Raza, S. A., Gao, T., Xiao, H., Betarbet, R., Duong, D. M., Webster, J. A., Hales, C. M., and Lah, J. J. (2018) Quantitative proteomics of acutely-isolated mouse microglia identifies novel immune Alzheimer's disease-related proteins, *Molecular neurodegeneration 13*, 34.

[82] Roher, A. E., Weiss, N., Kokjohn, T. A., Kuo, Y.-M., Kalback, W., Anthony, J., Watson, D., Luehrs, D. C., Sue, L., and Walker, D. (2002) Increased Aβ peptides and reduced cholesterol and myelin proteins characterize white matter degeneration in Alzheimer's disease, *Biochemistry 41*, 11080-11090.

[83] Desai, M. K., Mastrangelo, M. A., Ryan, D. A., Sudol, K. L., Narrow, W. C., and Bowers, W. J. (2010) Early oligodendrocyte/myelin pathology in Alzheimer's disease mice constitutes a novel therapeutic target, *The American journal of pathology 177*, 1422-1435.

[84] Desai, M. K., Sudol, K. L., Janelsins, M. C., Mastrangelo, M. A., Frazer, M. E., and Bowers, W. J. (2009) Triple-transgenic Alzheimer's disease mice exhibit region-specific abnormalities in brain myelination patterns prior to appearance of amyloid and tau pathology, *Glia 57*, 54-65.

[85] Bartzokis, G. (2011) Alzheimer's disease as homeostatic responses to age-related myelin breakdown, *Neurobiology of aging 32*, 1341-1371.

[86] Alzheimer, A. (1991) Über eigenartige Krankheitsfälle des späteren Alters: (On certain peculiar diseases of old age, *History of Psychiatry 2*, 74-101.
[87] Di Paolo, G., and Kim, T.-W. (2011) Linking lipids to Alzheimer's disease: cholesterol and beyond, *Nature Reviews Neuroscience 12*, 284-296.
[88] Chan, R. B., Oliveira, T. G., Cortes, E. P., Honig, L. S., Duff, K. E., Small, S. A., Wenk, M. R., Shui, G., and Di Paolo, G. (2012) Comparative lipidomic analysis of mouse and human brain with Alzheimer disease, *Journal of Biological Chemistry 287*, 2678-2688.
[89] Pimenova, A. A., Raj, T., and Goate, A. M. (2018) Untangling genetic risk for Alzheimer's disease, *Biological psychiatry 83*, 300-310.
[90] Kunkle, B. W., Grenier-Boley, B., Sims, R., Bis, J. C., Damotte, V., Naj, A. C., Boland, A., Vronskaya, M., van der Lee, S. J., and Amlie-Wolf, A. (2019) Genetic meta-analysis of diagnosed Alzheimer's disease identifies new risk loci and implicates Aβ, tau, immunity and lipid processing, *Nature genetics 51*, 414.
[91] Brown, G. C., and Neher, J. J. (2014) Microglial phagocytosis of live neurons, *Nature Reviews Neuroscience 15*, 209.
[92] Naj, A. C., Jun, G., Beecham, G. W., Wang, L.-S., Vardarajan, B. N., Buros, J., Gallins, P. J., Buxbaum, J. D., Jarvik, G. P., and Crane, P. K. (2011) Common variants at MS4A4/MS4A6E, CD2AP, CD33 and EPHA1 are associated with late-onset Alzheimer's disease, *Nature genetics 43*, 436-441.
[93] Bertram, L., Lange, C., Mullin, K., Parkinson, M., Hsiao, M., Hogan, M. F., Schjeide, B. M., Hooli, B., DiVito, J., and Ionita, I. (2008) Genome-wide association analysis reveals putative Alzheimer's disease susceptibility loci in addition to APOE, *The American Journal of Human Genetics 83*, 623-632.
[94] Rosenthal, S. L., and Kamboh, M. I. (2014) Late-onset Alzheimer's disease genes and the potentially implicated pathways, *Current genetic medicine reports 2*, 85-101.
[95] Yan, T., Liang, J., Gao, J., Wang, L., Fujioka, H., Zhu, X., and Wang, X. (2020) FAM222A encodes a protein which accumulates in plaques in Alzheimer's disease, *Nature communications 11*, 1-16.
[96] Strittmatter, W. J., Saunders, A. M., Schmechel, D., Pericak-Vance, M., Enghild, J., Salvesen, G. S., and Roses, A. D. (1993) Apolipoprotein E: high-avidity binding to beta-amyloid and increased frequency of type 4 allele in late-onset familial Alzheimer disease, *Proceedings of the National Academy of Sciences 90*, 1977-1981.
[97] Castellano, J. M., Kim, J., Stewart, F. R., Jiang, H., DeMattos, R. B., Patterson, B. W., Fagan, A. M., Morris, J. C., Mawuenyega, K. G., and Cruchaga, C. (2011) Human apoE isoforms differentially regulate brain amyloid-β peptide clearance, *Science translational medicine 3*, 89ra57-89ra57.

[98] Corder, E. H., Saunders, A. M., Strittmatter, W. J., Schmechel, D. E., Gaskell, P. C., Small, G., Roses, A. D., Haines, J., and Pericak-Vance, M. A. (1993) Gene dose of apolipoprotein E type 4 allele and the risk of Alzheimer's disease in late onset families, *Science 261*, 921-923.

[99] Saunders, A., Schmader, K., Breitner, J., Benson, M., Brown, W., Goldfarb, L., Goldgaber, D., Manwaring, M., Szymanski, M., and McCown, N. (1993) Apolipoprotein E epsilon 4 allele distributions in late-onset Alzheimer's disease and in other amyloid-forming diseases, *Lancet (London, England) 342*, 710-711.

[100] Strittmatter, W. J., and Roses, A. D. (1995) Apolipoprotein E and Alzheimer disease, *Proceedings of the National Academy of Sciences 92*, 4725-4727.

[101] Namba, Y., Tomonaga, M., Kawasaki, H., Otomo, E., and Ikeda, K. (1991) Apolipoprotein E immunoreactivity in cerebral amyloid deposits and neurofibrillary tangles in Alzheimer's disease and kuru plaque amyloid in Creutzfeldt-Jakob disease, *Brain research 541*, 163-166.

[102] Wisniewski, T., and Frangione, B. (1992) Apolipoprotein E: a pathological chaperone protein in patients with cerebral and systemic amyloid, *Neuroscience letters 135*, 235-238.

[103] Boyles, J. K., Pitas, R. E., Wilson, E., Mahley, R. W., and Taylor, J. (1985) Apolipoprotein E associated with astrocytic glia of the central nervous system and with nonmyelinating glia of the peripheral nervous system, *The Journal of clinical investigation 76*, 1501-1513.

[104] Mahley, R. W. (2016) Central nervous system lipoproteins: ApoE and regulation of cholesterol metabolism, *Arteriosclerosis, thrombosis, and vascular biology 36*, 1305-1315.

[105] Han, X., Cheng, H., Fryer, J. D., Fagan, A. M., and Holtzman, D. M. (2003) Novel Role for Apolipoprotein E in the Central Nervous System MODULATION OF SULFATIDE CONTENT, *Journal of Biological Chemistry 278*, 8043-8051.

[106] Cordero-Llana, O., Scott, S., Maslen, S., Anderson, J., Boyle, J., Chowhdury, R., Tyers, P., Barker, R., Kelly, C. M., and Rosser, A. E. (2011) Clusterin secreted by astrocytes enhances neuronal differentiation from human neural precursor cells, *Cell Death & Differentiation 18*, 907-913.

[107] Foster, E., Dangla Valls, A., Lovestone, S., Ribe, E. M., and Buckley, N. J. (2019) Clusterin in Alzheimer's disease: mechanisms, genetics, and lessons from other pathologies, *Frontiers in neuroscience 13*, 164.

[108] Nuutinen, T., Suuronen, T., Kauppinen, A., and Salminen, A. (2009) Clusterin: a forgotten player in Alzheimer's disease, *Brain research reviews 61*, 89-104.

[109] Cunin, P., Beauvillain, C., Miot, C., Augusto, J.-F., Preisser, L., Blanchard, S., Pignon, P., Scotet, M., Garo, E., and Fremaux, I. (2016) Clusterin facilitates apoptotic cell clearance and prevents apoptotic cell-induced autoimmune responses, *Cell death & disease 7*, e2215-e2215.
[110] Holtzman, D. M. (2004) In vivo effects of ApoE and clusterin on amyloid-β metabolism and neuropathology, *Journal of Molecular Neuroscience 23*, 247-254.
[111] Narayan, P., Orte, A., Clarke, R. W., Bolognesi, B., Hook, S., Ganzinger, K. A., Meehan, S., Wilson, M. R., Dobson, C. M., and Klenerman, D. (2012) The extracellular chaperone clusterin sequesters oligomeric forms of the amyloid-β 1− 40 peptide, *Nature structural & molecular biology 19*, 79.
[112] Oda, T., Wals, P., Osterburg, H. H., Johnson, S. A., Pasinetti, G. M., Morgan, T. E., Rozovsky, I., Stine, W. B., Snyder, S. W., and Holzman, T. F. (1995) Clusterin (apoJ) alters the aggregation of amyloid β-peptide (Aβ1-42) and forms slowly sedimenting Aβ complexes that cause oxidative stress, *Experimental neurology 136*, 22-31.
[113] DeMattos, R. B., O'dell, M. A., Parsadanian, M., Taylor, J. W., Harmony, J. A., Bales, K. R., Paul, S. M., Aronow, B. J., and Holtzman, D. M. (2002) Clusterin promotes amyloid plaque formation and is critical for neuritic toxicity in a mouse model of Alzheimer's disease, *Proceedings of the National Academy of Sciences 99*, 10843-10848.
[114] Jonsson, T., Stefansson, H., Steinberg, S., Jonsdottir, I., Jonsson, P. V., Snaedal, J., Bjornsson, S., Huttenlocher, J., Levey, A. I., and Lah, J. J. (2013) Variant of TREM2 associated with the risk of Alzheimer's disease, *New England Journal of Medicine 368*, 107-116.
[115] Guerreiro, R., Wojtas, A., Bras, J., Carrasquillo, M., Rogaeva, E., Majounie, E., Cruchaga, C., Sassi, C., Kauwe, J. S., and Younkin, S. (2013) TREM2 variants in Alzheimer's disease, *New England Journal of Medicine 368*, 117-127.
[116] Reitz, C., and Mayeux, R. (2013) TREM2 and neurodegenerative disease, *The New England journal of medicine 369*, 1564.
[117] Gratuze, M., Leyns, C. E., and Holtzman, D. M. (2018) New insights into the role of TREM2 in Alzheimer's disease, *Molecular neurodegeneration 13*, 1-16.
[118] Hickman, S. E., and El Khoury, J. (2014) TREM2 and the neuroimmunology of Alzheimer's disease, *Biochemical pharmacology 88*, 495-498.
[119] Wang, Y., Ulland, T. K., Ulrich, J. D., Song, W., Tzaferis, J. A., Hole, J. T., Yuan, P., Mahan, T. E., Shi, Y., and Gilfillan, S. (2016) TREM2-mediated early microglial response limits diffusion and

toxicity of amyloid plaques, *Journal of Experimental Medicine 213*, 667-675.
[120] Parhizkar, S., Arzberger, T., Brendel, M., Kleinberger, G., Deussing, M., Focke, C., Nuscher, B., Xiong, M., Ghasemigharagoz, A., and Katzmarski, N. (2019) Loss of TREM2 function increases amyloid seeding but reduces plaque-associated ApoE, *Nature neuroscience 22*, 191-204.
[121] Leyns, C. E., Gratuze, M., Narasimhan, S., Jain, N., Koscal, L. J., Jiang, H., Manis, M., Colonna, M., Lee, V. M., and Ulrich, J. D. (2019) TREM2 function impedes tau seeding in neuritic plaques, *Nature neuroscience 22*, 1217-1222.
[122] Meilandt, W., Ngu, H., Gogineni, A., Lalehzadeh, G., Lee, S., Srinivasan, K., Imperio, J., Wu, T., Weber, M., and Kruse, A. (2020) Trem2 deletion reduces late-stage amyloid plaque accumulation, elevates the Aβ42: Aβ40 ratio, and exacerbates axonal dystrophy and dendritic spine loss in the PS2APP Alzheimer's mouse model, *The Journal of neuroscience: the official journal of the Society for Neuroscience*.
[123] Colonna, M., and Wang, Y. (2016) TREM2 variants: new keys to decipher Alzheimer disease pathogenesis, *Nature Reviews Neuroscience 17*, 201.
[124] Ulrich, J. D., Ulland, T. K., Colonna, M., and Holtzman, D. M. (2017) Elucidating the role of TREM2 in Alzheimer's disease, *Neuron 94*, 237-248.
[125] Daws, M. R., Sullam, P. M., Niemi, E. C., Chen, T. T., Tchao, N. K., and Seaman, W. E. (2003) Pattern recognition by TREM-2: binding of anionic ligands, *The Journal of Immunology 171*, 594-599.
[126] Wang, Y., Cella, M., Mallinson, K., Ulrich, J. D., Young, K. L., Robinette, M. L., Gilfillan, S., Krishnan, G. M., Sudhakar, S., and Zinselmeyer, B. H. (2015) TREM2 lipid sensing sustains the microglial response in an Alzheimer's disease model, *Cell 160*, 1061-1071.
[127] Cannon, J. P., O'Driscoll, M., and Litman, G. W. (2012) Specific lipid recognition is a general feature of CD300 and TREM molecules, *Immunogenetics 64*, 39-47.
[128] Ulland, T. K., Song, W. M., Huang, S. C.-C., Ulrich, J. D., Sergushichev, A., Beatty, W. L., Loboda, A. A., Zhou, Y., Cairns, N. J., and Kambal, A. (2017) TREM2 maintains microglial metabolic fitness in Alzheimer's disease, *Cell 170*, 649-663. e613.
[129] Poliani, P. L., Wang, Y., Fontana, E., Robinette, M. L., Yamanishi, Y., Gilfillan, S., and Colonna, M. (2015) TREM2 sustains microglial expansion during aging and response to demyelination, *The Journal of clinical investigation 125*, 2161-2170.
[130] Takahashi, K., Rochford, C. D., and Neumann, H. (2005) Clearance of apoptotic neurons without inflammation by microglial triggering

receptor expressed on myeloid cells-2, *The Journal of experimental medicine 201*, 647-657.

[131] Boza-Serrano, A., Ruiz, R., Sanchez-Varo, R., García-Revilla, J., Yang, Y., Jimenez-Ferrer, I., Paulus, A., Wennström, M., Vilalta, A., and Allendorf, D. (2019) Galectin-3, a novel endogenous TREM2 ligand, detrimentally regulates inflammatory response in Alzheimer's disease, *Acta neuropathologica 138*, 251-273.

[132] Estus, S., Shaw, B. C., Devanney, N., Katsumata, Y., and Fardo, D. W. (2019) Evaluation of CD33 as a genetic risk factor for Alzheimer's disease, *Acta Neuropathologica*, 1-13.

[133] Lajaunias, F., Dayer, J. M., and Chizzolini, C. (2005) Constitutive repressor activity of CD33 on human monocytes requires sialic acid recognition and phosphoinositide 3-kinase-mediated intracellular signaling, *European journal of immunology 35*, 243-251.

[134] Huang, K.-l., Marcora, E., Pimenova, A. A., Di Narzo, A. F., Kapoor, M., Jin, S. C., Harari, O., Bertelsen, S., Fairfax, B. P., and Czajkowski, J. (2017) A common haplotype lowers PU. 1 expression in myeloid cells and delays onset of Alzheimer's disease, *Nature neuroscience 20*, 1052.

[135] Jehle, A. W., Gardai, S. J., Li, S., Linsel-Nitschke, P., Morimoto, K., Janssen, W. J., Vandivier, R. W., Wang, N., Greenberg, S., and Dale, B. M. (2006) ATP-binding cassette transporter A7 enhances phagocytosis of apoptotic cells and associated ERK signaling in macrophages, *The Journal of cell biology 174*, 547-556.

[136] Kim, W. S., Li, H., Ruberu, K., Chan, S., Elliott, D. A., Low, J. K., Cheng, D., Karl, T., and Garner, B. (2013) Deletion of Abca7 increases cerebral amyloid-β accumulation in the J20 mouse model of Alzheimer's disease, *Journal of Neuroscience 33*, 4387-4394.

[137] Sakae, N., Liu, C.-C., Shinohara, M., Frisch-Daiello, J., Ma, L., Yamazaki, Y., Tachibana, M., Younkin, L., Kurti, A., and Carrasquillo, M. M. (2016) ABCA7 deficiency accelerates amyloid-β generation and Alzheimer's neuronal pathology, *Journal of Neuroscience 36*, 3848-3859.

[138] Peng, Q., Malhotra, S., Torchia, J. A., Kerr, W. G., Coggeshall, K. M., and Humphrey, M. B. (2010) TREM2-and DAP12-dependent activation of PI3K requires DAP10 and is inhibited by SHIP1, *Science signaling 3*, ra38-ra38.

[139] Selkoe, D., Hardy, J., Selkoe, D., and Hardy, J. (2016) The amyloid hypothesis of Alzheimer's disease at 25 years. EMBO Mol Med 8: 595–608, DOI.

[140] Hardy, J. A., and Higgins, G. A. (1992) Alzheimer's disease: the amyloid cascade hypothesis, *Science 256*, 184.

[141] Karran, E., Mercken, M., and De Strooper, B. (2011) The amyloid cascade hypothesis for Alzheimer's disease: an appraisal for the

development of therapeutics, *Nature reviews Drug discovery 10*, 698-712.
[142] Barage, S. H., and Sonawane, K. D. (2015) Amyloid cascade hypothesis: Pathogenesis and therapeutic strategies in Alzheimer's disease, *Neuropeptides 52*, 1-18.
[143] Delaere, P., Duyckaerts, C., Masters, C., Beyreuther, K., Piette, F., and Hauw, J. (1990) Large amounts of neocortical βA4 deposits without neuritic plaques nor tangles in a psychometrically assessed, non-demented person, *Neuroscience letters 116*, 87-93.
[144] Glenner, G. G., and Wong, C. W. (1984) Alzheimer's disease and Down's syndrome: sharing of a unique cerebrovascular amyloid fibril protein, *Biochemical and biophysical research communications 122*, 1131-1135.
[145] Masters, C. L., Simms, G., Weinman, N. A., Multhaup, G., McDonald, B. L., and Beyreuther, K. (1985) Amyloid plaque core protein in Alzheimer disease and Down syndrome, *Proceedings of the National Academy of Sciences 82*, 4245-4249.
[146] Tanzi, R. E., Gusella, J. F., Watkins, P. C., Bruns, G., St George-Hyslop, P., Van Keuren, M. L., Patterson, D., Pagan, S., Kurnit, D. M., and Neve, R. L. (1987) Amyloid beta protein gene: cDNA, mRNA distribution, and genetic linkage near the Alzheimer locus, *Science 235*, 880-884.
[147] Kang, J., Lemaire, H.-G., Unterbeck, A., Salbaum, J. M., Masters, C. L., Grzeschik, K.-H., Multhaup, G., Beyreuther, K., and Müller-Hill, B. (1987) The precursor of Alzheimer's disease amyloid A4 protein resembles a cell-surface receptor, *Nature 325*, 733-736.
[148] Robakis, N. K., Ramakrishna, N., Wolfe, G., and Wisniewski, H. M. (1987) Molecular cloning and characterization of a cDNA encoding the cerebrovascular and the neuritic plaque amyloid peptides, *Proceedings of the National Academy of Sciences 84*, 4190-4194.
[149] Dyrks, T., Weidemann, A., Multhaup, G., Salbaum, J., Lemaire, H., Kang, J., Müller-Hill, B., Masters, C., and Beyreuther, K. (1988) Identification, transmembrane orientation and biogenesis of the amyloid A4 precursor of Alzheimer's disease, *The EMBO journal 7*, 949-957.
[150] Haass, C. (2004) Take five—BACE and the γ-secretase quartet conduct Alzheimer's amyloid β-peptide generation, *The EMBO journal 23*, 483-488.
[151] Haass, C., Kaether, C., Thinakaran, G., and Sisodia, S. (2012) Trafficking and proteolytic processing of APP, *Cold Spring Harbor perspectives in medicine 2*, a006270.
[152] Vassar, R., Bennett, B. D., Babu-Khan, S., Kahn, S., Mendiaz, E. A., Denis, P., Teplow, D. B., Ross, S., Amarante, P., and Loeloff, R. (1999) β-Secretase cleavage of Alzheimer's amyloid precursor

protein by the transmembrane aspartic protease BACE, *science 286*, 735-741.
[153] Tanzi, R. E., and Bertram, L. (2005) Twenty years of the Alzheimer's disease amyloid hypothesis: a genetic perspective, *Cell 120*, 545-555.
[154] Cao, X., and Südhof, T. C. (2001) A transcriptively active complex of APP with Fe65 and histone acetyltransferase Tip60, *Science 293*, 115-120.
[155] Levy-Lahad, E., Wasco, W., Poorkaj, P., Romano, D. M., Oshima, J., Pettingell, W. H., Yu, C.-e., Jondro, P. D., Schmidt, S. D., and Wang, K. (1995) Candidate gene for the chromosome 1 familial Alzheimer's disease locus, *Science 269*, 973-977.
[156] Rogaev, E., Sherrington, R., Rogaeva, E., Levesque, G., Ikeda, M., Liang, Y., Chi, H., Lin, C., Holman, K., and Tsuda, T. (1995) Familial Alzheimer's disease in kindreds with missense mutations in a gene on chromosome 1 related to the Alzheimer's disease type 3 gene, *Nature 376*, 775-778.
[157] Sherrington, R., Rogaev, E., Liang, Y. a., Rogaeva, E., Levesque, G., Ikeda, M., Chi, H., Lin, C., Li, G., and Holman, K. (1995) Cloning of a gene bearing missense mutations in early-onset familial Alzheimer's disease, *Nature 375*, 754-760.
[158] Wolfe, M. S., Xia, W., Ostaszewski, B. L., Diehl, T. S., Kimberly, W. T., and Selkoe, D. J. (1999) Two transmembrane aspartates in presenilin-1 required for presenilin endoproteolysis and γ-secretase activity, *Nature 398*, 513-517.
[159] Sisodia, S. S., and St George-Hyslop, P. H. (2002) γ-Secretase, Notch, Aβ and Alzheimer's disease: where do the presenilins fit in?, *Nature Reviews Neuroscience 3*, 281-290.
[160] Beyreuther, K., and Masters, C. L. (1991) Amyloid Precursor Protein (APP) and BZA4 Amyloid in the Etiology of Alzheimer's Disease: Precursor-Product Relationships in the Derangement of Neuronal Function, *Brain Pathology 1*, 241-251.
[161] Hardy, J. (1997) Amyloid, the presenilins and Alzheimer's disease, *Trends in neurosciences 20*, 154-159.
[162] Selkoe, D. J. (1998) The cell biology of β-amyloid precursor protein and presenilin in Alzheimer's disease, *Trends in cell biology 8*, 447-453.
[163] Haass, C., Hung, A. Y., Schlossmacher, M., Teplow, D. B., and Selkoe, D. J. (1993) beta-Amyloid peptide and a 3-kDa fragment are derived by distinct cellular mechanisms, *Journal of Biological Chemistry 268*, 3021-3024.
[164] Kummer, M. P., and Heneka, M. T. (2014) Truncated and modified amyloid-beta species, *Alzheimer's research & therapy 6*, 28.
[165] O'Brien, R. J., and Wong, P. C. (2011) Amyloid precursor protein processing and Alzheimer's disease, *Annual review of neuroscience 34*, 185-204.

[166] Zhang, Y.-w., Thompson, R., Zhang, H., and Xu, H. (2011) APP processing in Alzheimer's disease, *Molecular brain 4*, 3.
[167] Thinakaran, G., and Koo, E. H. (2008) Amyloid precursor protein trafficking, processing, and function, *Journal of Biological Chemistry 283*, 29615-29619.
[168] Bastrup, J., Kastaniegaard, K., Asuni, A. A., Volbracht, C., and Stensballe, A. (2019) Proteomic and Unbiased Post-Translational Modification Profiling of Amyloid Plaques and Surrounding Tissue in a Transgenic Mouse Model of Alzheimer's Disease, *Journal of Alzheimer's Disease*, 1-19.
[169] Wang, D.-S., Dickson, D. W., and Malter, J. S. (2006) β-Amyloid degradation and Alzheimer's disease, *BioMed Research International 2006*.
[170] Schieb, H., Kratzin, H., Jahn, O., Möbius, W., Rabe, S., Staufenbiel, M., Wiltfang, J., and Klafki, H. W. (2011) β-Amyloid Peptide Variants in Brains and Cerebrospinal Fluid from Amyloid Precursor Protein (APP) Transgenic Mice COMPARISON WITH HUMAN ALZHEIMER AMYLOID, *Journal of Biological Chemistry 286*, 33747-33758.
[171] Kalback, W., Watson, M. D., Kokjohn, T. A., Kuo, Y.-M., Weiss, N., Luehrs, D. C., Lopez, J., Brune, D., Sisodia, S. S., and Staufenbiel, M. (2002) APP transgenic mice Tg2576 accumulate Aβ peptides that are distinct from the chemically modified and insoluble peptides deposited in Alzheimer's disease senile plaques, *Biochemistry 41*, 922-928.
[172] Bouter, Y., Dietrich, K., Wittnam, J. L., Rezaei-Ghaleh, N., Pillot, T., Papot-Couturier, S., Lefebvre, T., Sprenger, F., Wirths, O., and Zweckstetter, M. (2013) N-truncated amyloid β (Aβ) 4-42 forms stable aggregates and induces acute and long-lasting behavioral deficits, *Acta neuropathologica 126*, 189-205.
[173] Guzmán, E. A., Bouter, Y., Richard, B. C., Lannfelt, L., Ingelsson, M., Paetau, A., Verkkoniemi-Ahola, A., Wirths, O., and Bayer, T. A. (2014) Abundance of Aβ 5-x like immunoreactivity in transgenic 5XFAD, APP/PS1KI and 3xTG mice, sporadic and familial Alzheimer's disease, *Molecular neurodegeneration 9*, 13.
[174] Haass, C., and Selkoe, D. J. (2007) Soluble protein oligomers in neurodegeneration: lessons from the Alzheimer's amyloid β-peptide, *Nature reviews Molecular cell biology 8*, 101-112.
[175] Lesne, S. E., Sherman, M. A., Grant, M., Kuskowski, M., Schneider, J. A., Bennett, D. A., and Ashe, K. H. (2013) Brain amyloid-β oligomers in ageing and Alzheimer's disease, *Brain 136*, 1383-1398.
[176] Sakono, M., and Zako, T. (2010) Amyloid oligomers: formation and toxicity of Aβ oligomers, *The FEBS journal 277*, 1348-1358.

[177] Karran, E., and De Strooper, B. (2016) The amyloid cascade hypothesis: are we poised for success or failure?, *Journal of Neurochemistry 139*, 237-252.
[178] Funato, H., Yoshimura, M., Kusui, K., Tamaoka, A., Ishikawa, K., Ohkoshi, N., Namekata, K., Okeda, R., and Ihara, Y. (1998) Quantitation of amyloid beta-protein (A beta) in the cortex during aging and in Alzheimer's disease, *The American journal of pathology 152*, 1633.
[179] Rodrigue, K., Kennedy, K., Devous, M., Rieck, J., Hebrank, A., Diaz-Arrastia, R., Mathews, D., and Park, D. (2012) β-Amyloid burden in healthy aging: regional distribution and cognitive consequences, *Neurology 78*, 387-395.
[180] Saido, T., and Leissring, M. A. (2012) Proteolytic degradation of amyloid β-protein, *Cold Spring Harbor perspectives in medicine 2*, a006379.
[181] Selkoe, D. J. (2001) Clearing the brain's amyloid cobwebs, *Neuron 32*, 177-180.
[182] Tanzi, R., Moir, R., and Wagner, S. (2004) Clearance of Alzheimer's Aβ peptide: the many roads to perdition, *Neuron 43*, 605-608.
[183] Haass, C., and Selkoe, D. J. (2007) Soluble protein oligomers in neurodegeneration: lessons from the Alzheimer's amyloid β-peptide, *Nature reviews Molecular cell biology 8*, 101.
[184] LaFerla, F. M., Green, K. N., and Oddo, S. (2007) Intracellular amyloid-β in Alzheimer's disease, *Nature Reviews Neuroscience 8*, 499-509.
[185] Wirths, O., Multhaup, G., and Bayer, T. A. (2004) A modified β-amyloid hypothesis: intraneuronal accumulation of the β-amyloid peptide–the first step of a fatal cascade, *Journal of neurochemistry 91*, 513-520.
[186] Lacor, P. N., Buniel, M. C., Chang, L., Fernandez, S. J., Gong, Y., Viola, K. L., Lambert, M. P., Velasco, P. T., Bigio, E. H., and Finch, C. E. (2004) Synaptic targeting by Alzheimer's-related amyloid β oligomers, *Journal of Neuroscience 24*, 10191-10200.
[187] Selkoe, D. J. (2008) Soluble oligomers of the amyloid β-protein: Impair synaptic plasticity and behavior, In *Synaptic Plasticity and the Mechanism of Alzheimer's Disease*, pp 89-102, Springer.
[188] Laurén, J., Gimbel, D. A., Nygaard, H. B., Gilbert, J. W., and Strittmatter, S. M. (2009) Cellular prion protein mediates impairment of synaptic plasticity by amyloid-β oligomers, *Nature 457*, 1128-1132.
[189] White, J. A., Manelli, A. M., Holmberg, K. H., Van Eldik, L. J., and LaDu, M. J. (2005) Differential effects of oligomeric and fibrillar amyloid-β1–42 on astrocyte-mediated inflammation, *Neurobiology of disease 18*, 459-465.

[190] Salminen, A., Ojala, J., Kauppinen, A., Kaarniranta, K., and Suuronen, T. (2009) Inflammation in Alzheimer's disease: amyloid-β oligomers trigger innate immunity defence via pattern recognition receptors, *Progress in neurobiology 87*, 181-194.
[191] Akiyama, H., Barger, S., Barnum, S., Bradt, B., Bauer, J., Cole, G. M., Cooper, N. R., Eikelenboom, P., Emmerling, M., and Fiebich, B. L. (2000) Inflammation and Alzheimer's disease, *Neurobiology of aging 21*, 383-421.
[192] Wyss-Coray, T. (2006) Inflammation in Alzheimer disease: driving force, bystander or beneficial response?, *Nature medicine 12*, 1005-1015.
[193] Glabe, C. G. (2006) Common mechanisms of amyloid oligomer pathogenesis in degenerative disease, *Neurobiology of aging 27*, 570-575.
[194] Nixon, R. A. (2017) Amyloid precursor protein and endosomal–lysosomal dysfunction in Alzheimer's disease: inseparable partners in a multifactorial disease, *The FASEB Journal 31*, 2729-2743.
[195] Ma, Q.-L., Yang, F., Rosario, E. R., Ubeda, O. J., Beech, W., Gant, D. J., Chen, P. P., Hudspeth, B., Chen, C., and Zhao, Y. (2009) β-amyloid oligomers induce phosphorylation of tau and inactivation of insulin receptor substrate via c-Jun N-terminal kinase signaling: suppression by omega-3 fatty acids and curcumin, *Journal of Neuroscience 29*, 9078-9089.
[196] Amar, F., Sherman, M. A., Rush, T., Larson, M., Boyle, G., Chang, L., Götz, J., Buisson, A., and Lesné, S. E. (2017) The amyloid-β oligomer Aβ* 56 induces specific alterations in neuronal signaling that lead to tau phosphorylation and aggregation, *Science signaling 10*.
[197] Jin, M., Shepardson, N., Yang, T., Chen, G., Walsh, D., and Selkoe, D. J. (2011) Soluble amyloid β-protein dimers isolated from Alzheimer cortex directly induce Tau hyperphosphorylation and neuritic degeneration, *Proceedings of the National Academy of Sciences 108*, 5819-5824.
[198] Hernández, F., de Barreda, E. G., Fuster-Matanzo, A., Lucas, J. J., and Avila, J. (2010) GSK3: a possible link between beta amyloid peptide and tau protein, *Experimental neurology 223*, 322-325.
[199] Zhang, F., Gannon, M., Chen, Y., Yan, S., Zhang, S., Feng, W., Tao, J., Sha, B., Liu, Z., and Saito, T. (2020) β-amyloid redirects norepinephrine signaling to activate the pathogenic GSK3β/tau cascade, *Science Translational Medicine 12*.
[200] Selkoe, D. J. (2002) Alzheimer's disease is a synaptic failure, *Science 298*, 789-791.
[201] Wang, H. Y., Lee, D. H., Davis, C. B., and Shank, R. P. (2000) Amyloid peptide Aβ1-42 binds selectively and with picomolar

affinity to α7 nicotinic acetylcholine receptors, *Journal of neurochemistry 75*, 1155-1161.
[202] Henstridge, C. M., Hyman, B. T., and Spires-Jones, T. L. (2019) Beyond the neuron–cellular interactions early in Alzheimer disease pathogenesis, *Nature Reviews Neuroscience 20*, 94-108.
[203] Schaeffer, E. L., Figueiro, M., and Gattaz, W. F. (2011) Insights into Alzheimer disease pathogenesis from studies in transgenic animal models, *Clinics 66*, 45-54.
[204] Duyckaerts, C., Potier, M.-C., and Delatour, B. (2008) Alzheimer disease models and human neuropathology: similarities and differences, *Acta neuropathologica 115*, 5-38.
[205] Elder, G. A., Gama Sosa, M. A., and De Gasperi, R. (2010) Transgenic mouse models of Alzheimer's disease, *Mount Sinai Journal of Medicine: A Journal of Translational and Personalized Medicine: A Journal of Translational and Personalized Medicine 77*, 69-81.
[206] Götz, J., and Ittner, L. M. (2008) Animal models of Alzheimer's disease and frontotemporal dementia, *Nature Reviews Neuroscience 9*, 532-544.
[207] Grabowski, T. J., Cho, H. S., Vonsattel, J. P. G., Rebeck, G. W., and Greenberg, S. M. (2001) Novel amyloid precursor protein mutation in an Iowa family with dementia and severe cerebral amyloid angiopathy, *Annals of Neurology: Official Journal of the American Neurological Association and the Child Neurology Society 49*, 697-705.
[208] Levy, E., Carman, M. D., Fernandez-Madrid, I. J., Power, M. D., Lieberburg, I., van Duinen, S. G., Bots, G., Luyendijk, W., and Frangione, B. (1990) Mutation of the Alzheimer's disease amyloid gene in hereditary cerebral hemorrhage, Dutch type, *Science 248*, 1124-1126.
[209] Goate, A., Chartier-Harlin, M.-C., Mullan, M., Brown, J., Crawford, F., Fidani, L., Giuffra, L., Haynes, A., Irving, N., and James, L. (1991) Segregation of a missense mutation in the amyloid precursor protein gene with familial Alzheimer's disease, *Nature 349*, 704-706.
[210] Murrell, J., Farlow, M., Ghetti, B., and Benson, M. D. (1991) A mutation in the amyloid precursor protein associated with hereditary Alzheimer's disease, *Science 254*, 97-99.
[211] Mullan, M., Crawford, F., Axelman, K., Houlden, H., Lilius, L., Winblad, B., and Lannfelt, L. (1992) A pathogenic mutation for probable Alzheimer's disease in the APP gene at the N–terminus of β–amyloid, *Nature genetics 1*, 345-347.
[212] Eckman, C. B., Mehta, N. D., Crook, R., Perez-tur, J., Prihar, G., Pfeiffer, E., Graff-Radford, N., Hinder, P., Yager, D., and Zenk, B. (1997) A new pathogenic mutation in the APP gene (I716V) increases the relative proportion of Aβ42 (43), *Human molecular genetics 6*, 2087-2089.

[213] Nilsberth, C., Westlind-Danielsson, A., Eckman, C. B., Condron, M. M., Axelman, K., Forsell, C., Stenh, C., Luthman, J., Teplow, D. B., and Younkin, S. G. (2001) The'Arctic'APP mutation (E693G) causes Alzheimer's disease by enhanced Aβ protofibril formation, *Nature neuroscience 4*, 887-893.

[214] Janssen, J., Beck, J., Campbell, T., Dickinson, A., Fox, N., Harvey, R., Houlden, H., Rossor, M., and Collinge, J. (2003) Early onset familial Alzheimer's disease: mutation frequency in 31 families, *Neurology 60*, 235-239.

[215] Ertekin-Taner, N. (2007) Genetics of Alzheimer's disease: a centennial review, *Neurologic clinics 25*, 611-667.

[216] Alexandru, A., Jagla, W., Graubner, S., Becker, A., Bäuscher, C., Kohlmann, S., Sedlmeier, R., Raber, K. A., Cynis, H., and Rönicke, R. (2011) Selective hippocampal neurodegeneration in transgenic mice expressing small amounts of truncated Aβ is induced by pyroglutamate–Aβ formation, *Journal of Neuroscience 31*, 12790-12801.

[217] Games, D., Adams, D., Alessandrini, R., Barbour, R., Borthelette, P., Blackwell, C., Carr, T., Clemens, J., Donaldson, T., and Gillespie, F. (1995) Alzheimer-type neuropathology in transgenic mice overexpressing V717F β-amyloid precursor protein, *Nature 373*, 523-527.

[218] Johnson-Wood, K., Lee, M., Motter, R., Hu, K., Gordon, G., Barbour, R., Khan, K., Gordon, M., Tan, H., and Games, D. (1997) Amyloid precursor protein processing and Aβ42 deposition in a transgenic mouse model of Alzheimer disease, *Proceedings of the National Academy of Sciences 94*, 1550-1555.

[219] Irizarry, M. C., Soriano, F., McNamara, M., Page, K. J., Schenk, D., Games, D., and Hyman, B. T. (1997) Aβ deposition is associated with neuropil changes, but not with overt neuronal loss in the human amyloid precursor protein V717F (PDAPP) transgenic mouse, *Journal of Neuroscience 17*, 7053-7059.

[220] Perez, R. G., Squazzo, S. L., and Koo, E. H. (1996) Enhanced Release of Amyloid-Protein from Codon 670/671 Swedish Mutant-Amyloid Precursor Protein Occurs in Both Secretory and Endocytic Pathways, *Journal of Biological Chemistry 271*, 9100-9107.

[221] Mann, D., Iwatsubo, T., Ihara, Y., Cairns, N., Lantos, P., Bogdanovic, N., Lannfelt, L., Winblad, B., Maat-Schieman, M., and Rossor, M. (1996) Predominant deposition of amyloid-beta 42 (43) in plaques in cases of Alzheimer's disease and hereditary cerebral hemorrhage associated with mutations in the amyloid precursor protein gene, *The American journal of pathology 148*, 1257.

[222] Irizarry, M. C., McNamara, M., Fedorchak, K., Hsiao, K., and Hyman, B. T. (1997) APPSw transgenic mice develop age-related Aβ

deposits and neuropil abnormalities, but no neuronal loss in CA1, *Journal of Neuropathology & Experimental Neurology 56*, 965-973.

[223] Chapman, P. F., White, G. L., Jones, M. W., Cooper-Blacketer, D., Marshall, V. J., Irizarry, M., Younkin, L., Good, M. A., Bliss, T., and Hyman, B. T. (1999) Impaired synaptic plasticity and learning in aged amyloid precursor protein transgenic mice, *Nature neuroscience 2*, 271-276.

[224] Chishti, M. A., Yang, D.-S., Janus, C., Phinney, A. L., Horne, P., Pearson, J., Strome, R., Zuker, N., Loukides, J., and French, J. (2001) Early-onset amyloid deposition and cognitive deficits in transgenic mice expressing a double mutant form of amyloid precursor protein 695, *Journal of Biological Chemistry 276*, 21562-21570.

[225] Lord, A., Kalimo, H., Eckman, C., Zhang, X.-Q., Lannfelt, L., and Nilsson, L. N. (2006) The Arctic Alzheimer mutation facilitates early intraneuronal Aβ aggregation and senile plaque formation in transgenic mice, *Neurobiology of aging 27*, 67-77.

[226] Knobloch, M., Konietzko, U., Krebs, D. C., and Nitsch, R. M. (2007) Intracellular Aβ and cognitive deficits precede β-amyloid deposition in transgenic arcAβ mice, *Neurobiology of aging 28*, 1297-1306.

[227] Wirths, O., Multhaup, G., Czech, C., Feldmann, N., Blanchard, V., Tremp, G., Beyreuther, K., Pradier, L., and Bayer, T. A. (2002) Intraneuronal APP/Aβ Trafficking and Plaque Formation in β-Amyloid Precursor Protein and Presenilin-1 Transgenic Mice, *Brain Pathology 12*, 275-286.

[228] Rutten, B. P., Van der Kolk, N. M., Schafer, S., van Zandvoort, M. A., Bayer, T. A., Steinbusch, H. W., and Schmitz, C. (2005) Age-related loss of synaptophysin immunoreactive presynaptic boutons within the hippocampus of APP751SL, PS1M146L, and APP751SL/PS1M146L transgenic mice, *The American journal of pathology 167*, 161-173.

[229] Oakley, H., Cole, S. L., Logan, S., Maus, E., Shao, P., Craft, J., Guillozet-Bongaarts, A., Ohno, M., Disterhoft, J., and Van Eldik, L. (2006) Intraneuronal β-amyloid aggregates, neurodegeneration, and neuron loss in transgenic mice with five familial Alzheimer's disease mutations: potential factors in amyloid plaque formation, *Journal of Neuroscience 26*, 10129-10140.

[230] Tomiyama, T., Matsuyama, S., Iso, H., Umeda, T., Takuma, H., Ohnishi, K., Ishibashi, K., Teraoka, R., Sakama, N., and Yamashita, T. (2010) A mouse model of amyloid β oligomers: their contribution to synaptic alteration, abnormal tau phosphorylation, glial activation, and neuronal loss in vivo, *Journal of Neuroscience 30*, 4845-4856.

[231] Oddo, S., Caccamo, A., Shepherd, J. D., Murphy, M. P., Golde, T. E., Kayed, R., Metherate, R., Mattson, M. P., Akbari, Y., and LaFerla, F. M. (2003) Triple-transgenic model of Alzheimer's disease with

plaques and tangles: intracellular Aβ and synaptic dysfunction, *Neuron 39*, 409-421.
[232] Billings, L. M., Oddo, S., Green, K. N., McGaugh, J. L., and LaFerla, F. M. (2005) Intraneuronal Aβ causes the onset of early Alzheimer's disease-related cognitive deficits in transgenic mice, *Neuron 45*, 675-688.
[233] Wirths, O., Breyhan, H., Cynis, H., Schilling, S., Demuth, H.-U., and Bayer, T. A. (2009) Intraneuronal pyroglutamate-Abeta 3–42 triggers neurodegeneration and lethal neurological deficits in a transgenic mouse model, *Acta neuropathologica 118*, 487-496.
[234] Herreman, A., Hartmann, D., Annaert, W., Saftig, P., Craessaerts, K., Serneels, L., Umans, L., Schrijvers, V., Checler, F., and Vanderstichele, H. (1999) Presenilin 2 deficiency causes a mild pulmonary phenotype and no changes in amyloid precursor protein processing but enhances the embryonic lethal phenotype of presenilin 1 deficiency, *Proceedings of the National Academy of Sciences 96*, 11872-11877.
[235] De Strooper, B. (2007) Loss-of-function presenilin mutations in Alzheimer disease, *EMBO reports 8*, 141-146.
[236] Luo, Y., Bolon, B., Kahn, S., Bennett, B. D., Babu-Khan, S., Denis, P., Fan, W., Kha, H., Zhang, J., and Gong, Y. (2001) Mice deficient in BACE1, the Alzheimer's β-secretase, have normal phenotype and abolished β-amyloid generation, *Nature neuroscience 4*, 231-232.
[237] Krohn, M., Bracke, A., Avchalumov, Y., Schumacher, T., Hofrichter, J., Paarmann, K., Fröhlich, C., Lange, C., Brüning, T., and von Bohlen und Halbach, O. (2015) Accumulation of murine amyloid-β mimics early Alzheimer's disease, *Brain 138*, 2370-2382.
[238] Huettenrauch, M., Baches, S., Gerth, J., Bayer, T. A., Weggen, S., and Wirths, O. (2015) Neprilysin deficiency alters the neuropathological and behavioral phenotype in the 5XFAD mouse model of Alzheimer's disease, *Journal of Alzheimer's Disease 44*, 1291-1302.
[239] Saito, T., Matsuba, Y., Mihira, N., Takano, J., Nilsson, P., Itohara, S., Iwata, N., and Saido, T. C. (2014) Single App knock-in mouse models of Alzheimer's disease, *Nature neuroscience 17*, 661-663.
[240] Nilsson, P., Saito, T., and Saido, T. C. (2014) New mouse model of Alzheimer's, ACS Publications.
[241] Piedrahita, J. A., Zhang, S. H., Hagaman, J. R., Oliver, P. M., and Maeda, N. (1992) Generation of mice carrying a mutant apolipoprotein E gene inactivated by gene targeting in embryonic stem cells, *Proceedings of the National Academy of Sciences 89*, 4471-4475.
[242] Kim, J., Jiang, H., Park, S., Eltorai, A. E., Stewart, F. R., Yoon, H., Basak, J. M., Finn, M. B., and Holtzman, D. M. (2011) Haploinsufficiency of human APOE reduces amyloid deposition in a

mouse model of amyloid-β amyloidosis, *Journal of Neuroscience 31*, 18007-18012.

[243] Leyns, C. E., Ulrich, J. D., Finn, M. B., Stewart, F. R., Koscal, L. J., Serrano, J. R., Robinson, G. O., Anderson, E., Colonna, M., and Holtzman, D. M. (2017) TREM2 deficiency attenuates neuroinflammation and protects against neurodegeneration in a mouse model of tauopathy, *Proceedings of the National Academy of Sciences 114*, 11524-11529.

[244] Griciuc, A., Patel, S., Federico, A. N., Choi, S. H., Innes, B. J., Oram, M. K., Cereghetti, G., McGinty, D., Anselmo, A., and Sadreyev, R. I. (2019) TREM2 Acts Downstream of CD33 in Modulating Microglial Pathology in Alzheimer's Disease, *Neuron 103*, 820-835. e827.

[245] Koldamova, R., Staufenbiel, M., and Lefterov, I. (2005) Lack of ABCA1 considerably decreases brain ApoE level and increases amyloid deposition in APP23 mice, *Journal of Biological Chemistry 280*, 43224-43235.

[246] Wahrle, S. E., Jiang, H., Parsadanian, M., Legleiter, J., Han, X., Fryer, J. D., Kowalewski, T., and Holtzman, D. M. (2004) ABCA1 is required for normal central nervous system ApoE levels and for lipidation of astrocyte-secreted apoE, *Journal of Biological Chemistry 279*, 40987-40993.

[247] Kayed, R., and Lasagna-Reeves, C. A. (2013) Molecular mechanisms of amyloid oligomers toxicity, *Journal of Alzheimer's Disease 33*, S67-S78.

[248] Cohen, R. M., Rezai-Zadeh, K., Weitz, T. M., Rentsendorj, A., Gate, D., Spivak, I., Bholat, Y., Vasilevko, V., Glabe, C. G., and Breunig, J. J. (2013) A transgenic Alzheimer rat with plaques, tau pathology, behavioral impairment, oligomeric aβ, and frank neuronal loss, *Journal of Neuroscience 33*, 6245-6256.

[249] Foley, P. (2010) Lipids in Alzheimer's disease: a century-old story, *Biochimica et Biophysica Acta (BBA)-Molecular and Cell Biology of Lipids 1801*, 750-753.

[250] Hartmann, T., Kuchenbecker, J., and Grimm, M. O. (2007) Alzheimer's disease: the lipid connection, *Journal of Neurochemistry 103*, 159-170.

[251] van der Kant, R., Langness, V. F., Herrera, C. M., Williams, D. A., Fong, L. K., Leestemaker, Y., Steenvoorden, E., Rynearson, K. D., Brouwers, J. F., and Helms, J. B. (2019) Cholesterol metabolism is a druggable axis that independently regulates tau and amyloid-β in iPSC-derived Alzheimer's disease neurons, *Cell stem cell 24*, 363-375. e369.

[252] Demuro, A., Mina, E., Kayed, R., Milton, S. C., Parker, I., and Glabe, C. G. (2005) Calcium dysregulation and membrane disruption as a ubiquitous neurotoxic mechanism of soluble amyloid oligomers, *Journal of Biological Chemistry 280*, 17294-17300.

[253] Berman, D. E., Dall'Armi, C., Voronov, S. V., McIntire, L. B. J., Zhang, H., Moore, A. Z., Staniszewski, A., Arancio, O., Kim, T.-W., and Di Paolo, G. (2008) Oligomeric amyloid-β peptide disrupts phosphatidylinositol-4, 5-bisphosphate metabolism, *Nature neuroscience 11*, 547-554.

[254] Grimm, M. O., Mett, J., Stahlmann, C. P., Grösgen, S., Haupenthal, V. J., Blümel, T., Hundsdörfer, B., Zimmer, V. C., Mylonas, N. T., and Tanila, H. (2015) APP intracellular domain derived from amyloidogenic β-and γ-secretase cleavage regulates neprilysin expression, *Frontiers in aging neuroscience 7*.

[255] Grimm, M. O., Grösgen, S., Rothhaar, T. L., Burg, V. K., Hundsdörfer, B., Haupenthal, V. J., Friess, P., Müller, U., Fassbender, K., and Riemenschneider, M. (2011) Intracellular APP domain regulates serine-palmitoyl-CoA transferase expression and is affected in Alzheimer's disease, *International Journal of Alzheimer's Disease 2011*.

[256] Palavicini, J. P., Wang, C., Chen, L., Hosang, K., Wang, J., Tomiyama, T., Mori, H., and Han, X. (2017) Oligomeric amyloid-beta induces MAPK-mediated activation of brain cytosolic and calcium-independent phospholipase A 2 in a spatial-specific manner, *Acta neuropathologica communications 5*, 56.

[257] Grimm, M. O., Grimm, H. S., Pätzold, A. J., Zinser, E. G., Halonen, R., Duering, M., Tschäpe, J.-A., De Strooper, B., Müller, U., and Shen, J. (2005) Regulation of cholesterol and sphingomyelin metabolism by amyloid-β and presenilin, *Nature cell biology 7*, 1118-1123.

[258] Onodera, T., Futai, E., Kan, E., Abe, N., Uchida, T., Kamio, Y., and Kaneko, J. (2014) Phosphatidylethanolamine plasmalogen enhances the inhibiting effect of phosphatidylethanolamine on γ-secretase activity, *The Journal of Biochemistry 157*, 301-309.

[259] Zha, Q., Ruan, Y., Hartmann, T., Beyreuther, K., and Zhang, D. (2004) GM1 ganglioside regulates the proteolysis of amyloid precursor protein, *Molecular psychiatry 9*, 946-952.

[260] Kalvodova, L., Kahya, N., Schwille, P., Ehehalt, R., Verkade, P., Drechsel, D., and Simons, K. (2005) Lipids as modulators of proteolytic activity of BACE involvement of cholesterol, glycosphingolipids, and anionic phospholipids in vitro, *Journal of Biological Chemistry 280*, 36815-36823.

[261] Kojro, E., Gimpl, G., Lammich, S., März, W., and Fahrenholz, F. (2001) Low cholesterol stimulates the nonamyloidogenic pathway by its effect on the α-secretase ADAM 10, *Proceedings of the National Academy of Sciences 98*, 5815-5820.

[262] Yanagisawa, K., Odaka, A., Suzuki, N., and Ihara, Y. (1995) GM1 ganglioside–bound amyloid β–protein (Aβ): A possible form of preamyloid in Alzheimer's disease, *Nature medicine 1*, 1062-1066.

[263] Hayashi, H., Kimura, N., Yamaguchi, H., Hasegawa, K., Yokoseki, T., Shibata, M., Yamamoto, N., Michikawa, M., Yoshikawa, Y., and Terao, K. (2004) A seed for Alzheimer amyloid in the brain, *Journal of Neuroscience 24*, 4894-4902.

[264] Martins, I. C., Kuperstein, I., Wilkinson, H., Maes, E., Vanbrabant, M., Jonckheere, W., Van Gelder, P., Hartmann, D., D'Hooge, R., and De Strooper, B. (2008) Lipids revert inert Aβ amyloid fibrils to neurotoxic protofibrils that affect learning in mice, *The EMBO journal 27*, 224-233.

[265] Osawa, S., Funamoto, S., Nobuhara, M., Wada-Kakuda, S., Shimojo, M., Yagishita, S., and Ihara, Y. (2008) Phosphoinositides suppress γ-secretase in both the detergent-soluble and-insoluble states, *Journal of Biological Chemistry 283*, 19283-19292.

[266] Sevastou, I., Kaffe, E., Mouratis, M.-A., and Aidinis, V. (2013) Lysoglycerophospholipids in chronic inflammatory disorders: the PLA2/LPC and ATX/LPA axes, *Biochimica et Biophysica Acta (BBA)-Molecular and Cell Biology of Lipids 1831*, 42-60.

[267] Yang, D.-S., Stavrides, P., Saito, M., Kumar, A., Rodriguez-Navarro, J. A., Pawlik, M., Huo, C., Walkley, S. U., Saito, M., and Cuervo, A. M. (2014) Defective macroautophagic turnover of brain lipids in the TgCRND8 Alzheimer mouse model: prevention by correcting lysosomal proteolytic deficits, *Brain 137*, 3300-3318.

[268] Tamboli, I. Y., Tien, N. T., and Walter, J. (2011) Sphingolipid storage impairs autophagic clearance of Alzheimer-associated proteins, *Autophagy 7*, 645-646.

[269] Wang, X., Wang, W., Li, L., Perry, G., Lee, H.-g., and Zhu, X. (2014) Oxidative stress and mitochondrial dysfunction in Alzheimer's disease, *Biochimica et Biophysica Acta (BBA)-Molecular Basis of Disease 1842*, 1240-1247.

[270] Moreira, P. I., Carvalho, C., Zhu, X., Smith, M. A., and Perry, G. (2010) Mitochondrial dysfunction is a trigger of Alzheimer's disease pathophysiology, *Biochimica et Biophysica Acta (BBA)-Molecular Basis of Disease 1802*, 2-10.

[271] Sayre, L. M., Zelasko, D. A., Harris, P. L., Perry, G., Salomon, R. G., and Smith, M. A. (1997) 4-Hydroxynonenal-derived advanced lipid peroxidation end products are increased in Alzheimer's disease, *Journal of neurochemistry 68*, 2092-2097.

[272] Cruchaga, C., Karch, C. M., Jin, S. C., Benitez, B. A., Cai, Y., Guerreiro, R., Harari, O., Norton, J., Budde, J., and Bertelsen, S. (2014) Rare coding variants in the phospholipase D3 gene confer risk for Alzheimer's disease, *Nature 505*, 550-554.

[273] van Echten-Deckert, G., and Walter, J. (2012) Sphingolipids: critical players in Alzheimer's disease, *Progress in lipid research 51*, 378-393.

[274] Yanagisawa, K. (2007) Role of gangliosides in Alzheimer's disease, *Biochimica et Biophysica Acta (BBA)-Biomembranes 1768*, 1943-1951.
[275] Monteiro-Cardoso, V. F., Oliveira, M. M., Melo, T., Domingues, M. R., Moreira, P. I., Ferreiro, E., Peixoto, F., and Videira, R. A. (2015) Cardiolipin profile changes are associated to the early synaptic mitochondrial dysfunction in Alzheimer's disease, *Journal of Alzheimer's Disease 43*, 1375-1392.
[276] Frisardi, V., Panza, F., Seripa, D., Farooqui, T., and Farooqui, A. A. (2011) Glycerophospholipids and glycerophospholipid-derived lipid mediators: a complex meshwork in Alzheimer's disease pathology, *Progress in lipid research 50*, 313-330.
[277] Hamilton, L. K., Dufresne, M., Joppé, S. E., Petryszyn, S., Aumont, A., Calon, F., Barnabé-Heider, F., Furtos, A., Parent, M., and Chaurand, P. (2015) Aberrant lipid metabolism in the forebrain niche suppresses adult neural stem cell proliferation in an animal model of Alzheimer's disease, *Cell stem cell 17*, 397-411.
[278] Su, X. Q., Wang, J., and Sinclair, A. J. (2019) Plasmalogens and Alzheimer's disease: a review, *Lipids in health and disease 18*, 100.
[279] Lim, G. P., Calon, F., Morihara, T., Yang, F., Teter, B., Ubeda, O., Salem, N., Frautschy, S. A., and Cole, G. M. (2005) A diet enriched with the omega-3 fatty acid docosahexaenoic acid reduces amyloid burden in an aged Alzheimer mouse model, *Journal of Neuroscience 25*, 3032-3040.
[280] Puglielli, L., Tanzi, R. E., and Kovacs, D. M. (2003) Alzheimer's disease: the cholesterol connection, *Nature neuroscience 6*, 345-351.
[281] Nugent, A. A., Lin, K., Van Lengerich, B., Lianoglou, S., Przybyla, L., Davis, S. S., Llapashtica, C., Wang, J., Xia, D., and Lucas, A. (2020) TREM2 Regulates Microglial Cholesterol Metabolism upon Chronic Phagocytic Challenge, *Neuron*.
[282] Burns, M. P., Noble, W. J., Olm, V., Gaynor, K., Casey, E., LaFrancois, J., Wang, L., and Duff, K. (2003) Co-localization of cholesterol, apolipoprotein E and fibrillar Aβ in amyloid plaques, *Molecular brain research 110*, 119-125.
[283] González-Domínguez, R., García-Barrera, T., and Gómez-Ariza, J. L. (2014) Combination of metabolomic and phospholipid-profiling approaches for the study of Alzheimer's disease, *Journal of proteomics 104*, 37-47.
[284] Stokes, C. E., and Hawthorne, J. N. (1987) Reduced phosphoinositide concentrations in anterior temporal cortex of Alzheimer-diseased brains, *Journal of neurochemistry 48*, 1018-1021.
[285] Bazan, N. G., Colangelo, V., and Lukiw, W. J. (2002) Prostaglandins and other lipid mediators in Alzheimer's disease, *Prostaglandins & other lipid mediators 68*, 197-210.

[286] Mulder, J., Zilberter, M., Pasquare, S. J., Alpar, A., Schulte, G., Ferreira, S. G., Köfalvi, A., Martín-Moreno, A. M., Keimpema, E., and Tanila, H. (2011) Molecular reorganization of endocannabinoid signalling in Alzheimer's disease, *Brain 134*, 1041-1060.
[287] Hannun, Y. A., and Obeid, L. M. (2008) Principles of bioactive lipid signalling: lessons from sphingolipids, *Nature reviews Molecular cell biology 9*, 139-150.
[288] Simons, K., and Toomre, D. (2000) Lipid rafts and signal transduction, *Nature reviews Molecular cell biology 1*, 31-39.
[289] Bartke, N., and Hannun, Y. A. (2009) Bioactive sphingolipids: metabolism and function, *Journal of lipid research 50*, S91-S96.
[290] Cheng, H., Vetrivel, K. S., Gong, P., Meckler, X., Parent, A., and Thinakaran, G. (2007) Mechanisms of disease: new therapeutic strategies for Alzheimer's disease—targeting APP processing in lipid rafts, *Nature Clinical Practice Neurology 3*, 374-382.
[291] Tamboli, I. Y., Prager, K., Barth, E., Heneka, M., Sandhoff, K., and Walter, J. (2005) Inhibition of glycosphingolipid biosynthesis reduces secretion of the β-amyloid precursor protein and amyloid β-peptide, *Journal of Biological Chemistry 280*, 28110-28117.
[292] Sawamura, N., Ko, M., Yu, W., Zou, K., Hanada, K., Suzuki, T., Gong, J.-S., Yanagisawa, K., and Michikawa, M. (2004) Modulation of amyloid precursor protein cleavage by cellular sphingolipids, *Journal of Biological Chemistry 279*, 11984-11991.
[293] Puglielli, L., Ellis, B. C., Saunders, A. J., and Kovacs, D. M. (2003) Ceramide stabilizes β-site amyloid precursor protein-cleaving enzyme 1 and promotes amyloid β-peptide biogenesis, *Journal of Biological Chemistry 278*, 19777-19783.
[294] Takasugi, N., Sasaki, T., Suzuki, K., Osawa, S., Isshiki, H., Hori, Y., Shimada, N., Higo, T., Yokoshima, S., and Fukuyama, T. (2011) BACE1 activity is modulated by cell-associated sphingosine-1-phosphate, *Journal of Neuroscience 31*, 6850-6857.
[295] Zhang, H., Ding, J., Tian, W., Wang, L., Huang, L., Ruan, Y., Lu, T., Sha, Y., and Zhang, D. (2009) Ganglioside GM1 binding the N-terminus of amyloid precursor protein, *Neurobiology of aging 30*, 1245-1253.
[296] Zha, Q., Ruan, Y., Hartmann, T., Beyreuther, K., and Zhang, D. (2004) GM1 ganglioside regulates the proteolysis of amyloid precursor protein, *Molecular psychiatry 9*, 946.
[297] Whyte, L. S., Lau, A. A., Hemsley, K. M., Hopwood, J. J., and Sargeant, T. J. (2017) Endo-lysosomal and autophagic dysfunction: a driving factor in Alzheimer's disease?, *Journal of neurochemistry 140*, 703-717.
[298] Kakio, A., Nishimoto, S.-i., Yanagisawa, K., Kozutsumi, Y., and Matsuzaki, K. (2001) Cholesterol-dependent formation of GM1 ganglioside-bound amyloid β-protein, an endogenous seed for

Alzheimer amyloid, *Journal of Biological Chemistry 276*, 24985-24990.

[299] Han, X., M Holtzman, D., W McKeel, D., Kelley, J., and Morris, J. C. (2002) Substantial sulfatide deficiency and ceramide elevation in very early Alzheimer's disease: potential role in disease pathogenesis, *Journal of neurochemistry 82*, 809-818.

[300] Han, X. (2005) Lipid alterations in the earliest clinically recognizable stage of Alzheimer's disease: implication of the role of lipids in the pathogenesis of Alzheimer's disease, *Current Alzheimer Research 2*, 65-77.

[301] Cheng, H., Zhou, Y., Holtzman, D. M., and Han, X. (2010) Apolipoprotein E mediates sulfatide depletion in animal models of Alzheimer's disease, *Neurobiology of aging 31*, 1188-1196.

[302] Han, X. (2007) Potential mechanisms contributing to sulfatide depletion at the earliest clinically recognizable stage of Alzheimer's disease: a tale of shotgun lipidomics, *Journal of neurochemistry 103*, 171-179.

[303] Cutler, R. G., Kelly, J., Storie, K., Pedersen, W. A., Tammara, A., Hatanpaa, K., Troncoso, J. C., and Mattson, M. P. (2004) Involvement of oxidative stress-induced abnormalities in ceramide and cholesterol metabolism in brain aging and Alzheimer's disease, *Proceedings of the National Academy of Sciences 101*, 2070-2075.

[304] Jana, A., and Pahan, K. (2004) Fibrillar Amyloid-β Peptides Kill Human Primary Neurons via NADPH Oxidase-mediated Activation of Neutral Sphingomyelinase IMPLICATIONS FOR ALZHEIMER'S DISEASE, *Journal of Biological Chemistry 279*, 51451-51459.

[305] Lee, J.-T., Xu, J., Lee, J.-M., Ku, G., Han, X., Yang, D.-I., Chen, S., and Hsu, C. Y. (2004) Amyloid-β peptide induces oligodendrocyte death by activating the neutral sphingomyelinase–ceramide pathway, *The Journal of cell biology 164*, 123-131.

[306] Hirano-Sakamaki, W., Sugiyama, E., Hayasaka, T., Ravid, R., Setou, M., and Taki, T. (2015) Alzheimer's disease is associated with disordered localization of ganglioside GM1 molecular species in the human dentate gyrus, *FEBS letters 589*, 3611-3616.

[307] Molander-Melin, M., Blennow, K., Bogdanovic, N., Dellheden, B., Månsson, J. E., and Fredman, P. (2005) Structural membrane alterations in Alzheimer brains found to be associated with regional disease development; increased density of gangliosides GM1 and GM2 and loss of cholesterol in detergent-resistant membrane domains, *Journal of neurochemistry 92*, 171-182.

[308] Ariga, T. (2017) The pathogenic role of ganglioside metabolism in Alzheimer's disease-cholinergic neuron-specific gangliosides and neurogenesis, *Molecular neurobiology 54*, 623-638.

[309] Camargo, N., Goudriaan, A., van Deijk, A.-L. F., Otte, W. M., Brouwers, J. F., Lodder, H., Gutmann, D. H., Nave, K.-A., Dijkhuizen, R. M., and Mansvelder, H. D. (2017) Oligodendroglial myelination requires astrocyte-derived lipids, *PLoS biology 15*.

[310] Saher, G., Brügger, B., Lappe-Siefke, C., Möbius, W., Tozawa, R.-i., Wehr, M. C., Wieland, F., Ishibashi, S., and Nave, K.-A. (2005) High cholesterol level is essential for myelin membrane growth, *Nature neuroscience 8*, 468-475.

[311] Mulder, M. (2009) Sterols in the central nervous system, *Current Opinion in Clinical Nutrition & Metabolic Care 12*, 152-158.

[312] Bodovitz, S., and Klein, W. L. (1996) Cholesterol modulates-secretase cleavage of amyloid precursor protein, *Journal of Biological Chemistry 271*, 4436-4440.

[313] Hutter-Paier, B., Huttunen, H. J., Puglielli, L., Eckman, C. B., Kim, D. Y., Hofmeister, A., Moir, R. D., Domnitz, S. B., Frosch, M. P., and Windisch, M. (2004) The ACAT inhibitor CP-113,818 markedly reduces amyloid pathology in a mouse model of Alzheimer's disease, *Neuron 44*, 227-238.

[314] Van Meer, G., Voelker, D. R., and Feigenson, G. W. (2008) Membrane lipids: where they are and how they behave, *Nature reviews Molecular cell biology 9*, 112-124.

[315] Han, X., Holtzman, D. M., and McKeel Jr, D. W. (2001) Plasmalogen deficiency in early Alzheimer's disease subjects and in animal models: molecular characterization using electrospray ionization mass spectrometry, *Journal of neurochemistry 77*, 1168-1180.

[316] Sundaram, J. R., Chan, E. S., Poore, C. P., Pareek, T. K., Cheong, W. F., Shui, G., Tang, N., Low, C.-M., Wenk, M. R., and Kesavapany, S. (2012) Cdk5/p25-induced cytosolic PLA2-mediated lysophosphatidylcholine production regulates neuroinflammation and triggers neurodegeneration, *Journal of Neuroscience 32*, 1020-1034.

[317] Desbène, C., Malaplate-Armand, C., Youssef, I., Garcia, P., Stenger, C., Sauvée, M., Fischer, N., Rimet, D., Koziel, V., and Escanyé, M.-C. (2012) Critical role of cPLA2 in Aβ oligomer-induced neurodegeneration and memory deficit, *Neurobiology of aging 33*, 1123. e1117-1123. e1129.

[318] Oliveira, T. G., and Di Paolo, G. (2010) Phospholipase D in brain function and Alzheimer's disease, *Biochimica et Biophysica Acta (BBA)-Molecular and Cell Biology of Lipids 1801*, 799-805.

[319] Krishnan, B., Kayed, R., and Taglialatela, G. (2018) Elevated phospholipase D isoform 1 in Alzheimer's disease patients' hippocampus: relevance to synaptic dysfunction and memory deficits, *Alzheimer's & Dementia: Translational Research & Clinical Interventions 4*, 89-102.

[320] Oliveira, T. G., Chan, R. B., Tian, H., Laredo, M., Shui, G., Staniszewski, A., Zhang, H., Wang, L., Kim, T.-W., and Duff, K. E.

(2010) Phospholipase d2 ablation ameliorates Alzheimer's disease-linked synaptic dysfunction and cognitive deficits, *Journal of Neuroscience 30*, 16419-16428.

[321] Shimohama, S., Homma, Y., Suenaga, T., Fujimoto, S., Taniguchi, T., Araki, W., Yamaoka, Y., Takenawa, T., and Kimura, J. (1991) Aberrant accumulation of phospholipase C-delta in Alzheimer brains, *The American journal of pathology 139*, 737.

[322] Jope, R. S., Song, L., Li, X., and Powers, R. (1994) Impaired phosphoinositide hydrolysis in Alzheimer's disease brain, *Neurobiology of aging 15*, 221-226.

[323] Landman, N., Jeong, S. Y., Shin, S. Y., Voronov, S. V., Serban, G., Kang, M. S., Park, M. K., Di Paolo, G., Chung, S., and Kim, T.-W. (2006) Presenilin mutations linked to familial Alzheimer's disease cause an imbalance in phosphatidylinositol 4, 5-bisphosphate metabolism, *Proceedings of the National Academy of Sciences 103*, 19524-19529.

[324] Di Paolo, G., and De Camilli, P. (2006) Phosphoinositides in cell regulation and membrane dynamics, *Nature 443*, 651.

[325] Morel, E., Chamoun, Z., Lasiecka, Z. M., Chan, R. B., Williamson, R. L., Vetanovetz, C., Dall'Armi, C., Simoes, S., Du Jour, K. S. P., and McCabe, B. D. (2013) Phosphatidylinositol-3-phosphate regulates sorting and processing of amyloid precursor protein through the endosomal system, *Nature communications 4*, 2250.

[326] Sun, G. Y., Xu, J., Jensen, M. D., and Simonyi, A. (2004) Phospholipase A2 in the central nervous system implications for neurodegenerative diseases, *Journal of lipid research 45*, 205-213.

[327] Gentile, M. T., Reccia, M., Sorrentino, P., Vitale, E., Sorrentino, G., Puca, A., and Colucci-D'Amato, L. (2012) Role of cytosolic calcium-dependent phospholipase A2 in Alzheimer's disease pathogenesis, *Molecular neurobiology 45*, 596-604.

[328] Han, X., Holtzman, D. M., and McKeel, D. W. (2001) Plasmalogen deficiency in early Alzheimer's disease subjects and in animal models: molecular characterization using electrospray ionization mass spectrometry, *Journal of neurochemistry 77*, 1168-1180.

[329] Farooqui, A. A., Rapoport, S. I., and Horrocks, L. A. (1997) Membrane phospholipid alterations in Alzheimer's disease: deficiency of ethanolamine plasmalogens, *Neurochemical research 22*, 523-527.

[330] Katafuchi, T., Ifuku, M., Mawatari, S., Noda, M., Miake, K., Sugiyama, M., and Fujino, T. (2012) Effects of plasmalogens on systemic lipopolysaccharide-induced glial activation and β-amyloid accumulation in adult mice, *Annals of the New York Academy of Sciences 1262*, 85-92.

[331] Farooqui, A. A. (2010) Studies on plasmalogen-selective phospholipase A 2 in brain, *Molecular neurobiology 41*, 267-273.

[332] Pope, S., Land, J. M., and Heales, S. J. (2008) Oxidative stress and mitochondrial dysfunction in neurodegeneration; cardiolipin a critical target?, *Biochimica et Biophysica Acta (BBA)-Bioenergetics 1777*, 794-799.
[333] Cremona, O., Di Paolo, G., Wenk, M. R., Lüthi, A., Kim, W. T., Takei, K., Daniell, L., Nemoto, Y., Shears, S. B., and Flavell, R. A. (1999) Essential role of phosphoinositide metabolism in synaptic vesicle recycling, *Cell 99*, 179-188.
[334] Buxbaum, J. D., Ruefli, A. A., Parker, C. A., Cypess, A. M., and Greengard, P. (1994) Calcium regulates processing of the Alzheimer amyloid protein precursor in a protein kinase C-independent manner, *Proceedings of the National Academy of Sciences 91*, 4489-4493.
[335] Jolles, J., Bothmer, J., Markerink, M., and Ravid, R. (1992) Phosphatidylinositol kinase is reduced in Alzheimer's disease, *Journal of neurochemistry 58*, 2326-2329.
[336] Miranda, A. M., Lasiecka, Z. M., Xu, Y., Neufeld, J., Shahriar, S., Simoes, S., Chan, R. B., Oliveira, T. G., Small, S. A., and Di Paolo, G. (2018) Neuronal lysosomal dysfunction releases exosomes harboring APP C-terminal fragments and unique lipid signatures, *Nature communications 9*, 291.
[337] Yang, C., Cai, C.-Z., Song, J.-X., Tan, J.-Q., Durairajan, S. S. K., Iyaswamy, A., Wu, M.-Y., Chen, L.-L., Yue, Z., and Li, M. (2017) NRBF2 is involved in the autophagic degradation process of APP-CTFs in Alzheimer disease models, *Autophagy 13*, 2028-2040.
[338] Miranda, A. M., Herman, M., Cheng, R., Nahmani, E., Barrett, G., Micevska, E., Fontaine, G., Potier, M.-C., Head, E., and Schmitt, F. A. (2018) Excess synaptojanin 1 contributes to place cell dysfunction and memory deficits in the aging hippocampus in three types of Alzheimer's disease, *Cell reports 23*, 2967-2975.
[339] Zhu, L., Zhong, M., Zhao, J., Rhee, H., Caesar, I., Knight, E. M., Volpicelli-Daley, L., Bustos, V., Netzer, W., and Liu, L. (2013) Reduction of synaptojanin 1 accelerates Aβ clearance and attenuates cognitive deterioration in an Alzheimer mouse model, *Journal of Biological Chemistry 288*, 32050-32063.
[340] Jenkins, G., and Frohman, M. (2005) Phospholipase D: a lipid centric review, *Cellular and Molecular Life Sciences CMLS 62*, 2305-2316.
[341] Stace, C. L., and Ktistakis, N. T. (2006) Phosphatidic acid-and phosphatidylserine-binding proteins, *Biochimica et Biophysica Acta (BBA)-Molecular and Cell Biology of Lipids 1761*, 913-926.
[342] Ramesh, S., Govindarajulu, M., Suppiramaniam, V., Moore, T., and Dhanasekaran, M. (2018) Autotaxin–Lysophosphatidic Acid Signaling in Alzheimer's Disease, *International journal of molecular sciences 19*, 1827.
[343] Aoki, J. (2004) Mechanisms of lysophosphatidic acid production, In *Seminars in cell & developmental biology*, pp 477-489, Elsevier.

[344] Umemura, K., Yamashita, N., Yu, X., Arima, K., Asada, T., Makifuchi, T., Murayama, S., Saito, Y., Kanamaru, K., and Goto, Y. (2006) Autotaxin expression is enhanced in frontal cortex of Alzheimer-type dementia patients, *Neuroscience letters 400*, 97-100.

[345] McLimans, K. E., and Willette, A. A. (2017) Autotaxin is related to metabolic dysfunction and predicts Alzheimer's disease outcomes, *Journal of Alzheimer's Disease 56*, 403-413.

[346] Yung, Y. C., Stoddard, N. C., Mirendil, H., and Chun, J. (2015) Lysophosphatidic acid signaling in the nervous system, *Neuron 85*, 669-682.

[347] Nogaroli, L., Yuelling, L. M., Dennis, J., Gorse, K., Payne, S. G., and Fuss, B. (2009) Lysophosphatidic acid can support the formation of membranous structures and an increase in MBP mRNA levels in differentiating oligodendrocytes, *Neurochemical research 34*, 182-193.

[348] Shi, J., Dong, Y., Cui, M.-Z., and Xu, X. (2013) Lysophosphatidic acid induces increased BACE1 expression and Aβ formation, *Biochimica et Biophysica Acta (BBA)-Molecular Basis of Disease 1832*, 29-38.

[349] Sierksma, A., Lu, A., Mancuso, R., Fattorelli, N., Thrupp, N., Salta, E., Zoco, J., Blum, D., Buée, L., and De Strooper, B. (2019) Novel Alzheimer risk genes determine the microglia response to amyloid-β but not to TAU pathology, *EMBO Molecular Medicine*.

[350] Nakai, M., Kawamata, T., Taniguchi, T., Maeda, K., and Tanaka, C. (1996) Expression of apolipoprotein E mRNA in rat microglia, *Neuroscience letters 211*, 41-44.

[351] Bandaru, V. V. R., Troncoso, J., Wheeler, D., Pletnikova, O., Wang, J., Conant, K., and Haughey, N. J. (2009) ApoE4 disrupts sterol and sphingolipid metabolism in Alzheimer's but not normal brain, *Neurobiology of aging 30*, 591-599.

[352] Han, X. (2007) Potential mechanisms contributing to sulfatide depletion at the earliest clinically recognizable stage of Alzheimer's disease: a tale of shotgun lipidomics, *Journal of neurochemistry 103*, 171-179.

[353] Salminen, A., and Kaarniranta, K. (2009) Siglec receptors and hiding plaques in Alzheimer's disease, *Journal of Molecular Medicine 87*, 697.

[354] Wang, Y., Ulland, T. K., Ulrich, J. D., Song, W., Tzaferis, J. A., Hole, J. T., Yuan, P., Mahan, T. E., Shi, Y., and Gilfillan, S. (2016) TREM2-mediated early microglial response limits diffusion and toxicity of amyloid plaques, *Journal of Experimental Medicine*, jem. 20151948.

[355] Thomson, J. (1910) LXXXIII. Rays of positive electricity, *The London, Edinburgh, and Dublin Philosophical Magazine and Journal of Science 20*, 752-767.

[356] Aston, F. W. (1919) LXXIV. A positive ray spectrograph, *The London, Edinburgh, and Dublin Philosophical Magazine and Journal of Science 38*, 707-714.
[357] Bleakney, W. (1929) A new method of positive ray analysis and its application to the measurement of ionization potentials in mercury vapor, *Physical Review 34*, 157.
[358] Nier, A. O. (1947) A mass spectrometer for isotope and gas analysis, *Review of Scientific Instruments 18*, 398-411.
[359] Inghram, M. G., and Gomer, R. (1954) Mass spectrometric analysis of ions from the field microscope, *The Journal of Chemical Physics 22*, 1279-1280.
[360] Gomer, R., and Inghram, M. G. (1955) Applications of field ionization to mass spectrometry, *Journal of the American Chemical Society 77*, 500-500.
[361] Munson, M. S., and Field, F.-H. (1966) Chemical ionization mass spectrometry. I. General introduction, *Journal of the American Chemical Society 88*, 2621-2630.
[362] Herzog, R., and Viehböck, F. (1949) Ion source for mass spectrography, *Physical Review 76*, 855.
[363] Macfarlane, R., and Torgerson, D. (1976) Californium-252 plasma desorption mass spectroscopy, *Science 191*, 920-925.
[364] Benninghoven, A., and Sichtermann, W. (1978) Detection, identification, and structural investigation of biologically important compounds by secondary ion mass spectrometry, *Analytical chemistry 50*, 1180-1184.
[365] Benninghoven, A., Jaspers, D., and Sichtermann, W. (1976) Secondary-ion emission of amino acids, *Applied physics 11*, 35-39.
[366] Barber, M., Bordoli, R., Sedgwick, R., and Tyler, A. (1981) Fast atom bombardment of solids as an ion source in mass spectrometry, *Nature 293*, 270-275.
[367] Barber, M., Bordoli, R. S., Sedgwick, R. D., and Tyler, A. N. (1981) Fast atom bombardment of solids (FAB): A new ion source for mass spectrometry, *Journal of the Chemical Society, Chemical Communications*, 325-327.
[368] Honig, R., and Woolston, J. (1963) Laser-induced emission of electrons, ions, and neutral atoms from solid surfaces, *Applied Physics Letters 2*, 138-139.
[369] Vastola, F., Mumma, R., and Pirone, A. (1970) Analysis of organic salts by laser ionization, *Organic Mass Spectrometry 3*, 101-104.
[370] Hillenkamp, F., UNSöLD, E., KAUFMANN, R., and NITSCHE, R. (1975) Laser microprobe mass analysis of organic materials, *Nature 256*, 119.
[371] Fenner, N., and Daly, N. (1966) Laser used for mass analysis, *Review of Scientific Instruments 37*, 1068-1070.

[372] Jonsson, G. P., Hedin, A. B., Hakansson, P. L., Sundqvist, B. U., Saeve, B. G. S., Nielsen, P. F., Roepstorff, P., Johansson, K. E., Kamensky, I., and Lindberg, M. S. (1986) Plasma desorption mass spectrometry of peptides and proteins adsorbed on nitrocellulose, *Analytical Chemistry 58*, 1084-1087.

[373] Hillenkamp, F., and Peter-Katalinic, J. (2013) *MALDI MS: a practical guide to instrumentation, methods and applications*, John Wiley & Sons.

[374] Karas, M., and Hillenkamp, F. (1988) Laser desorption ionization of proteins with molecular masses exceeding 10,000 daltons, *Analytical chemistry 60*, 2299-2301.

[375] Tanaka, K., Waki, H., Ido, Y., Akita, S., Yoshida, Y., Yoshida, T., and Matsuo, T. (1988) Protein and polymer analyses up to m/z 100 000 by laser ionization time-of-flight mass spectrometry, *Rapid communications in mass spectrometry 2*, 151-153.

[376] Fenn, J. B., Mann, M., Meng, C. K., Wong, S. F., and Whitehouse, C. M. (1989) Electrospray ionization for mass spectrometry of large biomolecules, *Science 246*, 64-71.

[377] Rayleigh, L. (1882) XX. On the equilibrium of liquid conducting masses charged with electricity, *The London, Edinburgh, and Dublin Philosophical Magazine and Journal of Science 14*, 184-186.

[378] Wong, S., Meng, C., and Fenn, J. (1988) Multiple charging in electrospray ionization of poly (ethylene glycols), *The Journal of Physical Chemistry 92*, 546-550.

[379] Reed, T. B. (1961) Induction-coupled plasma torch, *Journal of Applied Physics 32*, 821-824.

[380] Houk, R. S., Fassel, V. A., Flesch, G. D., Svec, H. J., Gray, A. L., and Taylor, C. E. (1980) Inductively coupled argon plasma as an ion source for mass spectrometric determination of trace elements, *Analytical Chemistry 52*, 2283-2289.

[381] Bandura, D. R., Baranov, V. I., Ornatsky, O. I., Antonov, A., Kinach, R., Lou, X., Pavlov, S., Vorobiev, S., Dick, J. E., and Tanner, S. D. (2009) Mass cytometry: technique for real time single cell multitarget immunoassay based on inductively coupled plasma time-of-flight mass spectrometry, *Analytical chemistry 81*, 6813-6822.

[382] Wiley, W., and McLaren, I. H. (1955) Time-of-flight mass spectrometer with improved resolution, *Review of scientific instruments 26*, 1150-1157.

[383] Mamyrin, B., Karataev, V., Shmikk, D., and Zagulin, V. (1973) The mass-reflectron, a new nonmagnetic time-of-flight mass spectrometer with high resolution, *Zh. Eksp. Teor. Fiz 64*, 82-89.

[384] Hipple, J., Sommer, H., and Thomas, H. A. (1949) A precise method of determining the Faraday by magnetic resonance, *Physical Review 76*, 1877.

[385] Sommer, H., Thomas, H., and Hipple, J. (1951) The measurement of e M by cyclotron resonance, *Physical Review 82*, 697.
[386] Comisarow, M. B., and Marshall, A. G. (1974) Fourier transform ion cyclotron resonance spectroscopy, *Chemical physics letters 25*, 282-283.
[387] Bowman, A. P., Blakney, G. T., Hendrickson, C. L., Ellis, S. R., Heeren, R. M., and Smith, D. F. (2020) Ultra-High Mass Resolving Power, Mass Accuracy, and Dynamic Range MALDI Mass Spectrometry Imaging by 21-T FT-ICR MS, *Analytical Chemistry 92*, 3133-3142.
[388] Spraggins, J. M., Rizzo, D. G., Moore, J. L., Rose, K. L., Hammer, N. D., Skaar, E. P., and Caprioli, R. M. (2015) MALDI FTICR IMS of intact proteins: using mass accuracy to link protein images with proteomics data, *Journal of the American Society for Mass Spectrometry 26*, 974-985.
[389] Kingdon, K. (1923) A method for the neutralization of electron space charge by positive ionization at very low gas pressures, *Physical Review 21*, 408.
[390] Makarov, A. (2000) Electrostatic axially harmonic orbital trapping: a high-performance technique of mass analysis, *Analytical chemistry 72*, 1156-1162.
[391] Paul, W., and Steinwedel, H. (1953) Ein neues massenspektrometer ohne magnetfeld, *Zeitschrift für Naturforschung A 8*, 448-450.
[392] Wolfgang, P., and Helmut, S. (1960) Apparatus for separating charged particles of different specific charges, Google Patents.
[393] Yost, R. A., Enke, C., McGilvery, D., Smith, D., and Morrison, J. (1979) High efficiency collision-induced dissociation in an rf-only quadrupole, *International Journal of Mass Spectrometry and Ion Physics 30*, 127-136.
[394] Shannon, T., and McLafferty, F. W. (1966) Identification of gaseous organic ions by the use of "Metastable Peaks", *Journal of the American Chemical Society 88*, 5021-5022.
[395] Jennings, K. R. (1968) Collision-induced decompositions of aromatic molecular ions, *International Journal of Mass Spectrometry and Ion Physics 1*, 227-235.
[396] Zubarev, R. A., Kelleher, N. L., and McLafferty, F. W. (1998) Electron capture dissociation of multiply charged protein cations. A nonergodic process, *Journal of the American Chemical Society 120*, 3265-3266.
[397] Gohlke, R. S. (1959) Time-of-flight mass spectrometry and gas-liquid partition chromatography, *Analytical Chemistry 31*, 535-541.
[398] Talroze, V., Karpov, G., IG, G., and Skurat, V. (1968) Capillary system for introduction of liquid mixtures into an analytical mass-spectrometer, pp 1658-&, Interperiodica PO Box 1831, Birmingham, Al 35201-1831.

[399] Blakley, C., McAdams, M., and Vestal, M. (1978) Crossed-beam liquid chromatoraph—mass spectrometer combination, *Journal of Chromatography A 158*, 261-276.
[400] McFadden, W., Schwartz, H., and Evans, S. (1976) Direct analysis of liquid chromatographic effluents, *Journal of Chromatography A 122*, 389-396.
[401] Pullen, F. (2010) The fascinating history of the development of LC-MS; a personal perspective, *Chromatography Today 3*, 4-6.
[402] Hoaglund, C. S., Valentine, S. J., Sporleder, C. R., Reilly, J. P., and Clemmer, D. E. (1998) Three-dimensional ion mobility/TOFMS analysis of electrosprayed biomolecules, *Analytical chemistry 70*, 2236-2242.
[403] Santos, C. R., and Schulze, A. (2012) Lipid metabolism in cancer, *The FEBS journal 279*, 2610-2623.
[404] Krauss, R. M. (2004) Lipids and lipoproteins in patients with type 2 diabetes, *Diabetes care 27*, 1496-1504.
[405] Grunfeld, C., Pang, M., Doerrler, W., Shigenaga, J., Jensen, P., and Feingold, K. (1992) Lipids, lipoproteins, triglyceride clearance, and cytokines in human immunodeficiency virus infection and the acquired immunodeficiency syndrome, *The Journal of Clinical Endocrinology & Metabolism 74*, 1045-1052.
[406] Ruipérez, V., Darios, F., and Davletov, B. (2010) Alpha-synuclein, lipids and Parkinson's disease, *Progress in lipid research 49*, 420-428.
[407] Wenk, M. R. (2005) The emerging field of lipidomics, *Nature reviews Drug discovery 4*, 594-610.
[408] Shevchenko, A., and Simons, K. (2010) Lipidomics: coming to grips with lipid diversity, *Nature reviews Molecular cell biology 11*, 593-598.
[409] Schmitt, S., Castelvetri, L. C., and Simons, M. (2015) Metabolism and functions of lipids in myelin, *Biochimica Et Biophysica Acta (BBA)-Molecular and Cell Biology of Lipids 1851*, 999-1005.
[410] Wang, C., Palavicini, J. P., and Han, X. (2018) Lipidomics Profiling of Myelin, In *Myelin*, pp 37-50, Springer.
[411] Han, X. (2007) Neurolipidomics: challenges and developments, *Frontiers in bioscience: a journal and virtual library 12*, 2601.
[412] Fernández, C., Hilty, C., Wider, G., and Wüthrich, K. (2002) Lipid–protein interactions in DHPC micelles containing the integral membrane protein OmpX investigated by NMR spectroscopy, *Proceedings of the National Academy of Sciences 99*, 13533-13537.
[413] Gupta, K., Li, J., Liko, I., Gault, J., Bechara, C., Wu, D., Hopper, J. T., Giles, K., Benesch, J. L., and Robinson, C. V. (2018) Identifying key membrane protein lipid interactions using mass spectrometry, *Nature protocols 13*, 1106-1120.

[414] Konijnenberg, A., Butterer, A., and Sobott, F. (2013) Native ion mobility-mass spectrometry and related methods in structural biology, *Biochimica et Biophysica Acta (BBA)-Proteins and Proteomics 1834*, 1239-1256.
[415] O'Donnell, V. B., Dennis, E. A., Wakelam, M. J., and Subramaniam, S. (2019) LIPID MAPS: Serving the next generation of lipid researchers with tools, resources, data, and training.
[416] Murphy, R. C., Fiedler, J., and Hevko, J. (2001) Analysis of nonvolatile lipids by mass spectrometry, *Chemical reviews 101*, 479-526.
[417] Blanksby, S. J., and Mitchell, T. W. (2010) Advances in mass spectrometry for lipidomics, *Annual Review of Analytical Chemistry 3*, 433-465.
[418] Han, X. (2016) Lipidomics for studying metabolism, *Nature Reviews Endocrinology 12*, 668.
[419] Schiller, J., Süß, R., Arnhold, J., Fuchs, B., Lessig, J., Müller, M., Petković, M., Spalteholz, H., Zschörnig, O., and Arnold, K. (2004) Matrix-assisted laser desorption and ionization time-of-flight (MALDI-TOF) mass spectrometry in lipid and phospholipid research, *Progress in lipid research 43*, 449-488.
[420] Winograd, N. (2005) The magic of cluster SIMS, ACS Publications.
[421] Passarelli, M. K., and Winograd, N. (2011) Lipid imaging with time-of-flight secondary ion mass spectrometry (ToF-SIMS), *Biochimica et Biophysica Acta (BBA)-Molecular and Cell Biology of Lipids 1811*, 976-990.
[422] Winograd, N. (2018) Gas cluster ion beams for secondary ion mass spectrometry, *Annual Review of Analytical Chemistry 11*, 29-48.
[423] Annesley, T. M. (2003) Ion suppression in mass spectrometry, *Clinical chemistry 49*, 1041-1044.
[424] Han, X., and Gross, R. W. (2003) Global analyses of cellular lipidomes directly from crude extracts of biological samples by ESI mass spectrometry a bridge to lipidomics, *Journal of lipid research 44*, 1071-1079.
[425] Oomen, P. E., Aref, M. A., Kaya, I., Phan, N. T., and Ewing, A. G. (2018) Chemical analysis of single cells, *Analytical chemistry 91*, 588-621.
[426] Zhang, L., and Vertes, A. (2018) Single-Cell Mass Spectrometry Approaches to Explore Cellular Heterogeneity, *Angewandte Chemie International Edition 57*, 4466-4477.
[427] Han, X., and Gross, R. W. (1994) Electrospray ionization mass spectroscopic analysis of human erythrocyte plasma membrane phospholipids, *Proceedings of the National Academy of Sciences 91*, 10635-10639.

[428] Kim, H.-Y., Wang, T.-C. L., and Ma, Y.-C. (1994) Liquid chromatography/mass spectrometry of phospholipids using electrospray ionization, *Analytical chemistry 66*, 3977-3982.
[429] Han, X., Yang, K., and Gross, R. W. (2012) Multi-dimensional mass spectrometry-based shotgun lipidomics and novel strategies for lipidomic analyses, *Mass spectrometry reviews 31*, 134-178.
[430] Han, X., and Gross, R. W. (2005) Shotgun lipidomics: electrospray ionization mass spectrometric analysis and quantitation of cellular lipidomes directly from crude extracts of biological samples, *Mass spectrometry reviews 24*, 367-412.
[431] Li, X., Wang, X., Zhang, X., Zhao, M., Tsang, W. L., Zhang, Y., Yau, R. G. W., Weisman, L. S., and Xu, H. (2013) Genetically encoded fluorescent probe to visualize intracellular phosphatidylinositol 3, 5-bisphosphate localization and dynamics, *Proceedings of the National Academy of Sciences 110*, 21165-21170.
[432] Bowman, A. P., Heeren, R. M., and Ellis, S. R. (2018) Advances in mass spectrometry imaging enabling observation of localised lipid biochemistry within tissues, *TrAC Trends in Analytical Chemistry*.
[433] Niehaus, M., Soltwisch, J., Belov, M., and Dreisewerd, K. (2019) Transmission-mode MALDI-2 mass spectrometry imaging of cells and tissues at subcellular resolution, *Nature methods 16*, 925-931.
[434] Castaing, R., and Slodzian, G. (1962) Microanalyse par émission ionique secondaire, *J Microsc 1*, I960.
[435] Galle, P. (1970) Sur une nouvelle méthode d'analyse cellulaire utilisant le phénomène d'émission ionique secondaire, *Ann Phys Biol Med 42*, 83-94.
[436] McDonnell, L. A., and Heeren, R. (2007) Imaging mass spectrometry, *Mass spectrometry reviews 26*, 606-643.
[437] Pacholski, M., and Winograd, N. (1999) Imaging with mass spectrometry, *Chemical reviews 99*, 2977-3006.
[438] Römpp, A., and Spengler, B. (2013) Mass spectrometry imaging with high resolution in mass and space, *Histochemistry and cell biology 139*, 759-783.
[439] Stoeckli, M., Chaurand, P., Hallahan, D. E., and Caprioli, R. M. (2001) Imaging mass spectrometry: a new technology for the analysis of protein expression in mammalian tissues, *Nature medicine 7*, 493-496.
[440] Vickerman, J. C. (2011) Molecular imaging and depth profiling by mass spectrometry—SIMS, MALDI or DESI?, *Analyst 136*, 2199-2217.
[441] van Hove, E. R. A., Smith, D. F., and Heeren, R. M. (2010) A concise review of mass spectrometry imaging, *Journal of chromatography A 1217*, 3946-3954.

[442] Wu, C., Dill, A. L., Eberlin, L. S., Cooks, R. G., and Ifa, D. R. (2013) Mass spectrometry imaging under ambient conditions, *Mass spectrometry reviews 32*, 218-243.
[443] Gode, D., and Volmer, D. A. (2013) Lipid imaging by mass spectrometry–a review, *Analyst 138*, 1289-1315.
[444] Spengler, B. (2015) Mass spectrometry imaging of biomolecular information, *Analytical chemistry 87*, 64-82.
[445] Becker, J. S., Matusch, A., and Wu, B. (2014) Bioimaging mass spectrometry of trace elements–recent advance and applications of LA-ICP-MS: A review, *Analytica chimica acta 835*, 1-18.
[446] Takáts, Z., Wiseman, J. M., Gologan, B., and Cooks, R. G. (2004) Mass spectrometry sampling under ambient conditions with desorption electrospray ionization, *Science 306*, 471-473.
[447] Wiseman, J. M., Ifa, D. R., Song, Q., and Cooks, R. G. (2006) Tissue imaging at atmospheric pressure using desorption electrospray ionization (DESI) mass spectrometry, *Angewandte Chemie International Edition 45*, 7188-7192.
[448] Wiseman, J. M., Ifa, D. R., Zhu, Y., Kissinger, C. B., Manicke, N. E., Kissinger, P. T., and Cooks, R. G. (2008) Desorption electrospray ionization mass spectrometry: Imaging drugs and metabolites in tissues, *Proceedings of the National Academy of Sciences 105*, 18120-18125.
[449] Garza, K. Y., Feider, C. L., Klein, D. R., Rosenberg, J. A., Brodbelt, J. S., and Eberlin, L. S. (2018) Desorption electrospray ionization mass spectrometry imaging of proteins directly from biological tissue sections, *Analytical chemistry 90*, 7785-7789.
[450] Ferguson, C. N., Benchaar, S. A., Miao, Z., Loo, J. A., and Chen, H. (2011) Direct ionization of large proteins and protein complexes by desorption electrospray ionization-mass spectrometry, *Analytical chemistry 83*, 6468-6473.
[451] Eikel, D., Vavrek, M., Smith, S., Bason, C., Yeh, S., Korfmacher, W. A., and Henion, J. D. (2011) Liquid extraction surface analysis mass spectrometry (LESA-MS) as a novel profiling tool for drug distribution and metabolism analysis: the terfenadine example, *Rapid Communications in Mass Spectrometry 25*, 3587-3596.
[452] Mikhailov, V. A., Griffiths, R. L., and Cooper, H. J. (2017) Liquid extraction surface analysis for native mass spectrometry: Protein complexes and ligand binding, *International Journal of Mass Spectrometry 420*, 43-50.
[453] Griffiths, R. L., and Cooper, H. J. (2016) Direct tissue profiling of protein complexes: toward native mass spectrometry imaging, *Analytical chemistry 88*, 606-609.
[454] Ryan, D. J., Patterson, N. H., Putnam, N. E., Wilde, A. D., Weiss, A., Perry, W. J., Cassat, J. E., Skaar, E. P., Caprioli, R. M., and Spraggins, J. M. (2019) MicroLESA: Integrating Autofluorescence

Microscopy, In Situ Micro-Digestions, and Liquid Extraction Surface Analysis for High Spatial Resolution Targeted Proteomic Studies, *Analytical chemistry 91*, 7578-7585.

[455] Takats, Z., Wiseman, J. M., and Cooks, R. G. (2005) Ambient mass spectrometry using desorption electrospray ionization (DESI): instrumentation, mechanisms and applications in forensics, chemistry, and biology, *Journal of mass spectrometry 40*, 1261-1275.

[456] Roach, P. J., Laskin, J., and Laskin, A. (2010) Molecular characterization of organic aerosols using nanospray-desorption/electrospray ionization-mass spectrometry, *Analytical Chemistry 82*, 7979-7986.

[457] Nguyen, S. N., Sontag, R. L., Carson, J. P., Corley, R. A., Ansong, C., and Laskin, J. (2017) Towards high-resolution tissue imaging using nanospray desorption electrospray ionization mass spectrometry coupled to shear force microscopy, *Journal of The American Society for Mass Spectrometry 29*, 316-322.

[458] Nemes, P., and Vertes, A. (2007) Laser ablation electrospray ionization for atmospheric pressure, in vivo, and imaging mass spectrometry, *Analytical chemistry 79*, 8098-8106.

[459] Nemes, P., Woods, A. S., and Vertes, A. (2010) Simultaneous imaging of small metabolites and lipids in rat brain tissues at atmospheric pressure by laser ablation electrospray ionization mass spectrometry, *Analytical chemistry 82*, 982-988.

[460] Appelhans, A. D., and Delmore, J. E. (1989) Comparison of polyatomic and atomic primary beams for secondary ion mass spectrometry of organics, *Analytical Chemistry 61*, 1087-1093.

[461] Blain, M., Della-Negra, S., Joret, H., Le Beyec, Y., and Schweikert, E. (1989) Secondary-ion yields from surfaces bombarded with keV molecular and cluster ions, *Physical review letters 63*, 1625.

[462] Wong, S., Hill, R., Blenkinsopp, P., Lockyer, N., Weibel, D., and Vickerman, J. (2003) Development of a C60+ ion gun for static SIMS and chemical imaging, *Appl. Surf. Sci. 203*, 219-222.

[463] Jones, E. A., Lockyer, N. P., and Vickerman, J. C. (2007) Mass spectral analysis and imaging of tissue by ToF-SIMS—the role of buckminsterfullerene, C60+, primary ions, *International Journal of Mass Spectrometry 260*, 146-157.

[464] Sjövall, P., Lausmaa, J., and Johansson, B. (2004) Mass spectrometric imaging of lipids in brain tissue, *Analytical chemistry 76*, 4271-4278.

[465] Weibel, D., Wong, S., Lockyer, N., Blenkinsopp, P., Hill, R., and Vickerman, J. C. (2003) A C60 primary ion beam system for time of flight secondary ion mass spectrometry: its development and secondary ion yield characteristics, *Analytical Chemistry 75*, 1754-1764.

[466] Touboul, D., Kollmer, F., Niehuis, E., Brunelle, A., and Laprévote, O. (2005) Improvement of biological time-of-flight-secondary ion mass

spectrometry imaging with a bismuth cluster ion source, *Journal of the American Society for Mass Spectrometry 16*, 1608-1618.

[467] Fletcher, J. S., Lockyer, N. P., Vaidyanathan, S., and Vickerman, J. C. (2007) TOF-SIMS 3D biomolecular imaging of Xenopus laevis oocytes using buckminsterfullerene (C60) primary ions, *Analytical Chemistry 79*, 2199-2206.

[468] Fletcher, J. S., Lockyer, N. P., and Vickerman, J. C. (2011) Developments in molecular SIMS depth profiling and 3D imaging of biological systems using polyatomic primary ions, *Mass spectrometry reviews 30*, 142-174.

[469] Tian, H., Six, D. A., Krucker, T., Leeds, J. A., and Winograd, N. (2017) Subcellular chemical imaging of antibiotics in single bacteria using C60-secondary ion mass spectrometry, *Analytical chemistry 89*, 5050-5057.

[470] Yamada, I., Matsuo, J., Toyoda, N., and Kirkpatrick, A. (2001) Materials processing by gas cluster ion beams, *Mat. Sci. Engineer. Rep. 34*, 231-295.

[471] Ninomiya, S., Ichiki, K., Yamada, H., Nakata, Y., Seki, T., Aoki, T., and Matsuo, J. (2009) Precise and fast secondary ion mass spectrometry depth profiling of polymer materials with large Ar cluster ion beams, *Rapid Communications in Mass Spectrometry: An International Journal Devoted to the Rapid Dissemination of Up-to-the-Minute Research in Mass Spectrometry 23*, 1601-1606.

[472] Tian, H., Maciążek, D., Postawa, Z., Garrison, B. J., and Winograd, N. (2016) CO2 cluster ion beam, an alternative projectile for secondary ion mass spectrometry, *Journal of The American Society for Mass Spectrometry 27*, 1476-1482.

[473] Angerer, T. B., Blenkinsopp, P., and Fletcher, J. S. (2015) High energy gas cluster ions for organic and biological analysis by time-of-flight secondary ion mass spectrometry, *International Journal of Mass Spectrometry 377*, 591-598.

[474] Tian, H., Sparvero, L. J., Amoscato, A. A., Bloom, A., Bayır, H. l., Kagan, V. E., and Winograd, N. (2017) Gas Cluster Ion Beam Time-of-Flight Secondary Ion Mass Spectrometry High-Resolution Imaging of Cardiolipin Speciation in the Brain: Identification of Molecular Losses after Traumatic Injury, *Analytical chemistry 89*, 4611-4619.

[475] Tian, H., Sparvero, L. J., Blenkinsopp, P., Amoscato, A. A., Watkins, S. C., Bayır, H., Kagan, V. E., and Winograd, N. (2019) Secondary-Ion Mass Spectrometry Images Cardiolipins and Phosphatidylethanolamines at the Subcellular Level, *Angewandte Chemie 131*, 3188-3193.

[476] Pareek, V., Tian, H., Winograd, N., and Benkovic, S. J. (2020) Metabolomics and mass spectrometry imaging reveal channeled de novo purine synthesis in cells, *Science 368*, 283-290.

[477] Sheraz née Rabbani, S., Barber, A., Fletcher, J. S., Lockyer, N. P., and Vickerman, J. C. (2013) Enhancing secondary ion yields in time of flight-secondary ion mass spectrometry using water cluster primary beams, *Analytical chemistry 85*, 5654-5658.

[478] Sheraz, S., Tian, H., Vickerman, J. C., Blenkinsopp, P., Winograd, N., and Cumpson, P. (2019) Enhanced Ion Yields Using High Energy Water Cluster Beams for Secondary Ion Mass Spectrometry Analysis and Imaging, *Analytical chemistry 91*, 9058-9068.

[479] Maharrey, S., Bastasz, R., Behrens, R., Highley, A., Hoffer, S., Kruppa, G., and Whaley, J. (2004) High mass resolution SIMS, *Appl. Surf. Sci. 231*, 972-975.

[480] Smith, D. F., Robinson, E. W., Tolmachev, A. V., Heeren, R. M., and Paša-Tolić, L. (2011) C60 secondary ion Fourier transform ion cyclotron resonance mass spectrometry, *Analytical chemistry 83*, 9552-9556.

[481] Passarelli, M. K., Pirkl, A., Moellers, R., Grinfeld, D., Kollmer, F., Havelund, R., Newman, C. F., Marshall, P. S., Arlinghaus, H., and Alexander, M. R. (2017) The 3D OrbiSIMS—label-free metabolic imaging with subcellular lateral resolution and high mass-resolving power, *Nature methods 14*, 1175.

[482] Scheltema, R. A., Hauschild, J.-P., Lange, O., Hornburg, D., Denisov, E., Damoc, E., Kuehn, A., Makarov, A., and Mann, M. (2014) The Q Exactive HF, a Benchtop mass spectrometer with a pre-filter, high-performance quadrupole and an ultra-high-field Orbitrap analyzer, *Molecular & Cellular Proteomics 13*, 3698-3708.

[483] Fletcher, J. S., Rabbani, S., Henderson, A., Blenkinsopp, P., Thompson, S. P., Lockyer, N. P., and Vickerman, J. C. (2008) A new dynamic in mass spectral imaging of single biological cells, *Analytical Chemistry 80*, 9058-9064.

[484] Hillion, F. (1993) A new high performance instrument: The Cameca Nano-SIMS 50, In *Secondary Ion Mass Spectrometry: SIMS IX. Proceedings of the 9th International Conference on Secondary Ion Mass Spectrometry, 1993*.

[485] Nuñez, J., Renslow, R., Cliff III, J. B., and Anderton, C. R. (2018) NanoSIMS for biological applications: current practices and analyses, *Biointerphases 13*, 03B301.

[486] Hindie, E., Coulomb, B., Beaupain, R., and Galle, P. (1992) Mapping the cellular distribution of labelled molecules by SIMS microscopy, *Biology of the Cell 74*, 81-88.

[487] Legin, A. A., Schintlmeister, A., Jakupec, M. A., Galanski, M., Lichtscheidl, I., Wagner, M., and Keppler, B. K. (2014) NanoSIMS combined with fluorescence microscopy as a tool for subcellular imaging of isotopically labeled platinum-based anticancer drugs, *Chemical Science 5*, 3135-3143.

[488] Lovrić, J., Dunevall, J., Larsson, A., Ren, L., Andersson, S., Meibom, A., Malmberg, P., Kurczy, M. E., and Ewing, A. G. (2016) Nano secondary ion mass spectrometry imaging of dopamine distribution across nanometer vesicles, *ACS nano 11*, 3446-3455.
[489] He, C., Weston, T. A., Jung, R. S., Heizer, P., Larsson, M., Hu, X., Allan, C. M., Tontonoz, P., Reue, K., and Beigneux, A. P. (2018) NanoSIMS analysis of intravascular lipolysis and lipid movement across capillaries and into cardiomyocytes, *Cell metabolism 27*, 1055-1066. e1053.
[490] Thomen, A., Najafinobar, N., Penen, F., Kay, E., Upadhyay, P. P., Li, X., Phan, N. T., Malmberg, P., Klarqvist, M., and Andersson, S. (2020) Sub-Cellular Mass Spectrometry Imaging and Absolute Quantitative Analysis across Organelles, *ACS nano*.
[491] Spitzer, M. H., and Nolan, G. P. (2016) Mass cytometry: single cells, many features, *Cell 165*, 780-791.
[492] Chang, Q., Ornatsky, O. I., Siddiqui, I., Loboda, A., Baranov, V. I., and Hedley, D. W. (2017) Imaging mass cytometry, *Cytometry part A 91*, 160-169.
[493] Giesen, C., Wang, H. A., Schapiro, D., Zivanovic, N., Jacobs, A., Hattendorf, B., Schüffler, P. J., Grolimund, D., Buhmann, J. M., and Brandt, S. (2014) Highly multiplexed imaging of tumor tissues with subcellular resolution by mass cytometry, *Nature methods 11*, 417-422.
[494] Angelo, M., Bendall, S. C., Finck, R., Hale, M. B., Hitzman, C., Borowsky, A. D., Levenson, R. M., Lowe, J. B., Liu, S. D., and Zhao, S. (2014) Multiplexed ion beam imaging of human breast tumors, *Nature medicine 20*, 436.
[495] Keren, L., Bosse, M., Thompson, S., Risom, T., Vijayaragavan, K., McCaffrey, E., Marquez, D., Angoshtari, R., Greenwald, N. F., and Fienberg, H. (2019) MIBI-TOF: A multiplexed imaging platform relates cellular phenotypes and tissue structure, *Science Advances 5*, eaax5851.
[496] Moon, D. W., Park, Y. H., Lee, S. Y., Lim, H., Kwak, S., Kim, M. S., Kim, H., Kim, E., Jung, Y., and Hoe, H.-S. (2020) Multiplex Protein Imaging with Secondary Ion Mass Spectrometry Using Metal Oxide Nanoparticle-Conjugated Antibodies, *ACS Applied Materials & Interfaces*.
[497] Knochenmuss, R. (2006) Ion formation mechanisms in UV-MALDI, *Analyst 131*, 966-986.
[498] Zenobi, R., and Knochenmuss, R. (1998) Ion formation in MALDI mass spectrometry, *Mass spectrometry reviews 17*, 337-366.
[499] Wei, J., Buriak, J. M., and Siuzdak, G. (1999) Desorption–ionization mass spectrometry on porous silicon, *Nature 399*, 243-246.
[500] Go, E., Apon, J., Luo, G., Saghatelian, A., Daniels, R., Sahi, V., Dubrow, R., Cravatt, B., Vertes, A., and Siuzdak, G. (2005)

Desorption/ionization on silicon nanowires, *Analytical chemistry 77*, 1641-1646.
[501] Jaskolla, T. W., and Karas, M. (2011) Compelling evidence for lucky survivor and gas phase protonation: the unified MALDI analyte protonation mechanism, *Journal of the American Society for Mass Spectrometry 22*, 976-988.
[502] Karas, M., and Krüger, R. (2003) Ion formation in MALDI: the cluster ionization mechanism, *Chemical reviews 103*, 427-440.
[503] Rubakhin, S. S., and Sweedler, J. V. (2010) A mass spectrometry primer for mass spectrometry imaging, In *Mass Spectrometry Imaging*, pp 21-49, Springer.
[504] Karbach, V., and Knochenmuss, R. (1998) Do single matrix molecules generate primary ions in ultraviolet matrix-assisted laser desorption/ionization, *Rapid communications in mass spectrometry 12*, 968-974.
[505] Allwood, D., Dyer, P., and Dreyfus, R. (1997) Ionization modelling of matrix molecules in ultraviolet matrix-assisted laser desorption/ionization, *Rapid communications in mass spectrometry 11*, 499-503.
[506] Ehring, H., and Sundqvist, B. U. (1995) Studies of the MALDI process by luminescence spectroscopy, *Journal of Mass Spectrometry 30*, 1303-1310.
[507] McCombie, G., and Knochenmuss, R. (2004) Small-molecule MALDI using the matrix suppression effect to reduce or eliminate matrix background interferences, *Analytical chemistry 76*, 4990-4997.
[508] Knochenmuss, R., Stortelder, A., Breuker, K., and Zenobi, R. (2000) Secondary ion–molecule reactions in matrix-assisted laser desorption/ionization, *Journal of mass spectrometry 35*, 1237-1245.
[509] Harrison, A. G. (1997) The gas-phase basicities and proton affinities of amino acids and peptides, *Mass Spectrometry Reviews 16*, 201-217.
[510] Baumgart, S., Lindner, Y., Kühne, R., Oberemm, A., Wenschuh, H., and Krause, E. (2004) The contributions of specific amino acid side chains to signal intensities of peptides in matrix-assisted laser desorption/ionization mass spectrometry, *Rapid communications in mass spectrometry 18*, 863-868.
[511] Chou, C.-W., Williams, P., and Limbach, P. A. (1999) Matrix influence on the formation of positively charged oligonucleotides in matrix-assisted laser desorption/ionization mass spectrometry, *International journal of mass spectrometry 193*, 15-27.
[512] Neubert, H., Knights, K. A., de Miguel, Y. R., and Cowan, D. A. (2003) MALDI TOF post-source decay investigation of alkali metal adducts of apolar polypentylresorcinol dendrimers, *Macromolecules 36*, 8297-8303.
[513] Jackson, A. U., Shum, T., Sokol, E., Dill, A., and Cooks, R. G. (2011) Enhanced detection of olefins using ambient ionization mass

spectrometry: Ag+ adducts of biologically relevant alkenes, *Analytical and bioanalytical chemistry 399*, 367-376.
[514] McCarley, T. D., McCarley, R. L., and Limbach, P. A. (1998) Electron-transfer ionization in matrix-assisted laser desorption/ionization mass spectrometry, *Analytical Chemistry 70*, 4376-4379.
[515] Dreisewerd, K. (2003) The desorption process in MALDI, *Chemical reviews 103*, 395-426.
[516] Spengler, B., Hubert, M., and Kaufmann, R. (1994) MALDI ion imaging and biological ion imaging with a new scanning UV-laser microprobe, In *Proceedings of the 42nd Annual Conference on Mass Spectrometry and Allied Topics*, p 1041, Chicago.
[517] Caprioli, R. M., Farmer, T. B., and Gile, J. (1997) Molecular imaging of biological samples: localization of peptides and proteins using MALDI-TOF MS, *Analytical chemistry 69*, 4751-4760.
[518] Cornett, D. S., Frappier, S. L., and Caprioli, R. M. (2008) MALDI-FTICR imaging mass spectrometry of drugs and metabolites in tissue, *Analytical chemistry 80*, 5648-5653.
[519] Greer, T., Sturm, R., and Li, L. (2011) Mass spectrometry imaging for drugs and metabolites, *Journal of proteomics 74*, 2617-2631.
[520] Zemski Berry, K. A., Hankin, J. A., Barkley, R. M., Spraggins, J. M., Caprioli, R. M., and Murphy, R. C. (2011) MALDI imaging of lipid biochemistry in tissues by mass spectrometry, *Chemical reviews 111*, 6491-6512.
[521] Goodwin, R. J., Pennington, S. R., and Pitt, A. R. (2008) Protein and peptides in pictures: imaging with MALDI mass spectrometry, *Proteomics 8*, 3785-3800.
[522] Kaya, I., Johansson, E., Lange, S., and Malmberg, P. (2017) Antisecretory Factor (AF) egg-yolk peptides reflects the intake of AF-activating feed in hens, *Clinical Nutrition Experimental 12*, 27-36.
[523] Hulme, H., Fridjonsdottir, E., Gunnarsdottir, H., Vallianatou, T., Zhang, X., Wadensten, H., Shariatgorji, R., Nilsson, A., Bezard, E., and Svenningsson, P. (2020) Simultaneous mass spectrometry imaging of multiple neuropeptides in the brain and alterations induced by experimental parkinsonism and L-DOPA therapy, *Neurobiology of Disease*, 104738.
[524] Chaurand, P., Norris, J. L., Cornett, D. S., Mobley, J. A., and Caprioli, R. M. (2006) New developments in profiling and imaging of proteins from tissue sections by MALDI mass spectrometry, *Journal of proteome research 5*, 2889-2900.
[525] Wiegelmann, M., Soltwisch, J., Jaskolla, T. W., and Dreisewerd, K. (2013) Matching the laser wavelength to the absorption properties of matrices increases the ion yield in UV-MALDI mass spectrometry, *Analytical and bioanalytical chemistry 405*, 6925-6932.

[526] Soltwisch, J., Jaskolla, T. W., Hillenkamp, F., Karas, M., and Dreisewerd, K. (2012) Ion yields in UV-MALDI mass spectrometry as a function of excitation laser wavelength and optical and physicochemical properties of classical and halogen-substituted MALDI matrixes, *Analytical chemistry 84*, 6567-6576.

[527] Niehaus, M., Schnapp, A., Koch, A., Soltwisch, J., and Dreisewerd, K. (2017) New Insights into the Wavelength Dependence of MALDI Mass Spectrometry, *Analytical Chemistry 89*, 7734-7741.

[528] Horneffer, V., Dreisewerd, K., Lüdemann, H.-C., Hillenkamp, F., Läge, M., and Strupat, K. (1999) Is the incorporation of analytes into matrix crystals a prerequisite for matrix-assisted laser desorption/ionization mass spectrometry? A study of five positional isomers of dihydroxybenzoic acid, *International journal of mass spectrometry 185*, 859-870.

[529] Jaskolla, T. W., Lehmann, W.-D., and Karas, M. (2008) 4-Chloro-α-cyanocinnamic acid is an advanced, rationally designed MALDI matrix, *Proceedings of the National Academy of Sciences 105*, 12200-12205.

[530] Fukuyama, Y., Tanimura, R., Maeda, K., Watanabe, M., Kawabata, S.-I., Iwamoto, S., Izumi, S., and Tanaka, K. (2012) Alkylated dihydroxybenzoic acid as a MALDI matrix additive for hydrophobic peptide analysis, *Analytical chemistry 84*, 4237-4243.

[531] Fukuyama, Y., Nakajima, C., Furuichi, K., Taniguchi, K., Kawabata, S.-i., Izumi, S., and Tanaka, K. (2013) Alkylated trihydroxyacetophenone as a MALDI matrix for hydrophobic peptides, *Analytical chemistry 85*, 9444-9448.

[532] Beavis, R. C., Chait, B. T., and Standing, K. (1989) Matrix-assisted laser-desorption mass spectrometry using 355 nm radiation, *Rapid Communications in Mass Spectrometry 3*, 436-439.

[533] Wenzel, T., Sparbier, K., Mieruch, T., and Kostrzewa, M. (2006) 2, 5-Dihydroxyacetophenone: a matrix for highly sensitive matrix-assisted laser desorption/ionization time-of-flight mass spectrometric analysis of proteins using manual and automated preparation techniques, *Rapid communications in mass spectrometry 20*, 785-789.

[534] Yang, J., and Caprioli, R. M. (2011) Matrix sublimation/recrystallization for imaging proteins by mass spectrometry at high spatial resolution, *Analytical chemistry 83*, 5728-5734.

[535] Yang, J., Zavalin, A., and Caprioli, R. M. Robust sample preparation with 2, 5-dihydroxyacetophenone for MALDI imaging mass spectrometry of proteins (2-70 kDa) at high spatial resolution (5μm).

[536] Zavalin, A., Yang, J., Hayden, K., Vestal, M., and Caprioli, R. M. (2015) Tissue protein imaging at 1 μm laser spot diameter for high spatial resolution and high imaging speed using transmission

geometry MALDI TOF MS, *Analytical and bioanalytical chemistry 407*, 2337-2342.
[537] Yang, J., Norris, J. L., and Caprioli, R. (2018) Novel vacuum stable ketone-based matrices for high spatial resolution MALDI imaging mass spectrometry, *Journal of Mass Spectrometry 53*, 1005-1012.
[538] Pashkova, A., Moskovets, E., and Karger, B. L. (2004) Coumarin tags for improved analysis of peptides by MALDI-TOF MS and MS/MS. 1. Enhancement in MALDI MS signal intensities, *Analytical chemistry 76*, 4550-4557.
[539] Pashkova, A., Chen, H.-S., Rejtar, T., Zang, X., Giese, R., Andreev, V., Moskovets, E., and Karger, B. L. (2005) Coumarin tags for analysis of peptides by MALDI-TOF MS and MS/MS. 2. Alexa Fluor 350 tag for increased peptide and protein identification by LC-MALDI-TOF/TOF MS, *Analytical chemistry 77*, 2085-2096.
[540] Franck, J., El Ayed, M., Wisztorski, M., Salzet, M., and Fournier, I. (2009) On-tissue N-terminal peptide derivatizations for enhancing protein identification in MALDI mass spectrometric imaging strategies, *Analytical chemistry 81*, 8305-8317.
[541] Sakakura, M., and Takayama, M. (2010) In-source decay and fragmentation characteristics of peptides using 5-aminosalicylic acid as a matrix in matrix-assisted laser desorption/ionization mass spectrometry, *Journal of the American Society for Mass Spectrometry 21*, 979-988.
[542] Demeure, K., Quinton, L., Gabelica, V., and De Pauw, E. (2007) Rational selection of the optimum MALDI matrix for top-down proteomics by in-source decay, *Analytical chemistry 79*, 8678-8685.
[543] Debois, D., Bertrand, V., Quinton, L., De Pauw-Gillet, M.-C., and De Pauw, E. (2010) MALDI-in source decay applied to mass spectrometry imaging: a new tool for protein identification, *Analytical chemistry 82*, 4036-4045.
[544] Calligaris, D., Longuespée, R. m., Debois, D., Asakawa, D., Turtoi, A., Castronovo, V., Noël, A. s., Bertrand, V., De Pauw-Gillet, M.-C., and De Pauw, E. (2013) Selected protein monitoring in histological sections by targeted MALDI-FTICR in-source decay imaging, *Analytical chemistry 85*, 2117-2126.
[545] Ellis, S. R., Jungmann, J. H., Smith, D. F., Soltwisch, J., and Heeren, R. M. (2013) Enhanced Detection of High-Mass Proteins by Using an Active Pixel Detector, *Angewandte Chemie International Edition 52*, 11261-11264.
[546] Prentice, B. M., Ryan, D. J., Van de Plas, R., Caprioli, R. M., and Spraggins, J. M. (2018) Enhanced ion transmission efficiency up to m/z 24 000 for MALDI protein imaging mass spectrometry, *Analytical chemistry 90*, 5090-5099.
[547] Spraggins, J. M., Rizzo, D. G., Moore, J. L., Noto, M. J., Skaar, E. P., and Caprioli, R. M. (2016) Next-generation technologies for spatial

proteomics: integrating ultra-high speed MALDI-TOF and high mass resolution MALDI FTICR imaging mass spectrometry for protein analysis, *Proteomics 16*, 1678-1689.
[548] Hillenkamp, F. (1998) Matrix-assisted laser desorption/ionization of non-covalent complexes, In *New methods for the study of biomolecular complexes*, pp 181-191, Springer.
[549] Jackson, S. N., and Woods, A. S. (2013) Imaging of noncovalent complexes by MALDI-MS, *Journal of The American Society for Mass Spectrometry 24*, 1950-1956.
[550] Woods, A., Buchsbaum, J., Worrall, T., Berg, J., and Cotter, R. J. (1995) Matrix-assisted laser desorption/ionization of noncovalently bound compounds, *Analytical Chemistry 67*, 4462-4465.
[551] Zehl, M., and Allmaier, G. (2005) Instrumental parameters in the MALDI-TOF mass spectrometric analysis of quaternary protein structures, *Analytical chemistry 77*, 103-110.
[552] Dashtiev, M., Wäfler, E., Röhling, U., Gorshkov, M., Hillenkamp, F., and Zenobi, R. (2007) Positive and negative analyte ion yield in matrix-assisted laser desorption/ionization, *International Journal of Mass Spectrometry 268*, 122-130.
[553] Vermillion-Salsbury, R. L., and Hercules, D. M. (2002) 9-Aminoacridine as a matrix for negative mode matrix-assisted laser desorption/ionization, *Rapid communications in mass spectrometry 16*, 1575-1581.
[554] Cerruti, C. D., Benabdellah, F., Laprévote, O., Touboul, D., and Brunelle, A. (2012) MALDI imaging and structural analysis of rat brain lipid negative ions with 9-aminoacridine matrix, *Analytical chemistry 84*, 2164-2171.
[555] Nonami, H., Tanaka, K., Fukuyama, Y., and Erra-Balsells, R. (1998) β-Carboline alkaloids as matrices for UV-matrix-assisted laser desorption/ionization time-of-flight mass spectrometry in positive and negative ion modes. Analysis of proteins of high molecular mass, and of cyclic and acyclic oligosaccharides, *Rapid communications in mass spectrometry 12*, 285-296.
[556] Ellis, S. R., Paine, M. R., Eijkel, G. B., Pauling, J. K., Husen, P., Jervelund, M. W., Hermansson, M., Ejsing, C. S., and Heeren, R. M. (2018) Automated, parallel mass spectrometry imaging and structural identification of lipids, *Nature methods 15*, 515-518.
[557] Wang, J., Qiu, S., Chen, S., Xiong, C., Liu, H., Wang, J., Zhang, N., Hou, J., He, Q., and Nie, Z. (2015) MALDI-TOF MS imaging of metabolites with a N-(1-naphthyl) ethylenediamine dihydrochloride matrix and its application to colorectal cancer liver metastasis, *Analytical chemistry 87*, 422-430.
[558] Ibrahim, H., Jurcic, K., Wang, J. S.-H., Whitehead, S. N., and Yeung, K. K.-C. (2017) 1, 6-Diphenyl-1, 3, 5-hexatriene (DPH) as a novel

matrix for MALDI MS imaging of fatty acids, phospholipids, and sulfatides in brain tissues, *Analytical chemistry 89*, 12828-12836.

[559] Korte, A. R., and Lee, Y. J. (2014) MALDI-MS analysis and imaging of small molecule metabolites with 1, 5-diaminonaphthalene (DAN), *Journal of Mass Spectrometry 49*, 737-741.

[560] Kaya, I., Jennische, E., Lange, S., and Malmberg, P. (2018) Dual polarity MALDI imaging mass spectrometry on the same pixel points reveals spatial lipid localizations at high-spatial resolutions in rat small intestine, *Analytical Methods 10*, 2428-2435.

[561] Liu, H., Zhou, Y., Wang, J., Xiong, C., Xue, J., Zhan, L., and Nie, Z. (2018) N-Phenyl-2-naphthylamine as a Novel MALDI matrix for analysis and in situ imaging of small molecules, *Analytical chemistry 90*, 729-736.

[562] He, H., Qin, L., Zhang, Y., Han, M., Li, J., Liu, Y., Qiu, K., Dai, X., Li, Y., and Zeng, M. (2019) 3, 4-Dimethoxycinnamic acid as a novel matrix for enhanced in situ detection and imaging of low-molecular-weight compounds in biological tissues by MALDI-MSI, *Analytical chemistry 91*, 2634-2643.

[563] Wang, J., Sun, J., Wang, J., Liu, H., Xue, J., and Nie, Z. (2017) Hexagonal boron nitride nanosheets as a multifunctional background-free matrix to detect small molecules and complicated samples by MALDI mass spectrometry, *Chemical Communications 53*, 8114-8117.

[564] Dong, X., Cheng, J., Li, J., and Wang, Y. (2010) Graphene as a novel matrix for the analysis of small molecules by MALDI-TOF MS, *Analytical chemistry 82*, 6208-6214.

[565] Shrivas, K., Hayasaka, T., Sugiura, Y., and Setou, M. (2011) Method for simultaneous imaging of endogenous low molecular weight metabolites in mouse brain using TiO2 nanoparticles in nanoparticle-assisted laser desorption/ionization-imaging mass spectrometry, *Analytical chemistry 83*, 7283-7289.

[566] Shanta, S. R., Kim, T. Y., Hong, J. H., Lee, J. H., Shin, C. Y., Kim, K.-H., Kim, Y. H., Kim, S. K., and Kim, K. P. (2012) A new combination MALDI matrix for small molecule analysis: application to imaging mass spectrometry for drugs and metabolites, *Analyst 137*, 5757-5762.

[567] Kudina, O., Eral, B., and Mugele, F. (2016) e-MALDI: an electrowetting-enhanced drop drying method for MALDI mass spectrometry, *Analytical chemistry 88*, 4669-4675.

[568] Lai, Y.-H., Cai, Y.-H., Lee, H., Ou, Y.-M., Hsiao, C.-H., Tsao, C.-W., Chang, H.-T., and Wang, Y.-S. (2016) Reducing spatial heterogeneity of MALDI samples with Marangoni flows during sample preparation, *Journal of The American Society for Mass Spectrometry 27*, 1314-1321.

[569] Ressine, A., Finnskog, D., Marko-Varga, G., and Laurell, T. (2008) Superhydrophobic properties of nanostructured–microstructured porous silicon for improved surface-based bioanalysis, *Nanobiotechnology 4*, 18-27.
[570] Soltwisch, J., Berkenkamp, S., and Dreisewerd, K. (2008) A binary matrix of 2, 5-dihydroxybenzoic acid and glycerol produces homogenous sample preparations for matrix-assisted laser desorption/ionization mass spectrometry, *Rapid Communications in Mass Spectrometry: An International Journal Devoted to the Rapid Dissemination of Up-to-the-Minute Research in Mass Spectrometry 22*, 59-66.
[571] Calvano, C. D., Ventura, G., Cataldi, T. R., and Palmisano, F. (2015) Improvement of chlorophyll identification in foodstuffs by MALDI ToF/ToF mass spectrometry using 1, 5-diaminonaphthalene electron transfer secondary reaction matrix, *Analytical and bioanalytical chemistry 407*, 6369-6379.
[572] Shroff, R., and Svatoš, A. (2009) Proton sponge: a novel and versatile MALDI matrix for the analysis of metabolites using mass spectrometry, *Analytical chemistry 81*, 7954-7959.
[573] Weißflog, J., and Svatoš, A. (2016) 1, 8-Di (piperidinyl)-naphthalene–rationally designed MAILD/MALDI matrix for metabolomics and imaging mass spectrometry, *RSC advances 6*, 75073-75081.
[574] Giampà, M., Lissel, M., Patschkowski, T., Fuchser, J., Hans, V., Gembruch, O., Bednarz, H., and Niehaus, K. (2016) Maleic anhydride proton sponge as a novel MALDI matrix for the visualization of small molecules (< 250 m/z) in brain tumors by routine MALDI ToF imaging mass spectrometry, *Chemical communications 52*, 9801-9804.
[575] Calvano, C. D., Cataldi, T. R., Kögel, J. F., Monopoli, A., Palmisano, F., and Sundermeyer, J. (2017) Structural characterization of neutral saccharides by negative ion MALDI mass spectrometry using a superbasic proton sponge as deprotonating matrix, *Journal of The American Society for Mass Spectrometry 28*, 1666-1675.
[576] Calvano, C. D., Monopoli, A., Cataldi, T. R., and Palmisano, F. (2018) MALDI matrices for low molecular weight compounds: an endless story?, *Analytical and bioanalytical chemistry*, 1-24.
[577] Calvano, C. D., Zambonin, C. G., and Palmisano, F. (2011) Lipid fingerprinting of Gram-positive lactobacilli by intact cells–matrix-assisted laser desorption/ionization mass spectrometry using a proton sponge based matrix, *Rapid Communications in Mass Spectrometry 25*, 1757-1764.
[578] Shroff, R., Rulíšek, L., Doubský, J., and Svatoš, A. (2009) Acid–base-driven matrix-assisted mass spectrometry for targeted metabolomics, *Proceedings of the National Academy of Sciences 106*, 10092-10096.

[579] Li, N., Wang, P., Liu, X., Han, C., Ren, W., Li, T., Li, X., Tao, F., and Zhao, Z. (2019) Developing IR-780 as a Novel Matrix for Enhanced MALDI MS Imaging of Endogenous High-Molecular-Weight Lipids in Brain Tissues, *Analytical chemistry 91*, 15873-15882.
[580] Brombacher, S., Owen, S. J., and Volmer, D. A. (2003) Automated coupling of capillary-HPLC to matrix-assisted laser desorption/ionization mass spectrometry for the analysis of small molecules utilizing a reactive matrix, *Analytical and bioanalytical chemistry 376*, 773-779.
[581] Vogel, M., Büldt, A., and Karst, U. (2000) Hydrazine reagents as derivatizing agents in environmental analysis–a critical review, *Fresenius' journal of analytical chemistry 366*, 781-791.
[582] Cobice, D. F., Mackay, C. L., Goodwin, R. J., McBride, A., Langridge-Smith, P. R., Webster, S. P., Walker, B. R., and Andrew, R. (2013) Mass spectrometry imaging for dissecting steroid intracrinology within target tissues, *Analytical chemistry 85*, 11576-11584.
[583] Zaikin, V. G., Borisov, R. S., Polovkov, N. Y., and Slyundina, M. S. (2015) Reactive matrices for matrix-assisted laser desorption/ionization mass spectrometry of primary amines, *European Journal of Mass Spectrometry 21*, 403-411.
[584] Shariatgorji, M., Nilsson, A., Goodwin, R. J., Källback, P., Schintu, N., Zhang, X., Crossman, A. R., Bezard, E., Svenningsson, P., and Andren, P. E. (2014) Direct targeted quantitative molecular imaging of neurotransmitters in brain tissue sections, *Neuron 84*, 697-707.
[585] Shariatgorji, M., Nilsson, A., Källback, P., Karlsson, O., Zhang, X., Svenningsson, P., and Andren, P. E. (2015) Pyrylium salts as reactive matrices for MALDI-MS imaging of biologically active primary amines, *Journal of the American Society for Mass Spectrometry 26*, 934-939.
[586] Monopoli, A., Calvano, C., Nacci, A., and Palmisano, F. (2014) Boronic acid chemistry in MALDI MS: a step forward in designing a reactive matrix with molecular recognition capabilities, *Chemical Communications 50*, 4322-4324.
[587] Kaya, I., Brülls, S. M., Dunevall, J., Jennische, E., Lange, S., Mårtensson, J., Ewing, A. G., Malmberg, P., and Fletcher, J. S. (2018) On-tissue chemical derivatization of catecholamines using 4-(N-Methyl) pyridinium boronic acid for ToF-SIMS and LDI-ToF mass spectrometry imaging, *Analytical chemistry 90*, 13580-13590.
[588] Shariatgorji, M., Nilsson, A., Fridjonsdottir, E., Vallianatou, T., Källback, P., Katan, L., Sävmarker, J., Mantas, I., Zhang, X., and Bezard, E. (2019) Comprehensive mapping of neurotransmitter networks by MALDI–MS imaging, *Nature methods 16*, 1021-1028.
[589] Ellis, S., Soltwisch, J., Paine, M., Dreisewerd, K., and Heeren, R. (2017) Laser post-ionisation combined with a high resolving power

orbitrap mass spectrometer for enhanced MALDI-MS imaging of lipids, *Chemical Communications 53*, 7246-7249.

[590] Belov, M. E., Ellis, S. R., Dilillo, M., Paine, M. R., Danielson, W. F., Anderson, G. A., de Graaf, E. L., Eijkel, G. B., Heeren, R. M., and McDonnell, L. A. (2017) Design and performance of a novel interface for combined matrix-assisted laser desorption ionization at elevated pressure and electrospray ionization with Orbitrap mass spectrometry, *Analytical chemistry 89*, 7493-7501.

[591] Soltwisch, J., Kettling, H., Vens-Cappell, S., Wiegelmann, M., Müthing, J., and Dreisewerd, K. (2015) Mass spectrometry imaging with laser-induced postionization, *Science*, aaa1051.

[592] Barré, F. P., Paine, M. R., Flinders, B., Trevitt, A. J., Kelly, P. D., Ait-Belkacem, R., Garcia, J. o. P., Creemers, L. B., Stauber, J., and Vreeken, R. J. (2019) Enhanced sensitivity using MALDI imaging coupled with laser postionization (MALDI-2) for pharmaceutical research, *Analytical chemistry 91*, 10840-10848.

[593] Spivey, E. C., McMillen, J. C., Ryan, D. J., Spraggins, J. M., and Caprioli, R. M. (2019) Combining MALDI-2 and transmission geometry laser optics to achieve high sensitivity for ultra-high spatial resolution surface analysis, *Journal of Mass Spectrometry 54*, 366-370.

[594] Nishizuka, Y. (1992) Intracellular signaling by hydrolysis of phospholipids and activation of protein kinase C, *Science 258*, 607-614.

[595] Kompauer, M., Heiles, S., and Spengler, B. (2017) Atmospheric pressure MALDI mass spectrometry imaging of tissues and cells at 1.4-μm lateral resolution, *nAture methods 14*, 90.

[596] Ellis, S. R., Cappell, J., Potočnik, N. O., Balluff, B., Hamaide, J., Van der Linden, A., and Heeren, R. M. (2016) More from less: high-throughput dual polarity lipid imaging of biological tissues, *Analyst*.

[597] Berry, K. A. Z., Li, B., Reynolds, S. D., Barkley, R. M., Gijón, M. A., Hankin, J. A., Henson, P. M., and Murphy, R. C. (2011) MALDI imaging MS of phospholipids in the mouse lung, *Journal of lipid research 52*, 1551-1560.

[598] Thomas, A. l., Charbonneau, J. L., Fournaise, E., and Chaurand, P. (2012) Sublimation of new matrix candidates for high spatial resolution imaging mass spectrometry of lipids: enhanced information in both positive and negative polarities after 1, 5-diaminonapthalene deposition, *Analytical chemistry 84*, 2048-2054.

[599] Hankin, J. A., Barkley, R. M., and Murphy, R. C. (2007) Sublimation as a method of matrix application for mass spectrometric imaging, *Journal of the American Society for Mass Spectrometry 18*, 1646-1652.

[600] Ogrinc Potočnik, N., Porta, T., Becker, M., Heeren, R., and Ellis, S. R. (2015) Use of advantageous, volatile matrices enabled by next-

generation high-speed matrix-assisted laser desorption/ionization time-of-flight imaging employing a scanning laser beam, *Rapid Communications in Mass Spectrometry 29*, 2195-2203.

[601] Wang, H.-Y. J., Jackson, S. N., and Woods, A. S. (2007) Direct MALDI-MS analysis of cardiolipin from rat organs sections, *Journal of the American Society for Mass Spectrometry 18*, 567-577.

[602] Jackson, S. N., Baldwin, K., Muller, L., Womack, V. M., Schultz, J. A., Balaban, C., and Woods, A. S. (2014) Imaging of lipids in rat heart by MALDI-MS with silver nanoparticles, *Analytical and bioanalytical chemistry 406*, 1377-1386.

[603] Amoscato, A., Sparvero, L., He, R., Watkins, S., Bayir, H., and Kagan, V. (2014) Imaging mass spectrometry of diversified cardiolipin molecular species in the brain, *Analytical chemistry 86*, 6587-6595.

[604] Sparvero, L. J., Amoscato, A. A., Fink, A. B., Anthonymuthu, T., New, L. A., Kochanek, P. M., Watkins, S., Kagan, V. E., and Bayır, H. (2016) Imaging mass spectrometry reveals loss of polyunsaturated cardiolipins in the cortical contusion, hippocampus, and thalamus after traumatic brain injury, *Journal of neurochemistry 139*, 659-675.

[605] Angel, P. M., Spraggins, J. M., Baldwin, H. S., and Caprioli, R. (2012) Enhanced sensitivity for high spatial resolution lipid analysis by negative ion mode matrix assisted laser desorption ionization imaging mass spectrometry, *Analytical chemistry 84*, 1557-1564.

[606] Hannun, Y. A., and Obeid, L. M. (2018) Sphingolipids and their metabolism in physiology and disease, *Nature reviews Molecular cell biology 19*, 175.

[607] Sugiura, Y., Shimma, S., Konishi, Y., Yamada, M. K., and Setou, M. (2008) Imaging mass spectrometry technology and application on ganglioside study; visualization of age-dependent accumulation of C20-ganglioside molecular species in the mouse hippocampus, *PLoS One 3*, e3232.

[608] Vens-Cappell, S., Kouzel, I. U., Kettling, H., Soltwisch, J., Bauwens, A., Porubsky, S., Müthing, J., and Dreisewerd, K. (2016) On-tissue phospholipase C digestion for enhanced MALDI-MS imaging of neutral glycosphingolipids, *Analytical chemistry 88*, 5595-5599.

[609] Dufresne, M., Patterson, N. H., Norris, J. L., and Caprioli, R. M. (2019) Combining Salt Doping and Matrix Sublimation for High Spatial Resolution MALDI Imaging Mass Spectrometry of Neutral Lipids, *Analytical chemistry 91*, 12928-12934.

[610] Kaya, I., Jennische, E., Dunevall, J., Lange, S., Ewing, A. G., Malmberg, P., Baykal, A. T., and Fletcher, J. S. (2019) Spatial Lipidomics Reveals Region and Long Chain Base Specific Accumulations of Monosialogangliosides in Amyloid Plaques in Familial Alzheimer's Disease Mice (5xFAD) Brain, *ACS chemical neuroscience 11*, 14-24.

[611] Caughlin, S., Maheshwari, S., Weishaupt, N., Yeung, K. K., Cechetto, D. F., and Whitehead, S. N. (2017) Age-dependent and regional heterogeneity in the long-chain base of A-series gangliosides observed in the rat brain using MALDI Imaging, *Scientific reports 7*, 1-12.

[612] Jackson, S. N., Muller, L., Roux, A., Oktem, B., Moskovets, E., Doroshenko, V. M., and Woods, A. S. (2018) AP-MALDI mass spectrometry imaging of gangliosides using 2, 6-dihydroxyacetophenone, *Journal of The American Society for Mass Spectrometry 29*, 1463-1472.

[613] Colsch, B., Jackson, S. N., Dutta, S., and Woods, A. S. (2011) Molecular microscopy of brain gangliosides: illustrating their distribution in hippocampal cell layers, *ACS chemical neuroscience 2*, 213-222.

[614] Jones, E. E., Dworski, S., Canals, D., Casas, J., Fabrias, G., Schoenling, D., Levade, T., Denlinger, C., Hannun, Y. A., and Medin, J. A. (2014) On-tissue localization of ceramides and other sphingolipids by MALDI mass spectrometry imaging, *Analytical chemistry 86*, 8303-8311.

[615] Barbacci, D. C., Roux, A., Muller, L., Jackson, S. N., Post, J., Baldwin, K., Hoffer, B., Balaban, C. D., Schultz, J. A., and Gouty, S. (2017) Mass spectrometric imaging of ceramide biomarkers tracks therapeutic response in traumatic brain injury, *ACS chemical neuroscience 8*, 2266-2274.

[616] Hankin, J. A., Farias, S. E., Barkley, R. M., Heidenreich, K., Frey, L. C., Hamazaki, K., Kim, H.-Y., and Murphy, R. C. (2011) MALDI mass spectrometric imaging of lipids in rat brain injury models, *Journal of the American Society for Mass Spectrometry 22*.

[617] Kaya, I., Brinet, D., Michno, W., Syvänen, S., Sehlin, D., Zetterberg, H., Blennow, K., and Hanrieder, J. r. (2017) Delineating Amyloid Plaque Associated Neuronal Sphingolipids in Transgenic Alzheimer's Disease Mice (tgArcSwe) Using MALDI Imaging Mass Spectrometry, *ACS chemical neuroscience 8*, 347-355.

[618] Nielsen, M. M., Lambertsen, K. L., Clausen, B. H., Meyer, M., Bhandari, D. R., Larsen, S. T., Poulsen, S. S., Spengler, B., Janfelt, C., and Hansen, H. S. (2016) Mass spectrometry imaging of biomarker lipids for phagocytosis and signalling during focal cerebral ischaemia, *Scientific reports 6*, 39571.

[619] Catalá, A. (2009) Lipid peroxidation of membrane phospholipids generates hydroxy-alkenals and oxidized phospholipids active in physiological and/or pathological conditions, *Chemistry and physics of lipids 157*, 1-11.

[620] Basu, S. (2010) Fatty acid oxidation and isoprostanes: oxidative strain and oxidative stress, *Prostaglandins, Leukotrienes and Essential Fatty Acids (PLEFA) 82*, 219-225.

[621] Hayasaka, T., Goto-Inoue, N., Zaima, N., Shrivas, K., Kashiwagi, Y., Yamamoto, M., Nakamoto, M., and Setou, M. (2010) Imaging mass spectrometry with silver naeoparticles reveals the distribution of fatty acids in mouse retinal sections, *Journal of the American Society for Mass Spectrometry 21*, 1446-1454.

[622] Dufresne, M., Masson, J.-F. o., and Chaurand, P. (2016) Sodium-doped gold-assisted laser desorption ionization for enhanced imaging mass spectrometry of triacylglycerols from thin tissue sections, *Analytical chemistry 88*, 6018-6025.

[623] Fincher, J. A., Korte, A. R., Dyer, J. E., Yadavilli, S., Morris, N. J., Jones, D. R., Shanmugam, V. K., Pirlo, R. K., and Vertes, A. (2019) Mass spectrometry imaging of triglycerides in biological tissues by laser desorption ionization from silicon nanopost arrays, *Journal of Mass Spectrometry*.

[624] Fincher, J. A., Dyer, J. E., Korte, A. R., Yadavilli, S., Morris, N. J., and Vertes, A. (2019) Matrix-free mass spectrometry imaging of mouse brain tissue sections on silicon nanopost arrays, *J Comp Neurol 527*, 2101-2121.

[625] Dufresne, M., Thomas, A. l., Breault-Turcot, J., Masson, J.-F. o., and Chaurand, P. (2013) Silver-assisted laser desorption ionization for high spatial resolution imaging mass spectrometry of olefins from thin tissue sections, *Analytical chemistry 85*, 3318-3324.

[626] Stopka, S. A., Rong, C., Korte, A. R., Yadavilli, S., Nazarian, J., Razunguzwa, T. T., Morris, N. J., and Vertes, A. (2016) Molecular imaging of biological samples on nanophotonic laser desorption ionization platforms, *Angewandte Chemie International Edition 55*, 4482-4486.

[627] Fincher, J. A., Jones, D. R., Korte, A. R., Dyer, J. E., Parlanti, P., Popratiloff, A., Brantner, C. A., Morris, N. J., Pirlo, R. K., and Shanmugam, V. K. (2019) Mass Spectrometry Imaging of Lipids in Human Skin Disease Model Hidradenitis Suppurativa by Laser Desorption Ionization from Silicon Nanopost Arrays, *Scientific reports 9*, 1-10.

[628] Soltwisch, J., Kettling, H., Vens-Cappell, S., Wiegelmann, M., Müthing, J., and Dreisewerd, K. (2015) Mass spectrometry imaging with laser-induced postionization, *Science 348*, 211-215.

[629] Rzagalinski, I., Hainz, N., Meier, C., Tschernig, T., and Volmer, D. A. (2018) MALDI mass spectral imaging of bile acids observed as deprotonated molecules and proton-bound dimers from mouse liver sections, *Journal of The American Society for Mass Spectrometry 29*, 711-722.

[630] Le, C. H., Han, J., and Borchers, C. H. (2012) Dithranol as a MALDI matrix for tissue imaging of lipids by Fourier transform ion cyclotron resonance mass spectrometry, *Analytical chemistry 84*, 8391-8398.

[631] Wang, X., Han, J., Pan, J., and Borchers, C. H. (2014) Comprehensive imaging of porcine adrenal gland lipids by MALDI-FTMS using quercetin as a matrix, *Analytical chemistry 86*, 638-646.
[632] Kaya, I., Brinet, D., Michno, W., Başkurt, M., Zetterberg, H., Blenow, K., and Hanrieder, J. r. (2017) Novel Trimodal MALDI Imaging Mass Spectrometry (IMS3) at 10 μm Reveals Spatial Lipid and Peptide Correlates Implicated in Aβ Plaque Pathology in Alzheimer's Disease, *ACS chemical neuroscience 8*, 2778-2790.
[633] Yang, J., and Caprioli, R. M. (2013) Matrix precoated targets for direct lipid analysis and imaging of tissue, *Analytical chemistry 85*, 2907-2912.
[634] Chaurand, P., Cornett, D. S., Angel, P. M., and Caprioli, R. M. (2011) From whole-body sections down to cellular level, multiscale imaging of phospholipids by MALDI mass spectrometry, *Molecular & Cellular Proteomics 10*, O110. 004259.
[635] Kaya, I., Michno, W., Brinet, D., Iacone, Y., Zanni, G., Blennow, K., Zetterberg, H., and Hanrieder, J. r. (2017) Histology-Compatible MALDI Mass Spectrometry Based Imaging of Neuronal Lipids for Subsequent Immunofluorescent Staining, *Analytical Chemistry 89*, 4685-4694.
[636] Andersson, M., Groseclose, M. R., Deutch, A. Y., and Caprioli, R. M. (2008) Imaging mass spectrometry of proteins and peptides: 3D volume reconstruction, *Nature Methods 5*, 101-108.
[637] Mallah, K., Quanico, J., Trede, D., Kobeissy, F., Zibara, K., Salzet, M., and Fournier, I. (2018) Lipid Changes Associated with Traumatic Brain Injury Revealed by 3D MALDI-MSI, *Analytical chemistry 90*, 10568-10576.
[638] Kompauer, M., Heiles, S., and Spengler, B. (2017) Autofocusing MALDI mass spectrometry imaging of tissue sections and 3D chemical topography of nonflat surfaces, *nature methods 14*, 1156.
[639] Woods, A. S., and Jackson, S. N. (2010) The application and potential of ion mobility mass spectrometry in imaging MS with a focus on lipids, In *Mass Spectrometry Imaging*, pp 99-111, Springer.
[640] Lanucara, F., Holman, S. W., Gray, C. J., and Eyers, C. E. (2014) The power of ion mobility-mass spectrometry for structural characterization and the study of conformational dynamics, *Nature chemistry 6*, 281.
[641] Jackson, S. N., Colsch, B., Egan, T., Lewis, E. K., Schultz, J. A., and Woods, A. S. (2011) Gangliosides' analysis by MALDI-ion mobility MS, *Analyst 136*, 463-466.
[642] Spraggins, J. M., Djambazova, K. V., Rivera, E. S., Migas, L. G., Neumann, E. K., Fuetterer, A., Suetering, J., Goedecke, N., Ly, A., and Van de Plas, R. (2019) High-Performance Molecular Imaging with MALDI Trapped Ion-Mobility Time-of-Flight (timsTOF) Mass Spectrometry, *Analytical chemistry 91*, 14552-14560.

[643] Neumann, E. K., Migas, L. G., Allen, J. L., Caprioli, R. M., Van de Plas, R., and Spraggins, J. (2020) Spatial Metabolomics of the Human Kidney using MALDI Trapped Ion Mobility Imaging Mass Spectrometry.
[644] Klein, D. R., and Brodbelt, J. S. (2017) Structural characterization of phosphatidylcholines using 193 nm ultraviolet photodissociation mass spectrometry, *Analytical chemistry 89*, 1516-1522.
[645] Ryan, E., Nguyen, C. Q. N., Shiea, C., and Reid, G. E. (2017) Detailed structural characterization of sphingolipids via 193 nm ultraviolet photodissociation and ultra high resolution tandem mass spectrometry, *Journal of The American Society for Mass Spectrometry 28*, 1406-1419.
[646] Ma, X., Chong, L., Tian, R., Shi, R., Hu, T. Y., Ouyang, Z., and Xia, Y. (2016) Identification and quantitation of lipid C= C location isomers: A shotgun lipidomics approach enabled by photochemical reaction, *Proceedings of the National Academy of Sciences 113*, 2573-2578.
[647] Wäldchen, F., Spengler, B., and Heiles, S. (2019) Reactive matrix-assisted laser desorption/ionization mass spectrometry imaging using an intrinsically photoreactive Paterno–Buchi matrix for double-bond localization in isomeric phospholipids, *Journal of the American Chemical Society 141*, 11816-11820.
[648] Paine, M. R., Poad, B. L., Eijkel, G. B., Marshall, D. L., Blanksby, S. J., Heeren, R. M., and Ellis, S. R. (2018) Mass spectrometry imaging with isomeric resolution enabled by ozone-induced dissociation, *Angewandte Chemie International Edition 57*, 10530-10534.
[649] Feng, Y., Chen, B., Yu, Q., and Li, L. (2019) Identification of double bond position isomers in unsaturated lipids by m-CPBA epoxidation and mass spectrometry fragmentation, *Analytical chemistry 91*, 1791-1795.
[650] Porta Siegel, T., Ekroos, K., and Ellis, S. R. (2019) Reshaping lipid biochemistry by pushing barriers in structural lipidomics, *Angewandte Chemie International Edition 58*, 6492-6501.
[651] Optimizing, U. (2006) laser focus profiles for improved MALDI performance Holle, Armin; Haase, Andreas; Kayser, Markus; Hoehndorf, *Journal of Mass Spectrometry 41*, 705-716.
[652] Suckau, D., Resemann, A., Schuerenberg, M., Hufnagel, P., Franzen, J., and Holle, A. (2003) A novel MALDI LIFT-TOF/TOF mass spectrometer for proteomics, *Analytical and bioanalytical chemistry 376*, 952-965.
[653] Demirev, P., Westman, A., Reimann, C., Håkansson, P., Barofsky, D., Sundqvist, B., Cheng, Y., Seibt, W., and Siegbahn, K. (1992) Matrix-assisted laser desorption with ultra-short laser pulses, *Rapid communications in mass spectrometry 6*, 187-191.

[654] Vestal, M., Juhasz, P., and Martin, S. (1995) Delayed extraction matrix-assisted laser desorption time-of-flight mass spectrometry, *Rapid Communications in Mass Spectrometry 9*, 1044-1050.
[655] Köcher, T., Engström, Å., and Zubarev, R. A. (2005) Fragmentation of peptides in MALDI in-source decay mediated by hydrogen radicals, *Analytical chemistry 77*, 172-177.
[656] Brown, R. S., Carr, B. L., and Lennon, J. J. (1996) Factors that influence the observed fast fragmentation of peptides in matrix-assisted laser desorption, *Journal of the American Society for Mass Spectrometry 7*, 225-232.
[657] Kaufmann, R., Chaurand, P., Kirsch, D., and Spengler, B. (1996) Post-source decay and delayed extraction in matrix-assisted laser desorption/ionization-reflectron time-of-flight mass spectrometry. Are there trade-offs?, *Rapid communications in mass spectrometry 10*, 1199-1208.
[658] Spengler, B. (1997) Post-source decay analysis in matrix-assisted laser desorption/ionization mass spectrometry of biomolecules, *Journal of Mass Spectrometry 32*, 1019-1036.
[659] Bradbury, N. E., and Nielsen, R. A. (1936) Absolute values of the electron mobility in hydrogen, *Physical Review 49*, 388.
[660] Lecchi, P., Le, H., and Pannell, L. K. (1995) 6-Aza-2-thiothymine: a matrix for MALDI spectra of oligonucleotides, *Nucleic acids research 23*, 1276.
[661] Kussmann, M., Nordhoff, E., Rahbek-Nielsen, H., Haebel, S., Rossel-Larsen, M., Jakobsen, L., Gobom, J., Mirgorodskaya, E., Kroll-Kristensen, A., and Palm‖, L. (1997) Matrix-assisted laser desorption/ionization mass spectrometry sample preparation techniques designed for various peptide and protein analytes, *Journal of Mass Spectrometry 32*, 593-601.
[662] Dai, Y., Whittal, R. M., and Li, L. (1999) Two-layer sample preparation: a method for MALDI-MS analysis of complex peptide and protein mixtures, *Analytical chemistry 71*, 1087-1091.
[663] Kaletaş, B. K., van der Wiel, I. M., Stauber, J., Dekker, L. J., Güzel, C., Kros, J. M., Luider, T. M., and Heeren, R. M. (2009) Sample preparation issues for tissue imaging by imaging MS, *Proteomics 9*, 2622-2633.
[664] Svensson, M., Skvld, K., Nilsson, A., Fdlth, M., Nydahl, K., Svenningsson, P., and Andrin, P. E. (2007) Neuropeptidomics: MS applied to the discovery of novel peptides from the brain, ACS Publications.
[665] Ly, A., Buck, A., Balluff, B., Sun, N., Gorzolka, K., Feuchtinger, A., Janssen, K.-P., Kuppen, P. J., van de Velde, C. J., and Weirich, G. (2016) High-mass-resolution MALDI mass spectrometry imaging of metabolites from formalin-fixed paraffin-embedded tissue, *Nature protocols 11*, 1428-1443.

[666] Lemaire, R., Desmons, A., Tabet, J., Day, R., Salzet, M., and Fournier, I. (2007) Direct analysis and MALDI imaging of formalin-fixed, paraffin-embedded tissue sections, *Journal of proteome research 6*, 1295-1305.

[667] Judd, A. M., Gutierrez, D. B., Moore, J. L., Patterson, N. H., Yang, J., Romer, C. E., Norris, J. L., and Caprioli, R. M. (2019) A recommended and verified procedure for in situ tryptic digestion of formalin-fixed paraffin-embedded tissues for analysis by matrix-assisted laser desorption/ionization imaging mass spectrometry, *Journal of Mass Spectrometry 54*, 716-727.

[668] Kawamoto, T. (2003) Use of a new adhesive film for the preparation of multi-purpose fresh-frozen sections from hard tissues, whole-animals, insects and plants, *Archives of histology and cytology 66*, 123-143.

[669] Altelaar, A. M., van Minnen, J., Jiménez, C. R., Heeren, R. M., and Piersma, S. R. (2005) Direct molecular imaging of Lymnaea stagnalis nervous tissue at subcellular spatial resolution by mass spectrometry, *Analytical chemistry 77*, 735-741.

[670] Stoeckli, M., Staab, D., Schweitzer, A., Gardiner, J., and Seebach, D. (2007) Imaging of a β-peptide distribution in whole-body mice sections by MALDI mass spectrometry, *Journal of the American Society for Mass Spectrometry 18*, 1921-1924.

[671] Schuerenberg, M., Luebbert, C., Deininger, S.-O., Ketterlinus, R., and Suckau, D. (2007) MALDI tissue imaging: mass spectrometric localization of biomarkers in tissue slices, *Nature Methods 4*, 462-462.

[672] Hamm, G., Bonnel, D., Legouffe, R., Pamelard, F., Delbos, J.-M., Bouzom, F., and Stauber, J. (2012) Quantitative mass spectrometry imaging of propranolol and olanzapine using tissue extinction calculation as normalization factor, *Journal of proteomics 75*, 4952-4961.

[673] Aerni, H.-R., Cornett, D. S., and Caprioli, R. M. (2006) Automated acoustic matrix deposition for MALDI sample preparation, *Analytical chemistry 78*, 827-834.

[674] Chaurand, P., Cornett, D. S., Angel, P. M., and Caprioli, R. M. (2011) From whole-body sections down to cellular level, multiscale imaging of phospholipids by MALDI mass spectrometry, *Molecular & Cellular Proteomics 10*.

[675] Bouschen, W., Schulz, O., Eikel, D., and Spengler, B. (2010) Matrix vapor deposition/recrystallization and dedicated spray preparation for high-resolution scanning microprobe matrix-assisted laser desorption/ionization imaging mass spectrometry (SMALDI-MS) of tissue and single cells, *Rapid Communications in Mass Spectrometry 24*, 355-364.

[676] Seeley, E. H., Oppenheimer, S. R., Mi, D., Chaurand, P., and Caprioli, R. M. (2011) Enhancement of protein sensitivity for MALDI imaging mass spectrometry after chemical treatment of tissue sections, *Journal of the American Society for Mass Spectrometry 19*, 1069-1077.

[677] Lemaire, R., Wisztorski, M., Desmons, A., Tabet, J., Day, R., Salzet, M., and Fournier, I. (2006) MALDI-MS direct tissue analysis of proteins: improving signal sensitivity using organic treatments, *Analytical chemistry 78*, 7145-7153.

[678] Yang, E., Dufresne, M., and Chaurand, P. (2019) Enhancing ganglioside species detection for MALDI-TOF imaging mass spectrometry in negative reflectron mode, *International Journal of Mass Spectrometry 437*, 3-9.

[679] Buchwalow, I. B., and Böcker, W. (2010) Immunohistochemistry, *Basics and Methods 1*, 1-149.

[680] Coons, A. H., Creech, H. J., and Jones, R. N. (1941) Immunological properties of an antibody containing a fluorescent group, *Proceedings of the society for experimental biology and medicine 47*, 200-202.

[681] Ino, H. (2004) Application of antigen retrieval by heating for double-label fluorescent immunohistochemistry with identical species-derived primary antibodies, *Journal of Histochemistry & Cytochemistry 52*, 1209-1217.

[682] Tsurui, H., Nishimura, H., Hattori, S., Hirose, S., Okumura, K., and Shirai, T. (2000) Seven-color fluorescence imaging of tissue samples based on Fourier spectroscopy and singular value decomposition, *Journal of Histochemistry & Cytochemistry 48*, 653-662.

[683] Roth, J., Bendayan, M., and Orci, L. (1978) Ultrastructural localization of intracellular antigens by the use of protein A-gold complex, *Journal of Histochemistry & Cytochemistry 26*, 1074-1081.

[684] Bendayan, M., and Garzon, S. (1988) Protein G-gold complex: comparative evaluation with protein A-gold for high-resolution immunocytochemistry, *Journal of Histochemistry & Cytochemistry 36*, 597-607.

[685] Pearson, K. (1901) LIII. On lines and planes of closest fit to systems of points in space, *The London, Edinburgh, and Dublin Philosophical Magazine and Journal of Science 2*, 559-572.

[686] Jackson, J. E. (2005) *A user's guide to principal components*, Vol. 587, John Wiley & Sons.

[687] Wold, S., Ruhe, A., Wold, H., and Dunn, I., WJ. (1984) The collinearity problem in linear regression. The partial least squares (PLS) approach to generalized inverses, *SIAM Journal on Scientific and Statistical Computing 5*, 735-743.

[688] Eriksson, L., Byrne, T., Johansson, E., Trygg, J., and Vikström, C. (2013) *Multi-and megavariate data analysis basic principles and applications*, Vol. 1, Umetrics Academy.
[689] Trygg, J., and Wold, S. (2002) Orthogonal projections to latent structures (O-PLS), *Journal of Chemometrics: A Journal of the Chemometrics Society 16*, 119-128.
[690] Ràfols, P., Vilalta, D., Brezmes, J., Cañellas, N., del Castillo, E., Yanes, O., Ramírez, N., and Correig, X. (2018) Signal preprocessing, multivariate analysis and software tools for MA (LDI)-TOF mass spectrometry imaging for biological applications, *Mass spectrometry reviews 37*, 281-306.
[691] Xu, D., and Tian, Y. (2015) A comprehensive survey of clustering algorithms, *Annals of Data Science 2*, 165-193.
[692] Deininger, S.-O., Ebert, M. P., Futterer, A., Gerhard, M., and Rocken, C. (2008) MALDI imaging combined with hierarchical clustering as a new tool for the interpretation of complex human cancers, *Journal of proteome research 7*, 5230-5236.
[693] McCombie, G., Staab, D., Stoeckli, M., and Knochenmuss, R. (2005) Spatial and spectral correlations in MALDI mass spectrometry images by clustering and multivariate analysis, *Analytical chemistry 77*, 6118-6124.
[694] Amantonico, A., Urban, P. L., Fagerer, S. R., Balabin, R. M., and Zenobi, R. (2010) Single-cell MALDI-MS as an analytical tool for studying intrapopulation metabolic heterogeneity of unicellular organisms, *Analytical chemistry 82*, 7394-7400.
[695] Scott, C., Kosmidis, C., Jia, W., Ledingham, K., and Singhal, R. (1994) Formation of atomic hydrogen in matrix-assisted laser desorption ionization, *Rapid Communications in Mass Spectrometry 8*, 829-832.
[696] Molin, L., Seraglia, R., Dani, F. R., Moneti, G., and Traldi, P. (2011) The double nature of 1, 5-diaminonaphthalene as matrix-assisted laser desorption/ionization matrix: some experimental evidence of the protonation and reduction mechanisms, *Rapid Communications in Mass Spectrometry 25*, 3091-3096.
[697] Maier, J. P. (1974) Photoelectron Spectroscopy of peri-Amino Naphthalenes, *Helvetica Chimica Acta 57*, 994-1003.
[698] Suzuki, T., Midonoya, H., and Shioi, Y. (2009) Analysis of chlorophylls and their derivatives by matrix-assisted laser desorption/ionization–time-of-flight mass spectrometry, *Analytical biochemistry 390*, 57-62.
[699] Wyatt, M. F., Stein, B. K., and Brenton, A. G. (2006) Characterization of Various Analytes Using Matrix-Assisted Laser Desorption/Ionization Time-of-Flight Mass Spectrometry and 2-[(2 E)-3-(4-Tert-Butylphenyl)-2-Methylprop-2-Enylidene] Malononitrile Matrix, *Analytical chemistry 78*, 199-206.

[700] Nazim Boutaghou, M., and Cole, R. B. (2012) 9, 10-Diphenylanthracene as a matrix for MALDI-MS electron transfer secondary reactions, *Journal of mass spectrometry 47*, 995-1003.
[701] Michno, W., Kaya, I., Nyström, S., Guerard, L., Nilsson, K. P. R., Hammarström, P., Blennow, K., Zetterberg, H., and Hanrieder, J. r. (2018) Multimodal chemical imaging of amyloid plaque polymorphism reveals Aβ aggregation dependent anionic lipid accumulations and metabolism, *Analytical chemistry 90*, 8130-8138.
[702] Scheffler, K., and Strupat, K. (2010) MALDI in-source decay fragment ions of peptides and proteins, *Application Note 30218*, 1-8.
[703] Kaya, I., Zetterberg, H., Blennow, K., and Hanrieder, J. r. (2018) Shedding light on the molecular pathology of amyloid plaques in transgenic Alzheimer's Disease mice using multimodal MALDI imaging mass spectrometry, *ACS chemical neuroscience 9*, 1802-1817.
[704] Michno, W., Nyström, S., Wehrli, P., Lashley, T., Brinkmalm, G., Guerard, L., Syvänen, S., Sehlin, D., Kaya, I., and Brinet, D. (2019) Pyroglutamation of amyloid-βx-42 (Aβx-42) followed by Aβ1–40 deposition underlies plaque polymorphism in progressing Alzheimer's disease pathology, *Journal of Biological Chemistry 294*, 6719-6732.
[705] Dyakov, Y. A., Tsai, S.-T., Bagchi, A., Tseng, C.-M., Lee, Y. T., and Ni, C.-K. (2009) 355 nm Multiphoton dissociation and ionization of 2, 5-dihydroxyacetophenone, *The Journal of Physical Chemistry A 113*, 14987-14994.
[706] Carlred, L., Michno, W., Kaya, I., Sjövall, P., Syvänen, S., and Hanrieder, J. (2016) Probing amyloid-β pathology in transgenic Alzheimer's disease (tgArcSwe) mice using MALDI imaging mass spectrometry, *Journal of neurochemistry 138*, 469-478.
[707] Carlred, L., Gunnarsson, A., Solé-Domènech, S., Johansson, B. r., Vukojević, V., Terenius, L., Codita, A., Winblad, B., Schalling, M., and Höök, F. (2014) Simultaneous imaging of amyloid-β and lipids in brain tissue using antibody-coupled liposomes and time-of-flight secondary ion mass spectrometry, *Journal of the American Chemical Society 136*, 9973-9981.
[708] Kakuda, N., Miyasaka, T., Iwasaki, N., Nirasawa, T., Wada-Kakuda, S., Takahashi-Fujigasaki, J., Murayama, S., Ihara, Y., and Ikegawa, M. (2017) Distinct deposition of amyloid-β species in brains with Alzheimer's disease pathology visualized with MALDI imaging mass spectrometry, *Acta neuropathologica communications 5*, 73.
[709] Bastrup, J., Birkelund, S., Asuni, A. A., Volbracht, C., and Stensballe, A. (2019) Dual strategy for reduced signal-suppression effects in matrix-assisted laser desorption/ionization mass spectrometry imaging, *Rapid Communications in Mass Spectrometry 33*, 1711-1721.

[710] Kelley, A. R., Perry, G., and Bach, S. B. (2018) Characterization of Proteins Present in Isolated Senile Plaques from Alzheimer's Diseased Brains by MALDI-TOF MS with MS/MS, *ACS chemical neuroscience*.

[711] Kelley, A. R., Perry, G., Castellani, R. J., and Bach, S. B. (2016) Laser-induced in-source decay applied to the determination of amyloid-beta in alzheimer's brains, *ACS chemical neuroscience 7*, 261-268.

[712] Strnad, Š., Pražienková, V., Sýkora, D., Cvačka, J., Maletínská, L., Popelová, A., and Vrkoslav, V. (2019) The use of 1, 5-diaminonaphthalene for matrix-assisted laser desorption/ionization mass spectrometry imaging of brain in neurodegenerative disorders, *Talanta 201*, 364-372.

[713] Sonnino, S., and Chigorno, V. (2000) Ganglioside molecular species containing C18-and C20-sphingosine in mammalian nervous tissues and neuronal cell cultures, *Biochimica et Biophysica Acta (BBA)-Reviews on Biomembranes 1469*, 63-77.

[714] Behrendt, G., Baer, K., Buffo, A., Curtis, M. A., Faull, R. L., Rees, M. I., Götz, M., and Dimou, L. (2013) Dynamic changes in myelin aberrations and oligodendrocyte generation in chronic amyloidosis in mice and men, *Glia 61*, 273-286.

[715] Kaya, I., Jennische, E., Lange, S., Baykal, A. T., Malmberg, P., and Fletcher, J. S. (2020) Brain Region Specific Amyloid Plaque Associated Myelin Lipid Loss, APOE Deposition and Disruption of the Myelin Sheath in Familial Alzheimer's Disease Mice, *Journal of Neurochemistry*.